



University
of Glasgow

Campanile, Daniel J. (2007) *The post-breakup evolution of the western Indian high-elevation passive margin*. PhD thesis.

<http://theses.gla.ac.uk/38/>

Copyright and moral rights for this thesis are retained by the author

A copy can be downloaded for personal non-commercial research or study, without prior permission or charge

This thesis cannot be reproduced or quoted extensively from without first obtaining permission in writing from the Author

The content must not be changed in any way or sold commercially in any format or medium without the formal permission of the Author

When referring to this work, full bibliographic details including the author, title, awarding institution and date of the thesis must be given

The post break-up evolution of the Western Indian high-elevation passive margin

Daniel Campanile

B.Sc. (Hons.), Glasgow

Thesis presented for the degree of Doctor of Philosophy (Ph.D.)

University of Glasgow

Department of Geographical and Earth Sciences

September 2007

Abstract

The tectonic development of the Western Indian high-elevation passive margin is complex. At least two major rifting events (India/Madagascar and India/Seychelles) and a major hotspot (The Reunion plume) are believed to have been instrumental in the formation and development of the margin. However, the temporal and spatial extent of these major tectonic events remains poorly constrained. The Western Ghats of India has also been cited as a type example of a downwarped, elevated passive continental margin. However, published low temperature thermochronometry suggests downwearing or parallel escarpment retreat as alternative models of margin evolution. Here are present the results of a sediment mass balance study utilising new data for the offshore portion of the Western Indian margin, new onshore apatite fission track and (U-Th)/He thermochronometry for the onshore portion of the Western Indian margin, and flexural isostatic modelling. The combined methodologies used within this study are used to resolve some of the fundamental questions regarding the tectonic development and subsequent long term landscape evolution of the Western Indian margin.

The Konkan-Kerala basin is a major depocentre for sediment from the onshore hinterland of Western India and as such provides a valuable record of the timing and magnitude of Cenozoic denudation along the continental margin. This study presents an analysis of sedimentation in the Konkan-Kerala basin, coupled with a mass balance study, in order to test competing conceptual models for the development of the Western Indian margin. An estimated 109,000 km³ of Cenozoic clastic sediment are present within the Konkan-Kerala basin, a volume difficult to reconcile with the denudation of a downwarped rift flank onshore, and more consistent with denudation of an elevated rift flank. There is evidence for two major pulses in sedimentation; an early phase in the Palaeocene, and a second beginning in the Pliocene. The Palaeocene increase in sedimentation can be interpreted in terms of a denudational response to the rifting between India and The Seychelles, whereas the mechanism responsible for the Pliocene pulse is more enigmatic.

Mass balance analysis only provides spatially and temporally averaged estimates for denudation; consequently, this study presents new low temperature thermochronology

from onshore regions to constrain the onshore pattern of denudation. Apatite fission track ages increase from c.55 Ma at the coast to <350 Ma at the escarpment with mean confined track length between 11.3 μm and 14.3 μm . Apatite (U-Th)/He ages range from 37 Ma to 123 Ma and zircon (U-Th)/He ages range from 324 Ma to 426 Ma. These data, when modelled, are consistent with accelerated denudation contemporaneous with rifting between India and The Seychelles. Inverse-modelling of the thermochronometric data suggest denudation of at least 4.5 km at the coast decreasing to more modest amounts of denudation of between 1.5km and 2.5km further inland towards the escarpment. The pattern of denudation inferred from low temperature thermochronometry is consistent with escarpment evolution into an elevated rift flank.

The flexural response of the Western Indian margin to sediment loading and denudational unloading can be modelled as a thin elastic beam overlying a fluid substratum. Modelling the isostatic response of the Western Indian lithosphere to sediment loading offshore and denudation onshore infer that flexural isostasy is an important component in the development of the Margin. However, flexural isostasy alone cannot account for the pattern of subsidence offshore or the pattern of uplift onshore and additional mechanisms must be invoked.

Table of contents

Abstract	i
Table of contents	iii
List of figures	vi
List of tables	viii
Acknowledgements	ix
Declaration	xi
1 Introduction	1
1.1 Introduction	1
1.2 Passive margins.....	2
1.2.1 Surface uplift mechanisms	2
1.2.2 Conceptual models of passive margin evolution	4
1.3 The Western Indian margin.....	7
1.3.1 Geological background.....	7
1.3.2 Margin physiography	10
1.3.3 Rifting and tectonic history	12
1.3.4 Margin geomorphology.....	15
1.4 The current study	20
1.5 Predictive forward modelling	21
1.5.1 Introduction.....	21
1.5.2 Methods and model parameters.....	21
1.5.3 Forward modelling results for the Northern field area.....	24
1.5.4 Forward modelling results for the Southern field area	26
2 Mass balance analysis	30
2.1 Introduction	30
2.2 The principles of mass balance analysis.....	33
2.2.1 The coupled erosional-depositional system	33
2.2.2 Mass balance analysis – methods and assumptions.....	36
2.3 Mass balance analysis of Western India	37
2.3.1 The offshore area	37
2.3.2 The onshore area	42
2.4 Methods	43
2.4.1 Quantifying sediment in the Konkan-Kerala basin.....	43
2.4.1.1 Obtaining compacted sediment volumes	43
2.4.1.2 Decompacting sediment volumes	46
2.4.2 Calculating the onshore denuded crustal prism.....	48
2.5 Results	50

2.6	Discussion and implications	52
3	Low temperature thermochronometry.....	55
3.1	Introduction	55
3.2	Apatite fission track thermochronometry	57
3.2.1	Introduction.....	57
3.2.2	AFTT annealing kinetics.....	58
3.2.3	Calculating AFTT ages.....	61
3.2.4	Fission track confined track length distributions (TLD's)	62
3.2.5	Interpreting AFTT data	62
3.2.5.1	AFTT age profiles and TLDs	63
3.2.5.2	Forward and inverse-modelling of AFTT data	67
3.3	(U-Th)/He thermochronometry	68
3.3.1	Introduction.....	68
3.3.2	(U-Th)/He ages.....	69
3.3.2.1	The accumulation of helium	69
3.3.2.2	The diffusive loss of helium.....	70
3.3.2.3	Alpha ejection	74
3.3.3	Analytical procedure.....	75
3.3.4	Interpreting (U-Th)/He ages	75
3.3.4.1	(U-Th)/He age profiles.....	75
3.3.4.2	Forward modelling of (U-Th)/He ages.....	77
3.4	Combining thermochronometers.....	77
3.5	Applying low temperature thermochronometry to long-term landscape development.....	79
4	Low temperature thermochronometry data for Goa and Karnataka	81
4.1	Introduction	81
4.2	Apatite fission track data	85
4.2.1	AFTT results.....	85
4.2.2	AFTT inverse-modelling	91
4.2.2.1	Model parameters	91
4.2.2.2	AFTT inverse modelling results.....	92
4.3	(U-Th)/He data	101
4.3.1	(U-Th)/He results.....	102
4.4	Simultaneous inverse-modelling	105
4.5	Summary and conclusions	108
5	Low temperature thermochronometry data for Kerala.....	110
5.1	Introduction	110
5.2	Apatite fission track data	113
5.2.1	AFTT results.....	114
5.2.2	AFTT inverse-modelling	118
5.3	(U-Th)/He data	125
5.3.1	Inverse-modelling (U-Th)/He data	128
5.4	Simultaneous inverse-modelling	133
5.5	Summary and conclusions	134
6	Flexure of the lithosphere.....	137
6.1	Introduction	137
6.2	Isostatic compensation mechanisms	140

6.2.1	Local isostasy.....	140
6.2.2	Regional isostasy	142
6.3	Isostasy and the Western Indian margin	147
6.4	Results	150
6.4.1	Continuous beam	150
6.4.2	Semi-continuous beam.....	152
6.5	Conclusions	153
7	Discussion and conclusions	157
7.1	Introduction	157
7.2	Plate tectonics and passive margin evolution	157
7.3	Long term landscape evolution of Western India	160
7.4	Methodological issues and future work	163
7.5	Conclusions and closing remarks	165
	Appendix A Analytical procedures for low temperature thermochronometry.....	167
A.1	Apatite and zircon mineral separation.....	167
A.2	Apatite fission track analytical techniques.....	167
A.3	Apatite and zircon (U-Th)/He analytical techniques	169
A.3.1	Sample preparation.....	169
A.3.2	Helium analysis.....	169
A.3.3	Uranium and thorium analysis.....	170
	Appendix B Calculating AFTT ages.....	171
B.1	The AFTT age equation	171
B.2	The zeta calibration method.....	173
	Appendix C AFTT data	174
C.1	Western Indian AFTT ages	174
C.1.1	Trackkey plots.....	175
C.2	Western Indian TLD's.....	187
C.2.1	Goa and Karnataka.....	187
C.2.2	Kerala	188
	References	190

List of figures

Chapter 1

Figure 1 Global distribution of elevated passive margins.....	3
Figure 2 Conceptual models of elevated passive margin development.	6
Figure 3 Regional Indian geology and associated major rifts, shear zones and faults.....	9
Figure 4 Pysiography of the Western Indian margin.	11
Figure 5 Tectonic map of India and adjacent oceanic regions.....	13
Figure 6 Plate reconstructions for the Indian, Seychelles and Madagascar.....	15
Figure 7 Different downwarp models for passive margin development.....	17
Figure 8 Panvel flexure alternative models.....	18
Figure 9 Procedure implemented for predictive forward modelling.....	23
Figure 10 Predictive forward modelling results for Goa and Karnataka (I).....	25
Figure 11 Predictive forward modelling results for Goa and Karnataka(II).....	26
Figure 12 Predictive forward modelling results for Kerala (I).....	28
Figure 13 Predictive forward modelling results for Kerala (II).....	29

Chapter 2

Figure 14 Different types of uplift.....	32
Figure 15 The coupled erosional-depositional system.....	35
Figure 16 Location map for onshore and offshore areas.....	39
Figure 17 Subsidence curve for the Kerala basin.....	40
Figure 18 Eustatic sea-level curve.....	41
Figure 19 Isopach maps for the Konkan-Kerala Basin.....	44
Figure 20 Seismic cross section for the Konkan-Kerala Basin.....	44
Figure 21 Simplified lithologies and stratigraphies of wells in the Konkan Kerala Basin..	46
Figure 22 Decompaction cartoon.....	47
Figure 23 Diagrammatic representation of the mass balance procedure.....	49
Figure 24 Sediment flux (a) and denudation rate (b) results.....	52

Chapter 3

Figure 25 Closure temperatures for thermochronometric systems.....	56
Figure 26 Synthetic AFTT ages for apatites with different chemical compositions.....	60
Figure 27 AFTT ages and TLD's within a hypothetical borehole.....	64
Figure 28 The apatite fission track age profile.....	65
Figure 29 The PAZ and the fossil PAZ.....	66
Figure 30 Relationship between AFTT age and TLD for evolving thermal histories.....	67
Figure 31 The concept of closure temperature.....	71
Figure 32 The Arrhenius relationship.....	72
Figure 33 Linear Arrhenius plots.....	73
Figure 34 The relationship between grain size, cooling rate and closure temperature.....	73
Figure 35 Alpha particle ejection.....	75
Figure 36 Apatite (U-Th)/He PRZ.....	76
Figure 37 Multiple thermochronometers.....	78

Chapter 4

Figure 38 Location of samples for Goa and Karnataka	83
Figure 39 Location of analysed samples for Goa and Karnataka	84
Figure 40 AFTT results for selected samples from Goa and Karnataka.....	86
Figure 41 Boomerang plot and age vs distance from the coast for Goa and Karnataka	89
Figure 42 Predictive forward modelling results and measured data	90
Figure 43 Inverse-modelling results of coastal samples from Goa and Karnataka.....	93
Figure 44 AFTT constraints on the time of accelerated cooling for Goa and Karnataka	95
Figure 45 AFT inverse-modelling results of inland samples from Goa and Karnataka	99
Figure 46 Inverse-modelling results for a margin normal transect.....	100
Figure 47 Apatite and zircon (U-Th)/He results ofr Goa and Karnataka.....	101
Figure 48 (U-Th)/He inverse-modelling of samples from Goa and Karnataka	104
Figure 49 ZrHe and AFTT simultaneous inverse modelling results for IND/9/04.....	106
Figure 50 Simultaneous inverse modelling results for Goa and Karnataka.....	107

Chapter 5

Figure 51 Location of samples for Kerala.....	112
Figure 52 Location of analysed samples for Kerala.....	113
Figure 53 AFTT results for Kerala	114
Figure 54 Boomerang plot and age vs distance from the coast for Kerala	117
Figure 55 Predictive forward modelling results and measured data for Kerala.....	118
Figure 56 AFTT inverse-modelling results for Kerala	123
Figure 57 AFTT constraints on the time of accelerated cooling for Kerala	124
Figure 58 Apatite (U-Th)/He plot from Kerala.....	127
Figure 59 Results from apatite and zircon (U-Th)/He inverse-modelling of samples.....	132
Figure 60 Simultaneous inverse-modelling results for Kerala.....	134

Chapter 6

Figure 61 Uplift, subsidence and isostasy.....	139
Figure 62 Models of local isostasy	142
Figure 63 Regional isostasy	146
Figure 64 Flexural modelling set-up.....	149
Figure 65 Model flexural isostatic response of a continuous beam	151
Figure 66 Model flexural isostatic response of a semi-continuous beam.....	153

Appendix

Figure 67 Apatite fission track sample preparation procedure	168
--	-----

List of tables

Chapter 2

Table 1 The chronologies of Rao & Srivastava (1984) and Chaubey et al. (2002)	45
Table 2 Mass balance results for Konkan-Kerala Basin	51

Chapter 3

Table 3 Averaged α -stopping distances for apatite and zircon	75
--	----

Chapter 4

Table 4 AFTT results from Goa and Karnataka	87
Table 5 Track length distribution and Dpar data for Goa and Karnataka	88
Table 6 Apatite (U-Th)/He results for Goa and Karnataka	102
Table 7 Zircon (U-Th)/He results for Goa and Karnataka	102
Table 8 Summary of magnitude of post break-up cooling of samples	94

Chapter 5

Table 9 Apatite fission track results for Kerala	115
Table 10 Track length distribution and Dpar data for Kerala	116
Table 11 Apatite (U-Th)/He results from Kerala	126
Table 12 Zircon (U-Th)/He results from Kerala	126
Table 13 Summary of magnitude of post break-up cooling for Kerala	124

Chapter 6

Table 14 Constants for modelling lithospheric flexure	145
Table 15 Variables for modelling lithospheric flexure	145
Table 16 Published constraints for T_e of the Indian sub-continent.	147
Table 17 Summary of cell parameters	150
Table 18 Results for a continuous beam	151
Table 19 Results for a semi-continuous beam	152

Chapter 7

Table 20 Conceptual models and methodologies	161
--	-----

Appendix

Table 21 AFTT TLD data for Goa and Karnataka	174
Table 22 AFTT TLD data for Kerala	174

Acknowledgements

Initially I would like to thank NERC for providing funding for this project, without which this research would not have been possible. The NERC studentship PhD award number for this study is NER/S/R/2003/12016. I would like to acknowledge my supervisors, Prof. Paul Bishop, Prof. Rod Brown, Dr. Fin Stuart and Dr. Mike Widdowson (listed alphabetically). I thank them for their guidance, individual and unique expertise but above all their tolerance and patients dealing with a difficult student. Within the department of Geographical and Earth Science I would also like to give special thanks to Dr. Cristina Persano for spending an inordinate amount of time with me, teaching valuable skills and providing advice throughout the PhD. Thanks also go to Dr. Tim Dempster for vital feedback and Dr. Kate Dobson for thoughtful discussions and indispensable support during the writing up process.

Thanks go to several members of staff for technical support. John Gilleece for help with fission track sample preparation, Bill Higginson for help with mineral separation, Sorcha Diskin, Jurgen Foeken and David Vilberts for Helium extraction, and Valerie Olive for Uranium and Thorium analysis. Essential IT support was provided by Brian Black and Kenny Roberts. I would like to acknowledge Dr. Andy Carter for providing additional AFT data on samples previously collected in India. During fieldwork, thanks go to Orlando Fernandez for sample collection in Goa and Karnataka, and Dr. Nambiar for sample collection in Kerala and help in obtaining and analysing the mass balance data. Thanks are also due for Tibi Codilean for assisting with computations and manipulation of DEMs.

All the postgraduates in the Gregory building have provided help throughout the project. However, particular mention goes to Jamie, Paul and Duncan for not only being good friends and dragging me to the pub to share our suffering but also for putting up with my complaining, and giving me a good kick when I needed it. Thanks also go to Lisa and Andy for exposing me to rare happiness only a young family can bring within my final year and for being sympathetic listeners. The list of friends that helped in one form or another outside of work is long but individual thanks are due for Antonio, Catarina, Claire, Graham, Katie, Steph, Fran, Tristan and Lynda. They all unknowingly provided vital

distractions and solace on snow, rock and ice, without which I would have lost my sanity long before the project was complete. I owe them all a huge dept of gratitude that will be difficult to repay. I also must thank my family, in particular my mum and dad, for support and belief despite my own continuous doubts. I cannot begin to imagine how difficult and frustrating it must have been as largely helpless parents unable to make things right for me in my final year.

Final thanks should go to Lindsay for unquestionable support, tolerance and love throughout most of the project, but above all, prior to writing up, for highlighting so effectively what it is to undertake a seemingly impossible personal challenge. She has undoubtedly helped make me the person I am today.

Declaration

The material presented in this thesis is the result of independent research undertaken by the Daniel Campanile between October 2003 and September 2007. This work was supervised by Prof. Paul Bishop, Prof. Roderick Brown, Dr. Finley Stuart and Dr. Mike Widdowson. All work by other researchers that is quoted in this thesis is given full acknowledgements in the text.

Daniel Campanile

September 2007

1 Introduction

1.1 Introduction

Long term landscape evolutions, and specifically the study of landforms, are generally the domain of the geomorphologist. Davis (1899), King (1955) and Penck (1953) devised and developed the classical models of landscape evolution by relating erosional features and rare onshore sedimentary deposits to pulses of rejuvenated uplift. Despite the popularity of these models, they lacked a detailed treatment of surface processes and failed to describe the tectonic mechanism for generating uplift. The theory of plate tectonics appeared to present a solution and a unifying conceptual framework for understanding the formation and distribution of the Earth's key surface features such as oceans, continents, mountains and basins.

One of the key areas of study has been passive margin evolution. Ollier (1985) related passive margin formation and in particular the presence of coast parallel escarpments to continental rifting. Nevertheless, incorporating passive margin morphology into prevailing ideas of plate tectonics remains challenging. Both tectonics and surface processes exert fundamental controls on landscape morphology along passive margins and strongly influence denudation and sedimentation (Beaumont et al., 2000). Understanding landscape morphology, tectonic processes (Gilchrist and Summerfield, 1990, 1994; Summerfield, 1985) and denudation rates is increasingly recognized as being crucial to improving theories of long term landscape development. Consequently, modern landscape evolution studies now incorporate a range of methodologies including low temperature thermochronometry (Brown et al., 2002a; Gallagher et al., 1994; Gunnell et al., 2003; Persano et al., 2002; Persano et al., 2005), cosmogenic isotope analysis (Brown et al., 2002a; Cockburn et al., 2000), offshore sediment analysis (Pazzaglia and Brandon, 1996; Pazzaglia and Gardner, 1994; Rust and Summerfield, 1990) and numerical surface process modelling (van der Beek et al., 2002).

This study presents new data derived using a variety of different methodologies with the aim of testing prevailing ideas of landscape development for the Western India elevated passive margin. Western India has undergone a complex tectonic history and, as a consequence, there is still an incomplete understanding of the spatial and temporal influences of the key tectonic

events and their effect on denudation. Accordingly, this project utilizes refined offshore data for denudational mass balance estimates and a combination of low temperature thermochronometers onshore to constrain denudation and provide solutions to the fundamental questions that remain unanswered for the Western Indian elevated passive margin.

The remainder of this chapter outlines the distribution, morphology and origin of passive margins, specifically focusing on elevated passive margin. The two key groups of conceptual models that have been developed to explain the evolution of passive margins are then described. An introduction to Western India summarizing the morphology, geological and tectonic history, together with a review of Western Indian landscape evolution studies is then provided followed by a final section on predictive forward modelling.

1.2 Passive margins

Passive margins are continental-scale features that develop on the trailing edges of plates in response to continental rifting, sea floor spreading and ocean basin development (Kearey and Vine, 1996). The macro-morphology of passive margins is highly variable; however, Gilchrist and Summerfield (1990) identified two end members; (i) low elevation passive margins and, (ii) high elevation passive margins. High elevation passive margins exhibit long-lived uplift regardless of age and may be characterised by marginal rift flank upwarps (Weissel and Karner, 1989). The primary morphological elements of high elevation passive margins are a highly dissected coastal plain and an elevated interior plateau, separated by kilometre high coast-parallel escarpments lying up to 200 km inland. Interestingly, the majority of the world's high elevation passive margins occur on the edges of the Gondwana continents (Figure 1) and have been intimately linked to the breakup and dispersal of Pangaea and Gondwana (King, 1950; Ollier, 1985).

1.2.1 Surface uplift mechanisms

Many mechanisms have been suggested for the both the initial cause of rifting and the generation and persistence of surface uplift at elevated passive margins (see Ollier (1985), Summerfield (1991b) and Summerfield (1991a) for general review), and although not fully understood the connection between rifting and denudation is well established. Proposed mechanisms can be grouped into two categories, active rifting processes and passive rifting processes. Determining the process(es) responsible for rifting is crucial because the timing of surface uplift differs for active and passive rifting. Surface uplift precedes continental splitting with active rifting whereas surface uplift occurs after continental splitting with passive rifting (Summerfield, 1991b).

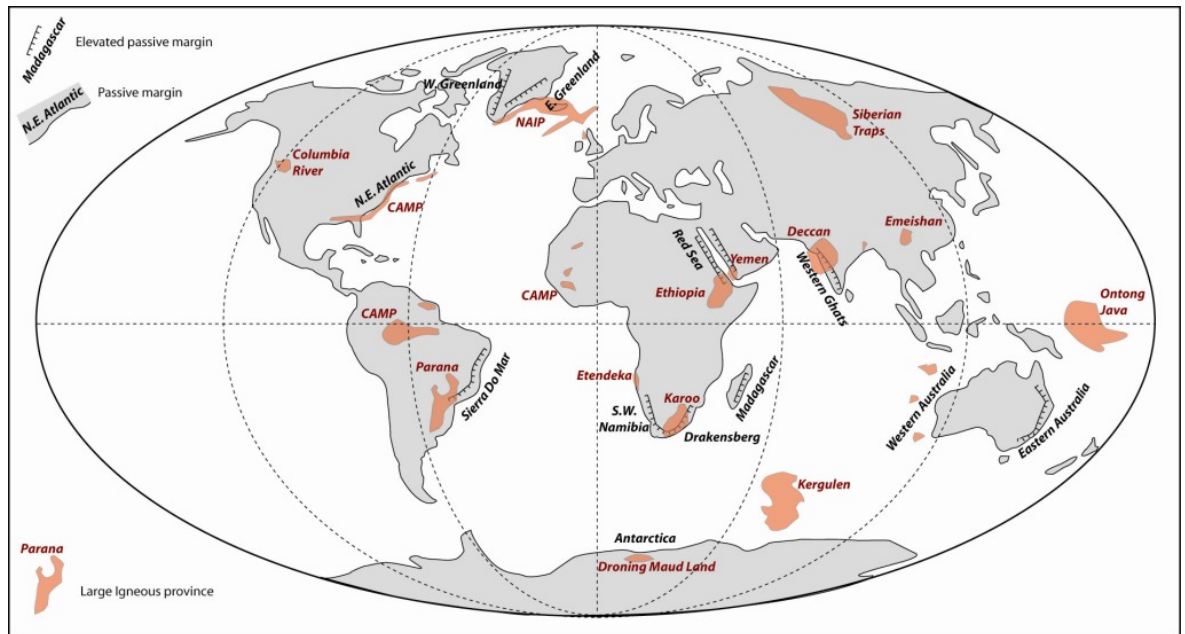


Figure 1 Global distribution of elevated passive margins.

Elevated passive margins (toothed ornament) and continental flood basalts (red fill). NAIP – North Atlantic Igneous Province. CAMP – Central Atlantic Magmatic Province.

Margins with extensive volcanic rocks are associated with active rifting and mantle plumes, and their distribution adjacent to many rifted margins (Figure 1) is central to the idea that hotspots can initiate continental rifting and the formation of volcanically rifted margins (Storey, 1995; White and McKenzie, 1989; White and McKenzie, 1995). With active, plume-related rifting and the formation of a volcanic rifted margin domal surface uplift of the order of 1-4 km occurs (Campbell and Griffiths, 1990), followed by the emplacement of volcanic rocks. Finally, continental splitting commences with the initiation of sea floor spreading (Summerfield, 1991b). A rising mantle plume impinging on the lithosphere results in thinning of the lithosphere and thermal expansion. These thermally-induced mechanisms initiate and drive surface uplift; however, such mechanisms are transient and decay after ca. 60 Ma (Richards et al., 1989) thus failing to explain the persistence of surface uplift at mature passive margins. Magmatic underplating (Cox, 1993) and subaerial emplacement of lavas are active rifting processes capable of generating permanent surface uplift through thickening of the lithosphere over timescales that extend beyond the duration of thermal decay associated with hotspots.

Margins lacking extensive volcanic rocks are associated with passive rifting where thinning of the lithosphere occurs not in response to a thermal anomaly such as a hot spot but as a consequence of tensional forces remote from the site of rifting. Thermal mechanisms associated with passive rifting include secondary mantle convection in response to thinning of the lithosphere (Steckler, 1985) and lateral heat flow from the thinned lithosphere at the site of rifting to the unthinned lithosphere beneath the rift flanks (Steckler et al., 1998). Non-thermal

or mechanical mechanisms for generating permanent uplift include; primary flexure in response to mechanical unloading of rift flanks (Weissel and Karner, 1989), lithospheric delamination (McKenzie, 1978) and depth dependant extension (McKenzie, 1978; Rowley and Sahagain, 1988). Post-rift secondary flexural uplift in response to denudational unloading onshore and sediment loading offshore is an additional mechanism that has been invoked to explain continual surface uplift at mature passive margins (Gilchrist and Summerfield, 1990, 1994). The timing of rift flank surface uplift differs for passive and active rifting; with active rifting, surface uplift precedes the rifting event, whereas with passive rifting, surface uplift post-dates the rifting event.

1.2.2 Conceptual models of passive margin evolution

Regardless of the mechanism(s) deemed responsible for surface uplift, elevated passive margins all display a broadly similar morphological pattern and consequently two groups of competing conceptual models have developed to explain post-rift passive margin evolution qualitatively. These models are: (i) escarpment retreat into a downwarped rift shoulder; and (ii) escarpment retreat or in-situ excavation into a high elevation rift shoulder.

Escarpment retreat into a downwarped rift shoulder (King, 1967a; Ollier and Pain, 1997) firstly envisages post-breakup formation of a broad, seaward-dipping monocline by lithospheric flexure (Figure 2A). Ollier (1982) suggested that the flexure is caused by tectonic uplift and is a direct consequence of continental breakup. Thereafter the lithosphere retains flexural strength and remains rigid. Faulting at the periphery of the new continental edge results in the formation of an escarpment, this then subsequently retreats landward via rejuvenated fluvial erosion (Figure 2A 1-4). This downwarp model does not incorporate isostatic rebound during the post-rift development of the margin. Erosion is minimal at the coast (a few hundred metres), increasing inland becoming greatest at the base of the escarpment (approximately equal to the height of the escarpment) and insignificant on the elevated interior plateau. Downwarped plateau remnants bypassed by escarpment retreat and seaward dipping strata on the coastal plain have been identified and are taken as supporting evidence for the downwarp model (Figure 2A 4) (Ollier, 1982; Ollier and Pain, 1997).

The second class of models differs from the downwarp model in that the rifted margin is initially elevated and bounded by steep normal faults as a consequence of either base level drop (due to breakup), tectonic rift flank uplift, or a combination of both (van der Beek, 1995) (Figure 2B and C) . The fault bounded escarpment at the edge of the rifted margin then evolves via either parallel retreat (Gilchrist and Summerfield, 1990, 1994; Kooi and Beaumont, 1994; Tucker and Slingerland, 1994) (Figure 2B 1-4), or by downwearing (Gilchrist et al.,

1994a; Kooi and Beaumont, 1994; van der Beek et al., 2002) (Figure 2C 1-4). The pre-rift topography effectively influences the mode of escarpment formation (van der Beek et al., 2002). For instance, if the pre-rift topography is horizontal and the escarpment lip is maintained as a drainage divide, then parallel retreat occurs. However, if there is a pre-existing drainage divide located inland of the rift axis, river incision will destroy the original fault generated escarpment followed by removal of interflaves and a new escarpment will be generated at the inland drainage divide, generating the so-called 'pinned divide' (Gilchrist et al., 1994a; Kooi and Beaumont, 1994).

Flexural isostasy in response to denudational unloading during formation of the escarpment and coastal plain is incorporated into this group of models, and is particularly important for the escarpment retreat scenario helping to maintain the escarpment by continuous backtilting (Kooi and Beaumont, 1994). The pattern and magnitude of denudation is characterized by kilometre-scale denudation having occurred near the coast and decreased denudation towards the base of the escarpment. This class of models therefore differs fundamentally from the downwarp model in the amount and timing of the denudation that it predicts.

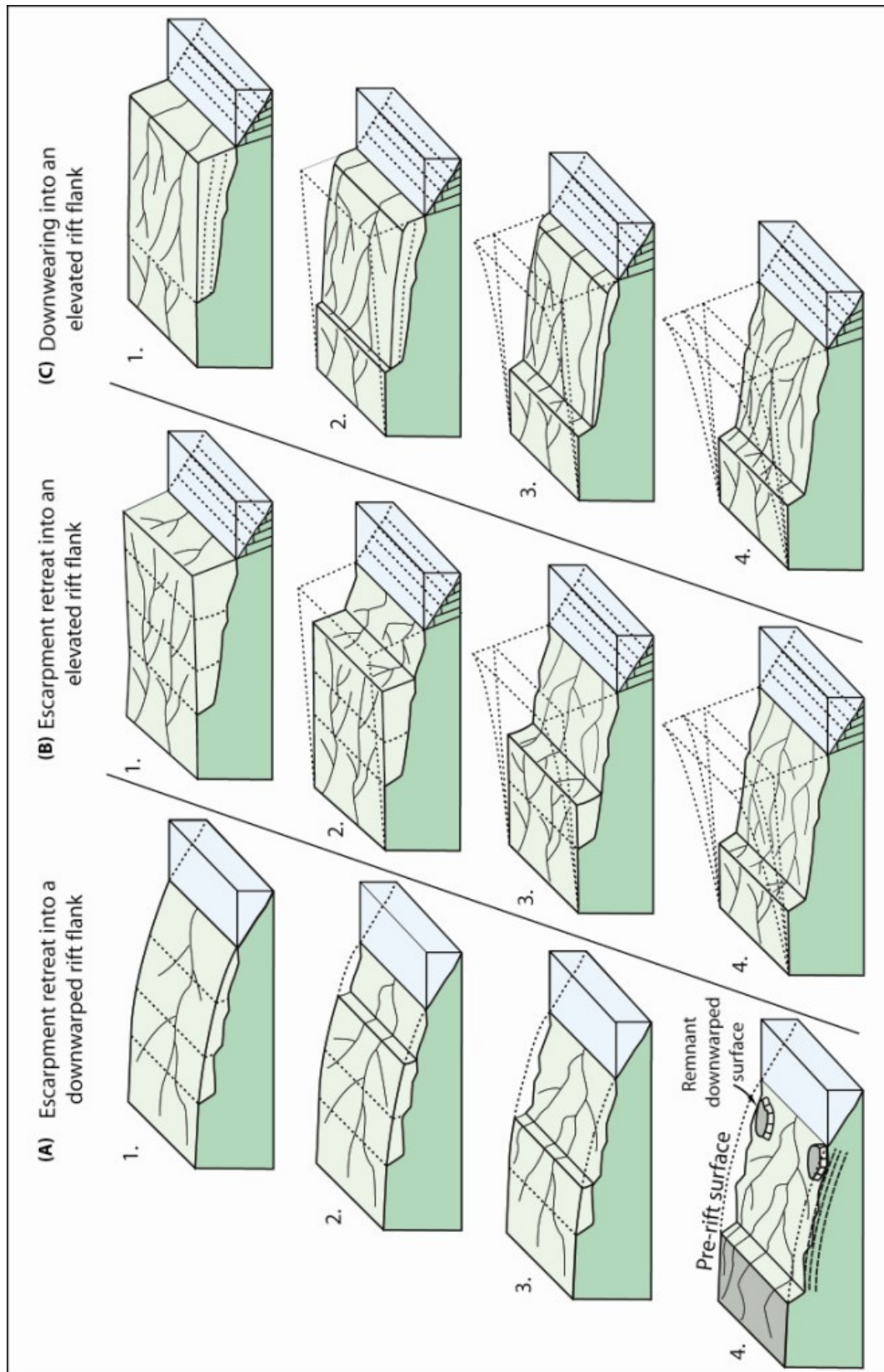


Figure 2 Conceptual models of elevated passive margin development.

Dashed lines represent missing crustal material: Escarpment retreat into a downwarped rift flank (A1-4), note the small volume of the crustal prism removed, and the remnant downwarped surface contemporaneous with the elevated plateau (grey areas). Denudation increases from the coast to the escarpment. Escarpment retreat into an elevated rift flank (B1-4), note the large volume of the crustal prism removed (with accompanied isostatic rebound) and denudation decreases from the coast to the escarpment. Downwearing into an elevated rift (C1-4), modification to escarpment retreat model but with an initial drainage divide located inland of the rift axis.

1.3 The Western Indian margin

Western India displays many of the geomorphic and structural features of an elevated passive margin, yet is unique in that the margin has experienced at least two major rifting events, the spatial extent, timing and magnitude of which are poorly constrained. Continental flood basalts within the Deccan volcanic province have been used as evidence to support active rifting in response to the impingement of a major hot spot (Kent et al., 1992; Richards et al., 1989; White and McKenzie, 1989; White and McKenzie, 1995). However, continental flood basalts are only restricted to the northern third of the margin (22 – 16 °N) and there is no clear evidence to support either active rifting or passive rifting for the remainder of the margin. Regardless of the mechanism responsible for the formation of the Western Indian passive margin, there is no clear consensus on the post-rift evolution of the margin. This section outlines the geology, physiography and debate over the tectonic development of Western India before addressing the aims of this study.

1.3.1 Geological background

The geology of the Western Indian passive margin can be separated into three broad regions: the southern granulite Proterozoic mobile belts of Kerala; the Archean granite-greenstone Dharwar craton of Goa and Karnataka; and the Cretaceous/Eocene Deccan volcanic province of Maharashtra (Figure 3). For the majority of the Proterozoic and Phanerozoic the margin has been exposed to sub-aerial processes of erosion and any stratigraphic information contained within the geology has predominantly been destroyed by the effect of erosion and denudation.

The Dharwar cratonic basement is composed of 2.9–3.4 Ga tonalite-trondjemite gneisses and granites (Beckinsale et al., 1980). Overlying and infolding this basement complex are the greenstone belts of the Dharwar supergroup, which is a metamorphosed (greenschist facies) volcano-sedimentary succession deposited 2.8–2.5 Ga (Chadwick et al., 1989; Chadwick et al., 1986; Taylor et al., 1984). In general, the metamorphic grade increases southwards from greenschist facies through to granulite facies, and the schists and gneisses of the Dharwar craton have been metamorphosed into charnokites from the Southern Granulite Terrain in Kerala (Naqvi and Rogers, 1987). Granulite facies metamorphism within the southern granulite terrain has been dated at 2.5–2.6 Ga (Crawford, 1969; Hansen et al., 1997; Santosh et al., 2006) and the charnokites and gneisses associated with this metamorphism are thought to be contiguous with the Dharwar basement to the north. There are limited Cenozoic sediments occurring in small isolated pockets on the coastal strip (Figure 3) and lie unconformably on the Precambrian basement (Soman, 1997).

The Deccan flood basalts were erupted relatively rapidly over 0.5-5 Myrs at the Cretaceous/Tertiary boundary (Allegre et al., 1999; Courtillot et al., 1986; Duncan and Pyle, 1988; Pande, 2002; Pande et al., 2001) and form the only major stratigraphic marker for the onshore portion of the Western Indian margin. The stratigraphy of the lava pile is now well established and individual units have been comprehensively mapped (Beane et al., 1986; Devey and Lightfoot, 1986; Mitchell and Widdowson, 1991; Subbarao et al., 1994). The lavas form maximum thicknesses along the Western Ghats, (i.e. Kalsubai Peak at 73° 40'E, 19° 35'N) where 1.2 – 1.7 km are exposed along the escarpment and provide first order constraints on the magnitude of denudation for the Deccan volcanic province. The sub-horizontal basalts cover an area of approximately 500,000 km² and lie unconformably on crystalline basement, infilling and blanketing the pre-existing shield topography (Wadia, 1989). The lavas form a broad lensoid structure (Widdowson, 1997), with maximum thicknesses along the western edge of the Deccan plateau towards the eastern and southern boundaries. The general structure of the lava pile comprises a broad anticline-monocline dipping gently to the south (Beane et al., 1986; Devey and Lightfoot, 1986) and locally forming the Westerly dipping Panvel Flexure in the Mumbai region (Figure 3) (Auden, 1949; Dessai and Bertrand, 1995; Sheth, 1998). The onshore outcrop of the Deccan can be traced offshore where it becomes covered by Cenozoic sediments (Naini and Talwani, 1982).

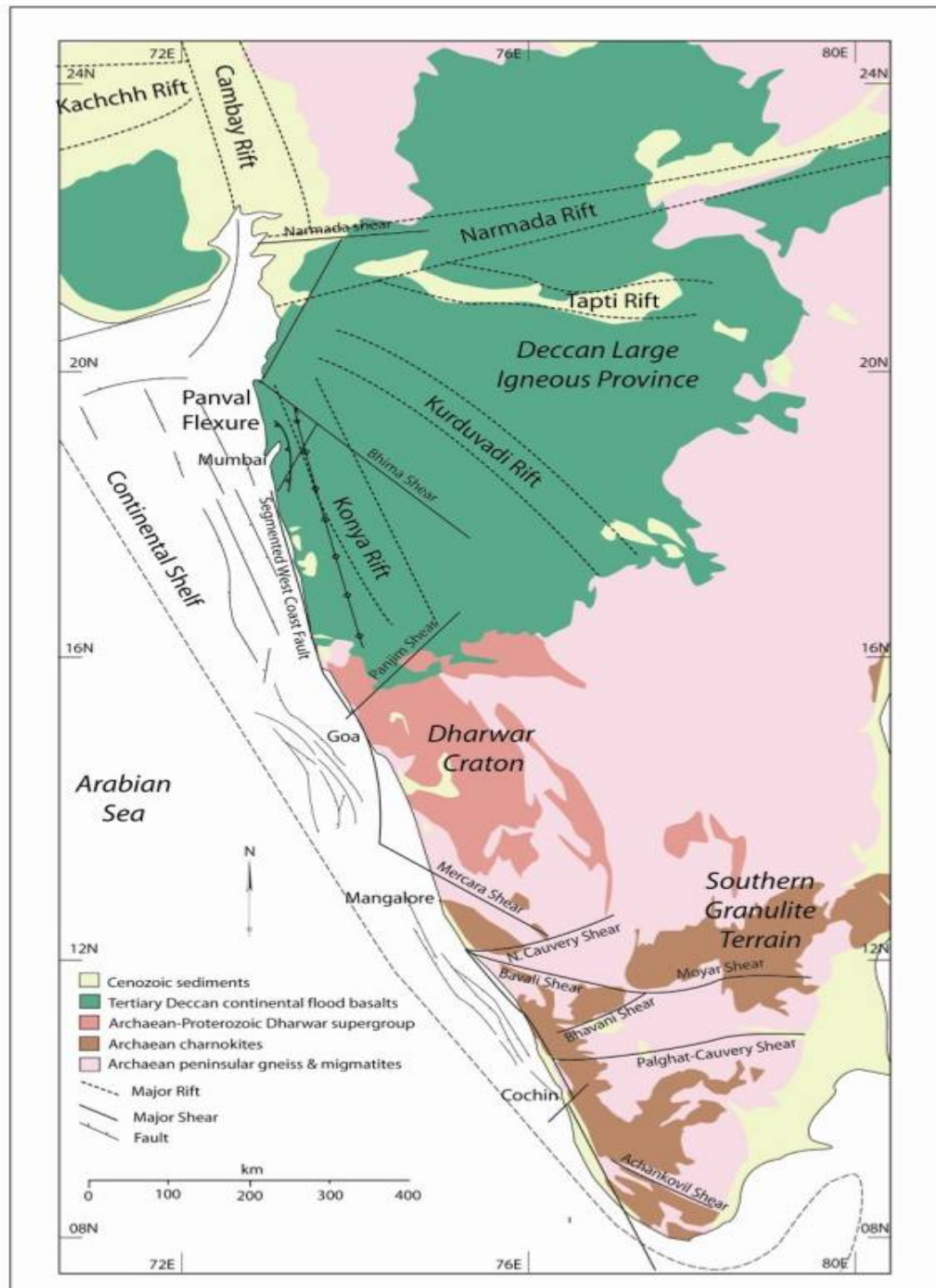


Figure 3 Regional Indian geology and associated major rifts, shear zones and faults.

1.3.2 Margin physiography

The physiography of the Western Indian margin is summarized in Figure 4. All three of the major geomorphological units characterising elevated passive margins are present: those being a low elevation, high-relief coastal plains (Konkan-Kanara lowlands) and elevated, low-relief interior plateaus (Maharashtra and Mysore plateaus) separated by a seaward-facing escarpment (The Western Ghats) parallel to the west coast. The width of the coastal plain ranges from 0 km to 100 km but on average rarely exceeds 60 km (Ollier and Power, 1985). Landward of the escarpment the Deccan, Karnataka and Mysore plateaus cover an area of approximately 4000 km², with an average elevation of 800 m (Kailasam, 1979) (Figure 4). The escarpment, whilst a continuous geomorphic feature is composed of several ‘ranges’ of the “Sahyadri” with elevations ranging from 500 m to 2200 m, can be traced for over 1500 km from the Tapti River north of Mumbai (21°10'N, 74°10'E) to Cape Comorin at the southern tip of the Indian peninsula (8°10'N, 77°30'E). Within the Deccan volcanic province the escarpment is linear, forming either an abrupt face, or a series of steps with short narrow spurs extending west onto the coastal plain. Within the crystalline basement, the escarpment becomes more sinuous with large embayments (Mangalore and Nilambur embayments) and in a few places a series of elongated gorges and spurs termed ‘Ghats breaches’ is present (Gunnell and Radhakrishna, 2001). The most notable of these is the 20 km-wide Palghat Gap that forms the only break in the escarpment along its entire length. North and south of the Palghat Gap the Nilgiri massif and Anaimalia/Cardomon hills form the highest elevations along the margin, with summits exceeding 2.5 km.

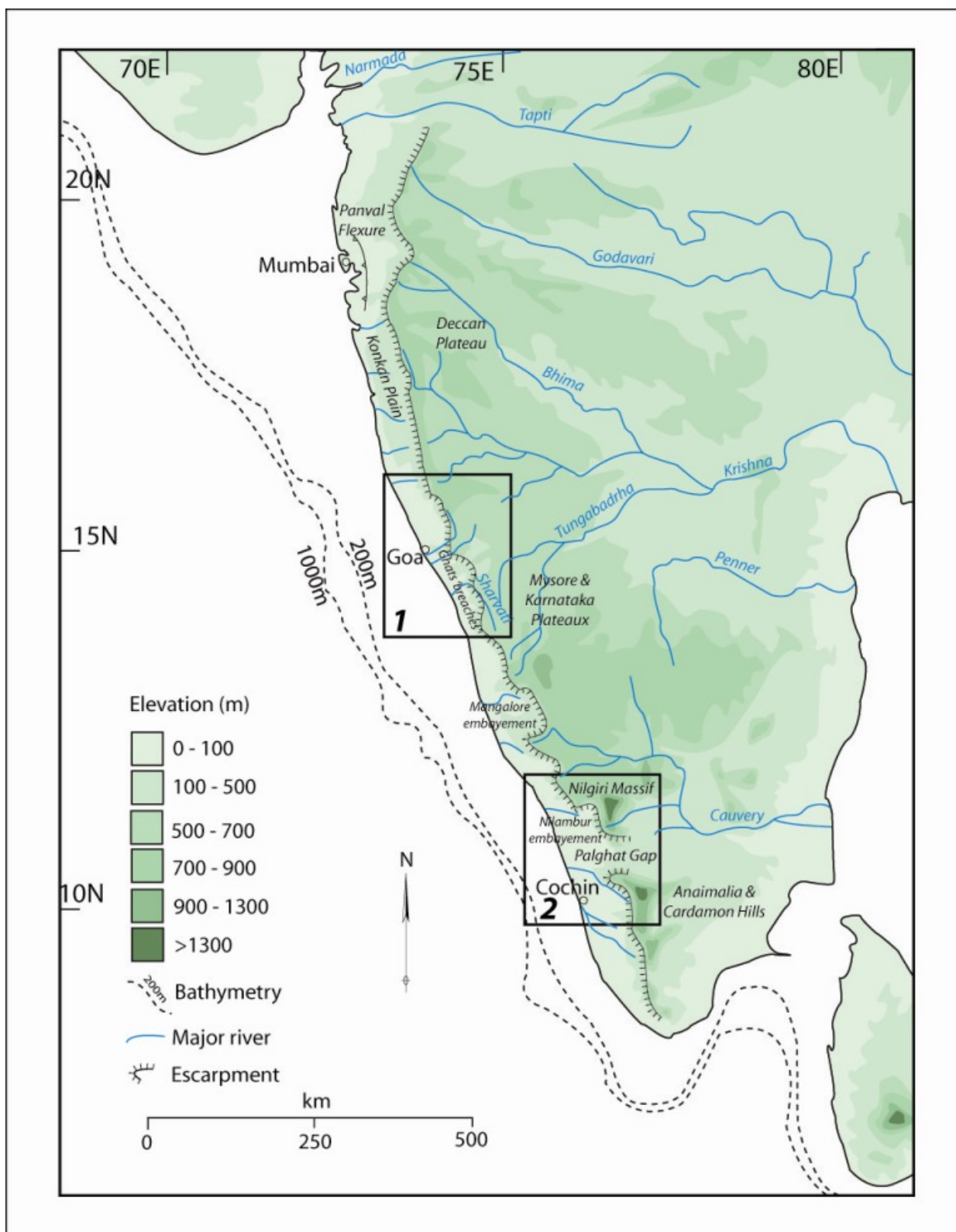


Figure 4 Pysiography of the Western Indian margin.

Toothed ornament is the great escarpment separating low elevation coastal plains from high elevation plateaus. Note the asymmetry of the drainage network, the top of the escarpment forms the major continental drainage divide. Box 1 is the northern onshore study area, Goa and Karnataka. Box 2 is the southern onshore study area, Kerala.

1.3.3 Rifting and tectonic history

The passive continental margins of India, and the adjacent oceanic regions are the result of a multi-stage rift history beginning with the breakup and dispersal of Gondwana in the early Jurassic ca. 180 Ma (Besse and Courtillot, 1991; Storey, 1995). At this time, Gondwana split into two large fragments, Eastern Gondwana (Madagascar, India, Antarctica and Australia) and Western Gondwana (Africa and South America) at 155 Ma (Reeves and de Wit, 2000). At 130 Ma India rifted from Antarctica to form the eastern continental margin of India (Embleton et al., 1980; Powell et al., 1980). Seafloor spreading began in the Mascarene basin between 118 Ma and 84 Ma during the breakup of Greater India (India and Seychelles) and Madagascar (Schlich, 1982; Todal and Edholm, 1998), this being the first major rifting event to affect the western margin of India (magnetic anomaly 34; Figure 5). Flood basalts along the east coast of Madagascar and felsic rocks on the St Mary's Islands off the west coast of India have been dated at 85-92 Ma (Pande et al., 2001; Storey, 1995; Torsvik et al., 2000). These volcanic rocks are thought to be linked to the Marion hotspot and the breakup of Greater India and Madagascar (Storey, 1995). Finally, a ridge jump in the nascent Indian Ocean resulted in the breakup of India and The Seychelles microcontinent at the end of the Late Cretaceous (McKenzie and Sclater, 1971; Naini and Talwani, 1982; Norton and Sclater, 1979; Schlich, 1982). The onset of rifting and sedimentation prior to this seafloor spreading is evident from sediments and volcanic rocks dated at 71-78 Ma in rift basins to the north of The Seychelles (Plummer and Belle, 1995). Emplacement of the Deccan flood basalts on the Indian sub-continent and volcanic rocks on The Seychelles at 65 Ma are contemporaneous with the final stages of breakup and the onset of seafloor spreading along the Carlsberg ridge (Courtillot et al., 1986; Miles and Roest, 1993) (Figure 5).

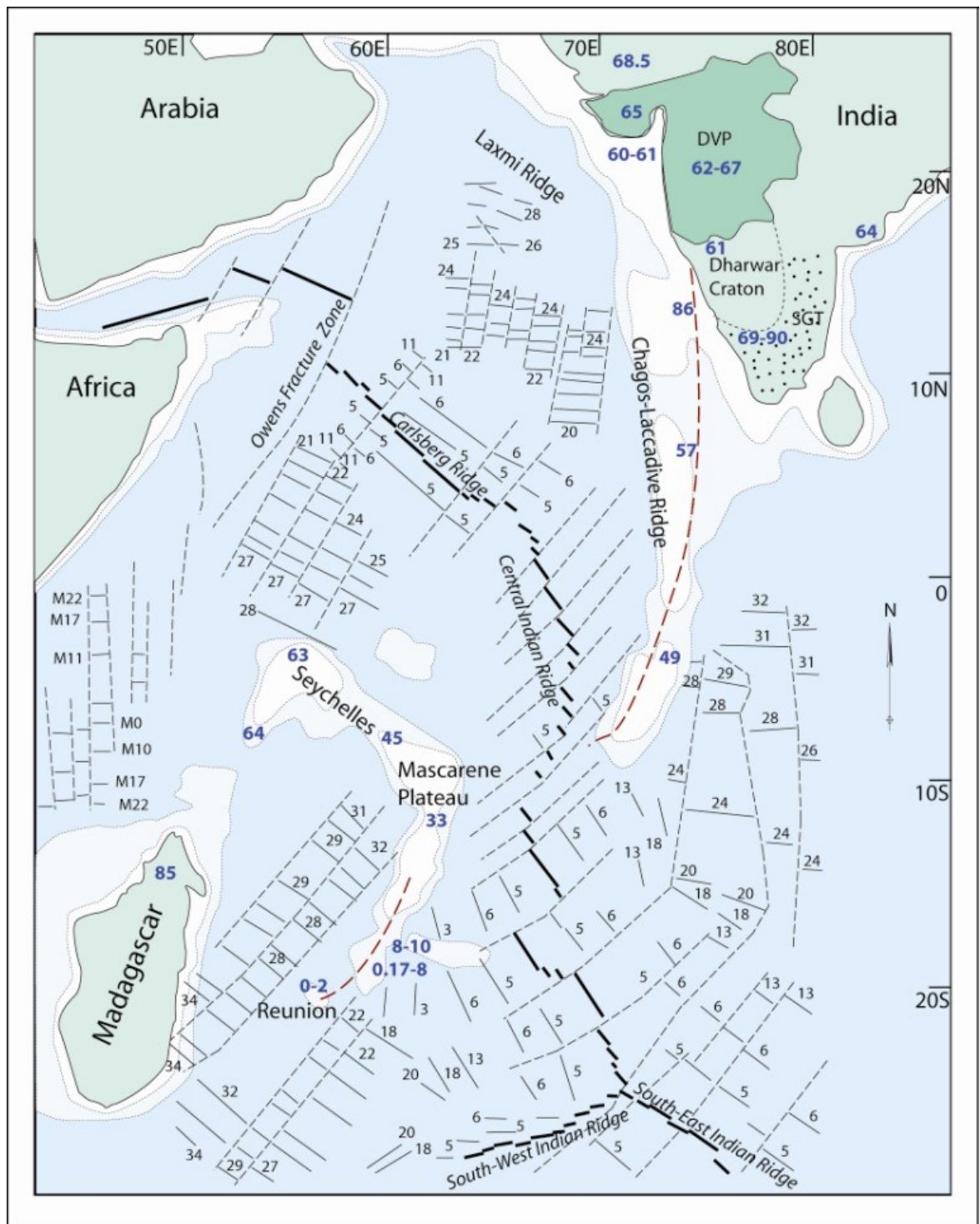


Figure 5 Tectonic map of India and adjacent oceanic regions.

DVP – Deccan Volcanic Province. SGT – Southern Granulite Terrain. Thick black lines are major spreading ridges, thin black lines are magnetic anomalies (no. adjacent in black text), and dashed black lines are ocean transforms. The thick dashed red line indicates the supposed north-south trace of the Reunion plume from the Deccan province to Reunion Islands. Blue numbers are igneous crystallisation ages (see Sheth (2005) figure 9 and references within). Note the apparent age decrease along the hotspot trace. Crystallization ages correlate well between the Deccan flood basalts and igneous rocks on the north of The Seychelles. Crystallization ages for the central and southern portion of Western India can be associated with either The Seychelles or Madagascar.

The India/Seychelles breakup and the emplacement of the Deccan continental flood basalts are believed to be a direct result of impingement of the proto-Reunion plume on the base of the Indian lithosphere (Courtilot et al., 1999; Hooper, 1990; Morgan, 1981). It has been suggested that the Reunion Islands on the African plate are the current position of the plume, and that the Chagos-Laccadive ridge is the trace of the hotspot as the Indian plate migrated northwards (Courtilot et al., 1999) (Figure 5). The role of such plumes in the development of a rifted continental margins is significant because of the implication for the timing and spatial pattern of uplift (see section 1.2.1). The plume impact model may account for the northern third of the Western Indian margin (where continental flood basalts are present) but fails to address the southern two thirds of the margin where plume effects are further to the west (i.e. the Chagos-Laccadive ridge). There is also a highly contentious view that the plume model may not even be necessary to explain the generation of flood basalts and the initiation of rifting for Western India (Anderson, 1994; King and Anderson, 1995; Sheth, 2005). A selective summary by Sheth (2005) argues that there is little petrological, geological and geophysical evidence to support the presence of abnormally hot mantle and the existence of the Reunion plume. The presence or absence of a plume has significant implications for the development of the Western Indian margin both spatially (plume effects on the north and south of the western margin) and temporally (active, pre-rift surface uplift or passive post-rift surface uplift).

Plate reconstructions of the Indian Ocean and the adjacent continental fragments have been attempted (Besse and Courtilot, 1988; Katz and Premoli, 1979; Muller et al., 1993; Scotese et al., 1988) but debate continues as to the precise palaeopositions of Madagascar and The Seychelles relative to the west coast of India. The palaeopositions of Madagascar and The Seychelles has important implications for the timing and spatial extend of rift related denudation. Plummer and Belle (1995) and, Todal and Edholm (1998) place The Seychelles continental fragment adjacent to the northern portion of the Western Indian margin, and its southerly continuation, the Mascarene plateau, adjacent to central and southern India. They also place Madagascar further west along the western boundary of The Seychelles (Figure 6). Reeves and de Wit (2000) position Madagascar adjacent to Western India prior to rifting, with The Seychelles detaching later but only in the north (Figure 6). Both the initial continental rifting and the rupture accompanied by sea floor spreading along the Western Indian margin have a direct effect on denudation and sedimentation, yet our understanding of the timing and location of the two major breakup events (Madagascar and later The Seychelles) remains unresolved. Magnetic lineations within the Arabian Sea have been extensively mapped (Chaubey et al., 1998) and the oldest sea floor (magnetic anomaly 28) formed 63 Ma. However, magnetic anomaly 28 can only be confidently mapped within the Laxmi basin with a large data gap at the Chagos-Laccadive ridge and further east (Figure 5). It is unclear if either

the India/Seychelles rifting event or the India/Madagascar rifting event affected the southern part of the Western Indian margin.

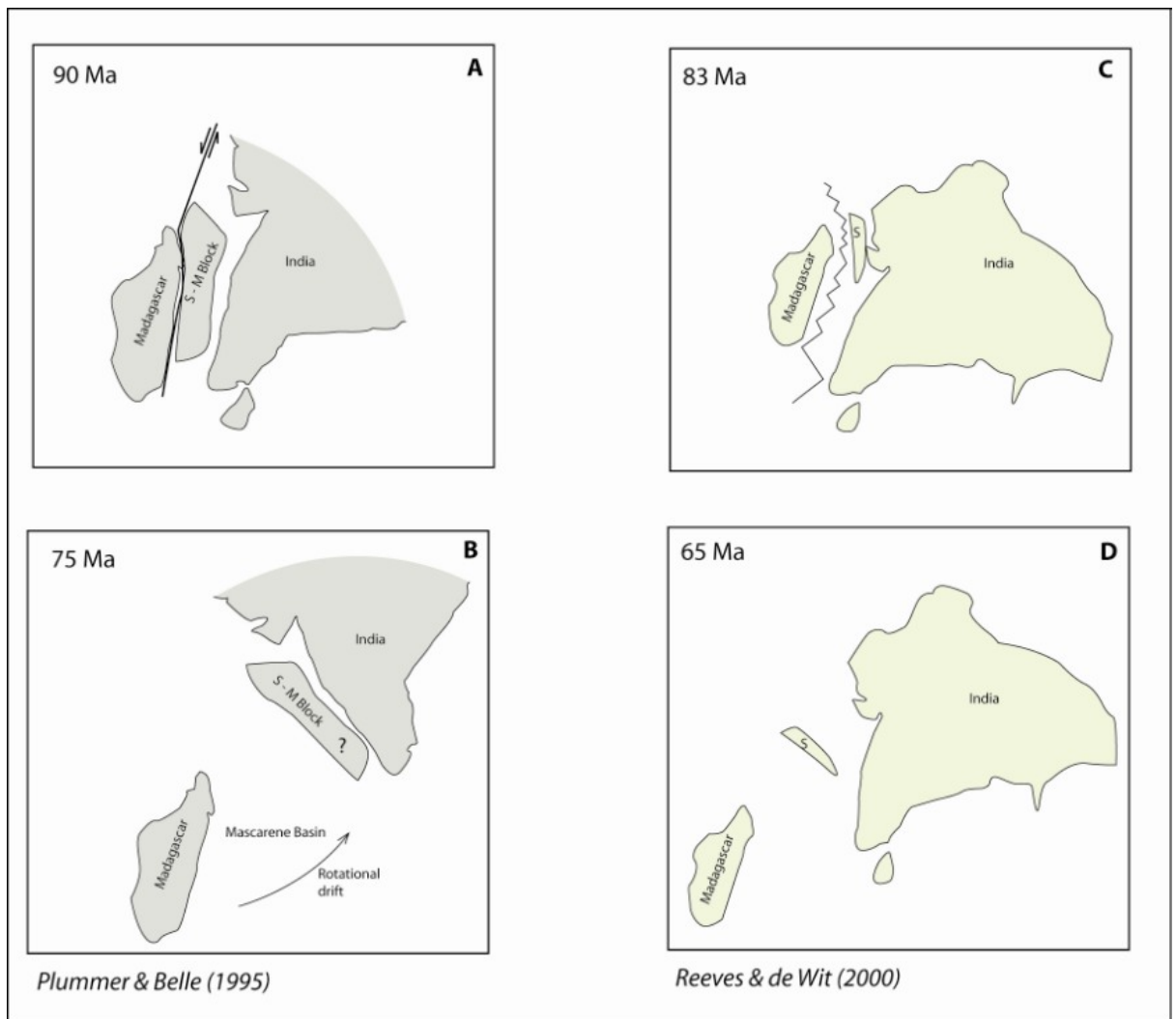


Figure 6 Plate reconstructions for the Indian, Seychelles and Madagascar microcontinents.

Reconstructions from Plummer & Belle, 1995 (a & b) and Reeves & de Wit, 2000 (c & d)

1.3.4 Margin geomorphology

Long-term landscape studies of the margin have been undertaken by geologists and geomorphologists since the late 1800s (Foote, 1876) in an attempt to explain the genesis, distribution and modification of large scale morphological features. Multidisciplinary reviews involving relative dating of erosion surfaces, fluvial network characteristics, laterite occurrences and distribution of relief have attempted to constrain a surface uplift chronology in order to understand the subsequent development of the Western Ghats (Gunnell, 1998; Gunnell and Fleitout, 1998; Radhakrishna, 1967, 1993; Vaidyanadhan, 1977; Widdowson, 1997; Widdowson and Cox, 1996). These studies acknowledge that although the Indian peninsula is an ancient craton, it has experienced ongoing surface uplift resulting in the elevation of erosion surfaces, their dissection and partial destruction, and the evolution of the escarpment since the

formation of the western margin. Within the Deccan volcanic province both the formation of the escarpment and the uplift of the Maharashtra plateau must have occurred after basalt emplacement at 64 – 67 Ma contemporaneous with rifting between Western Indian and The Seychelles. The remaining two thirds of the Ghats escarpment, south of the Deccan province, are devoid of stratigraphic markers and dateable sediments, preventing a more detailed surface uplift chronology from being established. The escarpment was originally believed to be either a marine cliff (Foote, 1876; Oldham, 1893) or a fault scarp (Pascoe, 1964; Radhakrishna, 1952), but it is now generally accepted that the escarpment is an erosional feature evolved from a fault-controlled rift flank that developed as a consequence of continental breakup (Ollier and Power, 1985; Subrahmanya, 1987; Widdowson, 1997). The absolute timing of escarpment formation is unclear especially south of the Deccan where there is no clear evidence of escarpment formation in response to rifting with The Seychelles. It has also been proposed that the presence and development of the escarpment south of the Deccan occurred in response to rifting between India and Madagascar much earlier during the Cretaceous (Chand and Subrahmanyam, 2003; Katz and Premoli, 1979; Pande et al., 2001; Torsvik et al., 2000). Regardless of the timing of escarpment formation, there is also no clear consensus on the style of escarpment development. The two groups of conceptual models discussed in Section 1.2.2 and Figure 2 have both been cited for the Western Indian margin, as outlined below.

A coastal monocline has been inferred from seaward dipping basalts in Maharashtra (manifested noticeably around Bombay as the Panvel Flexure), and from the geometry of geochemically mapped laterite surfaces (Widdowson, 1997). This monocline has been used as evidence to support margin evolution by means of the downwarp model (Widdowson, 1997; Widdowson and Cox, 1996; Widdowson and Gunnell, 1999). Two geochemically distinct post-eruptive laterite surfaces have been identified: an upper-level laterite, structurally concordant with the top of the basalt sequence, and a lower-level laterite, structurally discordant with the basalts. Formation of the upper-level laterite is interpreted as having ended with a phase of uplift resulting in denudation along the coast and the formation of the coastal plain. Both the laterite and the basalts on which they were formed were deformed and partially dissected simultaneously. The lower-level laterite developed on already-deformed basalts on the newly-formed coastal plain. Subsequent flexure modified the basalts further and warped the lower level laterite. From the structural relationships of the laterites the aforementioned authors envisage monoclinical development both as a consequence of syn-breakup primary tectonic downwarping and later post-breakup secondary flexure in response to coupled denudational unloading and sediment loading (Figure 7C). The downwarp model proposed by Widdowson (1997) differs from the model of Ollier and Pain (1997) where downwarping occurs in direct response to thermal subsidence soon after breakup. Ollier and Pain (1997) downwarp model assumes that after the initial rifting event and accompanying subsidence the lithosphere then

retains flexural strength and is not modified by any post-breakup flexure (Figure 2A & Figure 7B). Widdowson (1997) inferred the removal of 1–1.5 km of basalts seaward of the escarpment since Deccan emplacement, amounting to an average denudation rate of 15 - 23 m/Ma. Average escarpment retreat rates are 1 km/Ma if it is assumed that the locus of the proto-escarpment is the West Coast fault located immediately offshore (Balakrishnan, 2001; Chandrasekharam, 1985) (Figure 3).

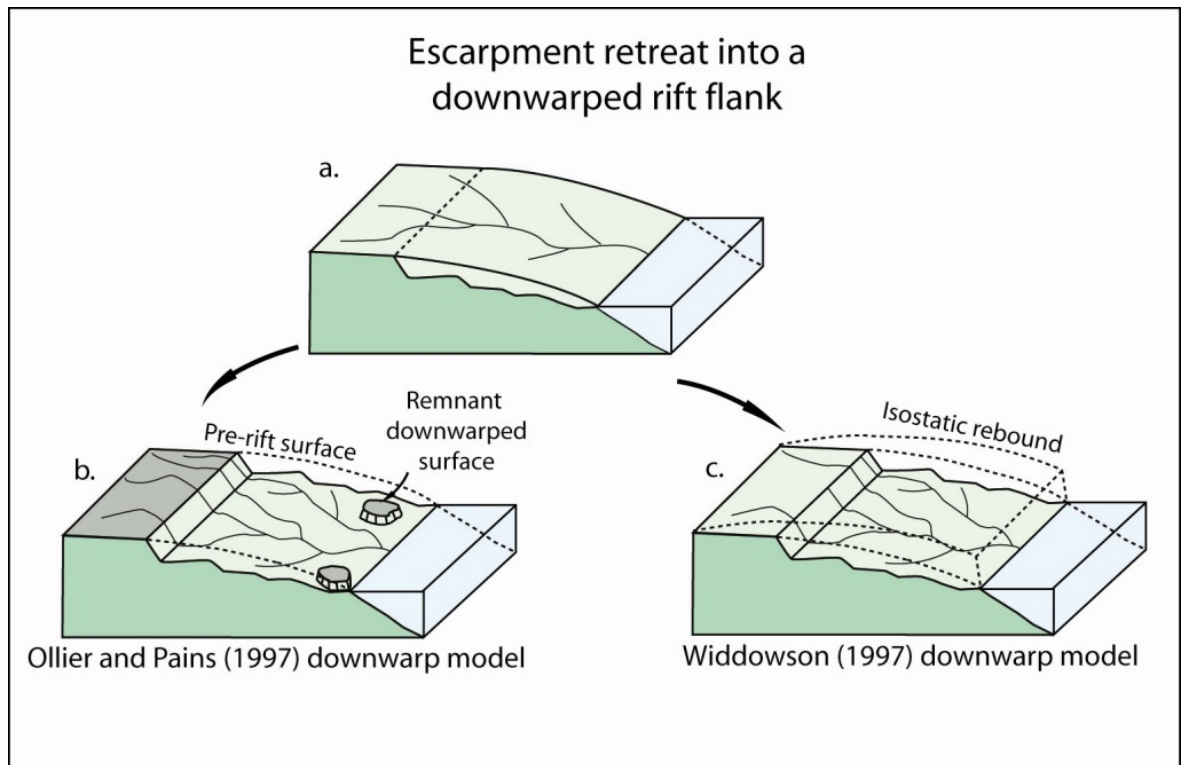


Figure 7 Different downwarp models for passive margin development

- a. Tectonically downwarped surface prior to escarpment retreat
- b. Ollier and Pains (1997) downwarp model incorporating escarpment retreat without accompanying isostatic rebound (see also Figure 2A).
- c. Widdowson (1997) modified downwarp model with accompanying isostatic rebound.

Both models are associated with a seaward dipping monoclinial camber but differ in the magnitude of crustal section removed.

The Panvel flexure is fundamental to the development of the downwarp hypothesis when the flexure is interpreted as either a simple monoclinial camber (Auden, 1949), a primary flexure resulting from rifting (Devey and Lightfoot, 1986) or a flexural response to uplift of the Western Ghats and accompanied subsidence offshore (Watts and Cox, 1989). A flexural origin for the Panvel flexure is a necessary condition for the downwarp model but is not universally accepted and alternative models have been developed. Dessai and Bertrand (1995), and Dessai and Viegas (1995) suggest that the Panvel flexure is a syn- or post-rift extensional fault structure composed of tilted fault blocks and is thus a brittle structure (Figure 8A). Sheth (1998) modified the extensional fault model and proposed that the Panvel flexure is a listric

fault-controlled reverse drag structure (Figure 8B). These non-flexural models bring into question the downwarp paradigm making it necessary to consider the competing group of models, escarpment development into an elevated rifted margin.

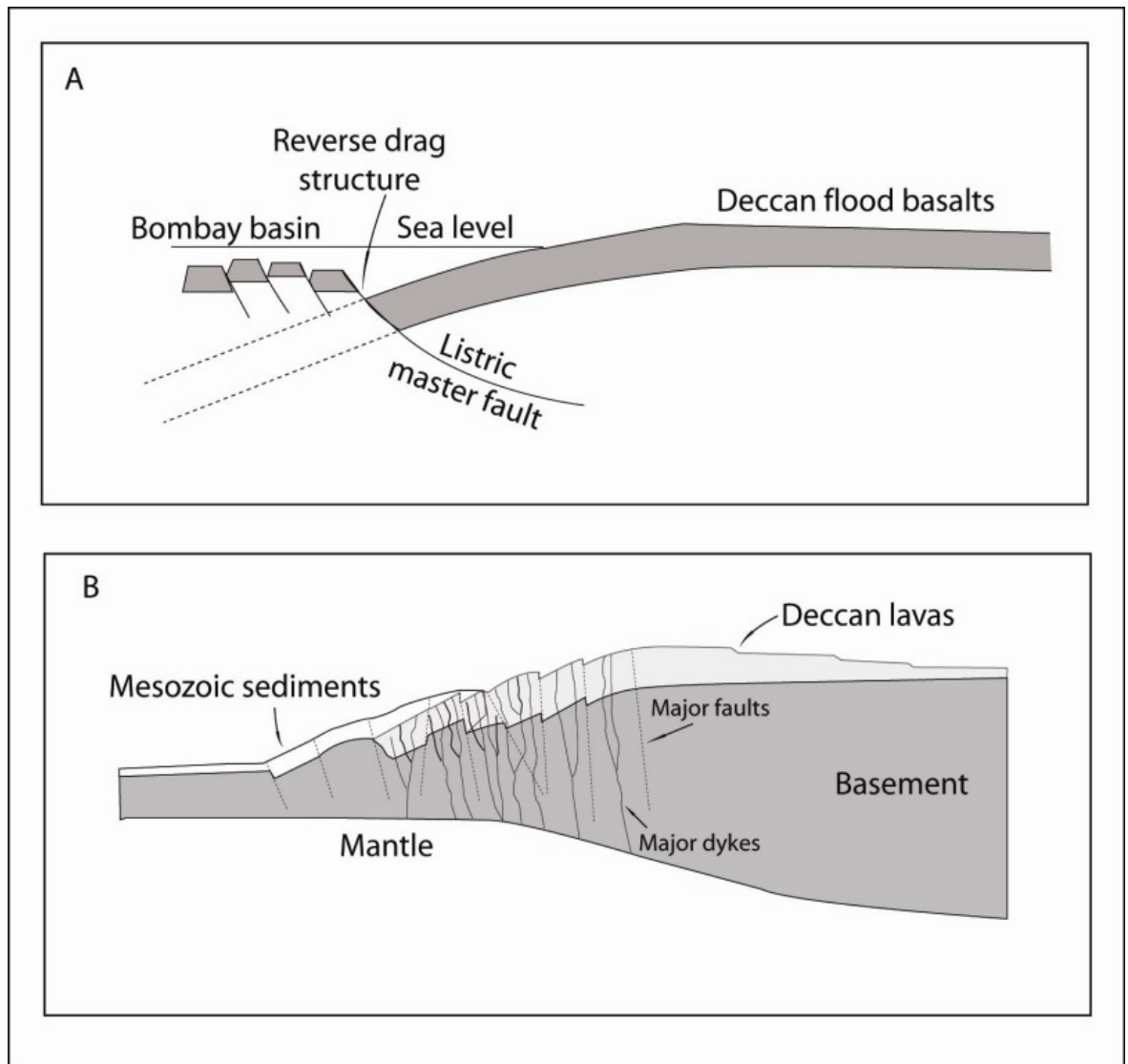


Figure 8 Panvel flexure alternative models

- a. Model proposed by Sheth (1998) viewing the Panvel flexure as a reverse drag structure.
 b. Model suggesting the Panvel flexure is an extensional fault structure (Dessai and Bertrand, 1995; Dessai and Viegas, 1995)

The second class of models differs from the downwarp model in that the rifted margin is initially elevated and bound by steep normal faults as a consequence of either base level drop (due to breakup), tectonic rift flank uplift or a combination of both (van der Beek, 1995). Escarpment development into an elevated rift flank incorporates initial elevation as a consequence of tectonic rift flank uplift, base level drop or a combination of both but also includes secondary flexural uplift in response to denudational unloading. Gunnell and Fleitout (1998) used computer simulations incorporating numerical modelling of lithospheric flexure

and escarpment development to examine the role of this secondary flexural response. Two plate configurations (with different values for the effective elastic thickness) were found to predict adequately the present rift flank morphology, either a discontinuous (broken) plate or a continuous plate. The broken plate configuration requires a lithospherically weak zone analogous to a master fault decoupling the continental and oceanic lithospheres. The West coast fault may represent this master fault located immediately offshore (Chandrasekharam, 1985). This de-coupling of the continental and oceanic lithospheres produces a concave-up flexure analogous to an elevated rift flank. The present topography can be reproduced as a result of denudational unloading only and does not require any additional tectonic uplift or an elevated initial palaeotopography. Conversely, a continuous plate configuration with the offshore and onshore areas coupled produces a concave down flexural monocline and is analogous to the downwarped model of Widdowson (1997). The continuous plate configuration predicts a much smaller degree of uplift in response to denudational unloading and hence requiring preexisting palaeoelevation or an additional pre-rift tectonic component of uplift. Both models have advantages. The broken plate model has the benefit of being less sensitive to initial model parameters, and denudational unloading alone can generate sufficient uplift. Nevertheless, the continuous plate model finds support from the geomorphology in the form of a coastal monocline and cambered palaeosurfaces (discussed above) and flexural modelling cannot discount the downwarp model altogether.

Gunnell et al. (2003) apatite fission-track thermochronometric (AFTT) study of the Western Indian margin aimed to quantify the spatial and temporal distribution in denudation rate either side of the escarpment. Landward of the escarpment the denudation rate fluctuated throughout the Mesozoic, with the maximum rates coinciding with the breakup of Gondwana and rifting with Australia, but rarely exceeding 60 m/Ma. Denudation rates then remained low throughout the Cenozoic (15 m/Ma) resulting in the removal of <1 km of crust. Seaward of the escarpment, denudation rates were low (20 m/Ma) throughout the Mesozoic but began to increase at 90 Ma peaking at 120 m/Ma before declining again at 50 Ma. The authors suggest that rifting between India/Madagascar and India/Seychelles initiated accelerated denudation in the Cenozoic. Inverse modelling of the AFTT data implies removal of over 2 km of crust from the coastal plain during this period of accelerated denudation. Such large amounts of rock removal are incompatible with Ollier and Pain (1997) downwarp model which requires much more modest amounts of denudation, or none at all, particularly along the coast. The AFTT data do not appear to be sensitive enough to distinguish between the denudational responses of the two major rifting events that have affected the western coast.

1.4 The current study

It is clear from this brief review that the post-rift evolution of the Western Indian margin remains a problematic issue. Some authors advocate escarpment retreat into a downwarped monocline, whereas others propose escarpment formation into an elevated rift flank, possibly accompanied by denudationally driven flexural rebound. The Panvel flexure and laterite surfaces support margin evolution into a downwarped monocline similar to the model developed by Ollier and Pain (1997) but modified to include post-rift flexural cambering (Widdowson, 1997; Widdowson and Cox, 1996; Widdowson and Mitchell, 1999). However, numerical flexural models (Gunnell and Fleitout, 1998, 2000) and apatite fission track thermochronometry (Gunnell et al., 2003) have been instrumental in fostering the opposing view that the margin developed from a flexural upwarp. Both groups of competing conceptual models incorporate post-rift flexural adjustment but differ fundamentally in their magnitude and spatial distribution of denudation. Obtaining accurate constraints on denudation are thus critical for determining long term landscape development of the Western Indian margin (and in particular its post-rift evolution). The tectonic development of the margin also remains an unresolved issue. The precise breakup history and influence of both Madagascar and The Seychelles are poorly constrained particularly south of the Deccan volcanic province, and the effect (if any) of the Reunion plume on the development of the margin is still not fully understood. This thesis therefore addresses the following questions:

1. What is the post-breakup evolution of the Western Indian margin? Has the margin developed into a downwarped rift flank similar to that proposed by Ollier and Pain (1997) or that of Widdowson (1997)? Alternatively, has the margin developed into an elevated rift flank either via parallel escarpment retreat or via downwearing?
2. Has The Seychelles rifting event triggered a denudational response along the entire length of the Western Indian margin?
3. Has the Reunion plume played a significant role in the long-term landscape development of the Western Indian margin?

Apatite fission track thermochronometry is a powerful tool for unravelling denudation histories and understanding long term landscape evolution at passive margins. Gunnell et al. (2003) utilised this technique in the most recent contribution to landscape development studies in Western India. However, the magnitude of denudation experienced by the Western Indian margin appears to be relatively small (1-2 km) and as such is at the sensitivity limits of AFTT system. This thesis will combine apatite fission track and (U-Th)/He methodologies to obtain

more accurate constraints on the magnitude and timing of denudation. Before applying low temperature thermochronometry to the Western Indian margin, predictive forward modelling is necessary to assess if apatite fission track and apatite (U-Th)/He data are capable of testing the hypotheses listed above. Section 1.5 outlines the methods and results for predictive forward modelling of low temperature thermochronometry data.

1.5 Predictive forward modelling

1.5.1 Introduction

Predictive forward modelling was used to model AHe and AFTT ages under different sets of conditions for different parts of a margin-normal transect (following a similar methodology to that of Persano et al. (2002)). The aims of the predictive forward modelling were:

- 1) To test if there is a significant difference in model ages for each of the competing groups of conceptual model of passive margin evolution, i.e. Ollier and Pains's (1997) downwarp model (DW), escarpment retreat into an elevated rift flank (ER) and downwarping into an elevated rift flank with a pinned divide (PD).
- 2) To test if there is a significant difference in model ages for a denudational response to either the Seychelles/India rifting event or the Madagascar/India rifting event.
- 3) to examine the effect on model ages for different magnitudes of denudational isostatic rebound (for the elevated rift flank models) and different rates of escarpment formation (for all conceptual models)
- 4) to determine which sections of a margin-normal transect are most sensitive to different model inputs.

1.5.2 Methods and model parameters

The initial model set-up is two hypothetical margin-normal transects, one for the northern study area (500 m high escarpment, see chapter 4), and one for the southern study area (2500 m escarpment, see chapter 5) with five modelled samples spaced from the coast to the escarpment (Figure 9a). Thermal histories for each sample for different model runs were generated and transferred into HeFTy to forward model the AHe and AFTT ages (Figure 9D). All model runs assume a geothermal gradient of 20 °C/km and all samples have an initial starting age of 0 Ma (i.e., samples are exhumed from a temperature in excess of 110 °C). If a

sample is exhumed during a simulated rifting event from lower temperatures than those at which complete annealing of fission tracks occurs, then the model run time is extended prior to rifting with cooling occurring at 5 m/Myr (Widdowson, 1997) (Figure 9c). The surface temperature for all model runs is 20 °C, the average present day surface temperature in Western India. The annealing model of Ketcham et al. (1999) was adopted for AFTT forward modelling. For forward modelling AHe ages, diffusion of helium in apatite was based on the parameters determined by Farley (2000) using a modelled spherical apatite grain with the same surface to volume ratio as the mean surface to volume ratio of the apatites used in the analyses. Both AFTT and AHe forward modelling was implemented through the software package HeFTy, version beta 6 (Ketcham, 2005) (Figure 9D).

Three model templates were used to represent the three groups of conceptual models, namely, escarpment retreat into a downwarped rift flank (DW), escarpment retreat into an elevated rift flank (ER), and downwearing into an elevated rift flank with a pinned divide inland (PD) (Figure 9a). DW was simulated with a small magnitude of cooling at the coast, equivalent to 300 m denudation, increasing to a maximum at the escarpment (i.e., the height of the escarpment). The downwarp model incorporates parallel escarpment retreat which was simulated by initiating cooling first at the coast then further inland in a series of time steps. ER was simulated with a large amount of cooling at the coast (the amount being dependent on the magnitude of rebound) decreasing to a magnitude of denudation equivalent to the height of the escarpment at the escarpment. Parallel escarpment retreat was simulated in the same way as for DW. The magnitude of cooling for PD is the same as with ER except that instead of parallel escarpment retreat, cooling begins at the same time for all positions across the transect. Each model template was adapted for:

- 1) Rapid cooling at 65 Ma (Seychelles-India rift) and 80 Ma (Madagascar-India rift)
- 2) Constant rate of escarpment retreat beginning at the initiation of rifting and lasting until 0 Ma, and rapid escarpment formation, beginning at the initiation of rifting and completed within 10 Myrs
- 3) the elevated rift flank model only, incorporating (i) a large magnitude of rebound (4.5 km at the coast decreasing to the height of the escarpment at the escarpment), and (ii) a small magnitude of rebound (2 km – 3km at coast decreasing to the height of the escarpment at the escarpment) (Figure 9B).

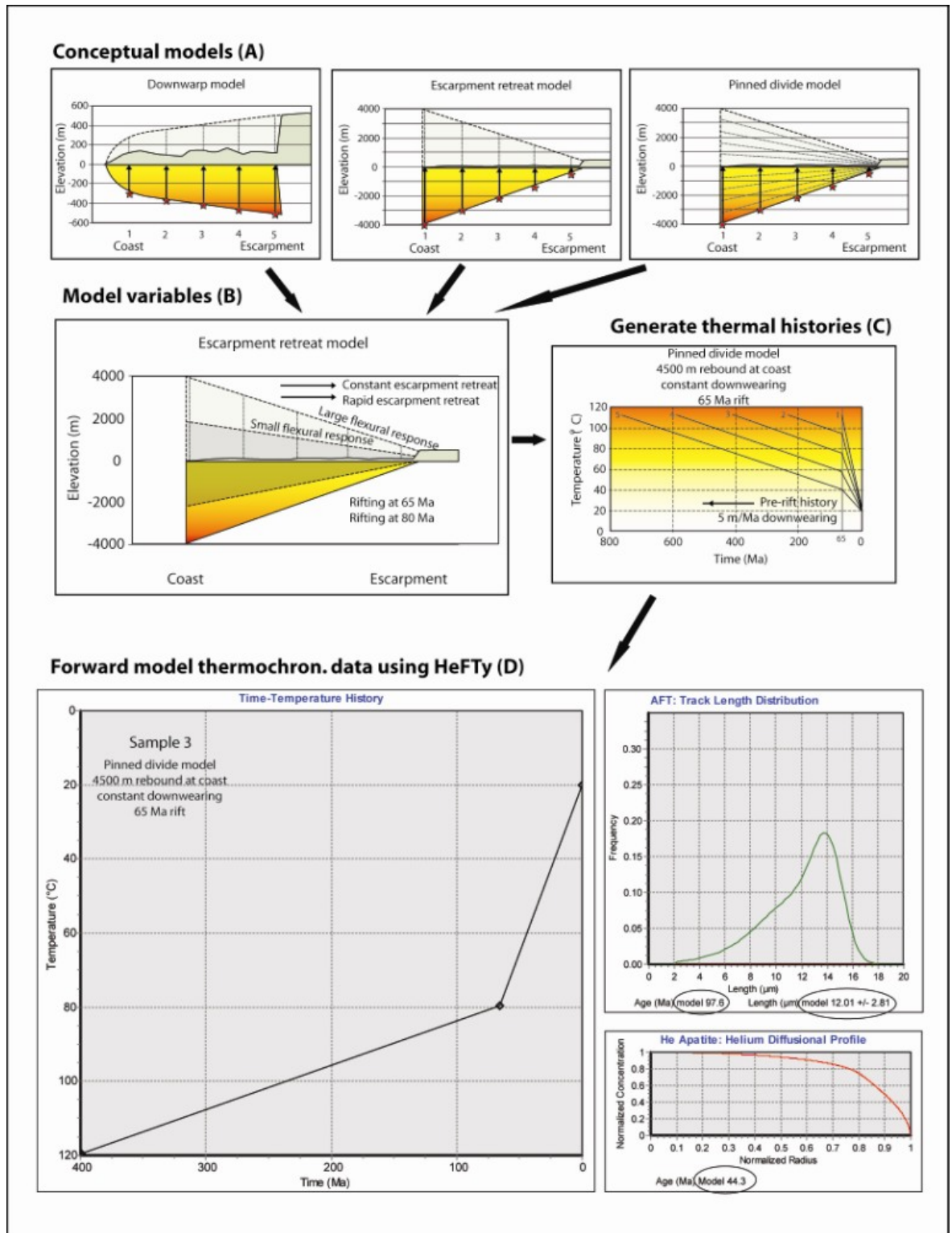


Figure 9 Procedure implemented for predictive forward modelling.

A) Hypothetical margin normal transects for each conceptual model. B) Model input parameters for each conceptual model. C) Generation of thermal histories for each hypothetical sample across the transect. D) importing thermal histories into software (HeFTy) to forward model thermochronometry data

1.5.3 Forward modelling results for the Northern field area

Forward modelled AHe ages for escarpment retreat into a downwarped rift flank predict ages that are four-times older than the time of cooling measured from the thermochronometry data in response to rifting furthest (seaward) from the escarpment. Predicted AHe ages become progressively younger towards the escarpment but still remain two to three-times older than the measured age of rifting (Figure 10). A similar trend is observed with predicted AFTT ages for the DW scenario except ages are eight-times older than the measured thermochronometry age furthest from the escarpment decreasing to six-times older than rifting at the escarpment (Figure 10). Forward modelled AHe and AFTT ages for both elevated rift flank models (ER and PD) show a general trend of ages that are youngest (similar to the timing of rifting) furthest from the escarpment, becoming progressively older towards the base of the escarpment (Figure 10). Predictive forward modelling indicates that the patterns of AHe and AFTT ages across a margin-normal transect could be used to differentiate between the escarpment evolution into a downwarped rift flank and escarpment evolution into an elevated rift flank but not between the ER and the PD models. The difference in ages between the conceptual models is most significant at the coast.

The downwarp model is insensitive to the timing of cooling in response to rifting and the pattern of modelled ages across a margin-normal transect remains the same (Figure 10). If the Western Indian escarpment has developed into a downwarped rift flank, then the rifting event responsible for an increase in denudation (either The Seychelles or Madagascar) will be difficult to determine. There is a difference in the pattern of modelled ages for different rifting events with the elevated rift flank models. The samples closest to the coast have modelled ages that are similar to the timing of the rifting event. If the Western Indian escarpment has developed into an elevated rift flank, then samples located furthest from the escarpment will record the timing of the initiation of escarpment development (i.e., the timing of the rifting event that triggered a denudational response).

With all the conceptual models, the predicted AHe and AFTT ages are not significantly affected by changes in rate of escarpment formation and the pattern of ages remains similar (Figure 11iii and iv). Regardless of the rate of escarpment formation it should still be possible to differentiate between the different conceptual models and the timing of the onset of escarpment development. With the elevated rift flank models, smaller magnitudes of rebound cause modelled ages to increase at the coast. Modelled ages also increase towards the escarpment but with decreasing effect and remain unchanged at the base of the escarpment (Figure 11i and ii). Predictive forward modelling for different magnitudes of flexure indicate that larger amounts of rebound enhance the difference in modelled ages between the

downwarped rift flank model and the elevated rift flank models. However, even for smaller magnitudes of denudation, it is still possible to differentiate between escarpment evolution into a downwarped rift flank and escarpment evolution into an elevated rift flank.

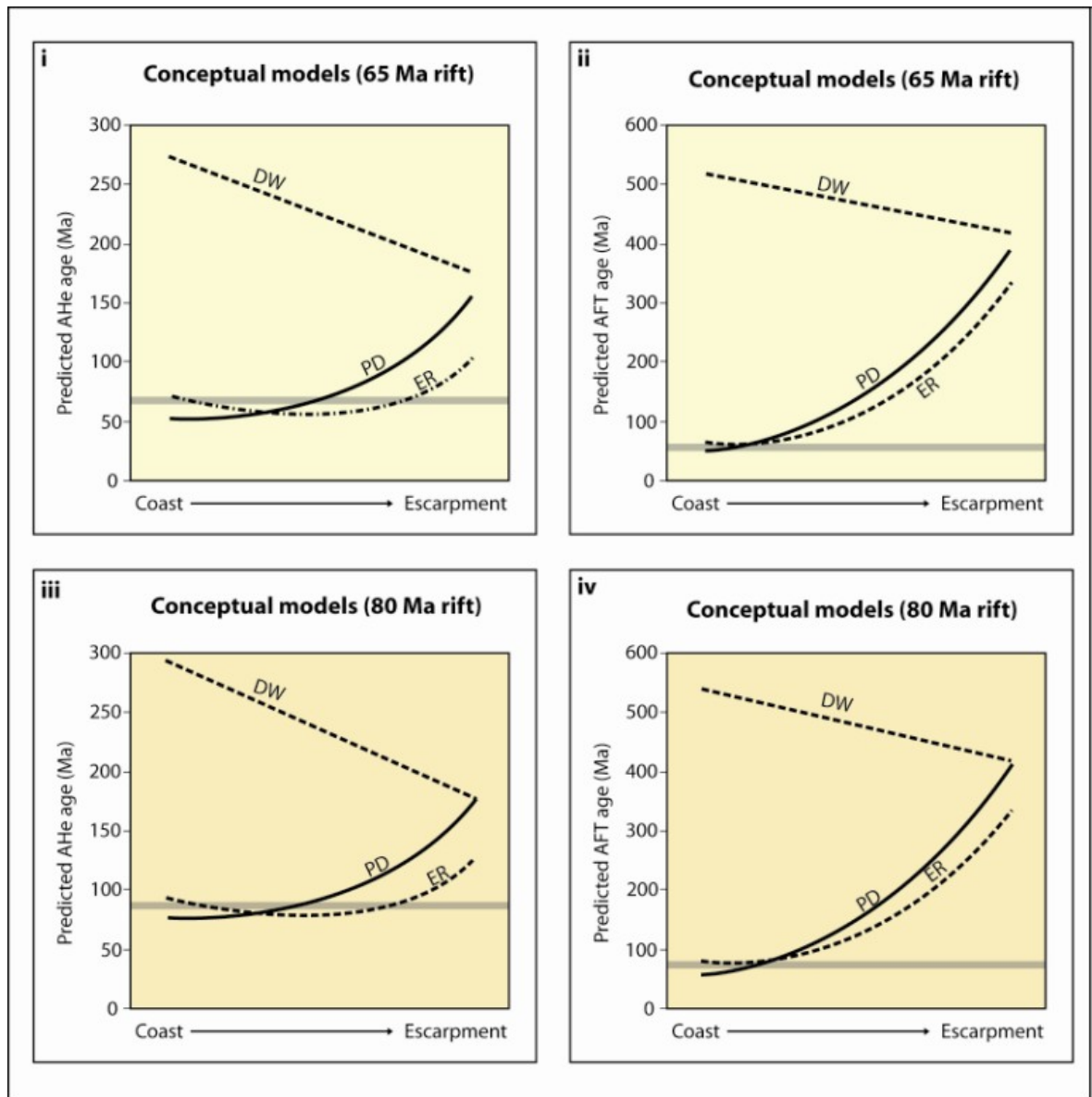


Figure 10 Predictive forward modelling results for Goa and Karnataka (I)

Predictive forward modelling results for constant escarpment evolution beginning at 65 Ma (i & ii) and 80 Ma (iii & iv) for each of the conceptual models. The grey bars demarcate the timing of rifting.

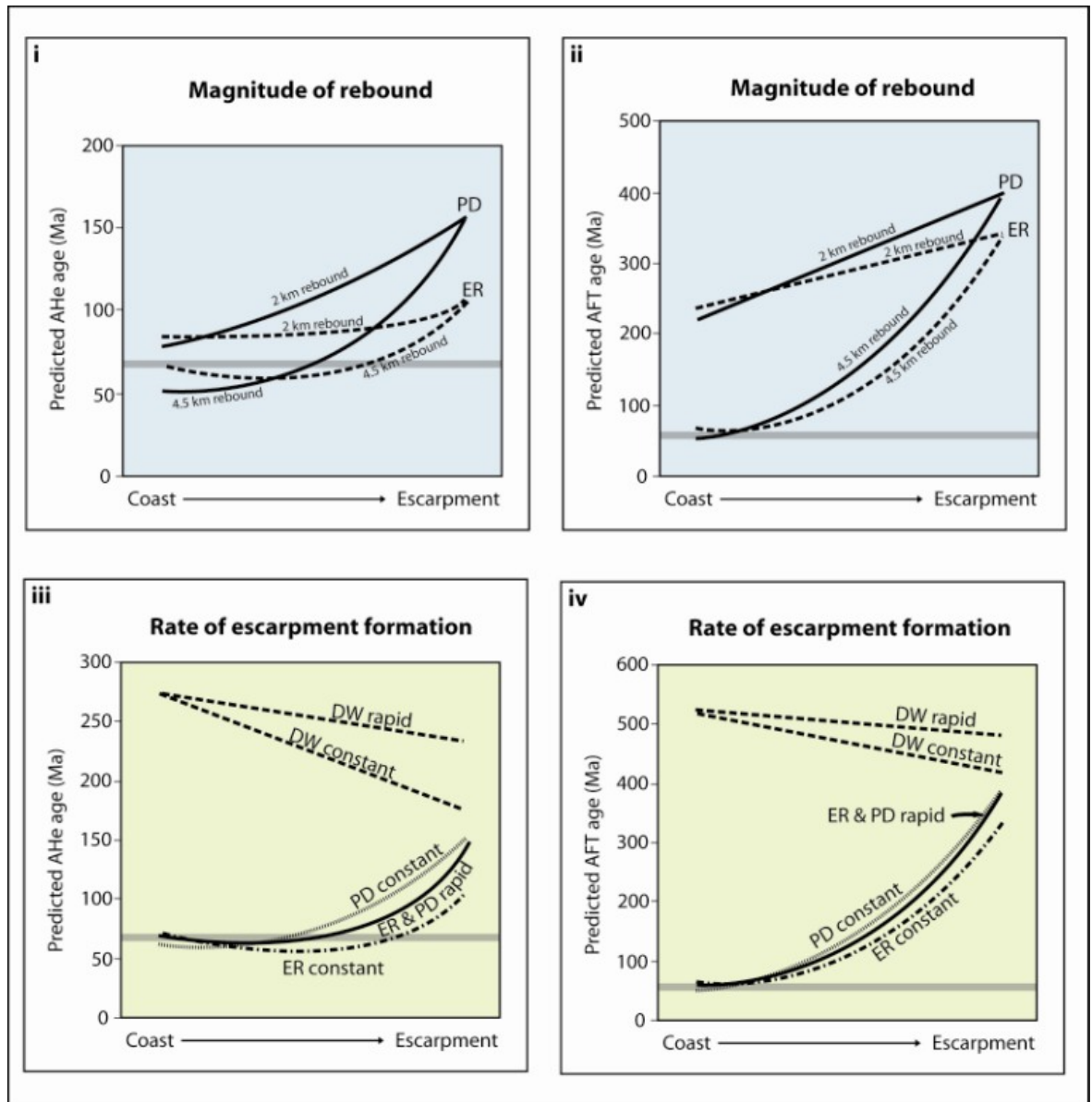


Figure 11 Predictive forward modelling results for Goa and Karnataka(II)

Predictive forward modelling results for different magnitudes of rebound with the elevated rift flank models (i & ii) for rifting at 65 Ma. Predictive forward modelling results for different rates of escarpment development with all the conceptual models (iii & iv) for rifting at 65 Ma.

1.5.4 Forward modelling results for the Southern field area

Predictive forward modelling for escarpment retreat into a downwarped rift shoulder predicts AHe ages at the coast that are over four times older than the age of rifting and the measured AHe ages at the coast. The modelled AHe ages decrease to a completely unrealistic ~ 0 Ma at the escarpment. Model results for AFTT ages provide a similar pattern with predicted ages at the coast eight times older than the time of rifting, decreasing to approximately 0 Ma at the escarpment (Figure 12 i & ii). Predictive forward modelling for escarpment formation into an elevated rift flank generates AHe ages that are all younger than the age of the simulated rifting event. The escarpment retreat model yields AHe ages that are similar to the age of rifting at the coast but decreasing to approximately 0 Ma at the escarpment. The pinned divide model yields

AHe ages that are almost half the age of the rifting event at the coast, increasing towards to the escarpment (Figure 12 i). Predictive forward modelled AFTT ages for the elevated rift flank models also differ from the downwarped rift flank model and are similar to the age of rifting at the coast increasing to approximately twice the age of rifting at the escarpment (Figure 12 ii). These results indicate that it should be possible to differentiate between the competing groups of conceptual models, with the coastal samples being the most sensitive to different scenarios (i.e., exhibiting the greatest difference in modelled ages for the different scenarios) and escarpment samples the least sensitive. However, it will be much more challenging to differentiate between the two elevated rift flank models, with the AHe age variations along the margin-normal transect offering the most hope in this regard.

Predicted AFTT and AHe ages for a denudational response to escarpment retreat into a downwarped rift flank initiated at either at 65 Ma or 80 Ma are similar (Figure 12). If the southern segment of the Western Indian margin evolved into a downwarped rift flank, it will be difficult to ascertain which rifting event triggered the onset of margin formation (i.e either 65 Ma for The Seychelles, or 80 Ma for Madagascar). Escarpment retreat into an elevated rift flank produces AHe and AFTT ages that are similar to the age of the rifting event at the coast and should be able to differentiate between a denudational response to rifting at 65 Ma or 80 Ma. Forward modelling of AFTT results for the pinned divide model also predicts coastal ages that are similar to the simulated rifting event and should be able to differentiate between a denudational response to either rifting at 65 Ma or rifting at 80 Ma (Figure 12).

The forward-modelling runs were adapted to simulate differing magnitudes of rebound for escarpment formation into an elevated rift flank beginning at 65 Ma. The two different magnitudes simulated were: 1) 4.5 km of rebound at the coast, decreasing to 2.5 km at the escarpment, and 2) 3 km of rebound at the coast decreasing to 2.5 km at the escarpment. Predicted AHe ages follow the same general trend along a transect for different magnitudes of rebound, but predicted ages are 5 – 10 Myr older at the coast for 3 km of rebound (Figure 13 i). A similar pattern is predicted for AFTT ages except that the age of coastal samples are 30 – 50 Myr older at the coast for 3 km of rebound (Figure 13 ii). Even for smaller magnitudes of rebound the pattern and magnitude of predicted AFTT and AHe ages are different (especially at the coast) between the downwarped rift flank model and the elevated rift flank models.

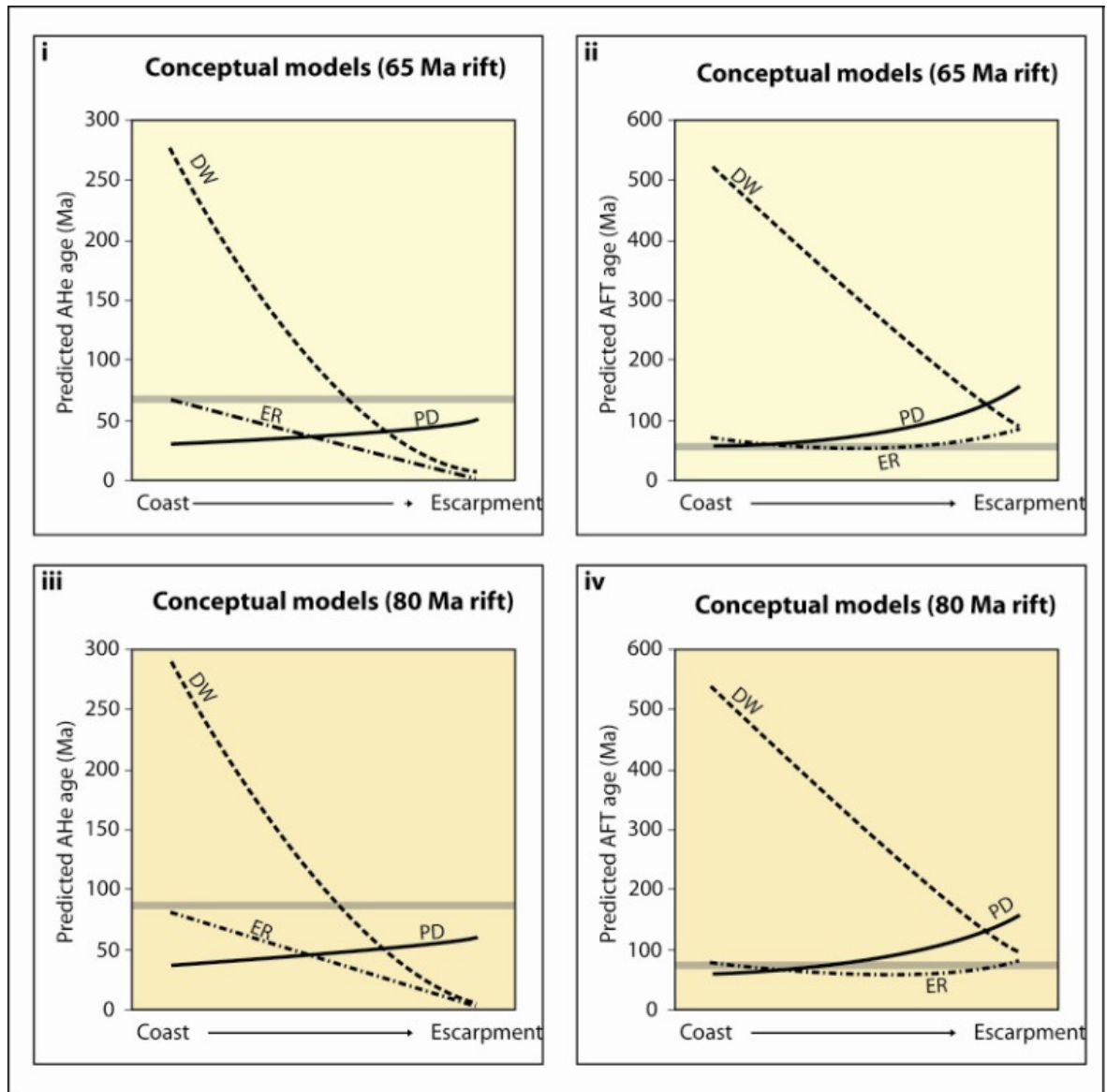


Figure 12 Predictive forward modelling results for Kerala (I)

Predictive forward modelling results for each of the three conceptual models for simulated rifting at 65 Ma and 80 Ma.

The solid grey bars are the time of each rifting event.

Predictive forward modelling was used to simulate constant escarpment formation (escarpment formation taking the full post-breakup time of 65 Myr) and rapid escarpment formation (escarpment formation completed after 10 Myr). Faster rates of escarpment formation result in older predicted AFTT and AHe ages for all three conceptual models, with samples closest to the escarpment producing the largest difference in predicted ages (Figure 13 iii & iv). Rapid escarpment formation within 10 Myrs of breakup reduces the differences in predicted ages between the escarpment retreat model and the pinned divide model, and the two conceptual models cannot be differentiated. At faster rates of escarpment formation, there is still a difference in predicted ages between escarpment retreat into a downwarped rift flank and escarpment formation into an elevated rift flank.

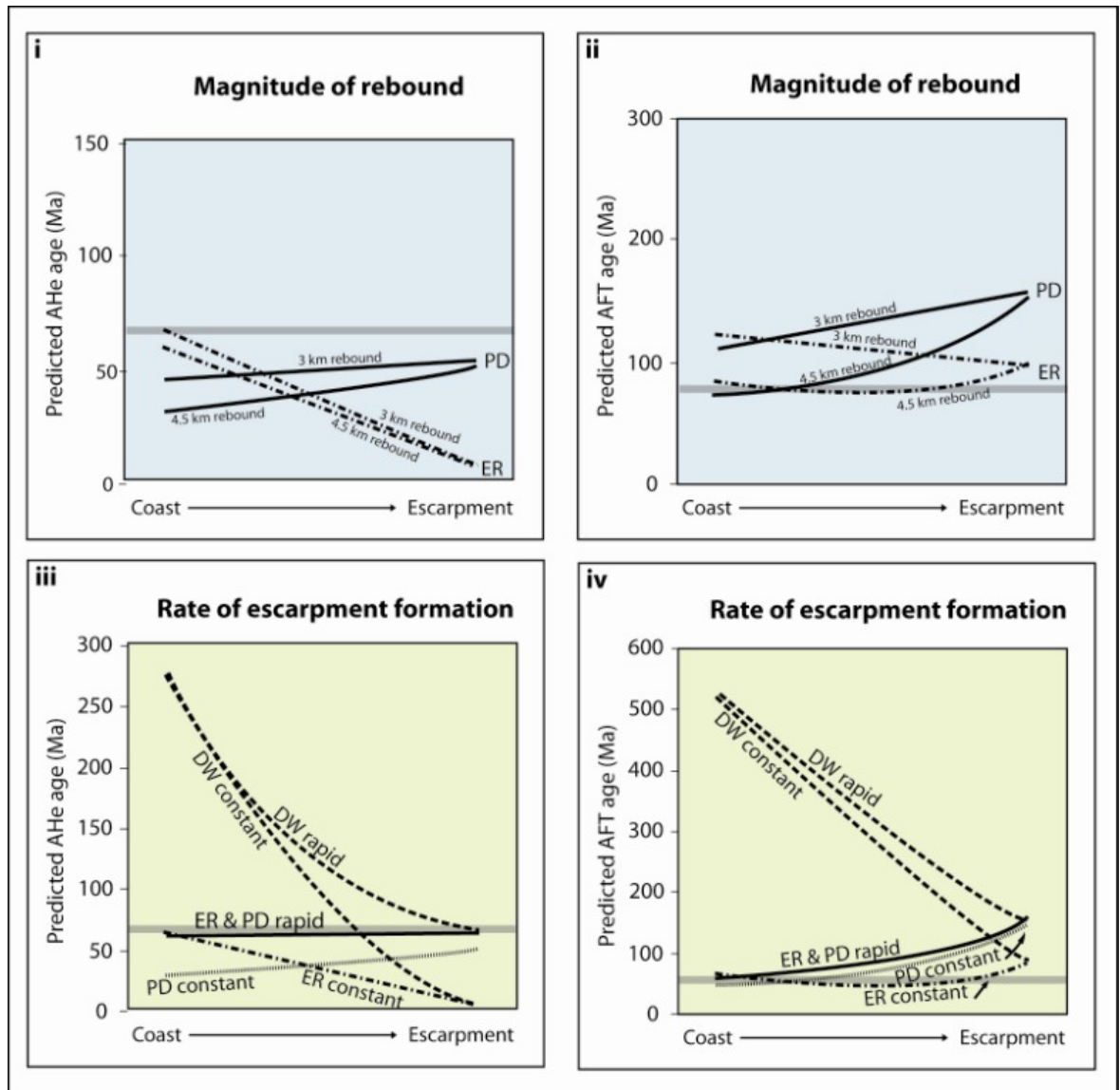


Figure 13 Predictive forward modelling results for Kerala (II)

Predictive forward modelling results for different magnitudes of rebound (ER and PD only) and different rates of escarpment formation (all three conceptual models) for simulated rifting at 65 Ma. The solid grey bars are the time of The Seychelles/India rifting event.

The onshore denudational component of a passive margin is intrinsically linked to the offshore depositional component, so this thesis also presents new data from a comprehensive offshore sedimentary analysis coupled with a mass balance study (Chapter 2). Chapter 3 describes the analytical procedures for undertaking apatite fission track and apatite (U-Th)/He analysis in addition to interpretation of data. Chapters 4 and 5 outline and interpret new low temperature thermochronometry data for two field areas, northern Karnataka and Kerala. Chapter 6 presents a detailed treatment of lithospheric flexure and its role in the development of the Western Indian margin. Such a multi disciplinary approach will help to provide a solution to some of the remaining problems facing geologist and geomorphologists studying the Western Indian elevated passive margin. The final chapter provides a general discussion and conclusions from the study.

2 Mass balance analysis

2.1 Introduction

Passive continental margins are commonly associated with offshore basins containing large volumes of sediment. The fact that many of these basins host hydrocarbons has stimulated research and improved our understanding of basin initiation, development and subsequent evolution. Most studies tend to focus on rifting processes (Cooper et al., 1991; Hubbard, 1988; Seranne and Anka, 2005), basin subsidence (Allen and Allen, 2005; Watts, 2001), basin thermal evolution (Allen and Allen, 2005; Steckler et al., 1993), hydrocarbons potential (Arthur et al., 2003; Cameron et al., 1999) or basin stratigraphy (Lawrence et al., 1990; Mohriak et al., 1988). There are fewer studies linking uplift and denudation to the generation of these sediments even though offshore basins are fundamentally connected to onshore hinterlands (Brown et al., 1990; Pazzaglia and Brandon, 1996; Pazzaglia and Gardner, 1994; Rust and Summerfield, 1990; van Balen et al., 1995). Sedimentary sequences in offshore basins can contain an almost continuous record of the magnitude, timing and variability of onshore denudation and thus quantifying these sediments can provide valuable information on passive margin development.

The concept of sediment mass balance assumes that material eroded from a defined source area over a certain period of time is equal to material deposited in a defined sink over the same period of time (Hay et al., 1989). Sedimentary mass balance analysis can be conducted over a range of temporal and spatial scales including short term (yrs) studies of river sediment discharge (Summerfield and Hulton, 1994), moderate term (ka) studies of lake and reservoir sediments (Einsele and Hinderer, 1998) or long term (Ma) studies of sedimentary basins (Hay et al., 1989). Mass balance analysis of offshore basins provides information on the longest temporal scale and largest spatial scale and is of greatest value to long term landscape development studies such as that conducted here on an elevated passive margin. Hinterland source areas (henceforth termed onshore) and peripheral sinks (henceforth termed offshore) are coupled erosional-depositional systems. If the source area onshore is known and the offshore basin retains all the sediment derived from the onshore area, then the volume of offshore terrigenous sediment can be used to calculate the average depth of onshore denudation.

Additionally, if the timing of increases in terrigenous sediment input is known it is possible to identify the timing of denudational pulses from the sedimentary record.

Understanding the dynamics of both erosional onshore systems and depositional offshore systems is a necessary pre-requisite to a mass balance analysis. The sediment routing system (Allen and Allen, 2005) encapsulates the processes and responses operating in the continental erosional domain and determines the resultant sediment flux into the oceanic depositional domain. Depositional basins are not passive stores and develop in response to sedimentary input, thermal subsidence, and changes in sea level. Section 2.2 outlines details of the sedimentary routing system and the depositional basin system and the methods of mass balance analysis.

To date, there has been only one mass balance analysis for Western India (Gunnell, 2001). Gunnell (2001) utilized isopach maps and the limited number of boreholes available at the time to establish sedimentation rates for the Bombay, Konkan and Kerala Basins. The aim of the study was to extract a denudation chronology for Western India from the sedimentary record, not to reconstruct the palaeogeography. Gunnell's (2001) work is important because it was the first attempt at mass balance analysis for the Western Indian PCM using temporal and spatial scales appropriate to long-term landscape development. However, there are a number of problems with their mass balance analysis. The Bombay Basin is not a closed system (see section 2.3), receiving sediments from rivers draining the Western Indian margin as well as receiving sediments from areas further north and east via rivers draining into the Gulf of Cambay. Gunnell and Radhakrishna (2001) removed 35% from the total sediment volume to account for sedimentological heterogeneity in the form of carbonates not derived from onshore denudation. Whereas this may be a reasonable approximation, it is now possible with the increasing availability of borehole data to refine this procedure.

The Western India mass balance analysis undertaken for this thesis does not attempt to undertake palaeogeographic reconstructions, having instead two other aims, namely, discerning the patterns in sediment flux offshore to constrain temporal variability of denudation onshore, and comparing the total volume of sediment offshore with the potential missing volume of crust onshore in order to test the two competing groups of conceptual models for passive continental margin development (downwarped and elevated rift flanks). This mass balance is only concerned with absolute volumes of rock removal (equivalent to denudation), not changes in surface elevation or the magnitude of rock uplift (England and Molnar, 1990) (Figure 14).

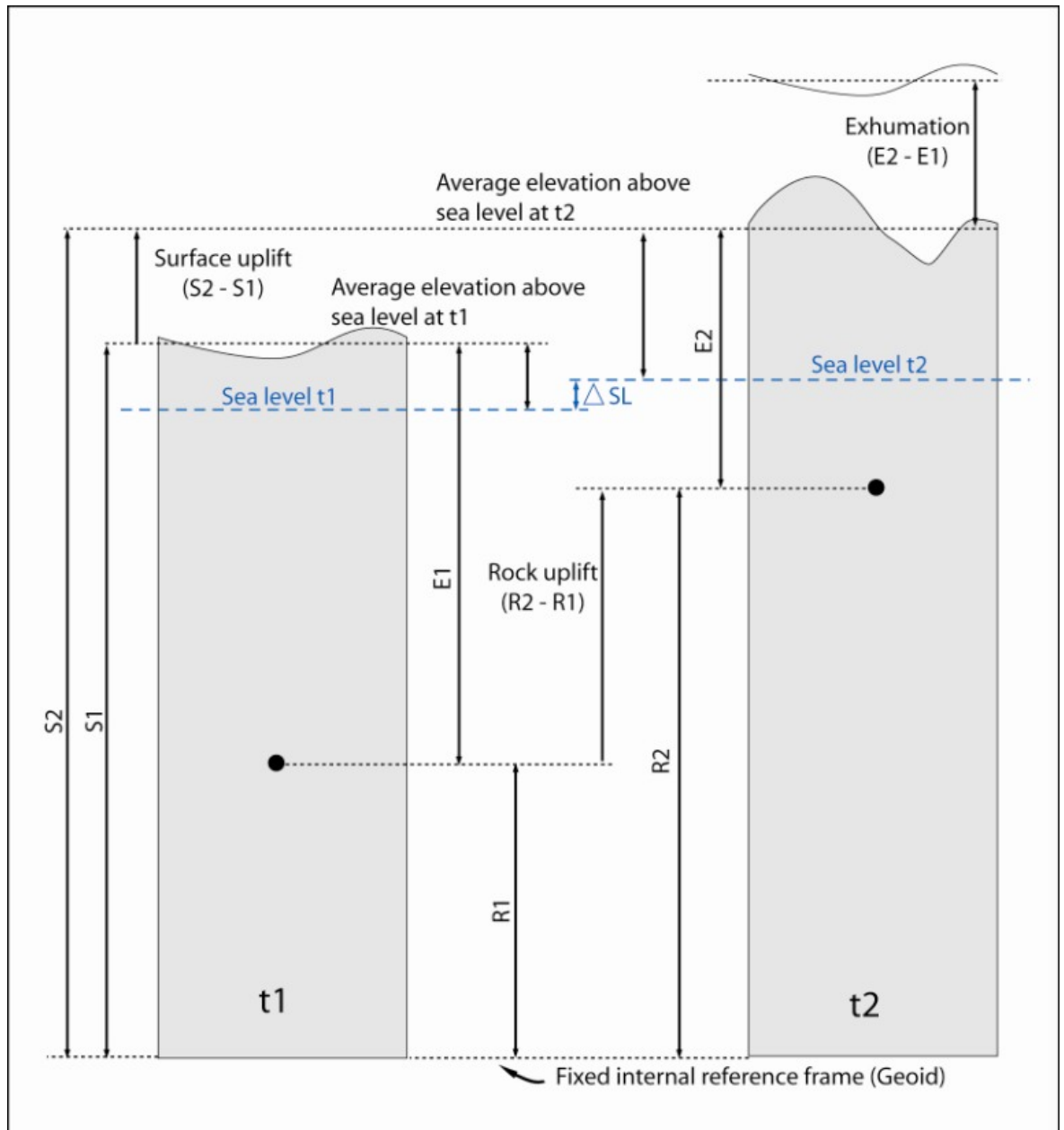


Figure 14 Different types of uplift

Rock uplift – the change in elevation between a specific point in the Earth's crust (black dot) measured from a fixed internal reference frame (such as the Geoid). Represented as $R_2 - R_1$.

Surface uplift – the change in average elevation of the surface measured from a fixed internal reference frame. Represented as $S_2 - S_1$

Exhumation – the volume of crust removed from the surface measured from a specific point in the Earth's crust. Represented as $E_2 - E_1$.

Mass balance analysis of Western India constrains the total volume of crust which has been eroded onshore (i.e. the amount of exhumation)

Section 2.2 summarises the principles of mass balance analysis followed by a brief review of the offshore and onshore areas selected for this study (section 2.3). Section 2.4 outlines the methods employed for the mass analysis of Western India and section 2.5 presents the results. Finally section 2.6 highlights the conclusion and implications focussing on the following issues:

1. What is the timing of major increases in sediment flux to the Western Indian offshore and what implications does the sediment flux have for changes in denudation rate?
2. Can these pulses in sediment flux be correlated with a particular rifting event or are the pulses related to other mechanisms?
3. Which conceptual model of passive margin evolution is more consistent with the volume of terrigenous sediment present offshore?

2.2 The principles of mass balance analysis

2.2.1 The coupled erosional-depositional system

Rocks exposed at the Earth's surface are subjected to in-situ mechanical and chemical weathering processes which are strongly controlled by climate, altitude and rock susceptibility. The disaggregated layer that forms in response to these processes is termed the regolith or weathered mantle. Although the thickness of regolith is dependent on the rate of production of weathered material, the thickness is also controlled by the rate of removal of weathered material by erosion (Summerfield, 1991a). Hillslope processes and fluvial processes are the erosive mechanisms that transport these weathered products from continental areas and transfer them to adjacent oceanic basins. Erosion is believed to be controlled largely by relief (Ahnert, 1970; Summerfield and Hulton, 1994), precipitation (Ohmori, 1983), and lithology. Surface runoff connects the onshore hinterland with the offshore basins and is the final link in the erosional-depositional system (Figure 15).

Material can be transferred offshore either in suspension or in solution. The proportions of suspended sediment and sediment in solution are highly variable globally but on average there is five times more sediment in suspension compared to sediment in solution Summerfield and Hulton (Summerfield and Hulton, 1994). The proportion of sediment in suspension to sediment in solution is important because suspended sediment is deposited and trapped in adjacent offshore basins but sediment in solution is dispersed and deposited throughout the world's

oceans. Sediment in solution can thus contribute significantly to denudation onshore but provides a much smaller constituent of the sediment volume deposited offshore.

Sedimentary basins do not passively receive and accumulate sediment but are dynamic systems. The key processes responsible for basin development are tectonic subsidence, thermal subsidence, subsidence in response to sediment loading, sea level change, and sediment input (Allen and Allen, 2005) (Figure 15). These processes determine the amount of accommodation space in a basin and ultimately its stratigraphy. Accommodation space determines whether sediments are deposited within the basin or they bypass the basin to be transported further offshore. If clastic sediment input is decreased, for example as a consequence of reduced relief onshore or a marine transgression, then biogenic processes become prevalent and carbonate sedimentation dominates. Periods of carbonate deposition correspond to low fluxes of clastic sediment (reflecting, in turn, low denudation rates onshore) whereas high denudation rates result in an increased offshore flux of clastic sediments. The timing and volume of clastic sediment input are therefore a proxy for spatially averaged denudation occurring within the source area of the basin.

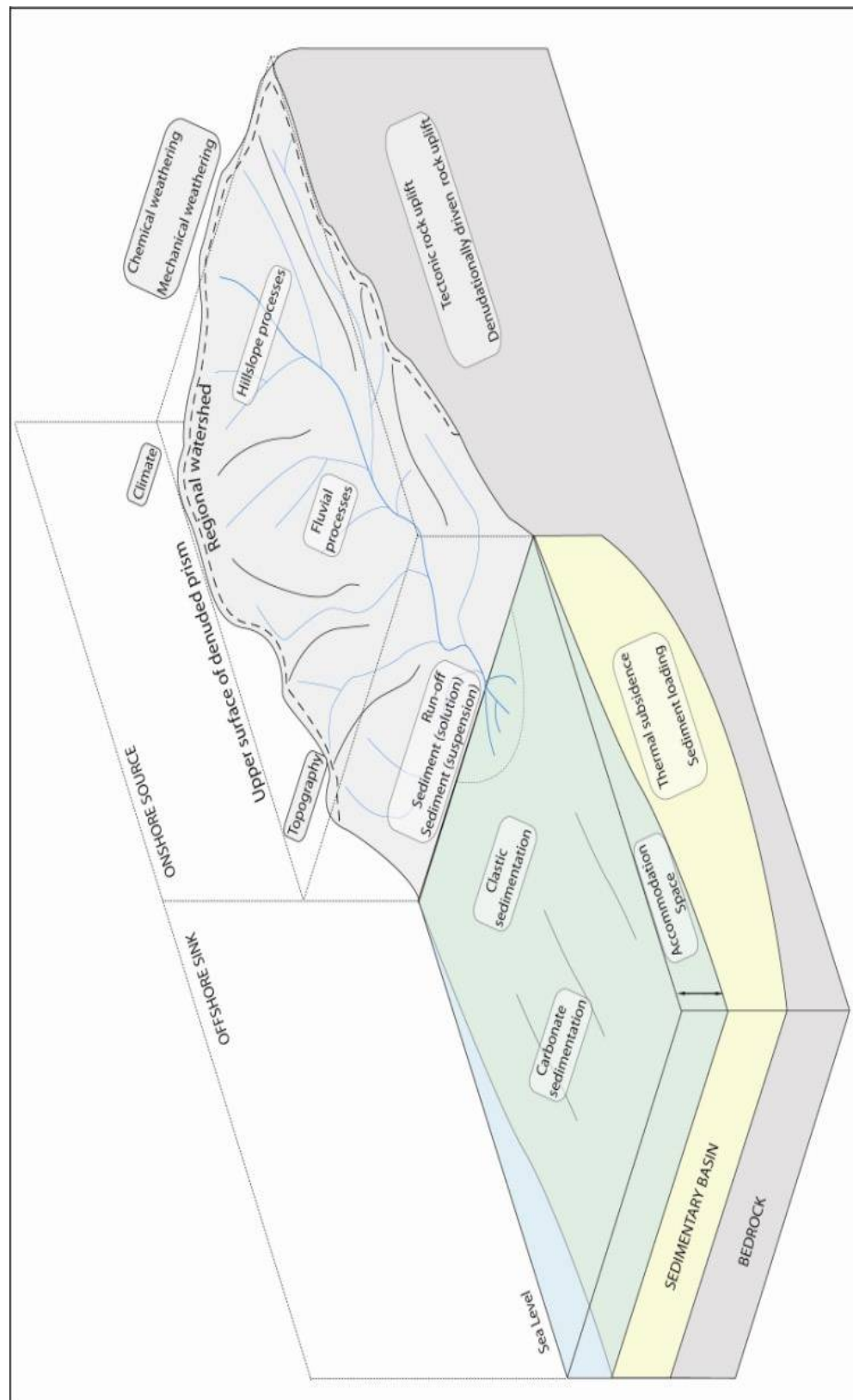


Figure 15 The coupled erosional-depositional system

Processes, forcing mechanism and transfers operating within the onshore and offshore domains. The regional watershed (thick dashed line) and coast are the boundaries for the onshore area. The volume of the onshore prism of denuded material is illustrated as the volume between the upper surface of the prism and the topography.

2.2.2 Mass balance analysis – methods and assumptions

The first stage in any mass balance analysis is to define an appropriate source area and an appropriate sink area. Regional mass balance analyses require the defining of large offshore basins and large onshore continental source areas. It is assumed that the boundaries for the onshore and offshore areas are known. These boundaries can alter through the time period of the mass balance study provided that any such changes in area can be quantified. Changes in offshore basin area tend to be well defined and are usually expressed as shifts in depocentres and facies changes within the basin stratigraphy. Changes in the onshore area such as migration of drainage divides should also be known; however, such changes are more challenging to quantify.

The next stage in the mass balance analysis is quantifying the volume of offshore sediment that was derived from erosion of the onshore hinterland, i.e. the terrigenous sediments only. A variety of sources such as isopach maps, seismic cross-sections and borehole data provide information on the lithostratigraphy, chronostratigraphy and thickness of each sedimentary sequence. The accuracy of the data on the clastic volume and its duration of deposition for each sedimentary sequence is highly dependent on the quality and quantity of available sources outlined above. The density of sediments increases with depth due to compaction by overlying sediment; therefore, the clastic volumes for each sedimentary sequence must be decompacted to allow for the effect of sediment loading. The resultant decompacted clastic volumes (and their ages) provide information on clastic sediment flux.

The final stage of the mass balance analysis is quantifying the eroded onshore volume from a pre-defined onshore area. Defining the source area for offshore sediments is a particularly challenging aspect of any mass balance analysis and some assumption must be made about the boundary conditions, the palaeotopography and the flexural properties of the eroding crust. The assumptions made for the mass balance analysis of Western India are outlined in section 2.4.2. Before a comparison can be made between the onshore eroded prism and offshore sediment volume, the decompacted sediments must be re-compacted to the equivalent average density of bedrock onshore.

There are two further assumptions required for a mass balance analysis, namely, that the system is closed and there is continuity between the onshore and offshore areas. The offshore area must be a closed system and there should be no loss of material further offshore or addition of material from unaccounted sources. All the material leaving the onshore area should be transferred into the offshore area used in the study. There must be continuity between the onshore and offshore areas, and the rate at which sediment is removed and

exported offshore must equal the rate of weathering and rate of removal by erosion. Continuity between the onshore and offshore areas ensures that the erosional and depositional systems are connected, allowing a direct comparison between the volume of terrigenous sediment offshore and denudation onshore.

2.3 Mass balance analysis of Western India

The Western Ghats and the coastal plain seaward of the continental drainage divide at the Ghats escarpment lip form a well-defined source area and offshore basins further west form depositional sinks, making Western India well suited to mass balance analysis. The discovery of petroleum within the Bombay platform has stimulated exploration along the entire Western Indian PCM and knowledge of the development of Indian West Coast basins is constantly improving (Mathur and Nair, 1993; Rao and Srivastava, 1984; Rao et al., 2002; Singh and Lal, 1993; Singh et al., 1999). This section provides a summary of the offshore and onshore areas selected for this mass balance analysis.

2.3.1 The offshore area

The sedimentary basins adjoining the west coast of India include the Northern Basins, comprising, from north to south, the Kutch Offshore Basin, the Cambay Basin, the Saurashtra Basin, the Surat Basin, and the Bombay Offshore Basin, and the southern basin, the Konkan-Kerala Basin (Figure 16). The Northern Basins are supplied by sediment derived from denudation of the northern one-third of the Western Indian margin but also receive sediments from the Cambay and Kutch grabens (Gunnell, 2001; Mathur and Nair, 1993). Additionally, the proportions of different clay minerals within sediments from the northern basins indicate that sediments are derived not only from the Deccan volcanic province but also from the Indus Fan to the west (Rao and Rao, 1995). The Northern basins are therefore not a closed system and are less suitable for mass balance analysis. The proportions of clay minerals within sediments entering the Konkan-Kerala Basin indicate that the sediments are derived exclusively from the remaining two-thirds of the margin (Rao and Rao, 1995). The shelf sediments along the western margin of India are strongly compartmentalised and show marked affinities along strike with their adjacent onshore areas. Thus, north of Goa modern shelf sediments have a clay content indicating a basaltic source, whereas south of Goa these sediments have a clay content indicating a gneissic source (Rao and Rao, 1995). There is a close relationship between the onshore geology and the offshore sediments, and, lacking evidence to the contrary, it is taken to be the case that there has been little longshore transport of sediment in the Konkan-Kerala Basin area. The Vengurla Arch basement high is a natural barrier at 17° N latitude, separating the Konkan-Kerala basin from the Northern Basins, and

the Chagos-Laccadive Ridge forms a barrier to westward sediment transport into the deeper abyssal plain (Gunnell and Radhakrishna, 2001). In effect, the inner shelf of the Konkan-Kerala Basin is a closed system and sediment sink for the erosional products of the Western Ghats, making it a suitable offshore area for mass balance analysis.

The Konkan-Kerala Basin hosts sediments from ca. 80 – 90 Ma onwards and represents the sag basin developed on the stretched pre-Deccan continental basement formed during the rifting of India from Madagascar (Singh and Lal, 1993). Sedimentation in the Konkan-Kerala Basin is within N-S trending grabens separated by local basement highs. Seismic profiles of the sediments show differential vertical movements in the sediments, as well as wrench faults, reverse faults and folds (Ghosh and Zutshi, 1989). Some of the faults may be inherited, and basement controlled since the thinned crust underlying the sediments is characterized by a coast-parallel Precambrian grain (Kolla and Coumes, 1990; Subrahmanyam et al., 1994; Subrahmanyam et al., 1995).

The early rift phase (Upper Cretaceous, Campanian) in the Konkan-Kerala Basin is localized in the southern part of the basin west of Cochin and restricted to narrow grabens. Sedimentation took place in a shallow continental setting (fan deltas, tidal flats and carbonate platforms) suggesting that a major part of the stretched portion of the crust on which the basin developed remained above sea-level until the Cretaceous-Tertiary boundary, ending in pre-Santonian time (Singh and Lal, 1993). The Upper Cretaceous sediments in the deepest wells of Konkan-Kerala Basin overlie altered volcanic rocks. These basal volcanic rocks are undated, but outcrops of volcanic rocks near the coast on St. Mary Islands (Figure 16) have been dated as 85.6 Ma (Pande et al., 2001), contemporaneous with Marion hot-spot magmatism (Joseph and Nambiar, 1996). Basin initiation must have occurred at 88 Ma, the time of India-Madagascar rifting and during the peak of Marion hotspot volcanism (Storey, 1995); nevertheless, the bulk of sediments in the Konkan-Kerala basin were deposited during the Cenozoic.

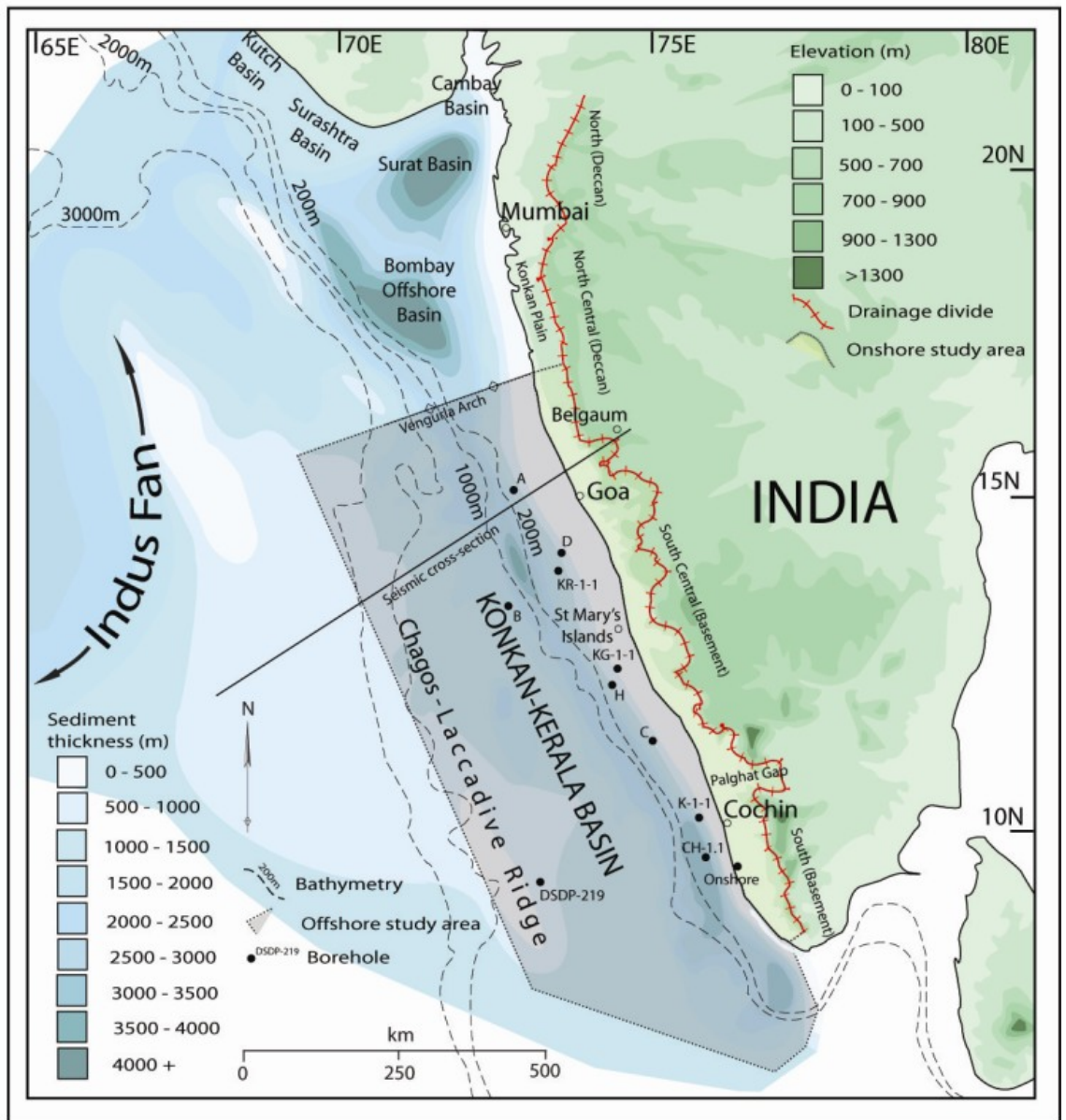


Figure 16 Location map for onshore and offshore areas

Total sediment thickness map of the offshore basins compiled from Rao & Srivastava, 1984; Rao et al., 2002. Also shown are the locations of wells used in the analysis and the location of the seismic profile of Chaubey et al., 2002. DEM-derived contours onshore, the regional watershed and the area used for mass-balance calculations are also shown.

Post-rift passive subsidence beginning at the start of the Cenozoic led to the development of an extensive marine basin and the deposition of the sediments whose volumes are quantified in this analysis. Sediment isopach maps in the Konkan-Kerala Basin indicate Cenozoic sediment thicknesses of up to 4 km (Rao and Srivastava, 1984). Total sediment thickness ranges from 500ms to 3500ms using seismic two way travel times (TWT) averaging 1300 ms for the Konkan-Kerala basin. The greatest accumulation occurs where Mesozoic sediments are present below Cenozoic sediments within coast-parallel graben structures that lie approximately 50-150 km offshore. However, sediments thin to less than 500 ms TWT over the Laccadive ridge, a portion of the Chagos-Laccadive volcanic ridge. Data from eleven bore-holes show a

generalized stratigraphy comprising of a thick carbonate accumulation (Eocene to Late Miocene) sandwiched between clastic-dominated sequences (Chaubey et al., 2002; Gunnell and Radhakrishna, 2001; Rao et al., 2002; Singh and Lal, 1993). The major breaks in deposition/unconformities in the basin occurred in the Middle Palaeocene, the Early Eocene and the Late Eocene-Early Oligocene, corresponding to an absence of sediments of these ages in the bore-hole logs.

Paleobathymetry estimates by Raju et al. (1999) imply shallow depths (<100 m) for the Konkan Kerala Basin during upper Cretaceous at 85 Ma. The basin became a depocentre at 85-75 Ma when its depth increased to >200 m. Uplift possibly due to the onset of rifting led to a decrease in basin depth to 0 m from 65-60 Ma, marking a period of non-deposition. Re-submergence then occurred in the Palaeocene/Eocene, followed by a further period of non-deposition from 28-38 Ma. The Konkan-Kerala Basin is interpreted to have followed a normal subsidence path for a rifted passive margin beginning with rapid initial subsidence in the Cretaceous, followed by slow thermal subsidence throughout the Cenozoic (Gombos et al., 1995) (Figure 17).

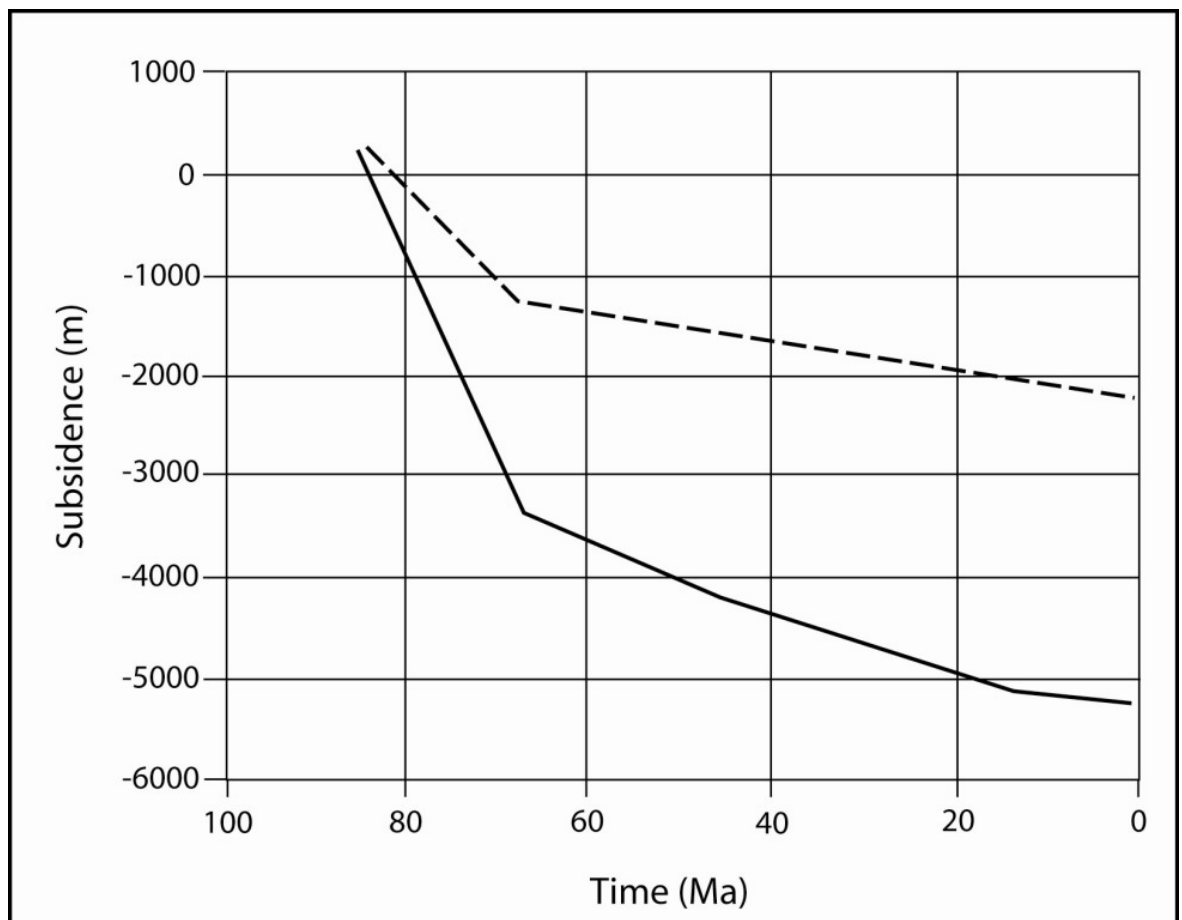


Figure 17 Subsidence curve for the Kerala basin

Subsidence curve for the Kerala basin (Gombos et al. (1995)). Basin initiation and rapid subsidence began at 85 Ma followed by slow thermal subsidence throughout the Cenozoic. The solid line indicates subsidence of the sediment-basement interface. The dashed line indicates backstripped thermo-tectonic subsidence

Sea-level may also play an important roll in the dynamics and nature of sediment transferred from the onshore portion of the margin to the Konkan-Kerlala basin (see section 2.2.2). Figure 18 displays the eustatic sea level curve (Haq et al., 1987). From the Palaeocene to middle Miocene sea level fluctuated but remained higher than present day. This is reflected in the style of sedimentation where aggradational sequences are observed indicating sufficient accommodation space for storage and steady sedimentation rates (Gunnell, 2001; Mathur and Nair, 1993; Singh and Lal, 1993). Fluctuating sea level and a series of regression occurred from the late Miocene to present, reflected in progradational sequences and coastal onlap (Gunnell, 2001). The present day continental shelf is wider than the Palaeocene and middle Miocene palaeoshelves as a result of these progradational sequences, however there is no evidence that accommodation space was reduced to such an extent that sediment was able to bypass the basin completely.

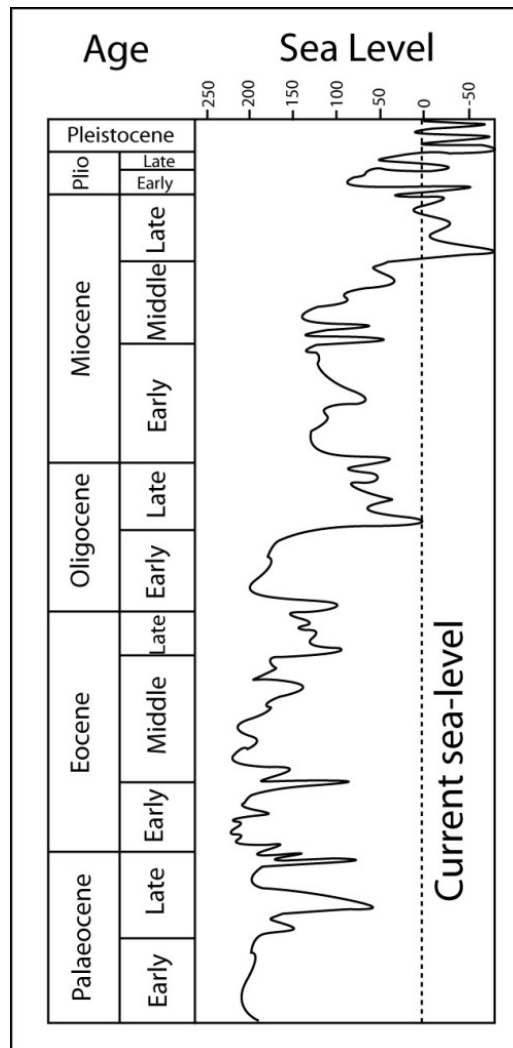


Figure 18 Eustatic sea-level curve

Adapted from Haq et al. (1987)

There are two potential sources of sediment that cannot be accounted for in the mass balance calculations, namely, sediment in solution from chemical weathering and clastic sediment sourced from the conjugate margins. Sediment in solution is derived from dissolution, chelation and lateritization, processes which are promoted by tropical weathering conditions predominating in Western India. The dissolved component of sediment is difficult to quantify and there are few constraints on the magnitude of sediment in solution relative to sediment in suspension. Approximate present day estimates for sediment in solution are available for Western India (Das et al., 2005; Prasad and Ramanatran, 2005) but the variability of dissolved sediment over timescales longer than ca. 20 years is unknown. Due to the sparse data on the volumes of sediment in suspension and in solution for the Western Indian margin, this mass balance analysis utilises the power law relationship whereby chemical weathering = 0.39 (physical weathering)^{0.66} developed from data collected from several global rivers including Western India (Millot et al., 2002). This power law assumes that there is 4.5 times more sediment in suspension than in solution (see section 2.4.2).

Sediment derived from the conjugate margins (Seychelles and Madagascar) could also possibly have contributed significant volumes of sediment to the basin. Madagascar rifted from Greater India at 88Ma (Storey, 1995); however, Mesozoic sediments are limited and restricted to the deeper central grabens within the Konkan-Kerala basin. Mesozoic sediments have not been included in the sediment volume calculations. The establishment of the Carlsberg ridge separated India from The Seychelles at 65 Ma, but there is little evidence of major sediment contribution from The Seychelles, a low lying microcontinental sliver. Where elevations on the microcontinent are significant, sediments are Eocene – Pleistocene carbonates and not extensive (Plummer and Belle, 1995).

2.3.2 The onshore area

The onshore segment of Western Indian is a typical high elevation passive margin (see Section 1.3) with a low elevation coastal plain, an erosional escarpment and a high elevation plateau inland of the escarpment. The escarpment lip coincides with the regional watershed for most of the length of the margin. Easterly flowing rivers drain the elevated interior plateau and deliver sediment to the Bay of Bengal, whereas westerly flowing rivers deliver sediment to the Arabian Sea derived from the denudation of the escarpment face and coastal plain (Figure 15). Apart from the northern third of the margin, the source of the sediment for the westerly flowing rivers is the coastal plain and the escarpment face; the southern two thirds of the margin therefore form a closed erosional-depositional system.

The regional watershed only forms the landward part of the boundary for the onshore area; the seaward part of the boundary is dependent on the location of the initial rift or proto-escarpment. A maximum onshore area would be defined if the proto-escarpment is placed at the ocean-continental crust transition 200km offshore from the present coast (Widdowson, 1997; Widdowson and Cox, 1996). However, a thick Palaeocene – early Eocene clastic fan has been identified (Basu et al., 1982; Parida and Mishra, 1992) at the coast near Mumbai. A clastic fan of this age could not develop if the proto-escarpment was located 200 km offshore and subsequently retreated towards its present position throughout the Cenozoic. This clastic fan is taken as evidence that the position for the proto-escarpment (and the seaward portion of the onshore boundary) would be near the present coast.

2.4 Methods

2.4.1 Quantifying sediment in the Konkan-Kerala basin

2.4.1.1 Obtaining compacted sediment volumes

The data used here to document Cenozoic sedimentation in the Konkan Kerala Basin is derived from 11 commercial wells (Chaubey et al., 2002; Gunnell and Radhakrishna, 2001; Rao et al., 2002; Singh and Lal, 1993), seismic profiles (Chaubey et al., 2002; Singh et al., 1999) and isopach maps (Rao and Srivastava, 1984). Total sediment thickness is based on the isopach maps of Rao and Srivastava (1984) and Rao et al. (2002). A regional seismic survey by Rao and Srivastava (1984) derived three Cenozoic sedimentary sequences in the Konkan-Kerala Basin (Figure 19): a lower succession, sequence II, with sediments of Palaeogene age ranging in thickness from 200 ms to 1200 ms (TWT); a middle succession, sequence III, of Miocene sediments ranging in thickness from 200 ms to 1200 ms (TWT); and an upper succession, sequence IV, of post-Miocene sediments ranging in thickness from 20 ms to 120 ms (TWT). Chaubey et al. (2002) identified six Cenozoic sequences (H1 to H6) on the basis of a multi-channel seismic reflection profile across the northern part of the Konkan Kerala Basin (Figure 20). The sequences of Chaubey et al. (2002) and the three sedimentary sequences of Rao and Srivastava (1984) have been combined. The boundary between Chaubey et al. (2002) sequences H2 and H3 has an inferred age of Late Oligocene (Chaubey et al. (2002) Table 1, p306) and thus correlates well with Rao and Srivastava (1984) boundary between sequences II and III. Similarly, the boundary between Chaubey et al. (2002) sequences H5 and H6 is Late Pleistocene and correlates well with the boundary between Rao and Srivastava (1984) sequences III and IV. The relationships between the chronologies of Chaubey et al. (2002) and Rao and Srivastava (1984) are summarised in Table 1. The revised chronostratigraphy refines the depositional periods for sequences II, III and IV of Rao and Srivastava (1984).

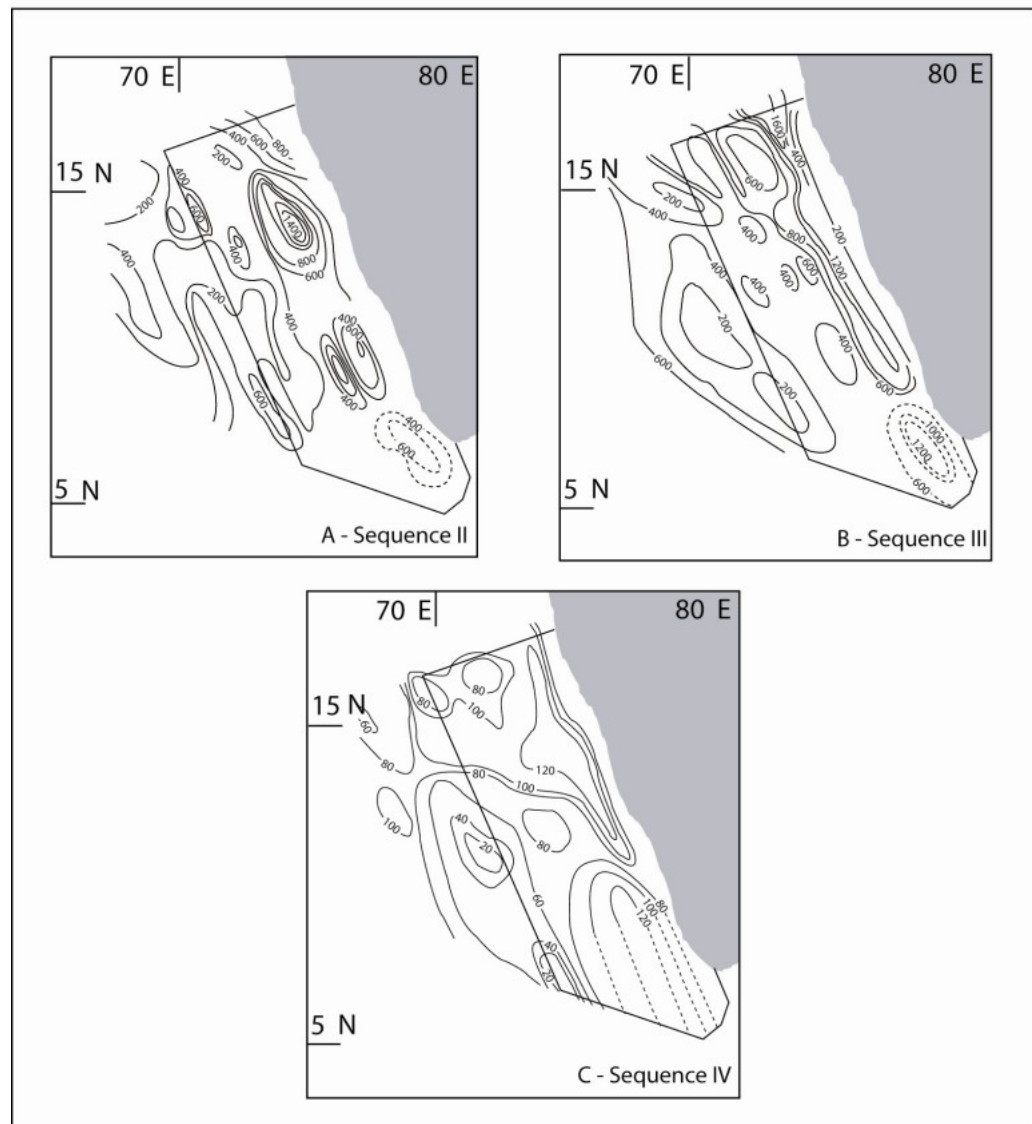


Figure 19 Isopach maps for the Konkan-Kerala Basin

Sediment-thickness maps of the three broad sequences as discussed in the text (modified after Rao & Srivastava, 1984). The broken lines are extrapolations based on the total sediment thickness data. Units are two way travel time.

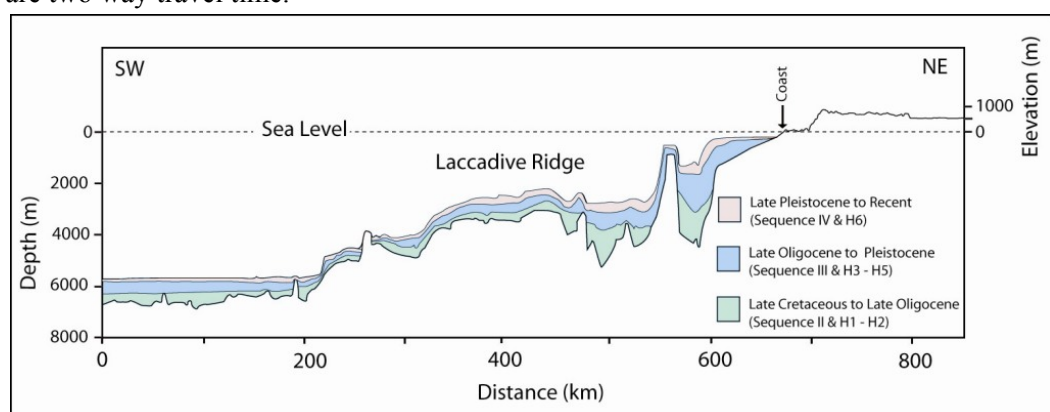


Figure 20 Seismic cross section for the Konkan-Kerala Basin

Generalized cross section along the northern part of the Konkan Kerala Basin (based on the seismic profile of Chaubey et al., 2002) showing the major lithostratigraphic units. The topographic profile onshore (extracted from the DEM) is also displayed.

TWT (ms)	Age	Rao & Srivastava (1984)	Chaubey et al. (2002)	Age (refined)
20 – 120	post Miocene	Sequence IV	H6	Late Pleistocene – Recent
200 – 1200	Miocene	Sequence III	H3, H4 & H5	Late Oligocene – Late Pleistocene
200 – 1200	Palaeogene	Sequence II	H1 & H2	Palaeocene – Late Oligocene

Table 1 The relationship between the sequence chronologies of Rao & Srivastava (1984) and Chaubey et al. (2002)

In this thesis sequences III and II have been further sub-divided based on a detailed analysis of the stratigraphy from ten litho-logs from the Konkan-Kerala Basin, and an additional stratigraphic column onshore in Kerala. Five sub-divisions (IV, IIIa, IIIb, IIa and IIb) and their equivalent ages are given in Figure 21. These sub-divisions were used for the sediment volume calculations.

Sediment volumes were calculated in a GIS using the (digitized) sediment isopach maps of Rao and Srivastava (1984), and assuming that 1 s two-way travel time is equivalent to 1 km thickness of sediment (Gunnell, 2001). Using lithologies in the eleven boreholes in the study area, percentages of clastic (terrigenous) and non-clastic sediments (biogenic and marine limestones) were obtained for each of the five sequences (IV, IIIa, IIIb, IIa, IIb). The non-clastic component of each of the sequences was then removed from the individual volumes extracted from the GIS to acquire the compacted clastic components.

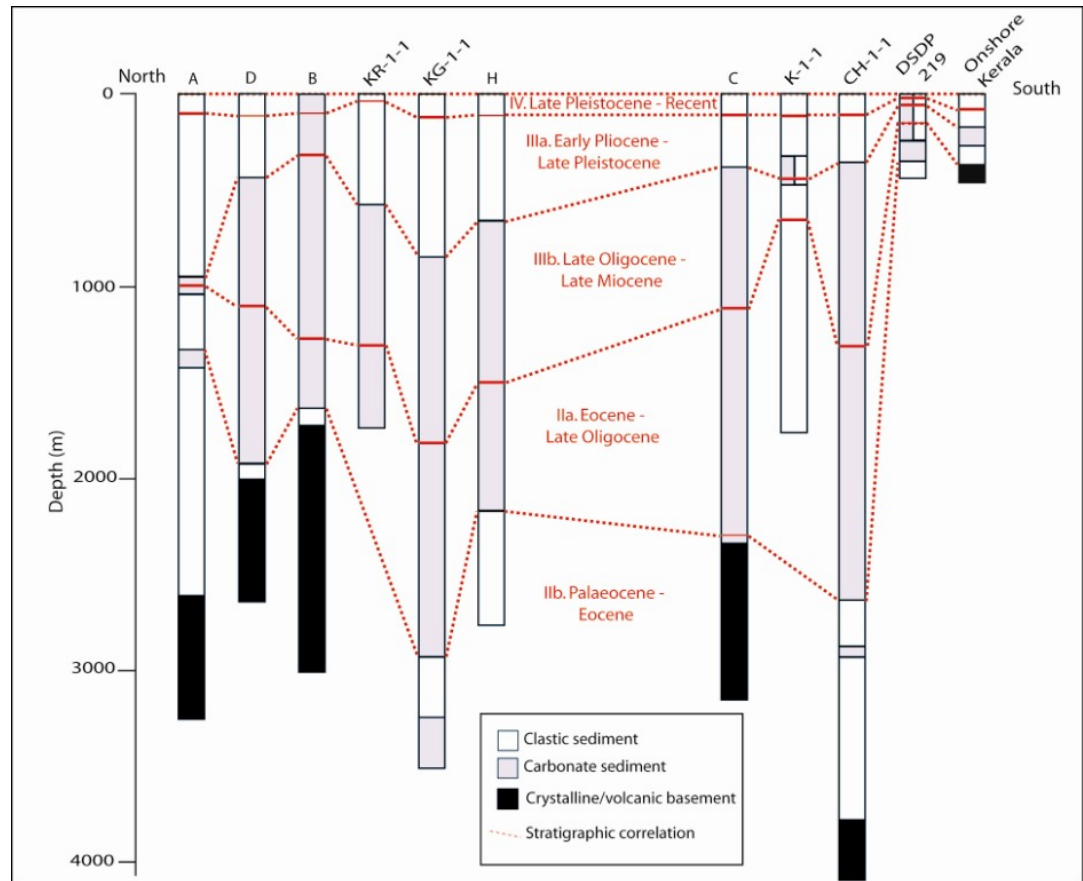


Figure 21 Simplified lithologies and stratigraphies of wells in the Konkan Kerala Basin

The red lines are stratigraphic correlations for the five sub-sequences used in the analysis. Wells A, B, C, D, H (Rao et al. 2002). K-R-1 and DSDP 219 (Chaubey et al. 2002). K-1-1 and CH-1-1 (Singh & Lal (1993). KG-1-1 and onshore Kerala (Gunnell & Radhakrishna, 2001).

2.4.1.2 Decompacting sediment volumes

To obtain true sediment volumes the clastic volumes were decompacted to allow for the effects of sediment loading with depth. The relationship between porosity and depth of burial for different sedimentary units must be understood for the decompaction procedure, and several relationships have been proposed (Athy, 1930; Audet and McConnell, 1994; Baldwin and Butler, 1985; Falvey and Deighton, 1982; Hedberg, 1936). Although each porosity-depth relationship differs subtly in detail, all assume a negative exponential decrease in porosity with depth. The Konkan-Kerala Basin lacks detailed porosity information needed to calibrate many of the porosity-depth curves; therefore, we apply the basic procedure of Athy (1930) and Hedberg (1936) summarised by Allen and Allen (2005), using the following equation:

$$y'_2 - y'_1 = y_2 - y_1 - \frac{\phi_0}{c} [\exp(-cy_1) - \exp(-cy_2)] + \frac{\phi_0}{c} [\exp(-cy'_1) - \exp(-cy'_2)]$$

Equation 1

where y'_2 and y_2 are the decompacted and compacted depths, respectively, to the base of the layer, y'_1 and y_1 are the decompacted and compacted depth, respectively, to the top of the layer

($y'_1 = 0$ for decompaction to sea level). ϕ_0 is a constant for the initial porosity prior to compaction, 0.56 for shaley sandstone (Allen and Allen, 2005), the most abundant terrigenous sediment in the basin (Chaubey et al., 2002; Gunnell and Radhakrishna, 2001; Rao and Srivastava, 1984; Rao et al., 2002; Singh and Lal, 1993; Singh et al., 1999). The porosity coefficient (c) is a constant which describes the gradient of the porosity-depth curve (0.39 for shaley sandstone (Allen and Allen, 2005)) and is equivalent to 'sliding' a given sedimentary layer up the porosity-depth curve (Figure 22). Average depths for the top and base of each of the five sedimentary sequences were used and their percentage increases in thickness were applied to their decompacted volumes. For example, the average depths to the base and top of sequence IIa are 2900m and 1000m respectively, giving an average compacted thickness of 1900m. If sequence IIa is decompacted, the thickness increases by 15% to 2200 m. This 15% increase is then applied to the compacted volume for sequence IIa to give a true decompacted volume.

Sediment accumulation rates can be calculated from decompacted sediment volumes if the depositional periods for the individual stratigraphic units are known. Sediment accumulation rates provide useful information on the changes in flux of sediment throughout the basins history but a direct comparison between the offshore clastic sediment volume and the volume of material eroded onshore can only be made by recompressing the decompacted volume of offshore clastic sediment to equivalent crystalline basement rock densities. A density of 1200 kg m^{-3} (average for shaley sandstone, the most abundant sediment in the basin) was adopted for the sediments and a density of 2700 kg m^{-3} for crystalline rocks (Rust and Summerfield, 1990). A density of 2700 kg m^{-3} was adopted for crystalline rocks because the majority of the rocks onshore are charnokites and gneisses with similar average densities.

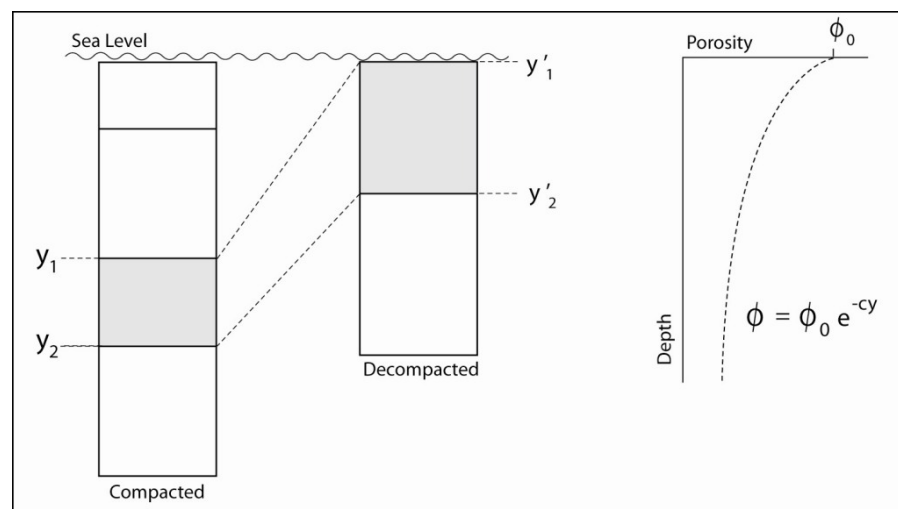


Figure 22 Decompaction cartoon

Modified from Allen and Allen (2005). y_1 and y_2 are the depths to the upper and lower layers of the sedimentary unit being decompacted. y'_1 and y'_2 are the depth to the upper and lower layers of the sedimentary unit after decompaction. The graph illustrates the relationship between porosity and depth (see text for explanation).

2.4.2 Calculating the onshore denuded crustal prism

The onshore denuded crustal prism is bounded to the east by the regional watershed and to the west by the coast of the Arabian Sea. The northern limit is onshore of the northern margin of the Konkan-Kerala basin east of the Vengurla arch basement high, and the southern limit is the tip of the Indian peninsula (Figure 16). The regional watershed was defined by extracting the boundary between easterly- and westerly-flowing river basins from the GTOPO30 DEM. The offshore sediment volume is a combination of the volume of prism eroded from the coastal plain (used to test the different conceptual models) and the additional volume eroded between the escarpment lip and the regional watershed (Figure 23).

The DEM was used to calculate the onshore area and volume of crust now missing from the coastal plain. The volume of eroded crust depends on the source area and the position of the upper surface of the prism (Figure 23). The position of the upper surface is controlled by both the geometry of the syn-rift palaeosurface and the flexural strength of the lithosphere. Flexurally strong lithosphere resists the isostatic effects resulting from erosion of the prism and the prism of material removed is either cubic where the prism has a horizontal upper surface corresponding to a syn-rift palaeosurface extending horizontally seawards from the crest of the escarpment or more likely wedge-shaped, thinning towards the coast (Figure 23A). A wedge-shaped prism is analogous to a downwarped margin geometry where syn-rift downwarping occurs, thereafter the lithosphere remains flexurally rigid (Ollier, 1982; Ollier and Pain, 1997). Denudational unloading may cause flexurally weaker lithosphere to rebound, increasing the volume of material that is eroded and subsequently transported offshore. The geometry of the crustal prism that incorporates an elevated pre-rift topography and/or flexural rebound is an inverted wedge thickening towards the coast, analogous to the elevated rift flank model (Figure 23B). Different lithospheric flexural properties cause different amounts of flexural rebound (and hence different dimensions of the eroded crustal prism). The flexural response of the lithosphere is explored more fully in Chapter 6.

For the purposes of this work, the eroded volumes were calculated as (i) a seaward tapering wedge-shaped geometry corresponding to Ollier and Pains (1997) downwarp model and (ii) an inverted wedge-shaped geometry corresponding to both the elevated rift flank models (i.e. escarpment retreat and pinned divide) (Figure 23A). It is the style of escarpment formation that differs between the two elevated rift flank models (escarpment retreat vs downwarping) not the magnitude of missing crustal section; therefore, the

calculated onshore eroded volumes for both the elevated rift flank models are treated the same. The eroded material between the escarpment lip and the regional watershed was then added to the eroded volume of each crustal prism (Figure 23B), constrained using palaeosurface reconstructions from the Deccan volcanic province (Widdowson, 1997) and from the northern Dharwar Craton (Gunnell, 1998). Sediment in solution contributes to the volume of material eroded onshore but is not deposited offshore; therefore to compensate for this, 19 % is removed from the calculated volumes of missing eroded crust (see section 2.3.1). Recompacting the decompacted volume of offshore clastic sediment to equivalent crystalline basement rock densities allows a comparison between the offshore sediment volume and onshore denuded material (for different crustal prisms), completing the mass balance.

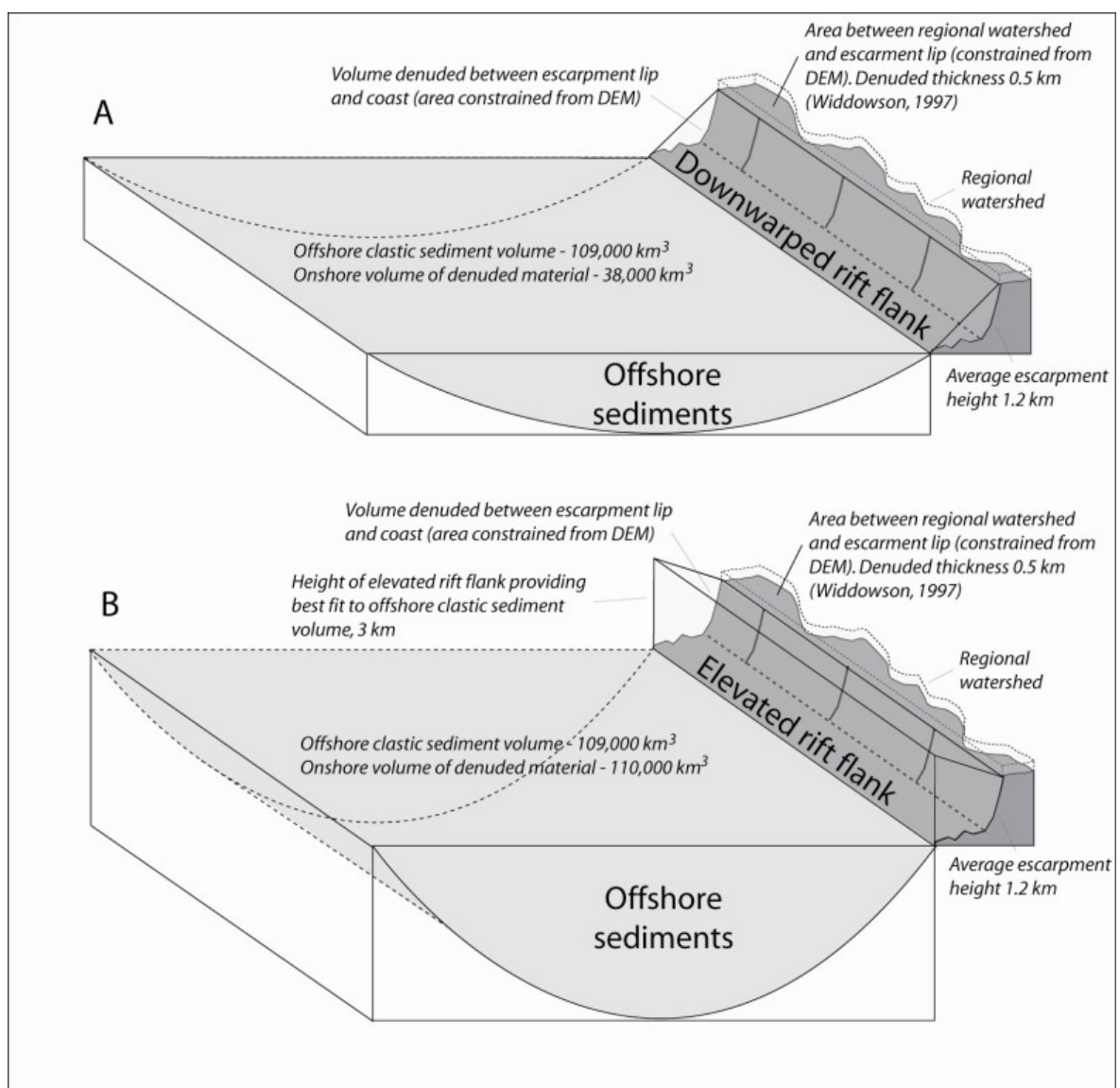


Figure 23 Diagrammatic representation of the mass balance procedure

Different onshore eroded prism produce different eroded volumes. The form of the crustal prism depends on both the pre-rift palaeoelevation and the flexural response of the lithosphere. A wedged shaped prism reflects a downwarped rift shoulder (A) and an inverted wedge shaped prism reflects an elevated rift shoulder (B).

2.5 Results

The results of backstacking are summarised in Table 2. The total equivalent rock volume calculated from the combined volumes of re-compacted clastic sediment is $108,740 \text{ km}^3$. The onshore source area for these sediments comprises of $6 \times 10^4 \text{ km}^2$ for the area between the escarpment and the coast, and $2.3 \times 10^4 \text{ km}^2$ for the area between the escarpment and the regional watershed (total of $8.3 \times 10^4 \text{ km}^2$). The total volume of denuded lithosphere (including the contribution landward of the escarpment lip) for a seaward tapering wedge-shaped prism (Ollier and Pain's (1997) downwarp geometry) would have been $38,000 \text{ km}^3$. Accordingly, denudation of a downwarped wedge-shaped prism would account for $\sim 30\%$ of the sediments present offshore. By contrast, an inverted wedge-shaped prism with 3 km of rebound at the coast (decreasing to 1.2 km at the escarpment) has a volume of $110,000 \text{ km}^3$, an amount more obviously consistent with the volume of sediment calculated as being present offshore.

The Konkan-Kerala Basin contains a total sediment accumulation (clastic and carbonate) of $464,000 \text{ km}^3$; the total clastic volumes and decompacted clastic volumes for each sequence are given in Table 2. The decompacted sediment volume and the depositional duration for each of the five sequences (the latter constrained by the borehole stratigraphy) allow clastic sediment volume accumulation rates to be calculated. Estimated onshore volumes of rock are also included in Table 2 as recompacted sediment volumes equivalent to crystalline basement. The final column of Table 2 displays the denudation rate for sequences IIb, IIa and IIIb. As a consequence of the very small duration of deposition (and hence denudation) of sequence IV, sequences IIIa and IV have been combined to avoid inappropriately high denudation rates. Sequences IIb, IIIa and IV have much greater proportions of clastic sediment compared to sequences IIa and IIIb which are carbonate dominated. Clastic sediment accumulation rates mirror the total clastic volumes calculated for each sequence, peak accumulation rates in the Palaeocene and Pliocene, separated by an intervening period of low clastic accumulation rates throughout the Eocene, Oligocene and Miocene (Figure 24).

OFFSHORE	Total sediment volume (km ³)	% clastic	Total compacted clastic volume (km ³)	Decompacted clastic volume (km ³)	Depositional duration (Myrs)	Clastic sediment accumulation rates (km ³ /Myrs)	Equivalent rock volume (km ³)	Denudation rate (m/Myrs)
IV Late Pleistocene – Recent	40,330	91	37,000	37,000	0.08	462,500	16,300	
IIIa Early Pliocene– Late Pleistocene	94,500	92	87,000	87,500	11.5	7,609	38,900	57.2
IIIb Late Oligocene – Late Miocene	140,000	2	2,800	3,808	16.8	227	1,370	0.9
IIa Eocene – Late Oligocene	89,000	11	9,800	11,400	27.4	416	5,070	2.2
IIb Palaeocene – Eocene	100,000	89	89,000	106,000	9.2	111,522	47,100	61.4
Total	463,830		225,600	245,708	64.9		108,740	

ONSHORE FROM DEM	Volume of denuded prism between the escarpment and the coast (km ³)	Total volume including material denuded landward of escarpment (km ³)	Total denuded volume corrected for chemical weathering contribution (comparable with offshore)
Ollier & Pain (1997) downwarp model	36,000	47,500	37,050
Elevated rift flank model	126,000	137,500	107,250

Table 1 Mass balance results for Konkan-Kerala Basin

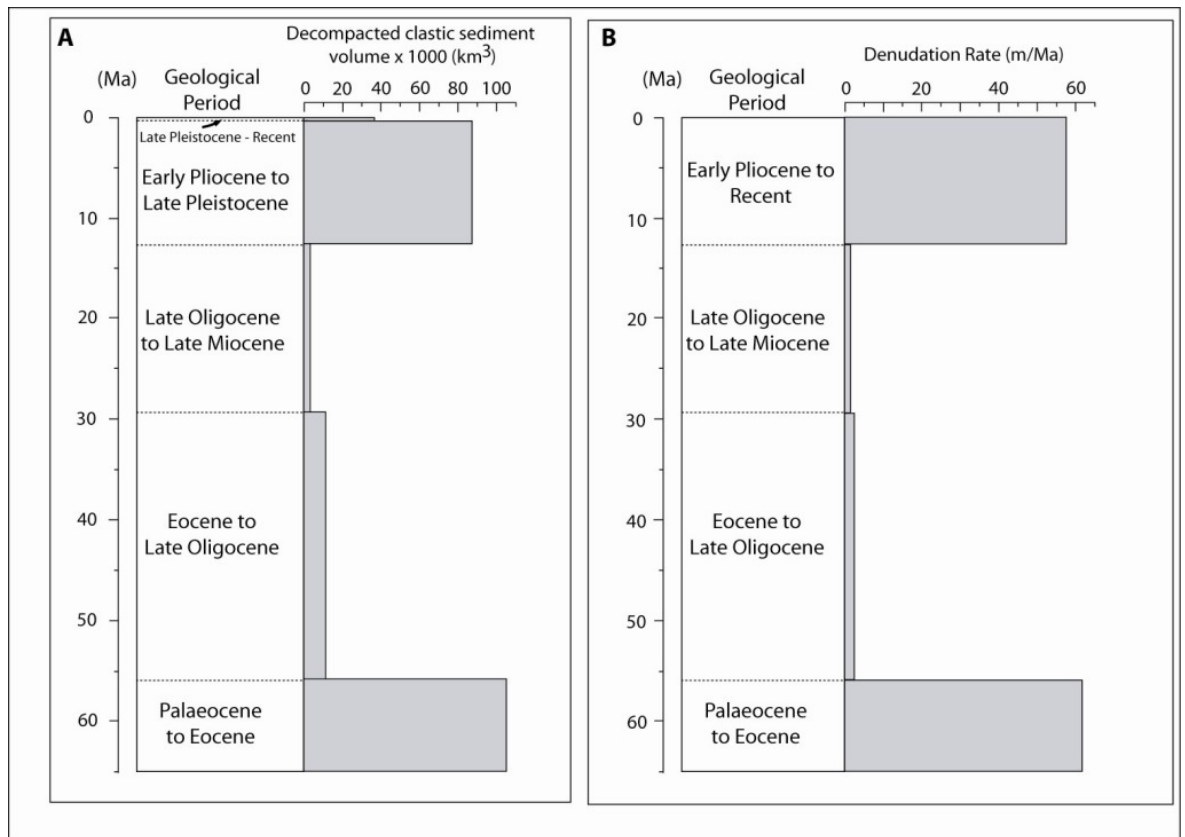


Figure 24 Sediment flux (a) and denudation rate (b) results

(a) The grey bars are the decompacted clastic sediment volumes for each of the five sub-sequences. (b) The grey bars are the denudation rates for each of the five sub-sequences with sequence IV & IIIb combined.

2.6 Discussion and implications

It is unclear how the separation between India/Madagascar at 85 Ma and India/The Seychelles at 65 Ma influenced the development of the Western Indian PCM (see Section 1.3). One of the consequences of rifting is a drop in base level at the new continental margin and the initiation of sedimentary basins receiving sediment from the new margin. The sediments should thus record the timing and spatial extent of rifting. Most of the sediments preserved in the Konkan-Kerala basin are Cenozoic with only limited Mesozoic sediments restricted to narrow coast-parallel grabens. The India/Madagascar rift may have initiated the formation of the Konkan-Kerala basin but that stretching of the crust and denudation were limited. The much larger volume of Cenozoic sediments implies that rifting between India and The Seychelles exerted a far greater influence on sediment delivery and basin subsidence.

Two maxima in sedimentation rates are interpreted as reflecting two phases of increased denudation. The first phase, beginning in the Palaeocene (Sequence IIb), yielded 106,000 km³

of clastic sediment. This phase of increased sediment flux is likely to have resulted from denudation and escarpment formation in response to rifting between India and The Seychelles. Plume-related regional surface uplift during rifting (Cox, 1989; Thakur and Nagarajan, 1992), secondary mantle convection and magmatic underplating (Cox, 1980, 1993) have all been suggested as possible active rifting mechanisms for triggering denudation along the western margin of India. Uplift tends to precede active rifting (Summerfield, 1991a) so if active rifting is responsible for an increase in sediment flux, the age of the sediments should pre-date the Palaeocene. Passive mechanisms such as lithospheric delamination, lithospheric necking and denudationally driven isostatic rebound onshore (Widdowson, 1997; Widdowson and Cox, 1996; Widdowson and Mitchell, 1999) provide alternative mechanisms for generating sediment of Cenozoic age in response to rifting.

A second pulse in sedimentation began in the late Miocene yielding 124,500 km³ of clastic sediment (ie: Sequence IIIa and IV). It is difficult to envisage this younger phase being related to the initial surface uplift in response to rifting and an alternative mechanism is more likely. The very high late Miocene sedimentation rates in the Konkan-Kerala basin may reflect climate change as a consequence of the Asian monsoon which commenced around 7-8 Ma (Prell and Kutzbach, 1992; Quade et al., 1989). Late Cenozoic uplift coupled with climate change has also been postulated as a possible mechanism for extremely high rates of sedimentation throughout Asia (Metivier et al., 1999; Molnar, 2004; Molnar and England, 1990). However, the link between tectonic surface uplift and climate change is tenuous with the Himalaya reaching their current elevation much earlier at ca. 15 Ma (Harris, 1995). Thus a combination of several factors, such as collision-related surface uplift, climatic variations, flexural and isostatic rebound, and contributions from the recycling of earlier sediments from coastal basins (marine regressions have been common since late Miocene, see Figure 18), may be responsible for the increased post-Miocene sedimentation in the Konkan-Kerala Basin.

The syn-rift topography, the magnitude of post-rift denudation and the scale of the flexural isostatic response of the margin to sediment loading and denudational unloading are different for the conceptual models for the evolution of Western India. The present mass balance analysis provides information on the magnitude of denudation, making it possible to test the downwarp hypothesis. The downwarped rift flank model proposed by (King, 1967b; Ollier and Pain, 1997) incorporates a flexurally rigid lithosphere and as such only envisages small magnitudes of denudation, which is incompatible with the volume of clastic sediment present offshore. The downwarp model has been subsequently modified for the Deccan Volcanic Province to not only account for the monoclinial structure of this segment of the margin (Auden, 1949) but also to include ongoing post-rift flexural uplift (Widdowson, 1997; Widdowson and Cox, 1996). The question remains if this modified downwarp model also

applies to the segment of the margin south of the Deccan Volcanic Province. The volume of clastic sediment within the study area can only be accounted for if there is denudational isostasy, which in Figure 23B, is modelled as a component of the elevated rift flank model. However, sediment mass balance alone does not have the spatial resolution to differentiate between the elevated rift flank model and the modified downwarp model of Widdowson, (1997). The volume of clastic sediment could equally be explained by a denuded prism ~ 2 km thick similar to the modified downwarp model illustrated in Widdowson's (1997) figure 12.

The offshore sedimentary record and mass balance analysis only provide spatially averaged denudation rates which are strongly dependent on initial conditions and assumptions about the source area and sink area. Furthermore, the sparse data available for quantifying sediments offshore can only provide an approximate estimate of denudation onshore. Too fully to understand the evolution of the Western Indian PCM a more detailed picture of the spatial and temporal variability of denudation across the margin is required. Low temperature thermochronometry provides information on the thermal history of rocks in the upper crust and offers a complementary approach for refining constraints on the timing, magnitude and spatial variability of denudation. Low temperature thermochronometry is capable of resolving the spatial differences in denudation between the elevated rift flank model (greatest magnitude of denudation at the coast) and the modified downwarp model (greatest denudation at the escarpment). Chapter 3 outlines the theory and application of three low temperature thermochronometers, the zircon (U-Th)/He system, the apatite fission track system and the apatite (U-Th)/He system. Chapters 4 and 5 report the results and interpretation of such data for two field areas along the Western Indian margin, Goa and Karnataka, and Kerala.

One of the key components separating Ollier and Pain's (1997) downwarped rift flank model from the elevated rift flank model is that the latter includes flexural isostatic response to denudational unloading onshore and sediment loading offshore. Denudation of a downwarped lithospherically rigid crust onshore cannot generate the volume of sediment present in the Konkan-Kerala basin and a flexural isostatic response may be required. The theory and processes of lithospheric flexure are examined more fully in Chapter 6 to determine the role of flexural isostasy in the development of the Western Indian PCM.

3 Low temperature thermochronometry

3.1 Introduction

Radioisotopes were first used as a dating tool in earth sciences over a century ago (Rutherford, 1906) and the discipline of radioisotopic geochronology subsequently developed. The rationale for many geochronologic studies was to establish crystallization ages (and therefore magmatic or stratigraphic ages) of individual rocks. However, it became apparent that some isotopic systems produce ages much younger than the formation age established by other isotopic systems on the same sample (Hurley, 1954). Geochronologists were aware that these ‘young’ ages were not rock crystallization ages but a measure of other processes such as diffusion and thermal resetting (Damon and Kulp, 1957; Hurley, 1954; Musset, 1960). It was not until after the late 1960s that the isotopic systems the geochronologists were having problems with started to be utilised to establish the thermal histories of rocks, in effect, the birth of thermochronometry (Clark and Jäger, 1969; Dodson, 1973; Purdy and Jäger, 1976; Wagner et al., 1977).

All geochronometers track the passage of rocks through a particular isotherm (or range of isotherms), the temperature being dependent on the host mineral and the isotopic system. Above the closure temperature of the isotopic system, all the daughter elements produced by radioactive decay diffuse out of the mineral at a greater rate than they accumulate. Below the closure temperature of the isotopic system, the daughter elements are retained within the mineral (Dodson, 1973). In the case of fission track formation, above the closure temperature, track fading due to annealing occurs at a rate faster than the formation of new fission tracks but tracks are retained below the closure temperature. The isotopic ages produced by thermochronometers are therefore a function of the rocks thermal history. Thermochronometers have been used to constrain a range of geological processes such as slip rates of faults (Carter et al., 2006; Ehlers and Farley, 2003; Stockli et al., 2003; Tagami, 2005), topographic evolution (Braun, 2005; House et al., 2001), magmatic processes (Ehlers, 2005; Tagami and Shimada, 1996), sedimentation (Armstrong, 2005) and denudation (Kohn et al., 2005; Spotila, 2005). In order to relate the thermal histories traced by thermochronometers to particular geological processes, there must be an understanding of the processes which allow

daughter elements to accumulate and the thermal structure of the lithosphere (Braun et al., 2006).

Individual thermochronometers are sensitive to different temperature ranges and a variety of thermochronometers have been developed (Figure 25). Low temperature thermochronometry (LTT) has the potential to constrain smaller magnitudes of denudation and near-surface processes than do other radioisotopic methods such as U-Pb and K-Ar. LTT is thus more suited to studies of passive margin evolution because the magnitude of cooling is generally small. The more effective techniques for passive margin studies are: zircon (U-Th)/He (Reiners, 2005); apatite fission tracks (Brown et al., 2002b; Gallagher et al., 1994; Gunnell et al., 2003; Moore et al., 1986; Omar and Steckler, 1995); and apatite (U-Th)/He (Balestrieri et al., 2005; Persano et al., 2002; Persano et al., 2005). All these techniques provide chronometers of cooling that are less than 200 °C.

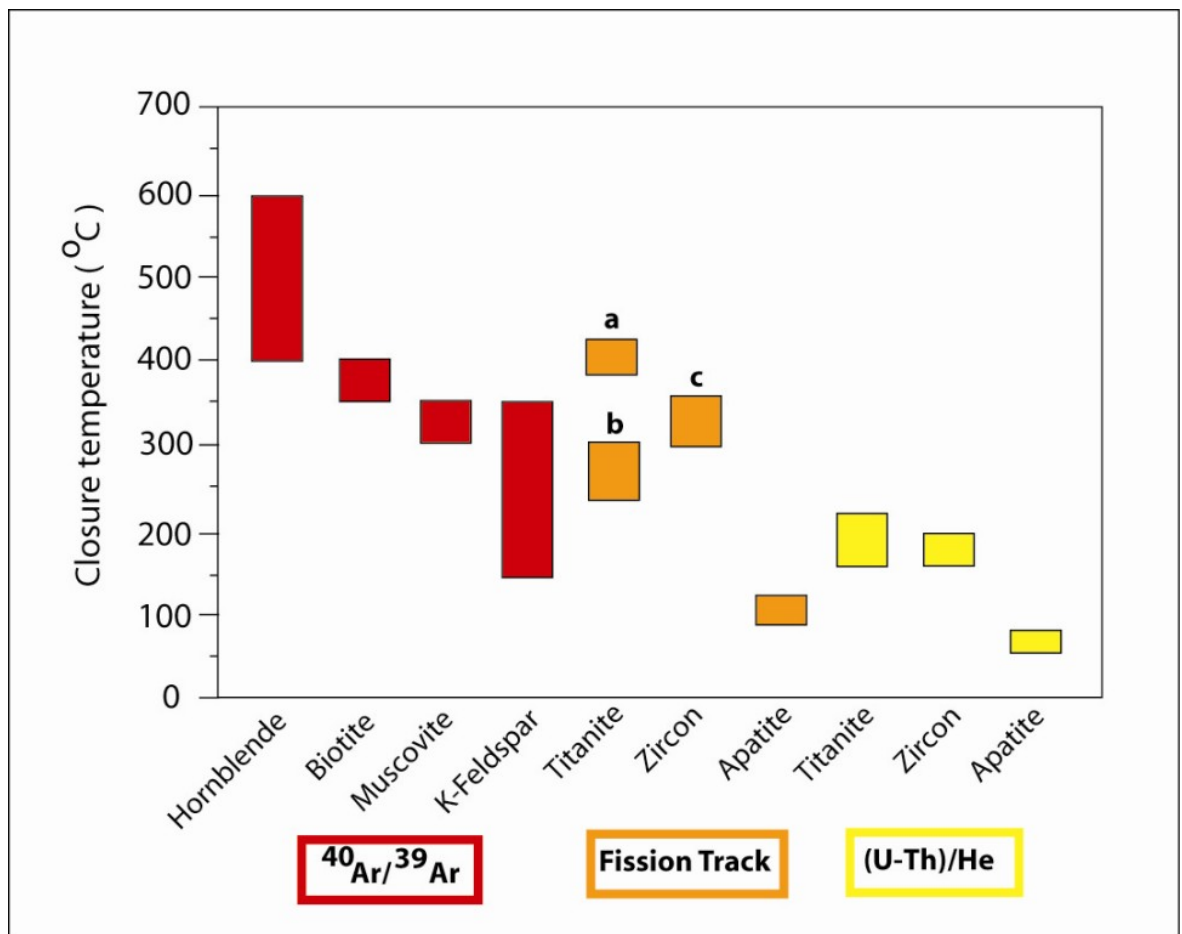


Figure 25 Closure temperatures for thermochronometric systems

$^{40}\text{Ar}/^{39}\text{Ar}$ - Hornblende (Dahl, 1996; Harrison, 1981), Biotite (Grove and Harrison, 1996; Harrison et al., 1985), Muscovite (Hames and Bowring, 1994), K-Feldspar (Lovera et al., 1997)
 Fission track – Titanite **a** (Coyle and Wagner, 1998) **b** (Naeser and Faul, 1967; Watt and Durrani, 1985), Zircon **c** (Tagami et al., 1998), Apatite (Ketcham et al., 1999; Laslett et al., 1987)
 (U-Th)/He – Titanite (Reiners and Farley, 1999), Zircon (Reiners et al., 2004), Apatite (Farley, 2000). Closure temperatures are for a cooling rate of 1-100 °C/ma

The Western Indian margin is almost completely devoid of stratigraphic markers, making reconstructing its origin, evolutionary history and vertical movements challenging (see Chapter 1). Western India does, however, show evidence of prolonged denudation since at least the emplacement of the Deccan Traps (Widdowson, 1997) and so low temperature thermochronometry has the potential to extract the denudational record. This chapter outlines the theory and application of three low temperature thermochronometers (apatite fission track, apatite (U-Th)/He and zircon (U-Th)/He) that have been used to constrain denudation for Western India. Chapters 4 and 5 outline the results and interpretations for two key field areas of the Western Indian margin: Goa and Karnataka, and Kerala (see Figure 4).

3.2 Apatite fission track thermochronometry

3.2.1 Introduction

The development of fission track thermochronometry began in the early 1960s with much of the pioneering work undertaken by Fleischer, Price and Walker (summarised by Fleischer et al. (1975)). Fission track thermochronometry (with apatite in particular) has advanced to become the most widely used technique for constraining low temperature thermal histories (see reviews by: Gallagher et al. (1998); Gleadow (2002); Hurford (1991); and Wagner and Van den Haute (1992))

Fission tracks form when heavy, radioactive nuclei decay and split, and the two positively charged fragments separate leaving a trail of damage within the crystal lattice of the host mineral. Although several radioactive isotopes undergo nuclear fission, ^{238}U occurs in sufficient concentrations in natural material and decays rapidly enough to dominate the production of fission tracks in naturally occurring minerals (Price and Walker, 1963). Unlike other isotopic systems, nuclear fission is unique in that there is no accumulation of an isotopic daughter product, only the accumulation of crystal damage in the form of latent fission tracks. Latent fission tracks are typically 10 – 20 μm in length and 4 – 10 nm in width (Tagami and O'Sullivan, 2005) and must be chemically etched to make them visible under an optical microscope.

The number of fission tracks preserved in a natural sample is dependent on the concentration of ^{238}U and the temperature history of the mineral. With apatite, latent fission tracks are only stable at moderately low temperatures (less than 60 $^{\circ}\text{C}$) and will anneal or shorten at a rate which is controlled by temperature, time and chemical composition of the host mineral (Fleischer et al., 1975). At temperatures greater than 110 $^{\circ}\text{C}$ fission tracks are thermally annealed as rapidly as they form and no fission tracks are preserved. At intermediate

temperatures between 110 °C and 60 °C fission tracks will only partially shorten or anneal. The annealing characteristics of fission tracks are a key property in their usefulness as a thermochronometer because different thermal histories produce distinctive ages and track length distributions. The temperature range over which fission tracks anneal over geological timescales has been termed the partial annealing zone (Gleadow and Fitzgerald, 1987; Laslett et al., 1987).

Apatite fission track samples from Western India were prepared using standard heavy mineral separation procedures (see section A.1). Apatite crystals from the separates were mounted in epoxy resin on a glass slide and prepared for analysis using the external detector method (Hurford and Green, 1982) (see section A.2).

3.2.2 AFTT annealing kinetics

Fission tracks in apatite only remain stable at less than ~110 °C over timescales of 10^6 - 10^7 yrs (for typical Durnago apatite) and will shorten or anneal at a rate which is controlled by time, chemical composition (Barbarand et al., 2003a; Barbarand and Pagel, 2001; Carlson et al., 1999; Crowley et al., 1991; Donelick, 1991; Gleadow and Duddy, 1981; Green et al., 1986; Green et al., 2005; Green et al., 1989; O'Sullivan and Parrish, 1995), track orientation (Donelick, 1991; Donelick et al., 1999; Green et al., 1986), alpha particle damage (Hendriks and Redfield, 2005) and possibly pressure (Kohn et al., 2003; Wendt et al., 2002, 2003); however, the primary control on fission track annealing is temperature (Fleischer et al., 1975). The annealing kinetics of fission tracks have been studied using laboratory induced tracks and extrapolating the result to natural tracks annealing on geological timescales (Carlson et al., 1999; Crowley et al., 1991; Donelick et al., 1990; Green et al., 1986), and natural tracks with established cooling histories such as boreholes (Gleadow and Duddy, 1981; Naeser and Forbes, 1976). From these studies it is now possible to, at least empirically, relate the formation and subsequent annealing of fission tracks to temperature.

It has been intimated that fission track annealing kinetics may be partly controlled by temperature and stress (Wendt et al., 2002, 2003). Experiments conducted on spontaneous tracks over laboratory temperature and time scales suggest that fission track annealing rates are reduced with increasing pressure. However, the experimental design and implementation has been severely criticised (Donelick et al., 2003; Kohn et al., 2003). Radiation damage from spontaneous α -particle decay is another possible mechanism effecting annealing kinetics, and it has been suggested that α -particle decay enhances apatite defect recovery (Hendriks and Redfield, 2005). AFTT ages that are 'too young' (relative to apatite (U-Th)/He ages), and the apparent negative correlation between the concentration of ^{238}U with the age of AFTT samples

from Fennoscandia have been used as evidence to support radiation enhanced annealing (Hendriks and Redfield, 2005; Lorencak, 2003; Murrell, 2003). However, radiation enhanced annealing does not seem to be a significant processes for anomalously young AFTT ages from other stable cratonic environments (e.g. Canadian, Australian or Brazilian Shields) (Kohn et al., 2006). Enhanced helium retention resulting in anomalously old apatite (U-Th)/He ages (rather than anomalously young AFTT ages) has also been proposed as an alternative mechanism (Green et al., 2006; Green and Duddy, 2006; Shuster et al., 2006).

Chemical composition influences the rate at which fission tracks anneal, and it has been demonstrated that fluorine-rich apatites tend to be less resistant to annealing than chlorine-rich apatites (Carlson et al., 1999; Green et al., 1986; Green et al., 1989). It is becoming increasingly common to measure either Cl wt % or Cl apfu to account for kinetic variability within an apatite population and incorporate the kinetic information into the modelling of data. However, the rate at which fission tracks anneal is controlled by a complex range of chemical substitution (Mn, Sr, Fe, OH and REE), not just Cl and F (Barbarand et al., 2003a; Barbarand and Pagel, 2001; Carlson et al., 1999). Different chemical substitutions will result in apatite structural variability and consequently will alter apatite solubility (Barbarand et al., 2003a) therefore, an alternative approach that accounts for kinetic variability is to measure etch pit width (D_{par}) (Donelick, 1993; Ketcham et al., 1999). Figure 26 summarises the effect of kinetic variability within apatites held at different temperatures (110 °C – 70 °C) for different times (10 Ma – 100 Ma). Kinetic variability is represented by different values of D_{par} which can be correlated with Cl wt % (Carlson et al., 1999; Donelick et al., 2005) but is also influenced by other apatite crystallographic properties (Donelick et al., 2005). To account for different annealing rates (and hence different ages) as a direct result of kinetic variability within a single apatite population, this project incorporates D_{par} values into the modelling of data (see section 3.2.5.2). Samples containing apatite grains that are less resistant to annealing (small D_{par} values) experience total annealing at lower temperatures, whereas samples containing apatites that are more resistant to annealing (large D_{par} values) experience total annealing at higher temperatures (Ketcham, 2005). Apatite grains with a D_{par} value of 1.50 μm will completely annealing at 100 °C, apatite grains with a D_{par} value of 3 μm will completely anneal at 160 °C (Ketcham, 2005).

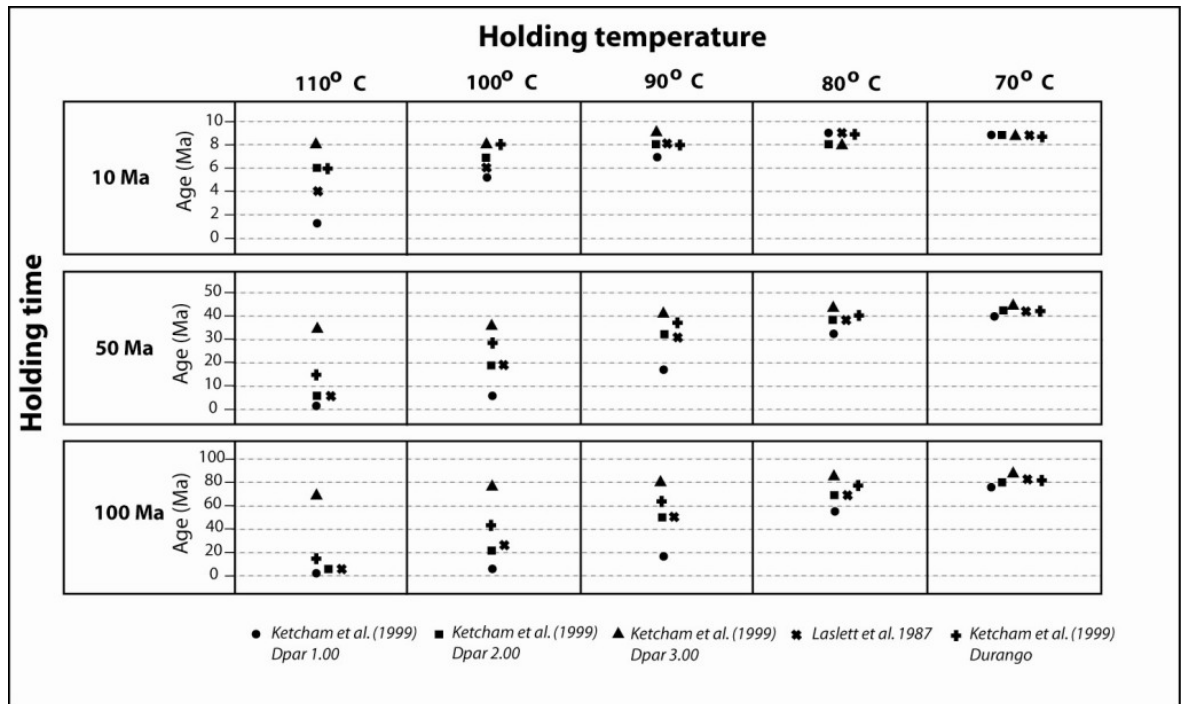


Figure 26 Synthetic AFTT ages for apatites with different chemical compositions

AFTT ages modelled using HeAFTy (Ketcham, 2005). The spread in AFTT ages is greatest for longer holding times and deeper levels within the AFTT PAZ.

Fission tracks also anneal at a rate which is partly controlled by crystal structure; fission tracks formed at high angles to the c-axis anneal faster than fission tracks formed at low angles to the c-axis (Donelick, 1991; Donelick et al., 1999; Green et al., 1986). The variation in annealing as a consequence of their angle to the c-axis can be corrected for using the c-axis projection method described by Ketcham (2005).

Latent fission tracks are chemically etched to make them visible under an optical microscope; however, the degree of track revelation is dependant on: the strength of the etchant, the temperature during etching, etch time, apatite chemistry and apatite crystal structure. Ideal etch times for track revelation have been determined from step etch experiments (Barbarand et al., 2003b; Crowley et al., 1991; Laslett et al., 1984; Watt and Durrani, 1985) and two well established protocols are now in general use, a ‘strong etch’ (5 M HNO₃, 20s at 20°C ±1 °C) and a ‘weak etch’ (0.8 M HNO₃, 45s at 21°C). (Barbarand et al., 2003b) found that the weak etch results in more isotropic revelation of tracks (i.e. with respect to angle to the crystallographic c-axis) but tracks are more challenging to define and c-axis parallel sections of crystals are more difficult to locate, the authors therefore advocate the use of the strong etch. Ravenhurst et al. (2003) found that although etch pit morphology is affected by the type of chemical etch, track anisotropy appears to be unaffected. Specific etching protocols have been used to develop the different annealing algorithms used to model AFTT data; therefore, to justify the use of a particular annealing model, identical etching protocol should be adhered to. AFTT data from Western India was modelled using HeFTy (Ketcham, 2005), software

developed for multi-kinetic modelling of low temperature thermochronological systems. AFTT samples from Western India were etched using 5 M HNO₃ for 20s at 21°C, identical to the etching protocol used to calibrate HeFTy.

3.2.3 Calculating AFTT ages

Full details on the derivation of the fission track age equation can be found in Section B.1, the standard age equation is:

$$t = \frac{1}{\lambda_{\alpha}} \ln \left\{ 1 + \lambda_{\alpha} \zeta \rho_D \left(\frac{\rho_s}{\rho_I} \right) G \right\}$$

Equation 2

where ζ is the empirically obtained zeta-calibration (see Section B.2) and ρ_D is the induced fission track density of a U-doped standard glass irradiated with the sample. Spontaneous fission tracks are sourced from both above (now polished away) and below the polished surface whereas induced tracks are only sourced from below the polished surface; therefore, a geometry factor of 0.5 is required (G). The spontaneous and induced track densities are ρ_s and ρ_I respectively.

In order to calculate a fission track age, ρ_s , ρ_I and ρ_D must be determined. The density of spontaneous tracks is normally calculated by counting the number of tracks that intersect the polished etched surfaces of twenty or more grains selected at random using an optical microscope (~1250 x magnification). Suitable grains must have well-polished surfaces with few crystal defects and well-revealed fission tracks with etch pits aligned parallel to the crystallographic c-axis (i.e. prismatic sections). The density of induced tracks is calculated by counting the number of tracks that intersect the etched surface of the detector using the prints of the same grains and equivalent area. The density of the standard U-doped glass used to determine the neutron flux for a particular irradiation is calculated by counting the number of tracks over a fixed area (~ 300,000 μm^2) for glasses at the top and base of the stack of samples (each with its own external detector). The densities are then linearly interpolated for the position of the sample within the stack to account for any gradient in the neutron flux density created between the top and base of the stack during irradiation.

3.2.4 Fission track confined track length distributions (TLD's)

The etching process used to expose fission tracks for age measurements also reveals tracks that are entirely confined within the host crystal. The etchant reaches these tracks either via an existing etched fission track (TINTs – Track IN Track) or via cracks and cleavages (TINCLES – Track IN CLEavage). Fission tracks form at a continuous and predictable rate determined by the fission of ^{238}U therefore each fission track forms at a different time and is exposed to a different segment of the host crystals complete thermal history. Younger tracks will always be longer because they have experienced less annealing compared to older tracks tend to be shorter. The confined track length distribution (TLD) consequently provides valuable information on the thermal history the host crystal has experienced (Gleadow et al., 1986; Green et al., 1989).

The initial length of a fission track that has not undergone any partial annealing has been determined from the length of induced tracks and is approximately 16.3 μm for Durango apatite (Laslett et al., 1987). However, the initial length of spontaneous tracks tends to be ~ 10 % shorter and it has been demonstrated that a degree of partial annealing occurs at ambient temperatures ~ 20 °C (Corrigan, 1993; Donelick et al., 1990; Ketcham et al., 1999). Defining the initial track length is important because it is a key parameter required for inversely modelling of AFTT data (see section 3.2.5.2).

Typically, the lengths of 100 confined tracks are measured to obtain track length distributions, with the mean, standard deviation and a histogram of track lengths being reported. Confined tracks are measured on grain sections oriented parallel to the crystallographic c-axis. It has been demonstrated that the annealing rate of fission tracks is anisotropic, with tracks perpendicular to the c-axis annealing more rapidly than tracks parallel to the c-axis particularly when there has been a large degree of annealing (Donelick, 1991; Donelick et al., 1999; Ketcham et al., 2003). To reduce the effect of this anisotropy, the angle to the c-axis for each confined track is also measured and a projection factor is applied (Ketcham et al., 2003).

3.2.5 Interpreting AFTT data

The apatite fission track system is sensitive to temperatures occurring in the upper few kilometres of the lithosphere, making it a useful technique for absolute dating of volcanic igneous rocks, sedimentary basin evolution, provenance studies, and long term landscape evolution in both active and passive tectonic settings (Brown et al., 1994; Gallagher et al., 1998; Gleadow, 1990; Gleadow et al., 2002). Although the apatite fission track system can be applied as an absolute dating tool, the power of the technique comes from the annealing

properties of fission tracks and the fact that annealing occurs over a large temperature range (60 – 110 °C). Commonly the AFTT age and TLD are the product of a particular thermal history and not a measure of an absolute geological event.

3.2.5.1 AFTT age profiles and TLDs

An apparent fission track age (as opposed to an absolute age) is best illustrated through the concept of a fission track ‘stratigraphy’ (Brown, 1991; Gleadow, 1990) or fission track age profile developed within a borehole in a tectonically stable region (Brown et al., 1994). Temperature increases with depth within the lithosphere and consequently the fission track age will decrease, and the TLD will become progressively shorter, with depth. Above a critical temperature (~ 120 °C for apatite) complete fission track annealing occurs, the system is reset and the apparent age is zero. Between 110 °C and 60 °C partial shortening of fission tracks occurs at a rate controlled by temperature, this temperature range being termed the partial annealing zone or PAZ (Gleadow and Fitzgerald, 1987). At shallower depths, less than 60 °C, little annealing occurs and the apparent age will be the oldest (Figure 27).

For a given section of crust, the shape of a fission track age profile depends on both the period of time the region has been stable and the denudation rate (Brown et al., 1994). If the denudation rate is negligible, and prior to the establishment of the age profile all ages were zero, then the age of the shallowest sample reflects the time the region has been stable for and ages become younger with depth. If the period of landscape stability is increased then the age of the shallowest sample will be greater and the entire age profile will be broadened (Figure 28a). If the denudation rate is increased then the fission track age profile becomes progressively smoother and changes from a concave up profile to a linear profile. The gradient of the linear profile approximates the denudation rate and the age of each sample roughly corresponds to the time of passage through the 110 °C isotherm (Figure 28b).

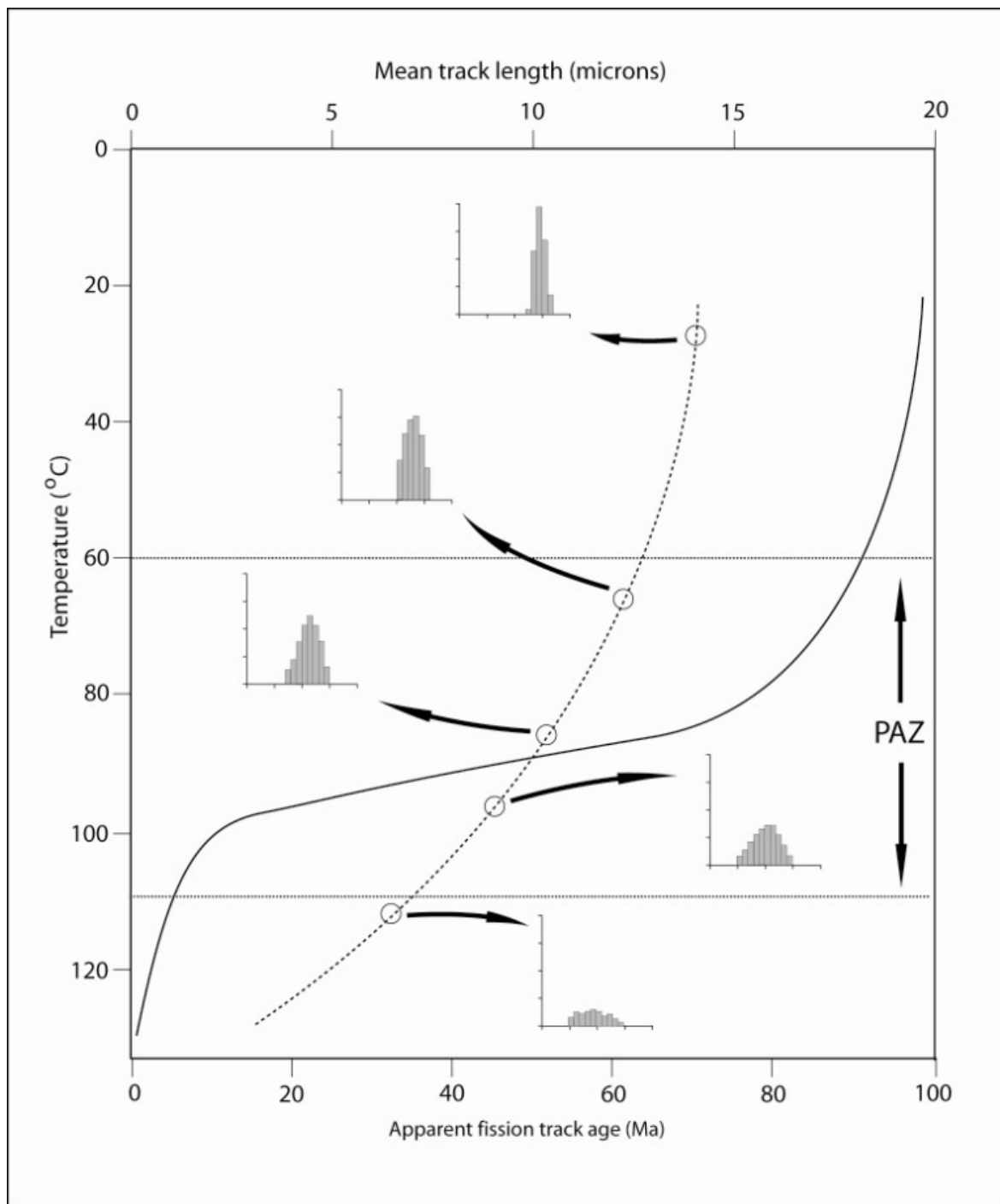


Figure 27 AFTT ages and TLD's within a hypothetical borehole

Variation in fission track age (solid line) and, track length distribution TLD: (dashed line) with temperature for a hypothetical borehole. Fission track age decreases with increasing temperature forming the partial annealing zone. TLD becomes progressively shorter and broader with increasing temperature.

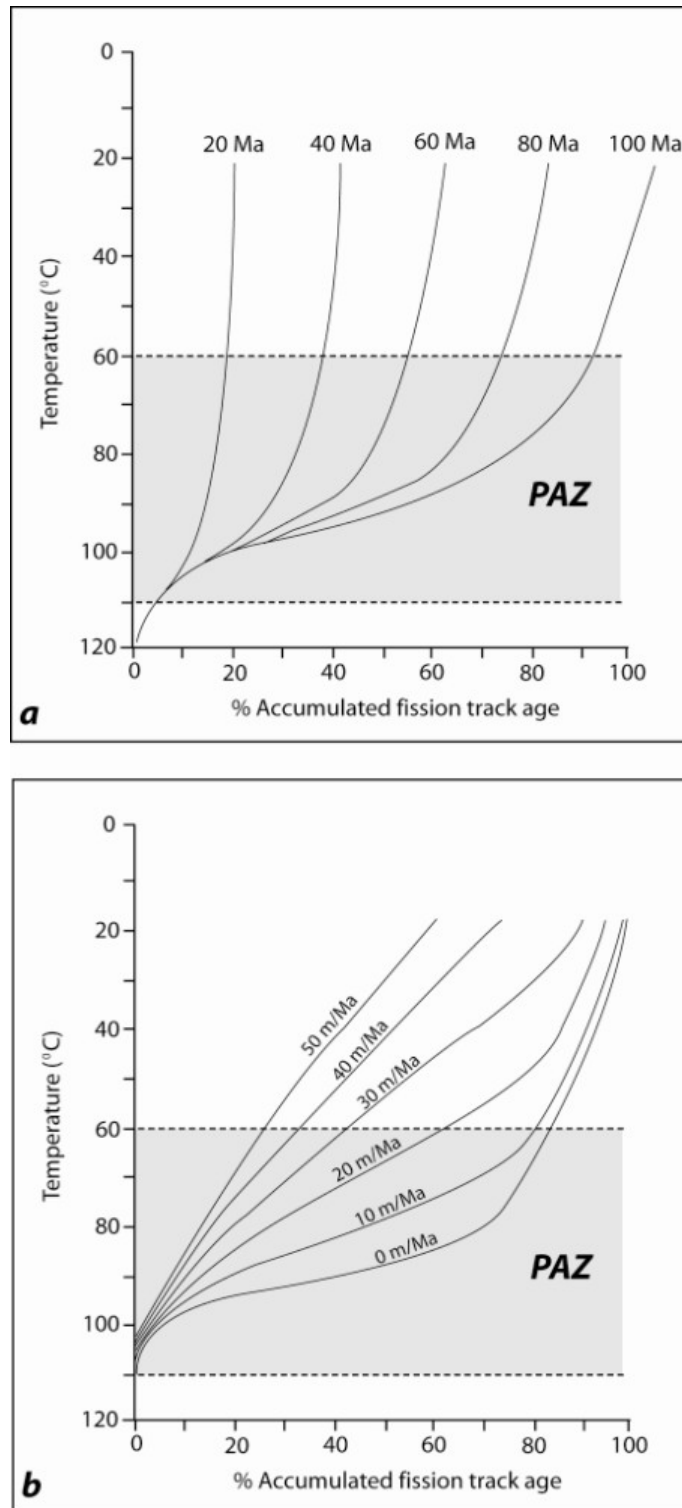


Figure 28 The apatite fission track age profile

a) Evolution of the apatite fission track partial annealing zone with time (adapted from (Brown et al., 1994)).

b) Relationship between fission track age, temperature and denudation rate (adapted from (Brown et al., 1994)).

If, after the development of a fission track age profile, there is a period of increased denudation then it is possible for the PAZ to be exhumed and exposed. This fossil PAZ may be preserved and a new PAZ will develop beneath it. The break in slope separating the fossil PAZ from the

newly developed PAZ corresponds to the timing of the exhumation of the fossil PAZ. Prior to exhumation, all the samples below the fossil PAZ were at >110 C and completely reset, and only accumulate fission tracks after exhumation. Samples within the fossil PAZ accumulate and retain fission tracks but each track will be annealed by different amounts depending on its temperature and duration within the PAZ, and therefore display older ‘mixed’ ages (Figure 29).

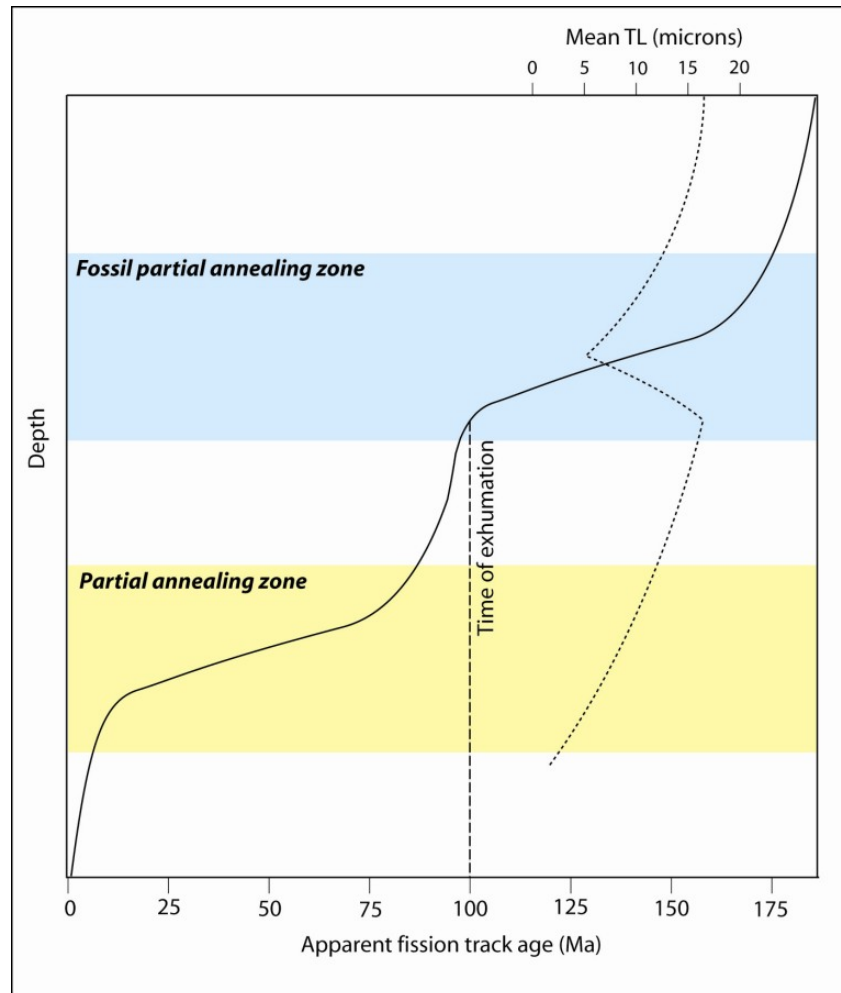


Figure 29 The PAZ and the fossil PAZ

Exhumed fission track partial annealing zone and existing partial annealing zone. The break in slope marks the time of exhumation. The solid line illustrates the decrease in age with depth, the dashed line illustrates the change in mean track length with depth (see text for explanation).

The relationship between fission track age and track length distribution is illustrated in Figure 30, which displays three hypothetical thermal histories with their corresponding AFTT ages and TLDs. Thermal history (a) undergoes rapid cooling through the PAZ at ~ 100 Ma and remains cool until time zero. Few tracks accumulate within the PAZ, the age approximates the cooling event and none of the tracks thermally anneal so the TLD is narrow and dominated by long tracks. Thermal histories (b) and (c) spend increased amounts of time within the PAZ so a proportion of their tracks are annealed resulting in a younger apparent fission track age.

Although thermal histories (a) and (b) cannot be differentiated on the basis of age alone, the annealing has produced different track length distributions. Simple thermal histories display simple TLDs, more complex thermal histories produce more intricate TLDs.

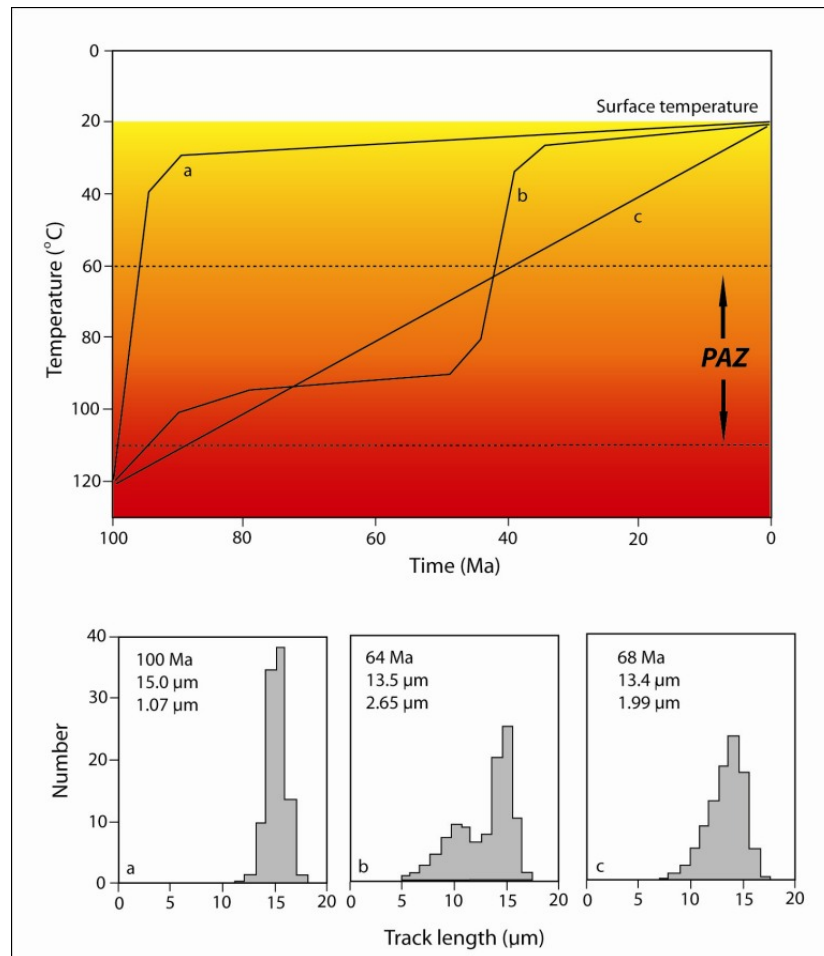


Figure 30 Relationship between AFTT age and TLD for evolving thermal histories

Three different fission track ages and track length distributions (bottom) produced from three hypothetical thermal histories (top) (adapted from (Gleadow and Brown, 2000)). Thermal history (a) rapid cooling at ~ 100 Ma produces an AFTT age of 100 Ma and a narrow, unimodal, long TLD. Thermal history (b) produces an AFTT which is a combination of rapid cooling at ~ 45 Ma and a prior history in the PAZ. The TLD is broad and bimodal, composed of long tracks produced during the 45 Ma cooling and short tracks produced and partially annealed as a consequence of residence time in the PAZ. Thermal history (c) monotonic cooling through the PAZ produces a similar age to thermal history (b) but a different TLD. All ages and track length distributions modelled using HeFTy (Ketcham, 2005).

3.2.5.2 Forward and inverse-modelling of AFTT data

AFTT thermochronometry is particularly effective for constraining the thermal histories of the upper few kilometres of the lithosphere because of the information provided by the combination of AFTT age and TLD data. However, to make the link between a specific thermal history and AFTT data, there must be an understanding of the kinetics of AFTT annealing. The kinetics of apatite fission track annealing have been studied extensively and a number of models have been developed (Carlson, 1990; Crowley et al., 1991; Donelick et al.,

2000; Green et al., 1989; Ketcham et al., 1999; Laslett et al., 1987). Such annealing algorithms have been used to provide forward models that predict the AFTT age and TLD for a particular thermal history. The modelled data can then be compared with data to test hypotheses.

Forward modelling is particularly useful for confirming how effective the various annealing algorithms are: However, as a predictive tool for extracting thermal history data, it can be time consuming. Consequently, numerical models have also been developed which inversely model fission track data to produce a the range of thermal histories that statistically fit the data (Gallagher, 1995; Ketcham et al., 2003). Due to an incomplete understanding of annealing kinetics, analytical uncertainty and the inherent non-uniqueness of a particular data set, inverse-modelling usually results in an envelope of thermal histories which must then be interpreted in a geological context. There are two main software packages available for inversely modelling AFTT data: MonteTrax (Gallagher, 1995) and HeFTy (Ketcham et al., 2003). MonteTrax uses a genetic algorithm which is a particularly efficient search procedure for extracting thermal histories, whereas HeFTy uses a Monte Carlo simulation to search for suitable thermal histories. HeFTy is used throughout this project for modelling AFTT data because the software is capable of incorporating a kinetic parameter (D_{par}) and a correction for track lengths that are not parallel to (but still in the plane of) the c-axis (see section 3.2.2).

Not all data are suitable for inverse-modelling, particularly if the spread in ages on individual grains from the same samples does not adhere to a Poission distribution. Variations in chemical composition (between grains) and different provenance sources can result in non-Poissionian distributions, but whatever the reason, such samples should be identified and rejected for inverse-modelling. The chi-square test is routinely applied in fission track studies to determine the homogeneity of a particular sample and is then assessed by calculating a corresponding p-value. In general p-values less than 0.05 are taken as evidence that a sample is not normally distributed and should not be inversely modelled. Chi-squared values and p-values are quoted for this project and only samples where the p-value exceeds 0.05 are considered for inverse-modelling.

3.3 (U-Th)/He thermochronometry

3.3.1 Introduction

The discovery that isotopes of uranium and thorium are radioactive and decay and produce helium initiated the start of geochronological dating (Rutherford, 1904; Strutt, 1908). However, the poor retention of He within many minerals meant that the system was of little use to geochronologists who were seeking absolute ages for the formation of rocks, and

development of the technique ceased (Hurley, 1954). Renewed interest in the (U-Th)/He system commenced three decades later when it was recognised that the loss of helium from apatite at temperatures below that of mineral crystallization could be used advantageously to constrain low temperature cooling (Zeitler et al., 1987). Quantification of the diffusion rate of helium from apatite has resulted in the establishment of the apatite (U-Th)/He system as an important low temperature thermochronometer (Farley, 2000; Farley and Stockli, 2002; Wolf et al., 1996).

A number of minerals contain suitable concentrations of uranium and thorium to produce measurable amounts of helium and thus have the potential to be utilised for (U-Th)/He dating. The accessory minerals apatite, and to a lesser extent zircon, are common in many lithologies, and have proved to be of great value for low temperature thermochronometry (Farley, 2002). The closure temperature of apatite is ~ 70 °C (Farley, 2000; Wolf et al., 1996), making it the lowest temperature thermochronometer in use. Zircon retains helium at higher temperatures, ~ 180 °C (Reiners et al., 2002). The following sections focus on the mechanism for the accumulation and loss of helium, obtaining (U-Th)/He ages and interpreting these ages for apatite and zircon.

3.3.2 (U-Th)/He ages

The (U-Th)/He age is controlled by the balance between the accumulation of radiogenic ^4He and the loss of ^4He . The accumulation of helium depends on the rate of production of helium and the concentration of U and Th within the host mineral. The loss of ^4He occurs via two mechanisms: 1) diffusion, which is controlled by temperature, time and the retentive properties of the host mineral; and 2) alpha ejection (section 3.3.2.3), which is controlled by the geometry of the host mineral, distribution of the parent elements and the stopping distance of He. The accumulation of He and loss of He are the focus of this section.

3.3.2.1 The accumulation of helium

^4He is produced via a chain of reactions when ^{238}U , ^{235}U , ^{232}Th and ^{147}Sm decay to ^{208}Pb , ^{207}Pb and ^{206}Pb . Except in rare circumstances, the abundance of ^{147}Sm is too low to produce a significant contribution to the total ^4He content. Helium production within a mineral can be defined by the following equation:

$$^4\text{He} = 8 \times ^{238}\text{U} (e^{(\lambda^{238}t)} - 1) + 7 \times \frac{^{238}\text{U}}{137.88} (e^{(\lambda^{235}t)} - 1) + 6 \times ^{232}\text{Th} (e^{(\lambda^{232}t)} - 1)$$

Equation 3

where ${}^4\text{He}$, ${}^{238}\text{U}$ and ${}^{232}\text{Th}$ are the measured concentrations, λ s are the decay constants for the different isotopes and t is the time (years). It is not necessary to measure the concentration of ${}^{235}\text{U}$ because the ${}^{238}\text{U}/{}^{235}\text{U}$ ratio is constant (1/137.88). The decay constants of ${}^{238}\text{U}$, ${}^{235}\text{U}$ and ${}^{232}\text{Th}$ are $1.55 \times 10^{-10} \text{ yr}^{-1}$, $9.85 \times 10^{-10} \text{ yr}^{-1}$ and $4.95 \times 10^{-11} \text{ yr}^{-1}$ respectively. The following assumptions must be made when calculating the amount of ${}^4\text{He}$. The parent isotope decay chains are in secular equilibrium. There is no initial ${}^4\text{He}$ in the crystal and the only source of ${}^4\text{He}$ is from the decay of U and Th (Sm contribution is insignificant). All ${}^4\text{He}$ is retained within the crystal lattice below the closure temperature.

3.3.2.2 The diffusive loss of helium

Diffusion is the net transport of material across a concentration gradient and is controlled by the atomic structure within which the material is being transported, the dimensions of the diffusive domain and the activation energy required to transport the material. The rate of diffusion is thermally-controlled (Walker, 2002), exponentially dependent on temperature and follows an Arrhenius relationship where:

$$\frac{D(T)}{a^2} = \frac{D_o}{a^2} e^{-E_a/(RT)}$$

Equation 4

where $D(T)$ is the diffusivity at temperature T (K) and a is the diffusion domain. The constants D_o , E_a and R are the diffusivity at infinite temperature, the activation energy and the gas constant. Each isotopic system and mineral will have specific values for D_o , E_a and a which define the diffusivity at a particular temperature. The higher the temperature, the higher the probability that a daughter atom will have enough energy to escape the mineral lattice and diffuse such that at high temperatures the system is effectively open and no daughter product will be retained. At low temperatures, diffusivity is so slow that any daughter product effectively remains within the host mineral. The temperature at which the transition from diffusive loss to accumulation occurs is defined as the blocking temperature (Dodson, 1973). However, parent-daughter isotope systems do not instantly switch from being open to closed but have a range of temperatures over which there is partial retention of the daughter product. At high temperatures diffusion exceeds accumulation, at moderate temperatures they become balanced, and at low temperatures diffusion exceeds accumulation. The isotopic age is

therefore a combination of daughter product accumulation when the system was fully closed combined with daughter product accumulation when the system was partially open. For constant monotonic cooling the isotopic age can be related to the closure temperature (Dodson, 1973) (see Figure 31)

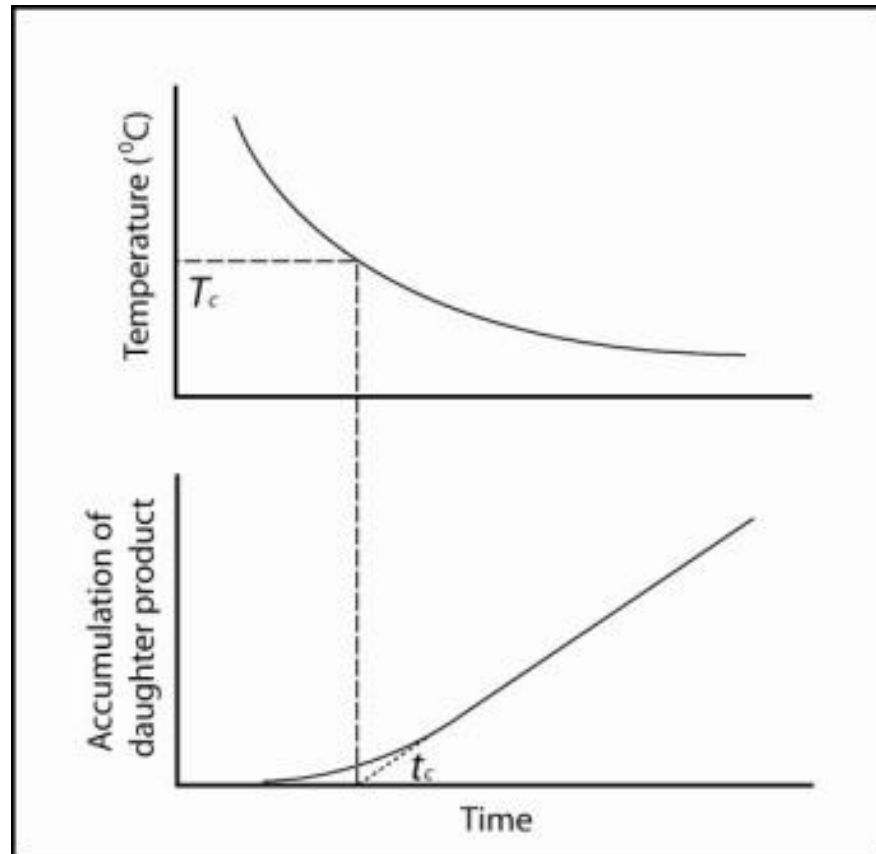


Figure 31 The concept of closure temperature

Adapted from (Harrison and Zeitler, 2005).

Incremental release of He from crystals by heating can be used to calculate the parameters for the Arrhenius relationship which can then be extrapolated to geological timescales provided the relationship holds over a range of temporal scales. If thermally-activated, volume-controlled diffusion is the dominant process, then data will form a straight line on an Arrhenius plot (Figure 32), where the y intercept is the log of the diffusion coefficient (D_0) and the gradient is related to the activation energy (E_a). From these parameters it is possible to calculate the closure temperature:

$$\frac{E}{RT_c} = \ln \left(\frac{ART_c^2 D_0 / a^2}{EdT/dt} \right)$$

Equation 5

where A is a geometric constant for the shape of the diffusion domain and T_c is the closure temperature which can be solved iteratively. For a given mineral chronometer, the closure temperature is dependent on the geometry and size of the diffusion domain, and the rate of cooling.

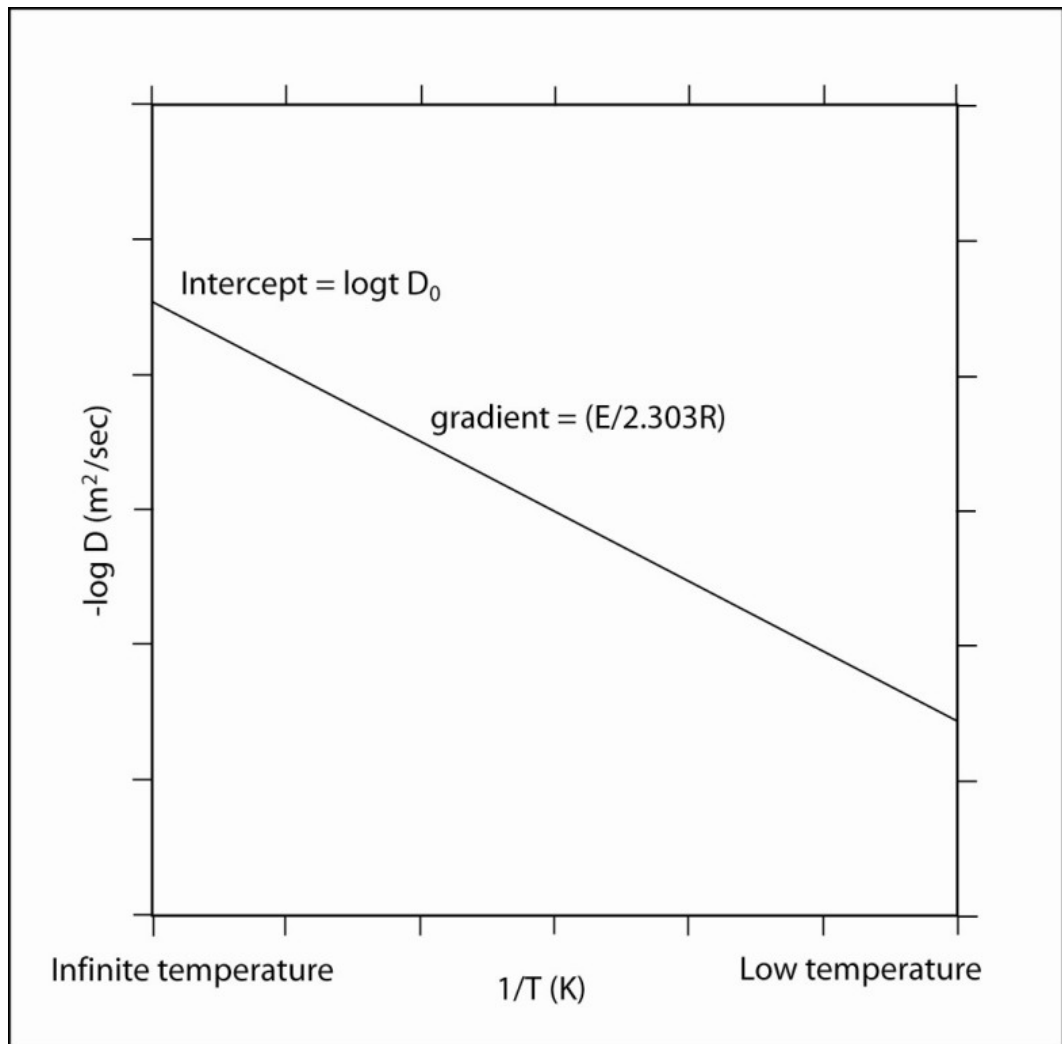


Figure 32 The Arrhenius relationship

Using the Arrhenius relationship to extract the diffusion coefficient and the activation energy (Harrison and Zeitler, 2005).

Incremental heating extraction of He from Durango apatite shows that thermally-activated diffusion is the dominant process (Farley, 2000). Arrhenius plots also indicate that diffusion varies with crystal volume (larger crystals are more retentive) implying that the diffusion domain is the whole crystal (Figure 33). The closure temperature also increases with increasing cooling rate (Figure 34) (Reiners and Farley, 2001). The closure temperature for apatite is ~ 70 °C for a 100 μm diameter grain (although T_c varies slightly with grain size) and the partial retention zone (PRZ) ranges from 70 °C to 40 °C in Durango apatite (Farley, 2000). The closure temperature concept, although useful, is only applicable when a sample has cooled

rapidly and monotonically. For more complex thermal histories, it is necessary to forward-model the data (see section 3.3.4.2).

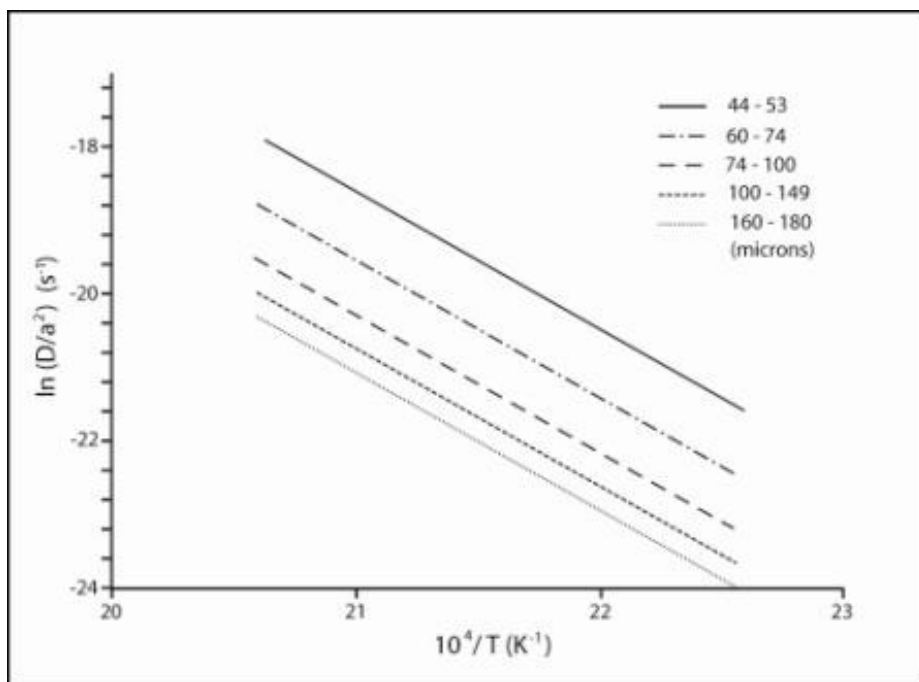


Figure 33 Linear Arrhenius plots

Linear Arrhenius plots for Durango apatite indicating that the diffusion domain is the grain size. Different lines are different grain sizes (adapted from (Farley, 2000)).

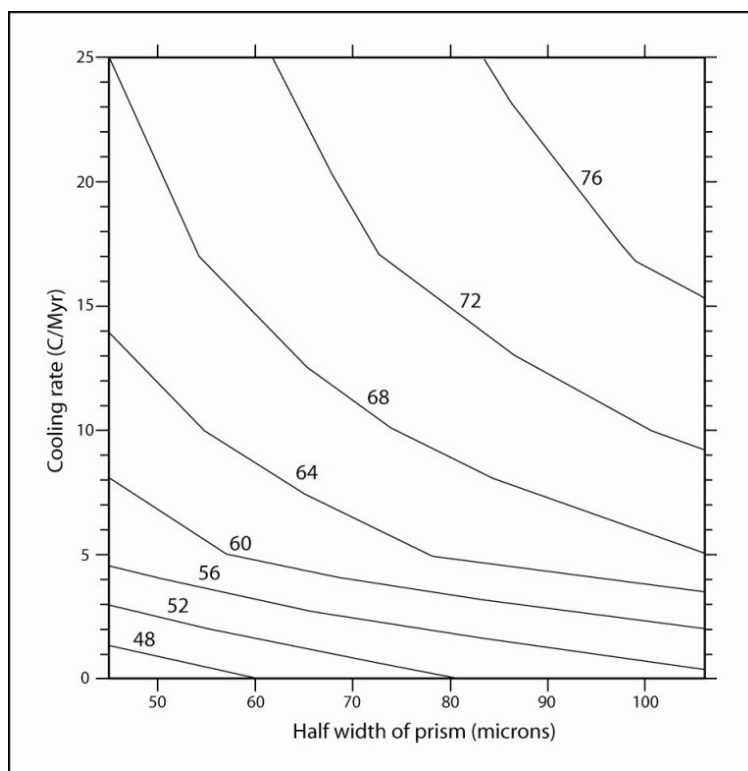


Figure 34 The relationship between grain size, cooling rate and closure temperature

The number marking the liens are closure temperatures for Durango apatite (adapted from (Farley,

2000).

Helium diffusion in zircon tends to be more complex than in apatite. Diffusion experiments show that zircon does not display a simple Arrhenius relationship, possibly as a result of α -damage or because there may be multiple diffusion domains of differing size within crystals (Reiners, 2005; Reiners et al., 2002; Reiners et al., 2004). Although diffusive behaviour in zircon is more challenging to understand, the closure temperature is estimated to be approximately 180 °C (Reiners et al., 2002; Reiners et al., 2004).

3.3.2.3 Alpha ejection

As well as diffusion, helium can also be lost from the host crystals via alpha ejection during radioactive decay. Helium atoms are ejected a distance that depends on both the crystal structure (primarily density) and the energy provided by the decaying parent isotope. The stopping distance from the decay of uranium and thorium for helium in apatite and zircon are summarised in Table 3. These stopping distances cause depletion in the concentration of helium at crystal boundaries (within one stopping distance) because a proportion of helium is ejected out of the crystal (Figure 35). Farley et al. (1996) describe a numerical solution that accounts for the ejection of helium and ‘corrects’ the (U-Th)/He age. The method requires knowledge of the α -stopping distance and the surface-to-volume ratio of the crystal. The α -ejection correction factor F_t is:

$$F_t = 1 + a_1\beta + a_2\beta^2$$

Equation 6

Where a_1 and a_2 are numerical parameters for the parent elements and β is a geometry factor controlled by the crystal shape and surface/volume ratio. The F_t correction is calculated for each crystal analysed in an aliquot and the mean (weighted against the crystal size) is applied to the age. When applying the alpha recoil correction, several assumptions must be made, namely, that implantation of ^4He is insignificant and need not be accounted for, U and Th are homogeneous in the crystal, and alpha recoil is unrelated to diffusion (but the correction is only strictly applicable for rapidly cooled samples, see section 3.3.4.2).

	Apatite	Zircon
^{238}U averaged (μm)	19.68	16.95
^{235}U averaged (μm)	22.83	19.64
^{232}Th averaged (μm)	22.46	19.32

Table 3 Averaged α -stopping distances for apatite and zircon

Data from Farley (2002)

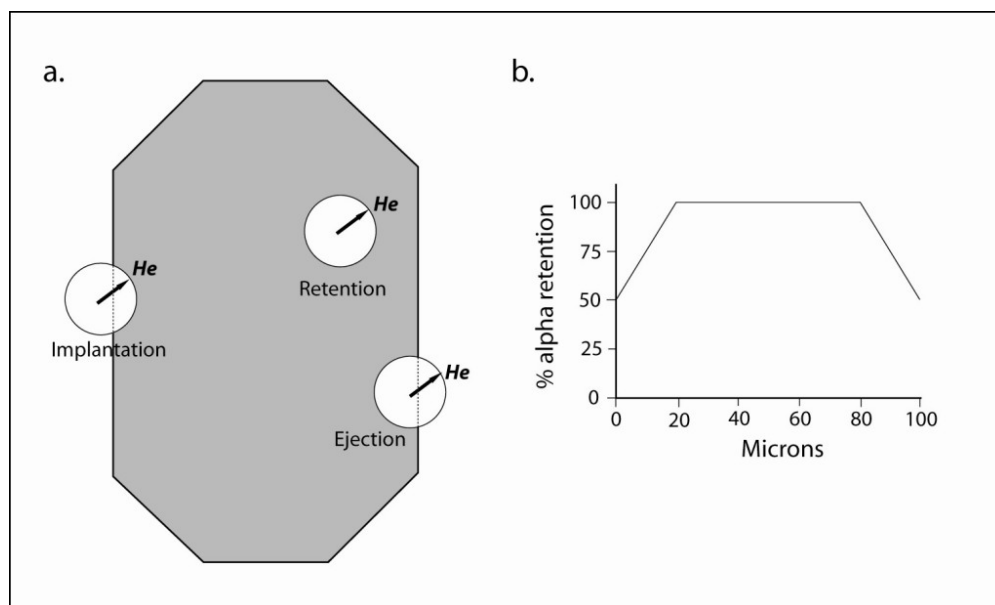


Figure 35 Alpha particle ejection

a. Three possibilities for a He atom produced via decay of U or Th: Retention, ejection or implantation. B. Relationship between the % of alpha particle retention and position within the apatite crystal. The % retention is a minimum at the crystal boundaries (50 %) increasing to a maximum (100 %) within one stopping distance at $\sim 20 \mu\text{m}$ (adapted from (Farley, 2002))

3.3.3 Analytical procedure

Standard rock crushing and heavy liquid techniques are employed to produce a concentrated mineral separate. Grains are then individually hand selected to insure that they are free from inclusions and crystal defects to preclude the chance of measuring parentless helium. Helium extraction was undertaken initially using an ultra-high vacuum furnace and in later studies a diode laser. Following extraction of He, the samples are recovered for U and Th analysis using isotopic dilution (see section A.3).

3.3.4 Interpreting (U-Th)/He ages

3.3.4.1 (U-Th)/He age profiles

Apatite (U-Th)/He (AHe) records information on cooling through 40 - 85 °C which depending on the palaeogeothermal gradient, is equivalent to removal of the upper 2-3 km of the upper

crust. Helium ages reflect the accumulation of helium since complete retention (i.e. less than 40 °C) but also the period when He is partially retained (i.e. 40 – 85 °C). As for AFTT, the effect of partial retention can be observed in vertical profiles or boreholes within a stable region that has not undergone significant denudation. AHe ages will be the oldest near the surface decreasing with depth until the age is zero at depths where the temperature is high enough for complete helium loss from crystals. The pattern of this age decrease is sigmoidal and the zone of partial accumulation is known as the partial retention zone (PRZ), analogous to the AFTT partial annealing zone (Figure 36). The PRZ occurs at temperatures between ~ 85 °C and 40 °C (Farley, 2000; Wolf et al., 1998). As with the AFTT partial annealing zone, the AHe partial retention zone can be exhumed and its base will be marked by an inflection with an age corresponding to the time of exhumation.

When dealing with AHe ages from surface samples, the concept of a PRZ is useful for interpretation. Provided it can be demonstrated that the lithosphere throughout the region has a similar thermal structure then the youngest AHe ages correspond to areas of greater denudation. In effect the different ages represent different exhumed sections of the PRZ. The prevailing conceptual models proposed for elevated passive margin evolution predict different magnitudes and spatial variations in denudation. It has been demonstrated that the pattern of AHe ages is a key discriminator between the conceptual models, particularly when the amount of denudation is low (Balestrieri et al., 2005; Persano et al., 2002; Persano et al., 2005).

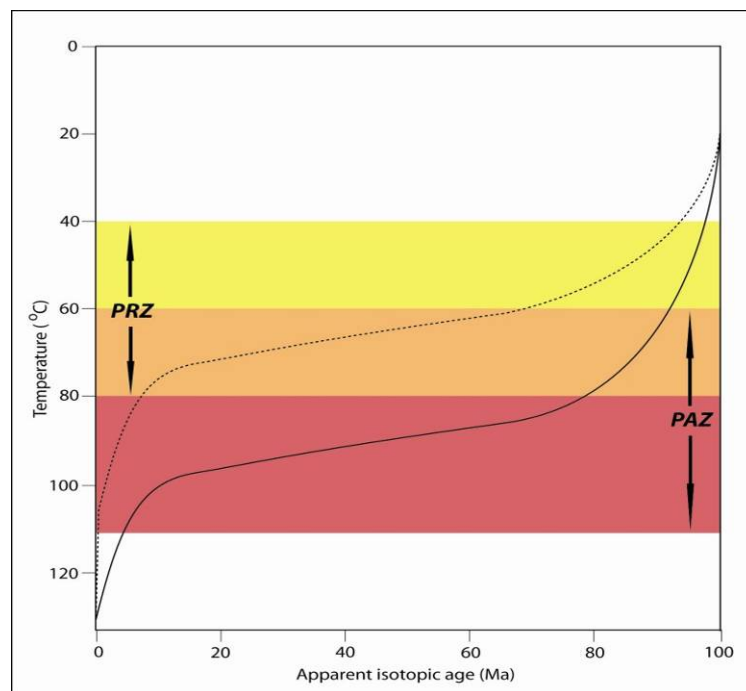


Figure 36 Apatite (U-Th)/He PRZ

Schematic illustration of the apatite helium partial retention zone (dashed line) and the apatite fission track partial annealing zone (solid line) for an isothermal holding time of 100 Ma. Thermal histories prior to 100 Ma have been reset.

3.3.4.2 Forward modelling of (U-Th)/He ages

When samples have cooled slowly through the He PRZ, it is more appropriate to forward model the AHe ages of samples in order to extract potential thermal histories to make meaningful geological interpretation. Forward modelling requires solving numerical solutions to both the radioactive decay responsible for the generation of helium and the mechanisms responsible for the loss of helium (i.e. diffusion and α -ejection) to produce a model age which can be compared to the measured age. To forward-model AHe ages it has been demonstrated that spheres of identical surface-to-volume ratio to the measured crystals not only provide rapid numerical solutions, but also produce accurate model ages (Dunai, 2005; Meesters and Dunai, 2002b). It has also been illustrated, particularly with samples that have resided within the PRZ for significant amounts of time, that the processes of diffusion and α -ejection must be treated simultaneously when forward modelling AHe data (Dunai, 2005; Meesters and Dunai, 2002a). With these points in mind, AHe data reported from this project have been forward modelled using DECOMP (Bikkar et al., 2002), a program that simultaneously solves the production-diffusion equation for the algorithms of (Meesters and Dunai, 2002a, 2002b).

Forward modelling can reduce the number of potential thermal histories a particular AHe age will produce; however, because AHe ages are always bulk ages, there are always multiple thermal histories that explain the data, i.e. model ages are not unique to a particular thermal history. Unlike AFTT data, conventional AHe data provide no information equivalent to track length distributions. One solution to this problem is to model AHe data with AFT thermochronometers to limit the range of possible thermal histories capable of reproducing the measured data (e.g. Persano et al. (2005)). Section 3.4 outlines the procedure of combined modelling of thermochronometers.

3.4 Combining thermochronometers

A large amount of information can be extracted from a single thermochronometer particularly if there are multiple samples from vertical profiles or multiple samples distributed across a region (Kohn et al., 2005). However, each thermochronometer has a unique temperature range in which the system is most sensitive and can only provide information on specific segments of a thermal history. Moreover, due to an incomplete understanding of the processes that control these isotopic systems and the errors associated with sample measurements, there is inherent non-uniqueness. A particular thermochronometric age can therefore be produced by a variety of different thermal histories. Although well planned sampling strategies (Braun and van der Beek, 2004) and appropriate treatment of modelling (Dunai, 2005; Ketcham, 2005) can be

effective, a complementary approach is to obtain multiple ages for different thermochronometers on the same sample.

The advantages of combining thermochronometers are schematically illustrated in Figure 37. It is now commonplace to inversely model AFTT data to extract thermal histories that are statistically acceptable as well as geologically reasonable. The AFTT system is sensitive to temperatures between 110 °C and 60 °C and will provide constraints on the time rock passes through these temperatures. AHe is sensitive to temperatures between 85 °C and 40 °C and therefore has the potential to constrain the cooler segment of the thermal history (Figure 37). ZrHe with its higher closure temperature of 180 °C, can provide even better control on higher temperatures.

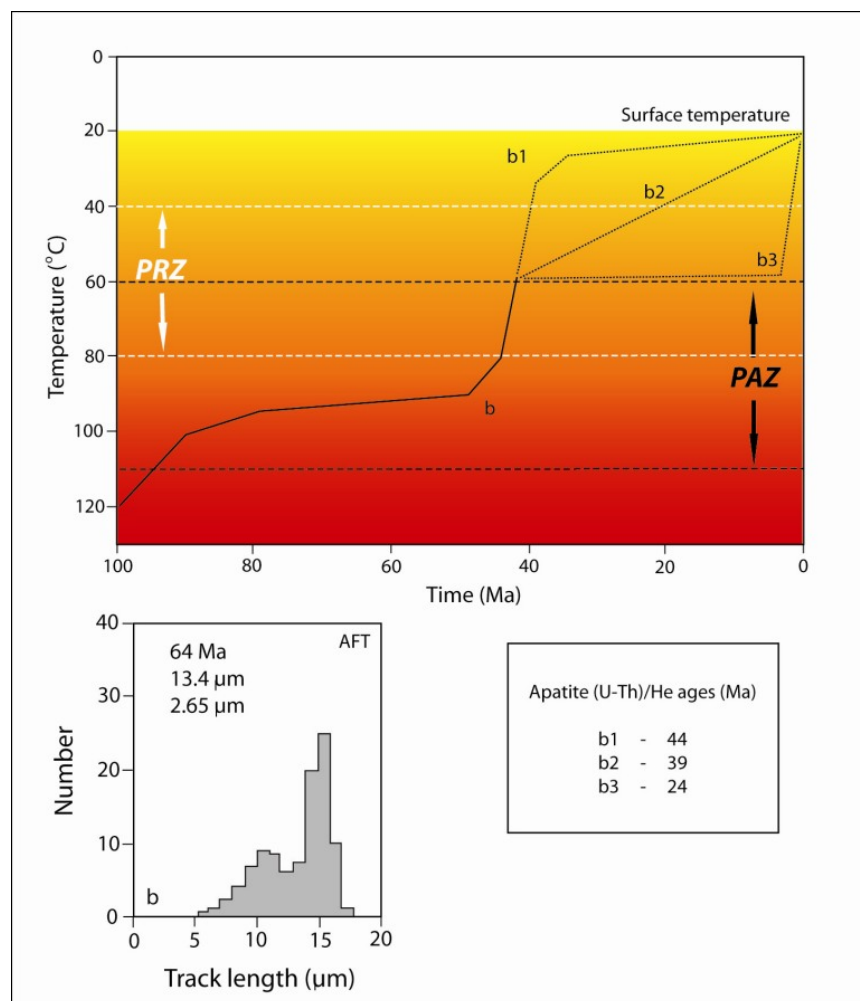


Figure 37 Multiple thermochronometers

Illustration of the advantages to applying multiple thermochronometers. Time temperature history (b) (same as fig. 3.5) with three late stage cooling pathways at ~40 Ma. The AFTT system is insensitive to these cooling pathways, and the modelled age and TLD remains the same for all three thermal histories. The AHe system is sensitive to temperatures less than 60 °C and modelled thermal histories predict different AHe ages. All ages modelled using HeFTy (Ketcham, 2005).

One of the aims of a thermochronology study is to use data from a sample to obtain a range of thermal histories that can be interpreted in a geological context by modelling the data. There are two potential approaches for modelling more than one thermochronometer on the same sample. The first method involves extracting statistically acceptable individual thermal histories that have been inversely modelled for AFTT and importing them into a forward model such as DECOMP (Bikkar et al., 2002) to test which thermal histories predict the AHe or ZrHe data (Persano et al., 2005). Although this method reduces the number of potential thermal histories predicted from AFTT alone, it has several disadvantages. It is time consuming, it can only be applied to two thermochronometers and it does not model each thermochronometer simultaneously. The availability of user-friendly and increasingly more sophisticated modelling software allows the simultaneous inversely modelling of two or more thermochronometers and provides the second method for combined modelling. Two computer programmes have been developed for simultaneous modelling, ContourTrax (Gallagher, 1995) and HeFTy (Ketcham, 2005; Ketcham et al., 2003). Although both programmes have their advantages, this project prefers the use of HeFTy because the software can incorporate a kinetic parameter into AFTT data (see section 3.2.2).

3.5 Applying low temperature thermochronometry to long-term landscape development

Low temperature thermochronometric data relate the thermal structure of the upper crust by directly relating temperature to depth, and as such, the cooling history provided from low temperature thermochronometry approximates movement of rocks to the surface or denudation. Both apatite fission track and (U-Th)/He analysis are particularly effective at constraining near surface processes and shallow level tectonism because both techniques are sensitive to temperatures and magnitude of denudation appropriate to long-term landscape development (Braun, 2003, 2005; Braun et al., 2006; Ehlers and Farley, 2003; House et al., 1998, 2001; Persano et al., 2002). Further more, the ages provided by low temperature thermochronometry are often the result of more complex cooling (e.g. apparent or 'mixed' ages) produced over longer periods of time and therefore have the ability to resolve more complex cooling (and denudational) histories.

At passive margins, denudation is the dominant process controlling cooling and the advection of rocks towards the earth surface (Gallagher and Brown, 1999; Gallagher et al., 1998). Denudationally driven cooling, couple with the timescales over which passive margins develop make low temperature thermochronometry ideally suited to improving our understanding of long-term landscape development within these tectonic settings. The

following two chapters outline the results of AFTT and (U-Th)/He data for two segments of the Western Indian elevated passive margin, outlining the effective use of low temperature thermochronometry for constraining denudation and long-term landscape development.

4 Low temperature thermochronometry data for Goa and Karnataka

4.1 Introduction

The northern field area is in Goa and Karnataka located between 16 °N and 14 °N. The exposed rocks are largely comprised of metasedimentary and metavolcanic rocks belonging to the Dharwar Supergroup overlying Dharwar cratonic basement gneisses and granites (see section 1.3.1). Within the field area, the Western Ghats range in height from 0.5 km to 1.5 km and the width of the coastal plain varies between 0 km and 50 km. North of the field area (within the Deccan Traps) the Ghats escarpment forms a steep barrier of high relief but to the south, it is more subdued and, in places, is replaced by a transition zone of smaller ‘foothills’ increasing in height towards the interior plateau. Here many truncated interfluvial ridges project seaward from the escarpment onto the coastal plain. Elevations on the coastal plain range from sea level to a maximum of 0.35 km, where granite domes and smaller outliers of the main escarpment are present. To the east (inland) of the escarpment lip, the low relief Maharashtra and Mysore plateaux are elevated at 0.4 – 0.6 km.

Goa and Karnataka were selected for study for several reasons. The Deccan Traps are a useful Phanerozoic stratigraphic marker along the Western Indian passive margin but only extend as far south as 16 °N (Figure 3). North of 16 °N, the escarpment is formed within the lavas, implying that escarpment development must have commenced following emplacement of the Deccan Traps at ca. 65 Ma in response to rifting between India and The Seychelles microcontinent (Widdowson, 1997)(see section 1.3.3). South of the lavas, the Dharwar basement lithologies are the first rocks to contain sufficient apatite and zircon for low temperature thermochronometry and they are therefore suitable for ascertaining the southerly influence of The Seychelles rifting event and the impact (if any) of the Reunion plume (see section 1.3.3). If The Seychelles rifted south of the Deccan lavas, the timing and magnitude of the denudational response should be detected in the thermal histories of the Dharwar rocks.

Apatite fission track thermochronometry (AFTT) has been previously undertaken in Goa and Karnataka to elucidate the denudational history of this segment of the Western Indian margin

(Gunnell et al., 2003; Kalaswad et al., 1993). Interpreting AFTT data and extracting thermal histories requires inversely modelling, which is influenced by input parameters (see section 3.2.5.2). Gunnell et al. (2003) found that the timing of rapid cooling associated with an increase in denudation is governed by the initial track length adopted (14.5 μm or 16 μm) for inverse-modelling and could not distinguish between an increase in denudation associated with The Seychelles or Madagascar rifting events. The timing of the development of the escarpment remains unresolved using AFTT. Gunnell et al. (2003) reported 92 AFTT results and, with the exception of five samples, all have ages between 100 and 400 Ma with mean track lengths shorter than 13.5 μm . If The Seychelles rift resulted in an increase in denudation, such relatively old ages and reduced mean track lengths would require the accumulation (and partial annealing) of tracks prior to rifting, a prolonged period of time within the PAZ, and (for a geothermal gradient of 20 °C) only 2-4 km of denudation. Although 2-4 km of denudation is within the sensitivity range for the AFTT system, such small magnitudes of denudation approach the limits of the AFTT technique. The apatite (U-Th)/He thermochronometer is sensitive to temperatures cooler than AFTT and has been used effectively, often in combination with AFTT, to constrain smaller magnitudes of denudation on other passive margins (Balestrieri et al., 2005; Persano et al., 2002; Persano et al., 2005). The zircon (U-Th)/He thermochronometer is sensitive to temperatures warmer than AFTT and is therefore valuable for constraining magnitudes of cooling that are greater than those which AFTT is less sensitive. This chapter reports the results of new AFTT, apatite (U-Th)/He and zircon (U-Th)/He data to constrain the thermal histories of the Goa and Karnataka segment of the Western Indian margin in order:

1. To test the competing conceptual models of passive margin evolution; and
2. To determine the timing of the rifting event responsible for initiating escarpment development.

Forty samples were collected in Goa and Karnataka, comprising two escarpment normal traverses, spot samples along the coast and spot samples on elevated areas of the coastal plain (Figure 38). This sampling strategy was adopted for two reasons: 1) thermochronometric data from samples along escarpment-normal traverses can differentiate between the competing models of escarpment evolution (Balestrieri et al., 2005; Gallagher et al., 1998; Persano et al., 2002; Persano et al., 2005; van der Beek and Braun, 1998).

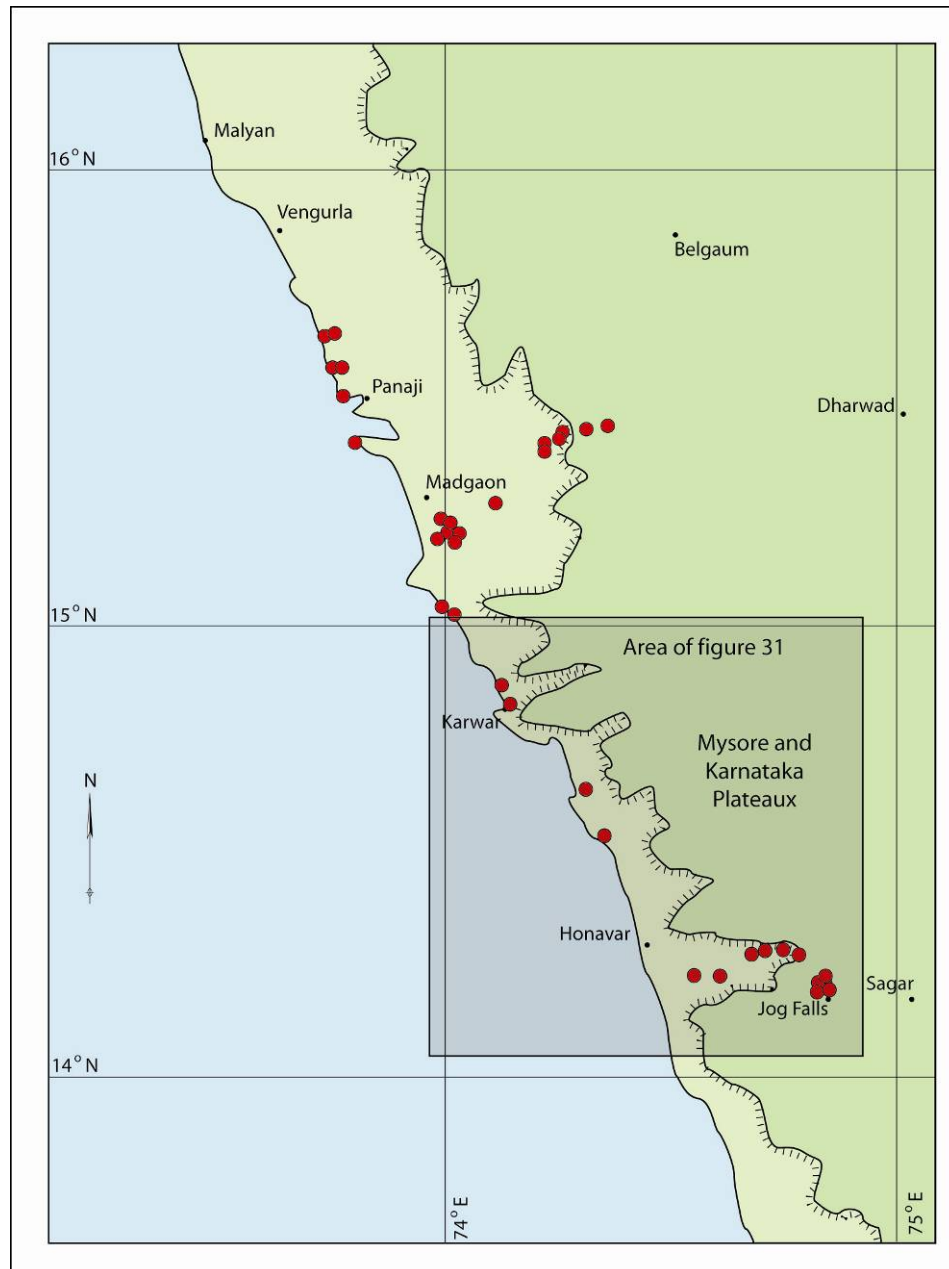


Figure 38 Location of samples for Goa and Karnataka

Samples are marked by red circles; the escarpment is marked by the ornamental line.

2) If the margin is elevated, thermochronometric ages from the coast should be similar to the age of rifting and can therefore be used to determine which rifting event is responsible for initiating margin development. Thick laterite cover, aggressive deep tropical weathering and thick vegetation precluded an ideal sampling strategy and limited the quality of apatite separates. Consequently, I report data from 23 AFTT samples (19 of which had been collected previously by M. Widdowson and Y. Gunnell, and analysed by A. Carter at UCL) (see section 4.2), five apatite (U-Th)/He samples and one zircon (U-Th)/He sample (see section 4.3). Two sample locations, one at the coast and one at the escarpment have also been modelled simultaneously using AFTT and (U-Th)/He data (see section 4.4). Analysed samples are displayed in Figure 39.

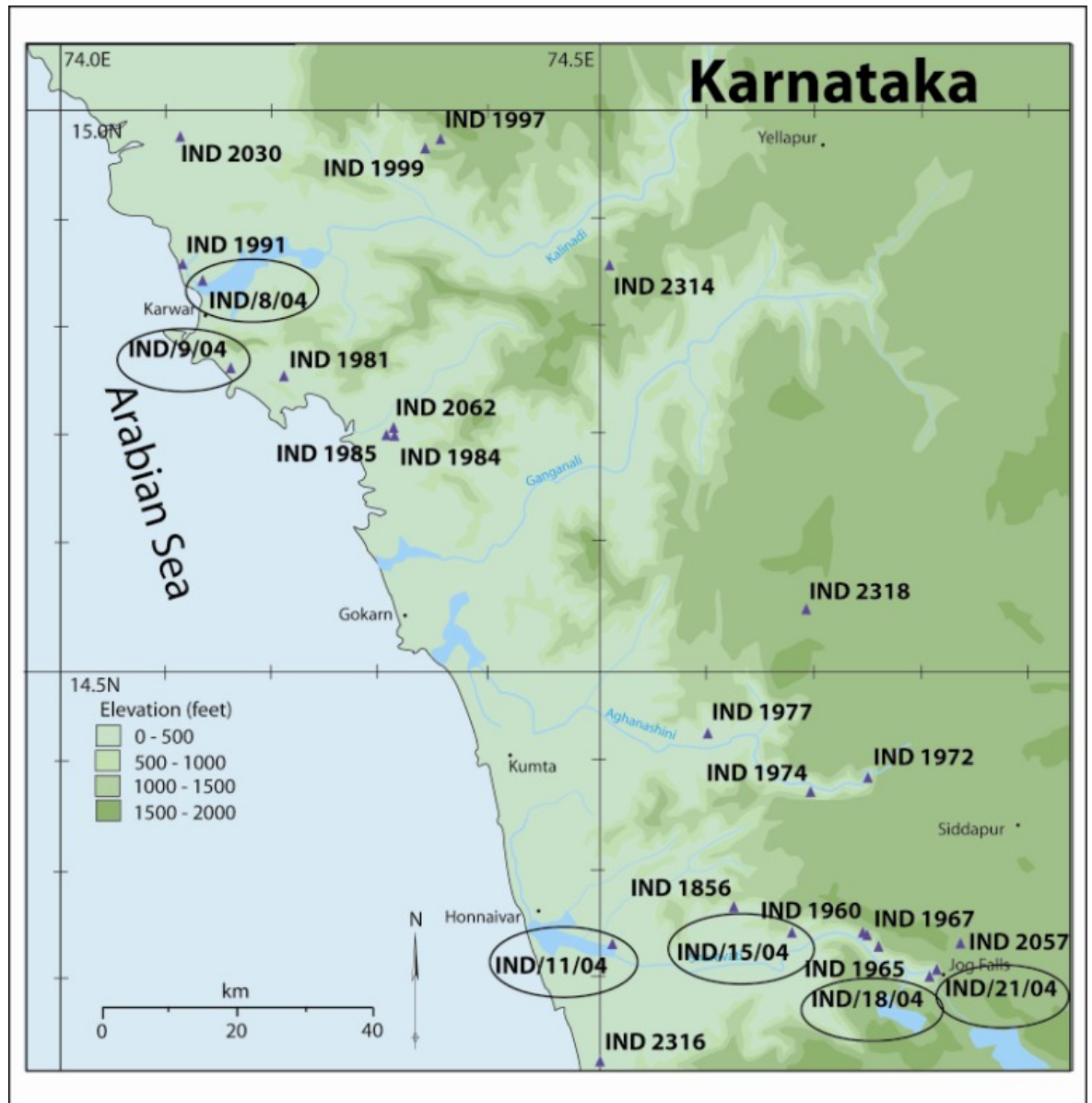


Figure 39 Location of analysed samples for Goa and Karnataka.

Ringed samples were analysed for this project, the remaining samples were analysed by A. Carter (UCL)

Thermochronometric data can only provide information on the magnitude of cooling a sample has experienced. To convert the magnitude of cooling into denudation, assumptions must be made about the palaeogeothermal gradient in the shallow lithosphere and palaeosurface temperature. Palaeogeothermal gradients are challenging to estimate and there are only limited data for present day geothermal gradients for the Western Indian margin. A geothermal gradient of between 11 – 13 °C/km has been calculated from current heat flow and thermal conductivity estimates for the Dharwar craton (Roy and Rao, 2000; Verma, 1991). Estimates of the offshore geothermal gradient range from 30 – 65 °C/km (Pandey and Agrawal, 2000; Rao et al., 2001; Shankar et al., 2004). As a consequence of the large range in estimates of the geothermal gradient, I assume an intermediate palaeogeothermal gradient of 20 °C/km for this study. The latitude of India has varied throughout the Cenozoic from ~ 30 °S prior to rifting

with Madagascar (Pande et al., 2001; Reeves and de Wit, 2000) to its current position $\sim 10^\circ\text{N} - 15^\circ\text{N}$. Although latitude variations will affect surface temperature the average surface temperature is unlikely to have fluctuated significantly from $c.20^\circ\text{C}$. Thus, it is assumed for the numerical modelling of thermal histories that the average surface temperature has remained a constant 20°C throughout the Cenozoic.

4.2 Apatite fission track data

Samples are located in three groups: 1) on the coastal plain at Karwar and on the plateau to the West of Karwar; 2) on the Aghanashini river; and 3) on the Sharavati river and at Jog Falls (see Figure 39). These locations were selected because they provide a range of elevations from sea level to 540 m on the elevated interior plateau. A large range of elevations are important for maximizing the range of palaeotemperatures from which samples have been exhumed (see section 3.2.5). The sample distribution also covers the three macro-geomorphological features of elevated passive margins, namely the coastal plain, the escarpment and the interior plateau. Nine of the samples (located along the Sharavati river) were selected because margin normal transects provide the most suitable sampling strategy for differentiating between the two competing groups of conceptual models (Gallagher et al., 1998; Persano et al., 2002).

Between 14 and 20 grains were analysed for each of the four samples collected for this study, using the external detector method (Gleadow and Duddy, 1981) and the zeta calibration technique (Hurford and Green, 1982, 1983). The 19 samples collected previously by M. Widdowson and Y. Gunnell had been analysed using the same method (A. Carter pers. comm.). The locations, elevations, fission track ages, mean track lengths and 1σ errors are reported in Table 4 & Table 5.

4.2.1 AFTT results

Apatite fission track ages range from 62 Ma to 281 Ma and generally increase in age from the coast to the elevated interior plateau. The youngest ages are between 62 Ma and 75 Ma and are in samples from closest to the coast (IND/9/04, IND 1991 and IND 2316). All other samples have AFTT ages older than 108 Ma. Mean track lengths (MTLs) range from $11.72\ \mu\text{m}$ to $14.33\ \mu\text{m}$ with the longest MTLs closest to the coast and the shortest MTLs inland on the coastal plain and on the elevated interior plateau (Figure 40, Table 4 & Table 5). The samples from closest to the coast are interpreted as having cooled rapidly from below the partial annealing zone (PAZ) at approximately the time of the Seychelles-India rift (65 Ma). All the samples further inland display older AFTT ages, shorter MTLs and more complex track length distributions, and are interpreted as having experienced a period of track accumulation within

the PAZ followed by cooling from within the PAZ. The timing of cooling from within the PAZ is difficult to ascertain and is discussed further in section 4.2.2.

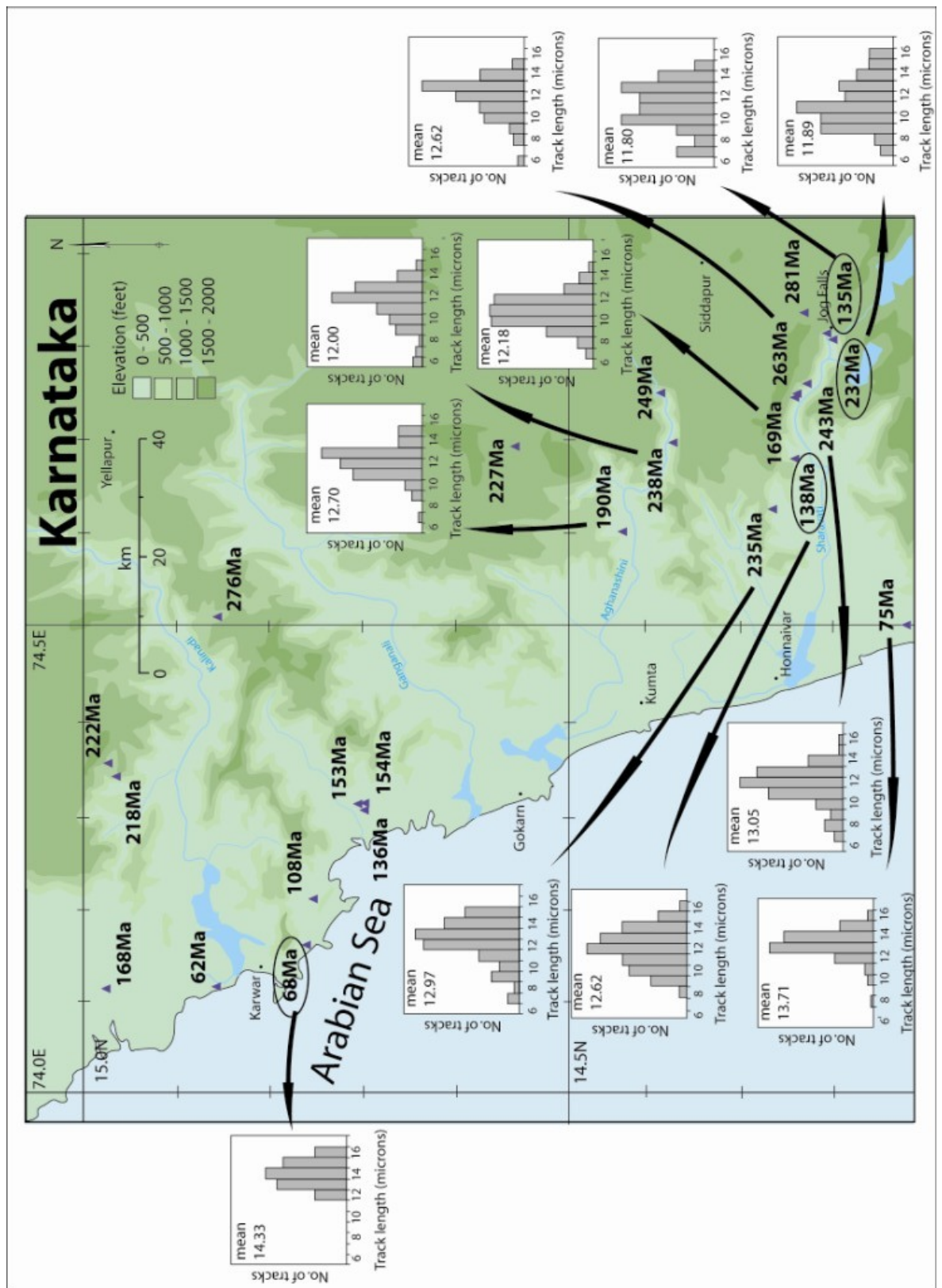


Figure 40 AFTT results for selected samples from Goa and Karnataka
 Ringed samples were analysed for this project, the remaining samples were analysed by A. Carter (UCL)

Sample name	Degrees (N)	Degrees (E)	Dosimeter		No of grains	Spontaneous tracks		Induced tracks		Age dispersion		Central age (Ma)
			(ρ_d)	(N_d)		(ρ_s)	(N_s)	(ρ_i)	(N_i)	Chi-sq	P(%)	
IND9	14.7752	74.1414	12.34	7139	14	3.53	276	8.594	672	5.34	96.69	67.8
IND15	14.2713	74.7048	12.28	7139	18	5.536	528	6.574	627	40.26	0.12	137.7
IND18	14.2237	74.8050	12.89	7139	20	3.723	467	2.727	342	5.87	99.82	232.3
IND21	14.2218	74.8056	12.51	7139	20	2.056	267	2.542	330	18.35	49.95	134.8
IND 1856	14.2486	74.6167	1.137	7737	20	3.92	3108	3.107	2463	20	3.9	235
IND 1960	14.2237	74.8102	1.289	8936	20	1.552	729	1.434	674	<1	23.2	243
IND 1965	14.2739	74.7106	1.36	9423	20	0.445	537	0.601	725	75	0.03	169
IND 1967	14.2773	74.7203	1.301	9015	20	1.437	769	1.181	632	40	4.3	263
IND 1972	14.3592	74.7355	1.289	8936	20	1.434	823	1.236	709	70	1.5	249
IND 1974	14.3932	74.6600	1.301	9015	20	1.005	461	0.913	419	40	5.9	238
IND 1977	14.4310	74.6098	1.289	8936	20	1.086	1275	1.229	1443	40	8.5	190
IND 1981	14.7635	74.2143	1.301	9015	20	0.442	754	0.893	1524	80	0.09	108
IND 1984	14.6953	74.3000	1.289	8936	20	0.745	1111	1.046	1560	40	7.6	154
IND 1985	14.6865	74.3580	1.36	9432	20	0.742	961	1.248	1617	<1	17.1	136
IND 1991	14.8463	74.1312	1.289	8936	20	0.328	351	1.141	1219	<1	19.9	62
IND 1997	14.9467	74.3597	1.289	8936	20	0.691	522	0.669	505	90	0	222
IND 1999	14.9775	74.3705	1.301	9015	20	1.193	620	1.21	629	<1	28.8	218
IND 2030	14.9922	74.1495	1.289	8936	20	0.73	583	0.938	749	40	4.7	168
IND 2057	14.2333	74.8444	1.301	9015	20	1.594	1014	1.228	781	20	8.6	281
IND 2062	14.6944	74.3583	1.301	9015	20	0.841	849	1.206	1217	20	13.4	153
IND 2314	14.3833	76.0833	1.344	7449	20	1.262	953	0.998	754	30	0.92	282
IND 2316	14.2667	76.3500	1.344	7449	20	1.494	557	1.478	551	90	0.03	226
IND 2318	14.8403	74.5097	1.364	7568	20	0.406	304	0.333	249	97	0	276

Table 4 AFTT age data for Goa and Karnataka

Sample name	Degrees (N)	Degrees (E)	Number of tracks	Mean TLD		D _{par}	
				(μm)	($\pm 1\sigma$)	(μm)	($\pm 1\sigma$)
IND9	14.7752	74.1414	58	14.33	1.3	2.16	0.39
IND15	14.2713	74.7048	63	12.62	1.8	3.71	0.68
IND18	14.2237	74.8050	66	11.89	2.2	2.65	0.23
IND21	14.2218	74.8056	67	11.80	2.1	2.04	0.31
IND 1856	14.2486	74.6167	110	12.97	0.19	-	-
IND 1960	14.2237	74.8102	103	13.05	0.2	-	-
IND 1965	14.2739	74.7106	100	12.18	0.18	-	-
IND 1967	14.2773	74.7203	102	12.62	0.22	-	-
IND 1972	14.3592	74.7355	100	12.31	0.16	-	-
IND 1974	14.3932	74.6600	103	12.00	0.19	-	-
IND 1977	14.4310	74.6098	100	12.70	0.14	-	-
IND 1981	14.7635	74.2143	100	12.42	0.2	-	-
IND 1984	14.6953	74.3000	100	11.91	0.2	-	-
IND 1985	14.6865	74.3580	100	12.13	0.18	-	-
IND 1991	14.8463	74.1312	100	13.65	0.13	-	-
IND 1997	14.9467	74.3597	100	12.08	0.22	-	-
IND 1999	14.9775	74.3705	100	11.99	0.18	-	-
IND 2030	14.9922	74.1495	100	12.07	0.2	-	-
IND 2057	14.2333	74.8444	100	11.72	0.21	-	-
IND 2062	14.6944	74.3583	101	12.22	0.16	-	-
IND 2314	14.3833	76.0833	100	12.60	0.22	-	-
IND 2316	14.2667	76.3500	100	13.71	0.15	-	-
IND 2318	14.8403	74.5097	100	12.88	0.17	-	-

Table 5 Track length distribution and D_{par} data for Goa and Karnataka

Figure 41a is a ‘boomerang’ plot showing the relationship between AFTT age and mean track length for the northern study area. If a region has experienced a single cooling event, the data should form a coherent boomerang shape with the youngest ages and longest MTLs corresponding to the last thermal event (Brown et al., 1994; Gallagher et al., 1998; Gladow and Brown, 2000). The boomerang plot for the northern study area displays such a relationship for the youngest samples with the last thermal event contemporaneous with the timing of The Seychelles/India rift (Figure 41a). However, the boomerang plot exhibits a less distinct relationship with the older ages and shorter MTLs, indicating that more than one cooling event may be recorded by the AFTT data further inland, or there are compositional effects. Gallagher et al. (1998) demonstrated that the trend in AFTT ages differs along a margin-normal transect for the competing groups of conceptual models. Figure 41b displays the relationship between

AFTT age and distance from the coast (analogous to several margin normal transects) for the northern study area. The trend of AFTT ages is qualitatively more consistent with the pattern of denudation associated with the elevated rift flank model.

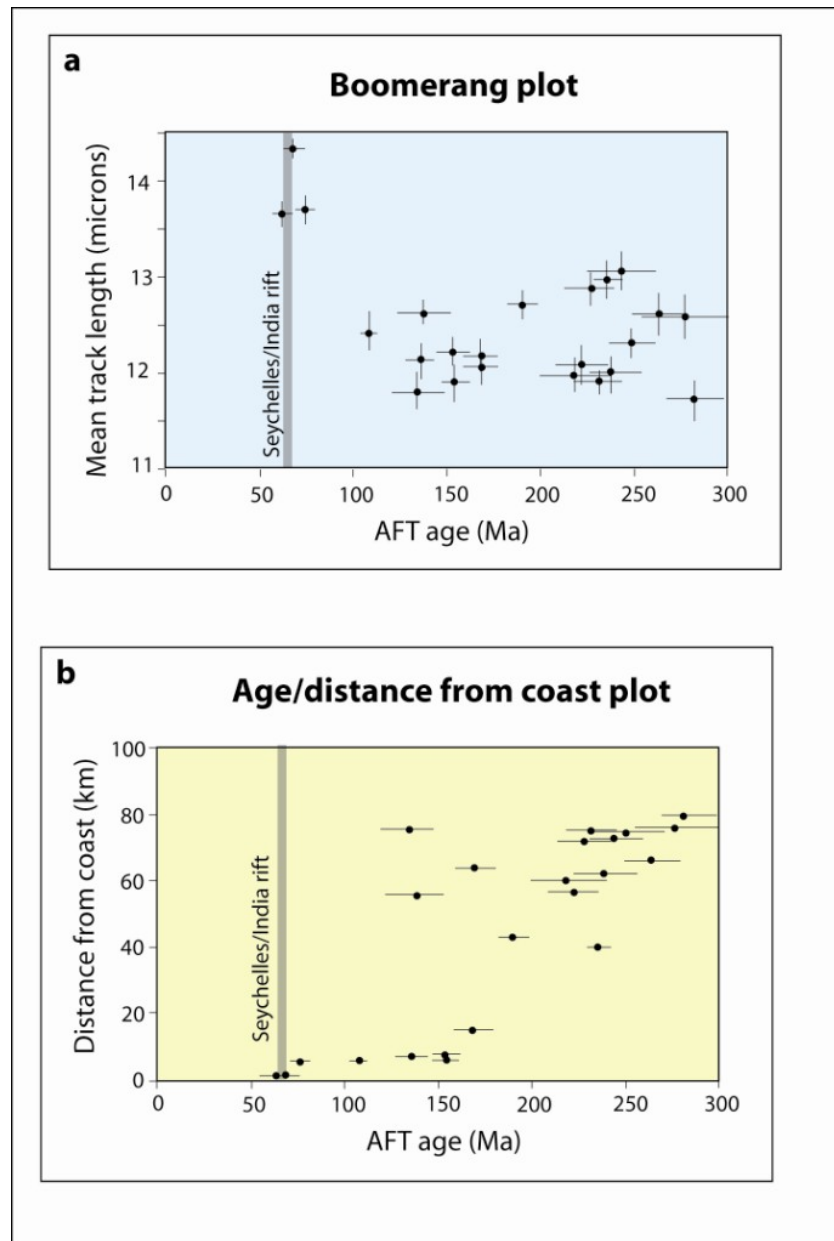


Figure 41 Boomerang plot and age vs distance from the coast for Goa and Karnataka
a - Boomerang plot (AFTT age vs mean track length) for AFTT samples from Goa and Karnataka. The timing of The Seychelles/India rift is marked by the solid bar.
b - AFTT age vs distance from the coast for AFTT samples from Goa and Karnataka. The timing of The Seychelles/India rift is marked by the solid bar.

Figure 42 shows the predictive forward modelling results for AFTT ages (dashed lines) and the measured AFTT data (closed circles). The forward modelled results for all three conceptual models are for constant escarpment evolution initiated at 65 Ma. The two elevated rift flank models were forward modelled with 4.5 km of denudation furthest from the escarpment

decreasing to 0.5 km at the base of the escarpment. The forward modelled results from both the elevated rift flank models provide the best fit to the measured data.

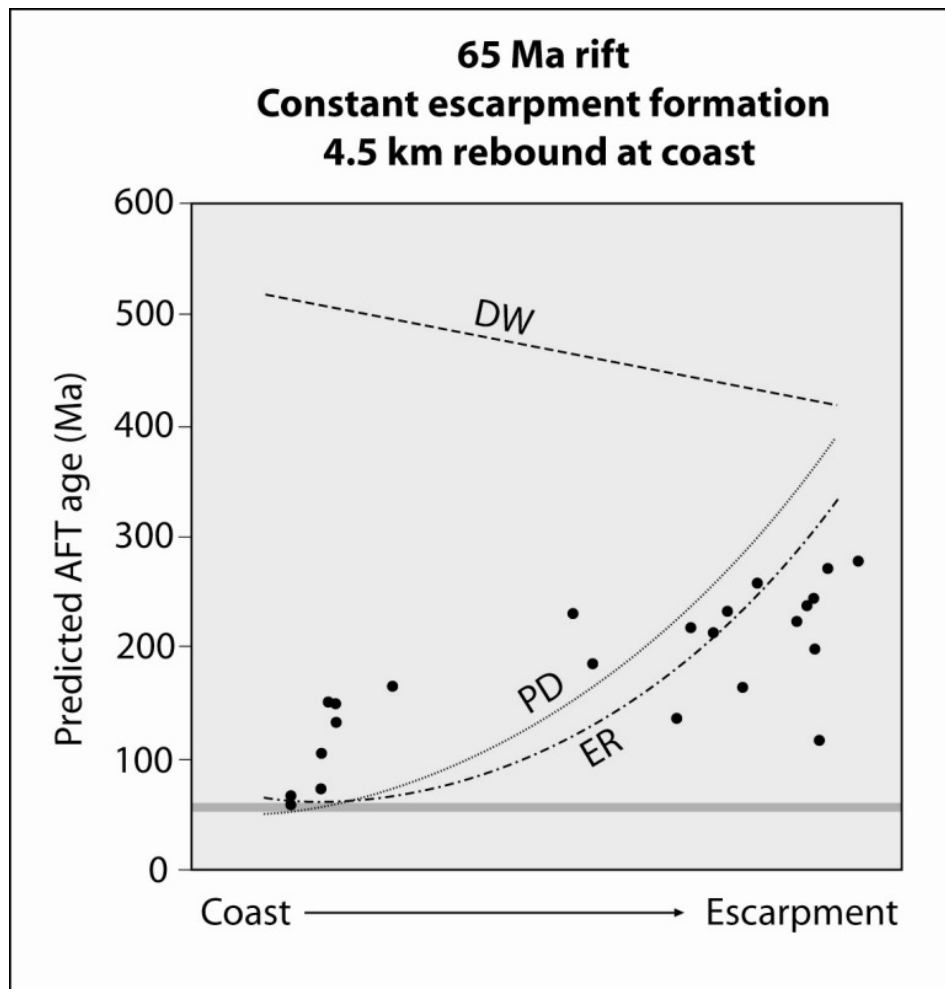


Figure 42 Predictive forward modelling results and measured data from Goa and Karnataka

Predictive forward modelling results for each conceptual model with constant escarpment evolution beginning at 65 Ma. The elevated rift flank models have 4.5 km of rebound at the coast decreasing to 0.5 km of rebound at the escarpment. The measured data are closed circles and fit the elevated rift flank models more suitably than the downwarped rift flank model.

Such qualitative interpretation of the AFTT data is an important step in interpreting the denudational history of the Western Indian margin. Inverse-modelling is a more rigorous methodology for extracting information from AFTT data and was used to explore two fundamental questions about the denudational history of the Western Indian margin: 1) Did The Seychelles-India rift or Madagascar-India rift trigger a denudational response? and 2) Which conceptual model is more consistent with the pattern in denudation across the margin?

4.2.2 AFTT inverse-modelling

Inverse-modelling involves searching for thermal histories that statistically fit the measured data by linking a set of assumed starting conditions and measured ending conditions (e.g. AFTT age, TLD, surface temperature) (Ketcham, 2005) (see section 3.2.5.2). This section reports the results from inverse-modelling a sub-set of samples from the northern study area using the computer program HeFTy. HeFTy was selected for inverse-modelling because unlike other modelling software, HeFTy incorporates a c-axis projection correction for confined tracks and a parameter for kinetic variability (Dpar for this study) within a particular AFTT population (see section 3.2.5.2). Only samples that pass the chi-squared test, with p-values greater than 0.05 (see section 3.2.5.2) were selected for model inversions.

4.2.2.1 Model parameters

The time-temperature point from which the thermal history evolves (i.e. the starting conditions) was selected such that it exceeded the measured AFTT age of the modelled sample and began at temperatures in excess of complete annealing. The ending conditions were present day average surface temperatures (20 °C) at 0 Ma. Ten thousand thermal history paths were generated for each model run using a Monte-Carlo search approach providing random and independent thermal histories which can be statistically compared to the measured data. Both statistically ‘acceptable’ modelled thermal histories and statistically ‘good’ modelled thermal histories are retained at the end of each model run. A statistically ‘good’ modelled thermal history corresponds to a p-value greater than 0.5 and a statistically ‘acceptable’ modelled thermal history corresponds to a p-value greater than 0.05 (Ketcham et al., 2003). Model runs were set up to test how well the data can be used to distinguish between different tectonic scenarios. The first model runs were given no constraints to ascertain if the data can be reproduced by a wide or narrow range of thermal histories. Subsequent model runs were constrained to mimic reburial from Deccan emplacement, accelerated cooling at the time of the Sechelles/India rift and accelerated cooling at the time of the Madagascar India rift. Four samples from this study were inversely modelled using Dpar as a kinetic parameter. Five additional samples with complete track length data (i.e. all individual track lengths not just mean track length) were provided by A. Carter at UCL. However, the five UCL samples do not have any information to constrain a kinetic parameter (such as Dpar) so were modelled as a single population. Model results are displayed in Figure 43 and Figure 45 as green envelopes for ‘acceptable’ thermal histories and purple envelopes for ‘good’ thermal histories.

4.2.2.2 AFTT inverse modelling results

Inverse-modelling results of the AFTT data from the two youngest samples from the coast (IND/9/04 and IND1991) provide evidence for a rapid cooling event from the base of the PAZ at $\sim 75 - 65$ Ma when the model is unconstrained (Figure 43). There are no 'good' modelled thermal histories when these data are forced to cool at ~ 80 Ma or if the model mimics re-burial (Figure 43). If accelerated cooling is imposed at 65 Ma there is a good fit between the modelled data and the measured data. The two youngest samples can be interpreted as having been rapidly exhumed at the time of The Seychelles/India rift. The temperature from which the samples have been exhumed depends on how resistant the apatite grains within them are to annealing. IND/9/04 has an average D_{par} value of $2.16 \mu\text{m}$ and is expected to completely anneal at ~ 125 °C, a degree of cooling which equates to more than ~ 5.25 km of denudation based on the assumption outlined in section 4.1. The inverse modelling of AFTT data from the coast provides no evidence for accelerated cooling in response to the Madagascar/India rift for this segment of the margin.

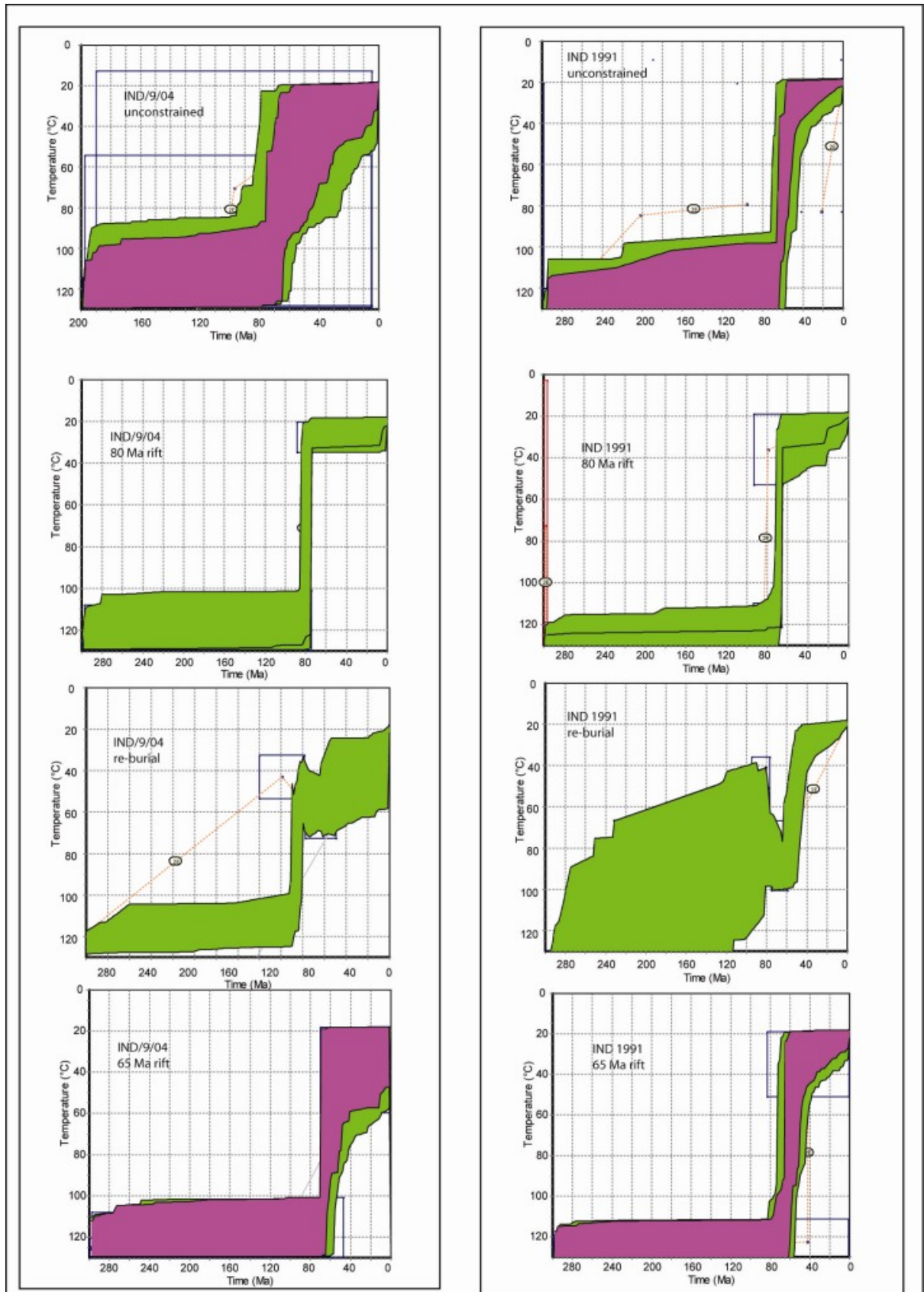


Figure 43 Inverse-modelling results of coastal samples from Goa and Karnataka

Inverse modelling-results of coastal samples from Goa and Karnataka for different tectonic scenarios. 'Acceptable' thermal histories fall within the green envelope and 'good' thermal histories fall within the purple envelope.

Inverse-modelling results from the samples further inland are more challenging to interpret. All the samples have reduced mean track lengths, complex track length distributions and ages older than the two major rifting events. The data can be reproduced by initiating cooling at either 65 Ma or 80 Ma; however, for the majority of samples, the inverse-modelling locates more ‘good’ thermal histories if rapid cooling occurs at 65 Ma (Figure 45 A - D and Figure 44). The data from inland samples are not reproduced successfully if re-burial is modelled. Inversely modelled samples south of 14.5 °N illustrate the spatial variability in denudation across the coastal plain and demonstrate which conceptual model best explains the data. IND 1991 has already been discussed above and is modelled as having been rapidly cooled from temperatures in excess of 110 °C. Data from IND/15/04 (on the coastal plain but not at the escarpment) are reproduced if the sample is modelled as having cooled from 80 to 90 °C. Data from samples at the escarpment (IND/21/04 and IND/18/04) are reproduced if they are modelled as having cooled from 60 to 70 °C (Figure 46). If the temperatures from which these samples have cooled are the result of being exhumed from different depths within the lithosphere (and not the result of variable geothermal gradient) then this pattern of cooling is more consistent with an escarpment that has developed into an elevated rift flank with 5.25 km of denudation at the coast, decreasing to 2 – 2.5 km at the escarpment. Table 6 summarises the magnitude of denudation for different palaeogeothermal gradients for each of the samples analysed for Goa and Karnataka.

Sample Name	Degrees (N)	Degrees (E)	Post break-up cooling (°C) 65 Ma – 0 Ma	Magnitude of denudation (km) for variable palaeogeothermal gradients		
				20 °C/km	40 °C/km	60 °C/km
IND/9/04	14.7752	74.1414	90	5.25	2.63	1.75
IND1991	14.8463	74.1312	90	4.50	2.25	1.50
IND1984	14.6953	74.3000	30	1.50	0.75	0.50
IND1985	14.6865	74.3580	40	2.00	1.00	0.67
IND1977	14.4310	74.6098	30	1.50	0.75	0.50
IND1856	14.2486	74.6167	20	1.00	0.50	0.33
IND/15/04	14.2713	74.7048	70	3.50	1.75	1.12
IND1965	14.2739	74.7106	40	2.00	1.00	0.67
IND1960	14.2237	74.8102	30	1.50	0.75	0.50
IND/18/04	14.2237	74.8050	40	2.00	1.00	0.67
IND/21/04	14.2218	74.8056	50	2.50	1.25	0.83

Table 6 Summary of magnitude of post break-up cooling of samples from Goa and Karnataka

Summary of magnitude of post break-up cooling from modelled AFTT data and magnitude of denudation based on variable palaeogeothermal gradients.

With the exception of the two young samples at the coast, it is not possible with any of the other samples to identify a precise time and, therefore, the rifting event that resulted in a denudational response. The magnitude of cooling, particularly for samples close to the escarpment, is small (from 60 - 70 °C) and the denudational response to rifting (if any) is difficult to identify. Modelling these samples provides information on the thermal histories prior to any cooling in response to rifting during which the majority of tracks formed and partially annealed. The small degree of syn-rift and post-rift cooling is at the limit of the sensitivity of the AFTT system making it difficult to measure the effects of the rifting event and the precise magnitude of denudation. To address these limitations, the next section reports on the results from (U-Th)/He thermochronometry which is capable of constraining smaller magnitudes of denudation.

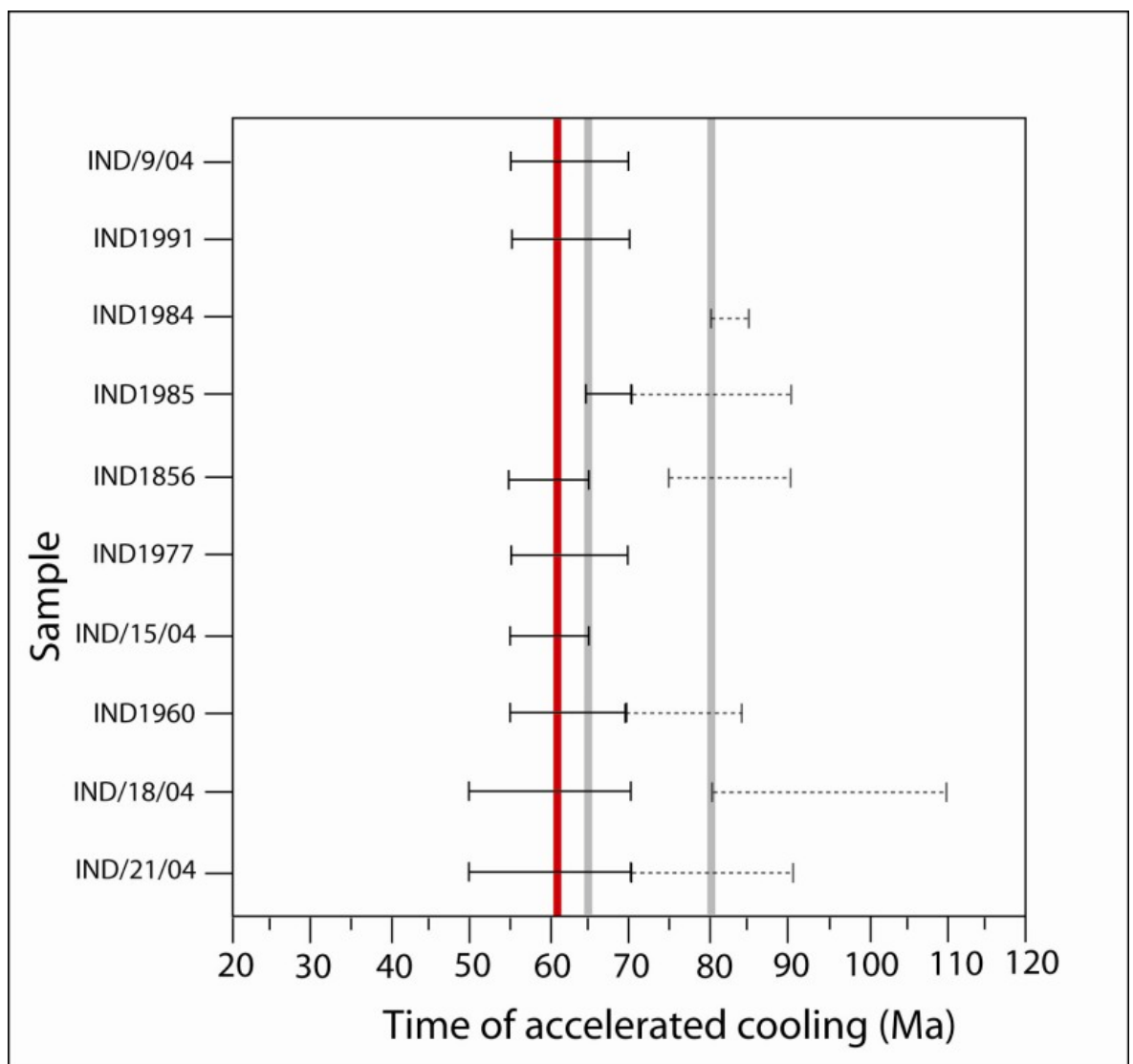
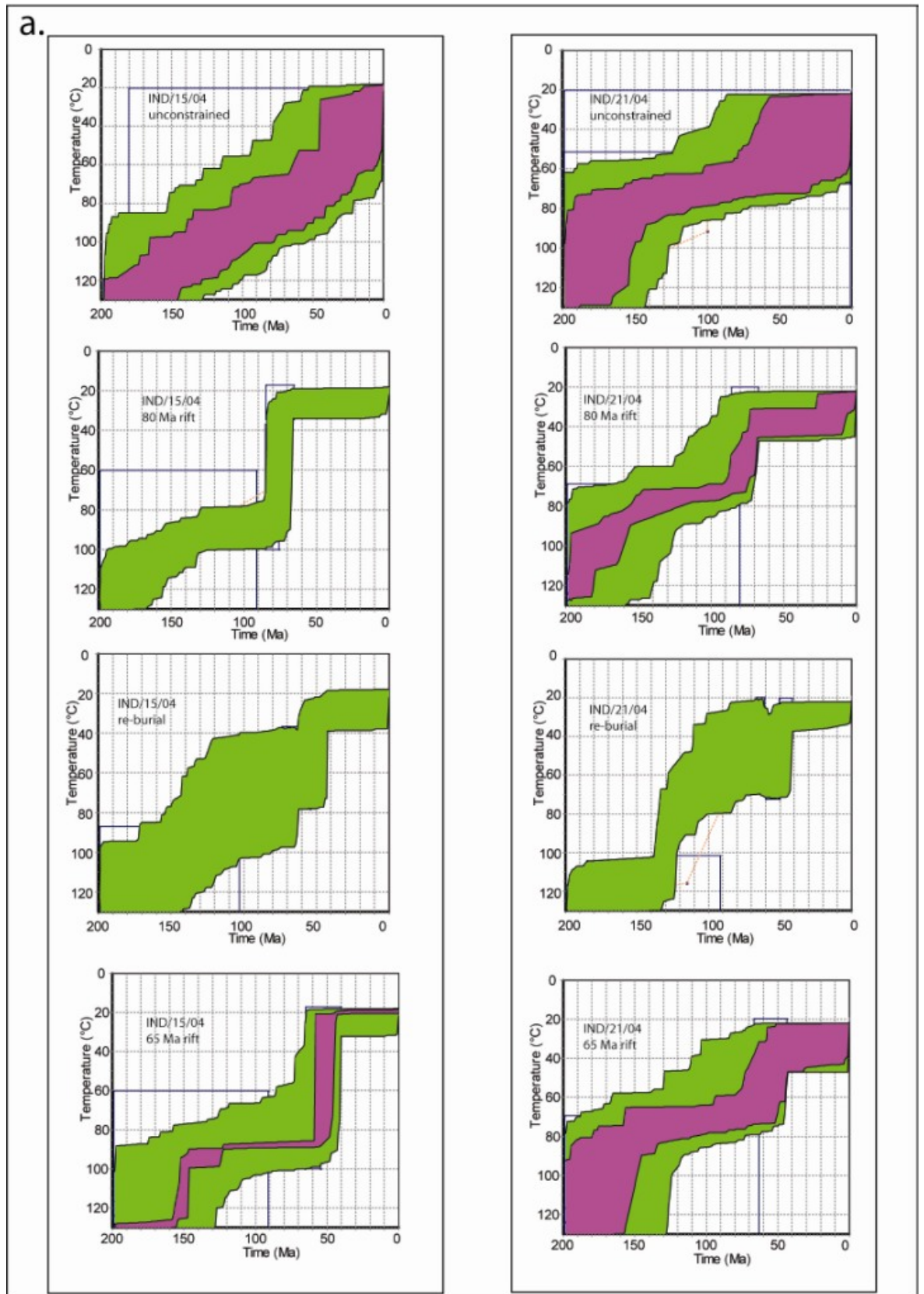
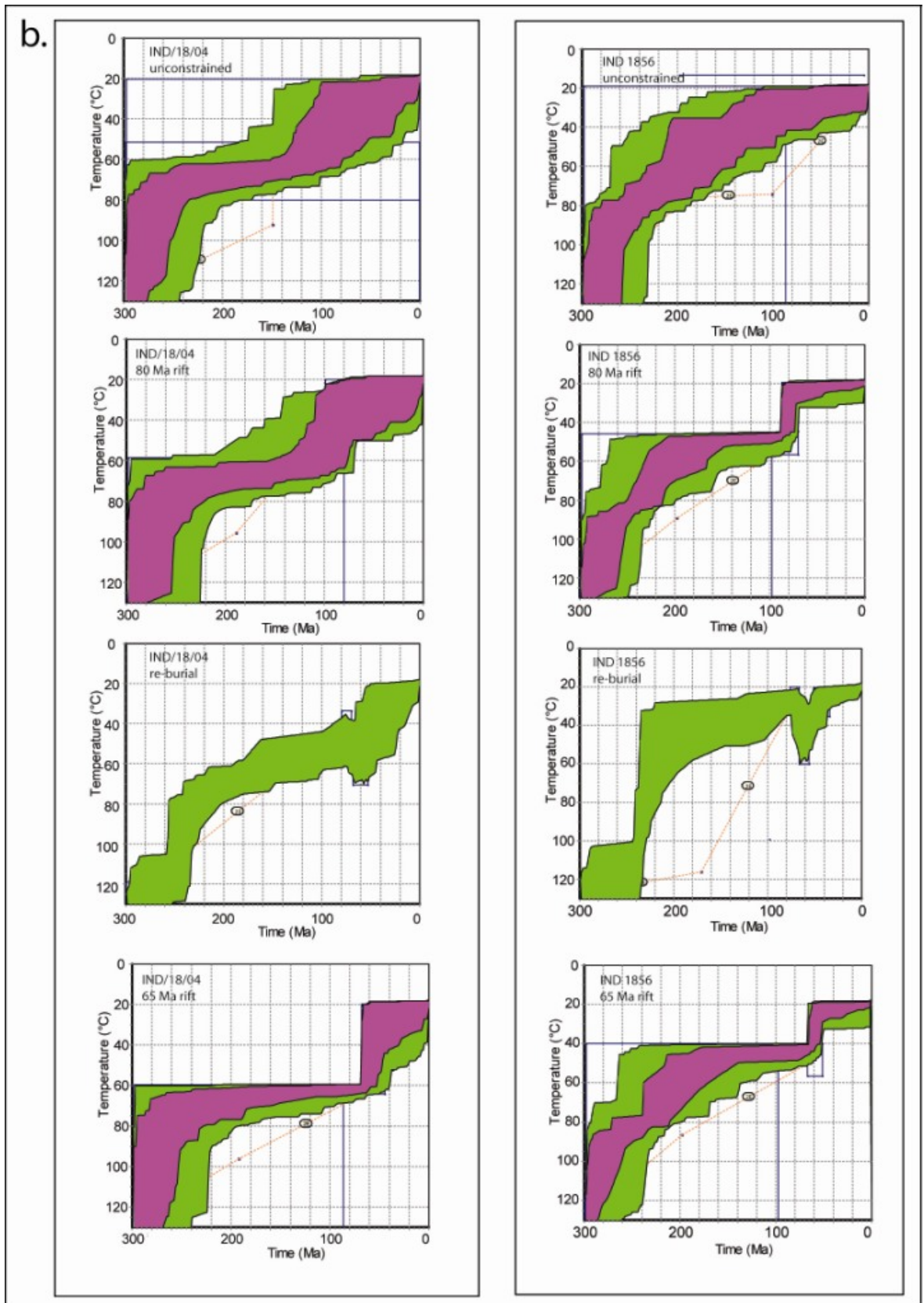
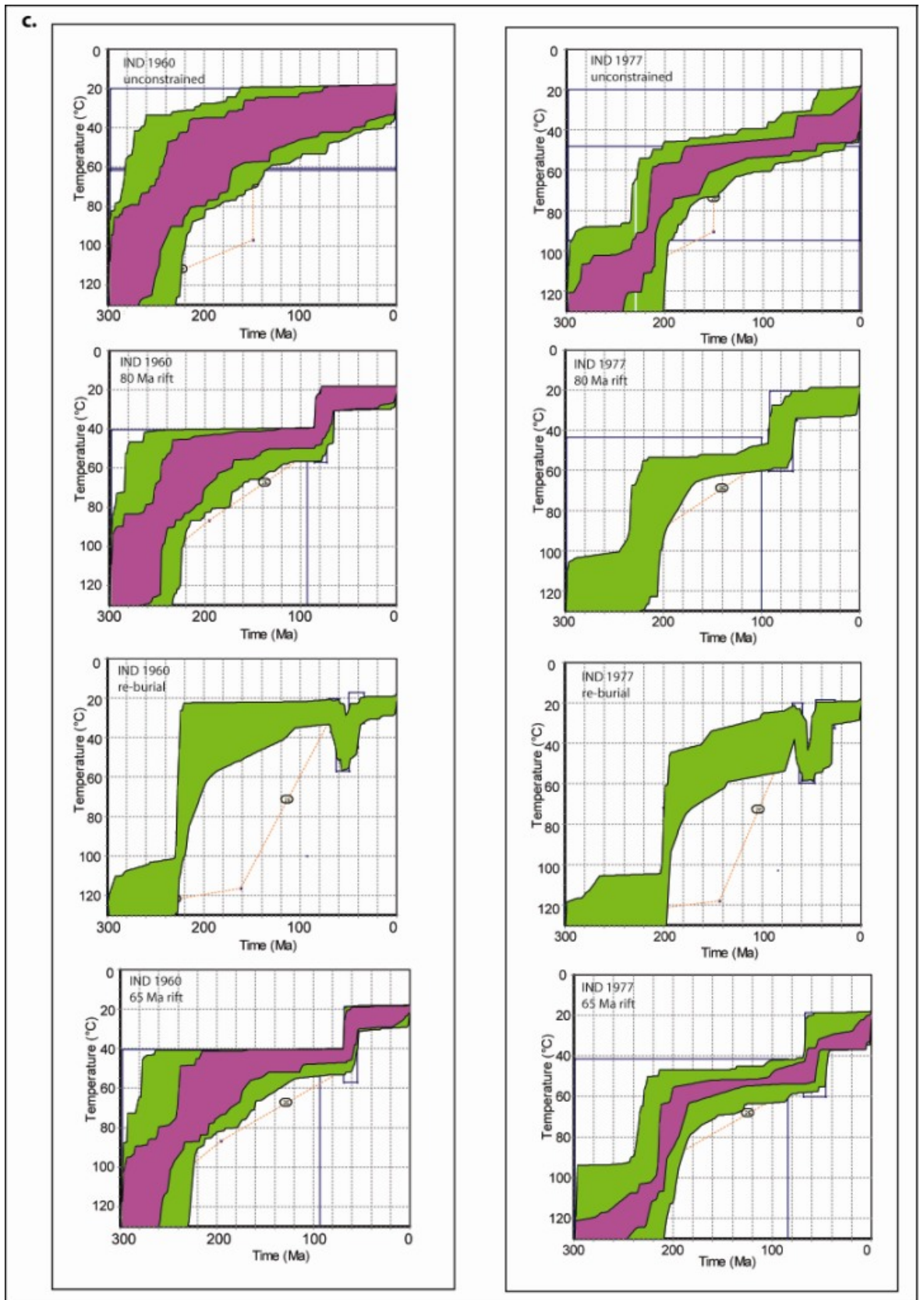


Figure 44 AFTT constraints on the time of accelerated cooling for Goa and Karnataka

Apatite fission track constraints on the time of accelerated cooling (x-axis) for individual inversely modelled samples (y-axis). The majority of samples can be successfully modelled with an accelerated cooling event at ~ 65 Ma (solid bars); however some samples can also be modelled successfully with accelerated cooling at ~ 80 Ma (dashed bars). The red solid line is the average time of cooling (62.5 Ma) for the modelled samples.







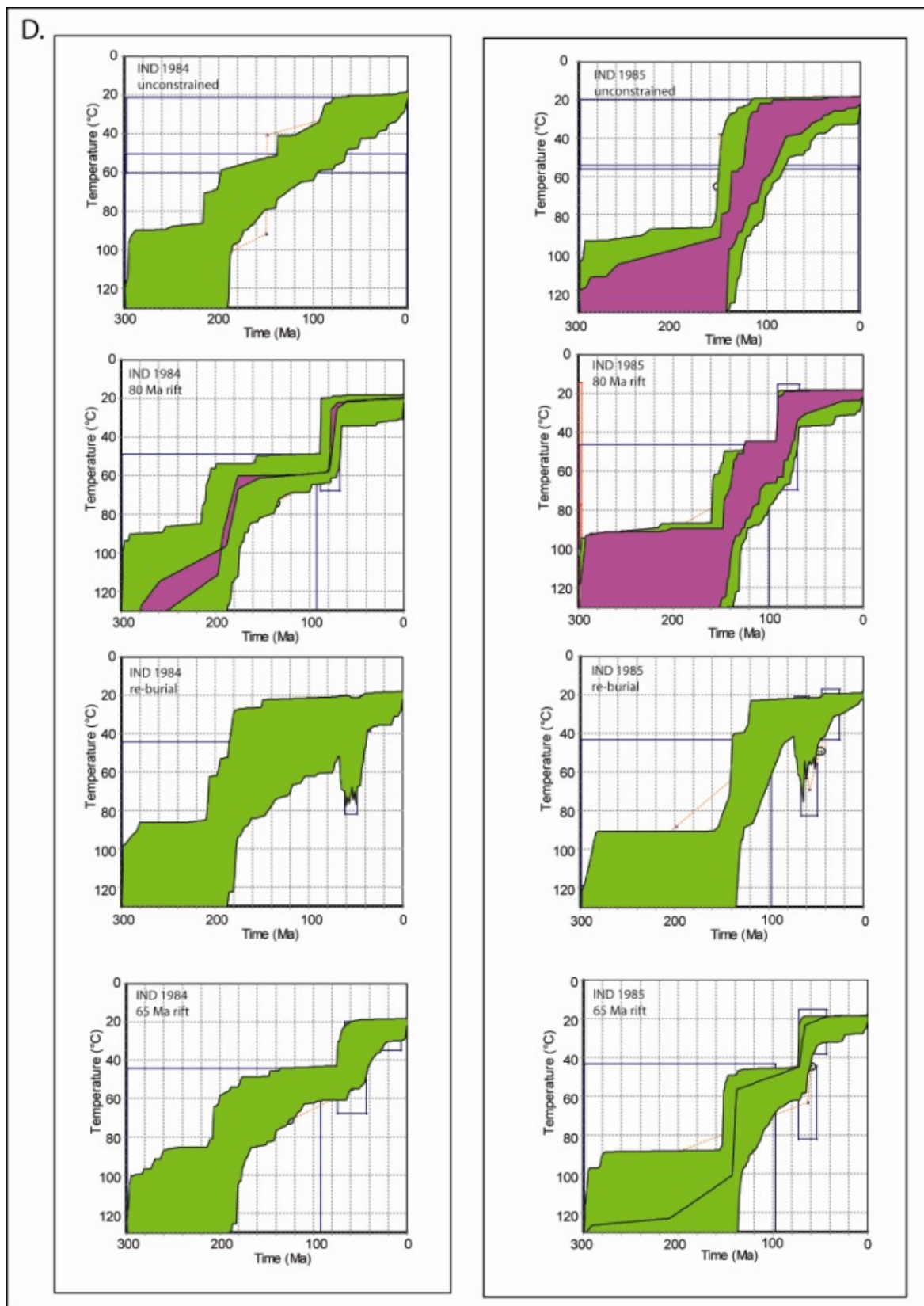


Figure 45 AFT inverse-modelling results of inland samples from Goa and Karnataka
 Inverse-modelling results of inland samples from Goa and Karnataka for unconstrained cooling, accelerated cooling at 65 Ma, accelerated cooling at 80 Ma and re-burial. 'Acceptable' thermal histories fall within the green envelope and 'good' thermal histories fall within the purple envelope.

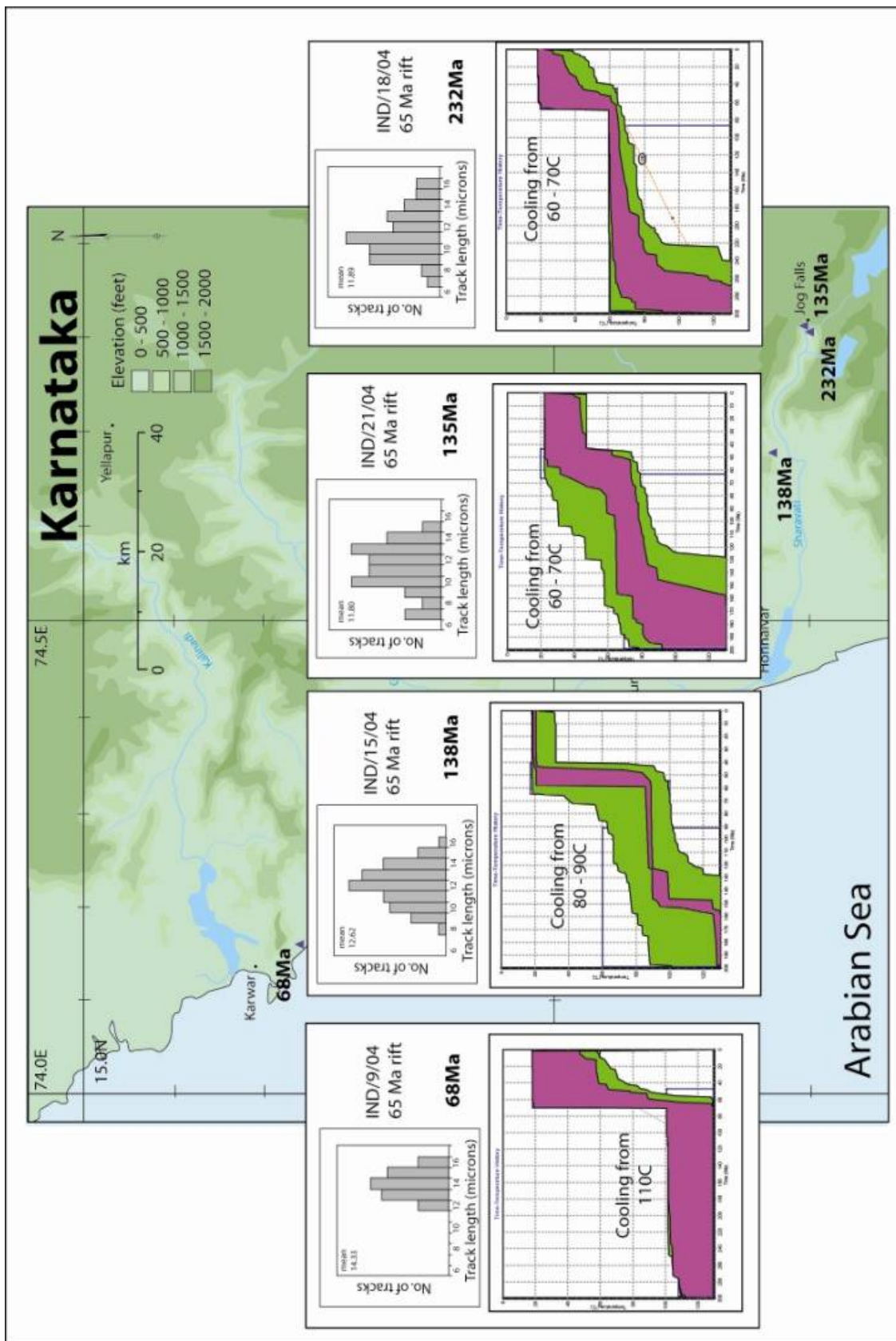


Figure 46 Inverse-modelling results for a margin normal transect for Goa and Karnataka.

Samples closest to the coast are modelled most effectively with cooling from 110 °C. Samples further inland are modelled most effectively with cooling from between 80 – 90 °C. Samples at the escarpment are modelled most effectively with cooling from between 80 – 90 °C.

4.3 (U-Th)/He data

The sampling strategy for (U-Th)/He included: 1) coastal samples and 2) margin-normal transects. The greatest difference in apatite (U-Th)/He ages between the two competing groups of conceptual models should be from samples located the greatest distance seaward of the escarpment (i.e. nearest the coast). Transects have the greatest potential to constrain the spatial variability in cooling across the coastal plain. Constraining cooling is particularly important for samples located close to the escarpment where the magnitude of cooling inferred from the AFTT data appears to be small. The ideal sampling strategy was difficult to meet for the northern study area and was inhibited by low apatite concentrations and poor apatite quality. Consequently, only five samples were analysed for apatite (U-Th)/He (Figure 47). IND/8/04, IND/9/04 and IND/11/04 are located close to the coast, and IND/18/04 and IND/19/04 are located at the escarpment. Two to six inclusion free crystals were analysed in each aliquot using the methods outlined in section 3.3.3. The smallest dimensions of crystals (i.e. the width) range between 65 μm and 200 μm . The range in width was kept to a minimum within separate aliquots to minimise uncertainties on the alpha recoil corrections (see section 3.3.3). Results are reported in Table 7 and Table 8.

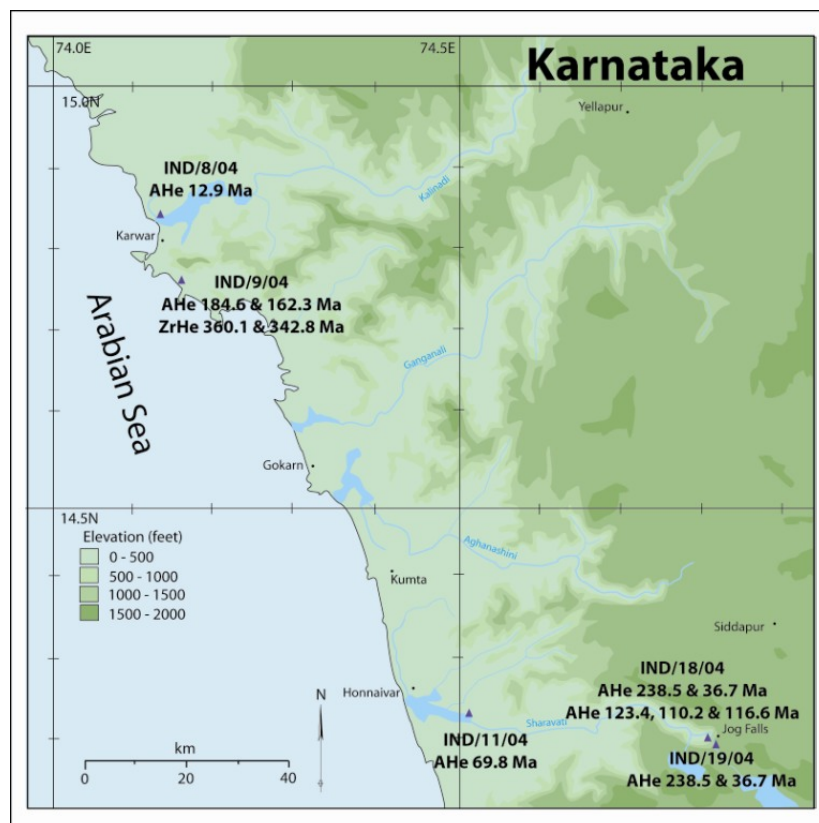


Figure 47 Apatite and zircon (U-Th)/He results ofr Goa and Karnataka

The location and results from samples analysed for apatite (U-Th)/He and zircon (U-Th)/He

Apatite (U-Th)/He

Sample name	Degrees (N)	Degrees (E)	Elevation (m)	Replicate	²³⁸ U (ng)	²³² Th (ng)	⁴ He (cc)	Uncorrected He age (Ma)	Corrected He age (Ma)	Mean age (Ma)	2σ	Analytical Error (Ma)	AFT age (Ma)
IND-8-A	14.8428	74.1253	10	I	0.62141	1.09922	9.63x10 ⁻¹⁰	9.0	12.9	12.9	0.7	0.3	
IND-9-A	14.7752	74.1414	28	I	0.12404	0.08712	2.70x10 ⁻⁹	151.6	184.0	173.2	30.7	3.7	67.8
IND-9-B				II	0.02896	0.01315	4.70x10 ⁻¹⁰	119.3	162.3			7.1	
IND-11-A	14.2418	74.5555	24	I	0.03216	0.10629	4.01x10 ⁻¹⁰	57.4	69.8	69.8	4.2	2.4	
IND-18-A	14.2237	74.805	220	I	0.04894	0.82027	3.90x10 ⁻¹¹	1.4	2.2	73.9	49.1	0.1	232.3
IND-18-B				II	0.00487	0.00344	3.57x10 ⁻¹¹	51.5	71.7			10.8	
IND-18-C	14.2237	74.805	220	I	0.0269	0.0272	3.842x10 ⁻¹⁰	94.2	123.4	116.7	13.2	0.3	232.3
IND-18-D				I	0.0198	0.0203	2.597x10 ⁻¹⁰	86.1	110.2			3.7	
IND-18-E				II	0.0186	0.0156	2.267x10 ⁻¹⁰	83.2	116.6			7.1	
IND-19-A	14.2234	74.8063	290	I	0.20656	0.16249	5.22x10 ⁻⁹	172.9	238.5	137.6	142.7	4.8	
IND-19-B				II	0.03161	0.07124	1.70x10 ⁻¹⁰	28.8	36.7			1.1	

Zircon (U-Th)/He

Sample name	Degrees (N)	Degrees (E)	Elevation (m)	Replicate	²³⁸ U (ng)	²³² Th (ng)	⁴ He (cc)	Uncorrected He age (Ma)	Corrected He age (Ma)	Mean age (Ma)	2σ	Analytical Error (Ma)	AFT age (Ma)
IND-9-1	14.7752	74.1414	28	I	3.321	0.831	9.249x10 ⁻⁰⁸	212.2	360.1	351.5	24.5	7.5	67.8
IND-9-2				II	3.330	0.688	8.770x10 ⁻⁰⁸	202.8	342.8			7.4	

Table 7 and 8 (U-Th)/He data from Goa and Karnataka

Errors are quoted to 2σ for multiple analyses. Single analyses are quoted to 6%, the same errors associated with analysis of Durnago apatite.

The quality of many of the samples was problematic. In particular, the apatite surfaces were often ‘frosted’ preventing detailed examination of the interior of grains and the identification of any inclusions. IND/8/04, IND/18/04 (A) and IND /19/04 (B) yielded very young apatite (U-Th)/He ages between 2.2 Ma and 36.7 Ma (alpha recoil-corrected). The measured concentrations of ^4He , U and Th are low for each of these aliquots and difficult to measure with precision; therefore, they are treated as suspect ages which cannot be meaningfully interpreted. IND/9/04 (A and B) and IND/19/04 (A) yielded very old AHe ages between 162.3 Ma and 238.5 Ma. Old AHe ages can be the result of unidentified inclusions providing parentless ^4He (Farley, 2000). The AFTT system is a deeper thermochronometer and provides older ages than the AHe system; therefore, another indicator that AHe ages may be erroneous is if they exceed the AFTT age. IND/9/04 provided a younger AFTT age (68 Ma) and although there is no AFTT age for IND/19/04, the AFTT ages of samples in close proximity are all younger than 160 Ma. IND/9/04 yielded ZrHe ages that replicate within 2 standard deviations and IND/18/04 (C - E) yielded AHe ages that replicate within 2 standard deviations. Both these samples are therefore treated more rigorously with inverse-modelling. The AHe inverse-modelling follows the same methods as AFTT modelling but uses a production-diffusion model to provide thermal histories (see section 3.3).

Sample IND/9/04 yielded two zircon (U-Th)/He (ZrHe) ages between 343 and 360 Ma. These are much older than either rifting event. To generate the old ZrHe ages, IND/9/04 can be interpreted as having spent time within the ZrHe PRZ prior to rifting. Inverse-modelling results indicate that IND/9/04 has cooled from temperatures between 125 and 140 °C, equating to 5.25 – 6 km of denudation (Figure 48a).

Samples IND/18/04 (C - E) have alpha recoil-corrected AHe ages of between 110 Ma and 123 Ma. These ages are older than IND/11/04 and reflect the time spent accumulating He within the He PRZ, prior to cooling to surface temperatures. Inverse-modelling results indicate that cooling at either 80 Ma or 65 Ma provides equally plausible thermal histories that fit the data and it is not possible based on modelled AHe ages alone to ascertain which rifting event initiated a denudational response (Figure 48b). However, in both modelled scenarios (cooling at 65 Ma and 80 Ma) the AHe data provides tighter constraints on the magnitude of cooling to surface temperatures: cooling cannot be less than 40 °C (otherwise the modelled AHe ages are too old) and cooling cannot be more than 60 °C (otherwise the modelled AHe ages are too young). The inverse-modelling of the AHe data also provides narrower constraints on the late stage segment of the cooling history (i.e., cooling from ~60 °C), with the result that the possible range of modelled thermal histories has been reduced when compared to inverse-modelling results from AFTT data for IND/18/04.

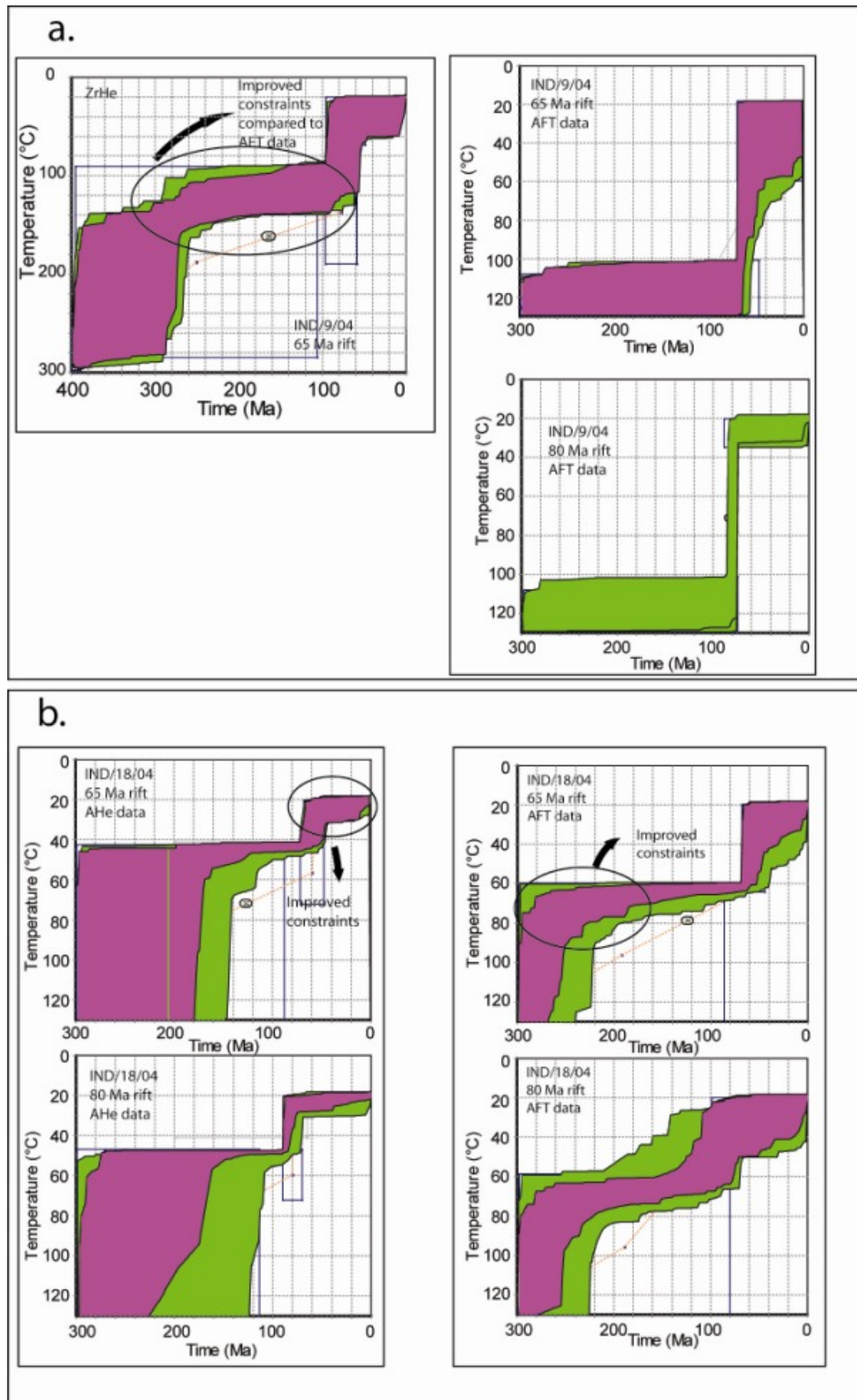


Figure 48 (U-Th)/He inverse-modelling of samples from Goa and Karnataka

a. Results from ZrHe inverse-modelling of IND/9/04 compared to results from AFTT inverse-modelling of IND/9/04. Note better constraints on the range of thermal histories with ZrHe for temperatures in excess of 110 °C

b. Results from AHe inverse-modelling of IND/18/04 compared to results from AFTT inverse-modelling of IND/18/04. Each thermochronometer provides tighter constraints on the range of thermal histories for the temperatures they are most sensitive to.

AHe ages are bulk ages and there is no additional information equivalent to AFTT TLD. Consequently, inverse-modelling often provides a large range of thermal histories which

reproduce the data suitably, and, as illustrated by the modelling results of IND/18/04, more than one tectonic history may be plausible. Inverse-modelling of IND/18/04 also demonstrates how AFTT and AHe data provide narrower constraints for the portion of the thermal history to which they are most sensitive (Figure 48b). The AFTT data constrain the pre-rift history, and the AHe data constrain the post-rift history (Figure 48). However, inverse-modelling of the data separately implies that the two thermochronometers are working independently when in reality fission tracks are formed and annealed at the same time that helium is being produced and diffused. Software is now available which allows simultaneous modelling of both AFTT data and AHe data to generate better defined thermal histories (see section 4.4).

4.4 Simultaneous inverse-modelling

This section reports the results of simultaneous modelling (AFT and AHe) from a sample at the escarpment (IND/18/04) and Simultaneous modelling (AFT and ZrHe) from a sample at the coast (IND/9/04). As with the individual modelling, simultaneous modelling was used to test if a particular rift initiated a rapid cooling event and what the magnitude of the cooling event was.

IND/9/04 was simultaneously modelled using ZrHe data and AFTT data. Figure 49 indicates improved constraints on both the high temperature segment of the thermal history (i.e., for temperatures >110 °C, as constrained by ZrHe data) and lower temperature segment of the thermal history (constrained by AFTT data). To satisfy the data, IND/9/04 must have been exhumed from between 140 °C and 110 °C at 65 – 75 Ma.

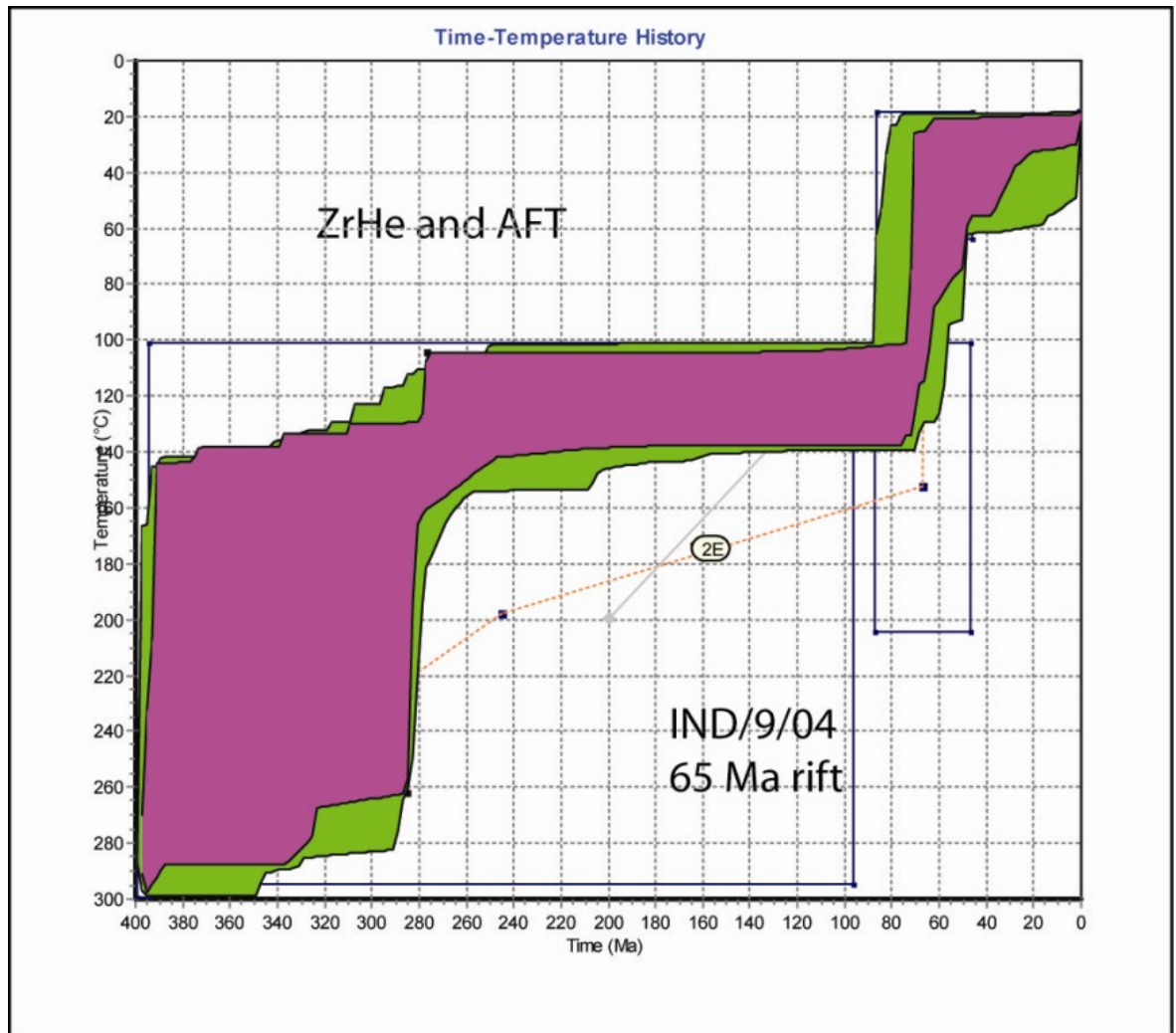


Figure 49 ZrHe and AFTT simultaneous inverse modelling results for IND/9/04

Individual inverse-modelling of IND/18/04 failed to resolve whether rifting at 80 Ma or 65 Ma resulted in a rapid cooling event (Figure 45a and Figure 48), an issue that simultaneous modelling may be able to resolve. Results from simultaneously modelling of AFTT data and AHe data are reported in Figure 50, but simultaneous modelling fails to satisfy both sets of data. There are several possible reasons for this: 1) incomplete understanding (and/or incomplete integration into the modelling software) of either the kinetics of fission track annealing or the diffusive behaviour of helium in apatite. 2) The data are erroneous or of poor quality. 3) The sample has experienced a complex thermal history that cannot adequately be replicated by the modelling software. Simultaneous modelling can provide additional information on a sample thermal history (as with IND/9/04); however, IND/18/04 demonstrates that in some circumstances simultaneous modelling is ineffective.

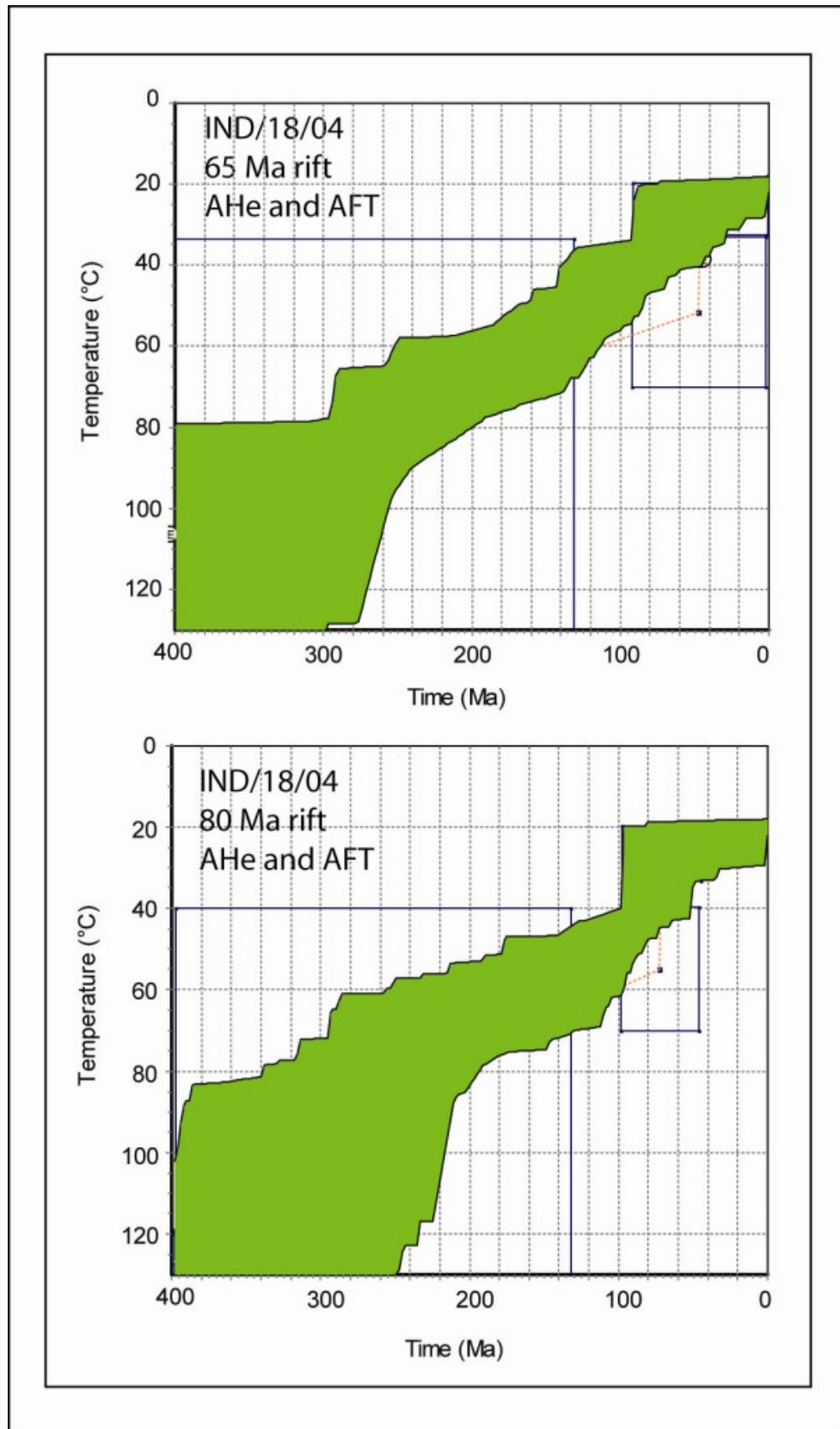


Figure 50 Simultaneous inverse modelling results for Goa and Karnataka
Simultaneous inverse modelling results for IND/18/04 (escarpment).

4.5 Summary and conclusions

Low temperature thermochronometry of rocks from the Goa and Karnataka provide specific information on the evolutionary history of the onshore portion of the Western Indian margin which complement the information provided from the offshore sedimentary record (see chapter 2). Samples at the coast have long uni-modal AFTT TLDs and AFTT ages that are indistinguishable from the timing of The Seychelles/India rift. The coastal samples can be interpreted as having been rapidly cooled from at least 110 °C at 65 Ma. AHe ages from the coast are consistent with AFTT ages and can be interpreted as having been rapidly cooled from at least 80 °C at 65 Ma. The AFTT or the AHe data do not provide constraints on the upper limit of cooling (both thermochronometers are insensitive to temperatures greater than 110 °C). However, ZrHe ages and modelling indicate that coastal samples must have been exhumed from less than 140 °C. The timing of the onset of increased cooling at the coast is inconsistent with either a denudational response to the Madagascar/India rift or active rifting (incorporating pre-rift rock uplift) associated with The Seychelles/India rift.

Samples located inland from the coast have short mean track lengths, complex TLDs and AFTT ages older than the timing of either The Seychelles/India rift or the Madagascar/India rift. These samples can be interpreted as having spent time in the PAZ prior to being exhumed to surface temperatures with the majority of fission tracks accumulating prior to cooling to surface temperatures. Inverse-modelling results indicate that the data can be reproduced equally well if rapid cooling occurred in response to either of the rifting events; however, the amount of cooling is small (~ 20 – 40 °C) and is at the limit of the sensitivity of the AFTT technique. AHe data from samples inland of the coast also fail to highlight if a particular rifting event initiated rapid cooling but provide improved constraints on the magnitude of cooling. Nonetheless, the fact that the coastal samples indicate that accelerated cooling must have occurred at 65 Ma means that it is reasonable to suggest that further inland is also likely to have experienced accelerated cooling in response to the same event.

Predictive forward modelled thermochronometry ages for the downwarp hypothesis should be old at the coast (as old as ages found on the interior plateau) and become younger towards the escarpment. The opposite trend in measured AFTT and AHe ages is observed from the Goa and Karnataka study area and is more consistent with escarpment formation into an elevated rift flank with 5.25 km of rock uplift at the coast decreasing to 0.5 – 1.5 km at the base of the escarpment. Predictive forward modelling also indicates that the measured data are best explained by a denudational response to rifting at 65 Ma, not 80 Ma.

Simultaneous inverse-modelling of AFTT data and (U-Th)/He data from samples at the coast demonstrates that this approach can be effective for providing improved resolution on the thermal history experienced by this segment of the margin. However, simultaneous inverse-modelling of thermochronometry data from samples close to the escarpment was less successful and did not yield any additional information. IND/18/04 highlights some of the potential challenges of inverse-modelling multiple thermochronometers (see section7).

The next chapter reports low temperature thermochronometry data from the southern field area within the state of Kerala, over 600 km south of the northern field area. Kerala is geographically distinct from Goa and Karnataka, the coastal plain is much wider (~100 km), and the escarpment is higher (2.5 km). The tectonic history of Kerala is poorly understood, and there is no clear consensus on the timing of formation of this portion of the margin. Kerala is a suitable field area to test if the Madagascar/India rifting event has influenced the development of this segment of the Western Indian margin using low temperature thermochronometry.

5 Low temperature thermochronometry data for Kerala

5.1 Introduction

The southern field area is in the state of Kerala between 9°N and 12°N. The bedrock is predominantly 2.5 – 2.6 Ga charnockites and gneisses of the Southern Granulite Terrane, that are locally overlain by Cenozoic sediments (see section 1.3.1). In Kerala the Ghats are separated into the Western Ghats and the Nilgiri Block, and the Southern Ghats by the 20 km-wide Palghat Gap (Figure 51). The Ghats are on average 1 – 2 km high reaching a maximum height of 2.9 km north of Munnar. Unlike the northern study area, the Ghats in Kerala are a more distinct linear feature with the escarpment rising abruptly from the coastal plain and foothills (here termed, for simplicity, the coastal plain). The coastal plain has an average elevation of 0.5 km and ranges in width from 30 km, to the north of Calicut, to a maximum of 70 km, south of Cochin. East of the crest of the escarpment there is a 5 – 10 km wide elevated region of dissected hills and inselbergs, bounded further to the east by a prominent east-facing escarpment that rises from an extensive interior plateau with an average elevation of 0.7 km.

Kerala was selected as a suitable area of study because the timing of initiation of escarpment formation is incompletely understood as there are few stratigraphic markers. As an alternative, the alignment of Precambrian structural lineaments has been used in plate reconstructions to place Madagascar adjacent to Western India prior to rifting at 80 Ma (Katz and Premoli, 1979). Spectral analysis of gravity and bathymetric data has also been used to ascertain the conjugate nature of Madagascar and Western India (Chand and Subrahmanyam, 2003; Subrahmanyam and Chand, 2006). Igneous rocks have been dated and tentatively linked to Marion hotspot volcanism and rifting between India and Madagascar (Pande et al., 2001; Storey, 1995; Torsvik et al., 2000) with little evidence from the volcanic record that The Seychelles/India rift propagated as far south as Kerala (see section 1.3.3). The rifting event responsible for the formation of the southern segment of the Western Indian margin remains unknown.

Low temperature thermochronometry has the potential to provide information on the thermal history of this portion of the margin to elucidate its tectonic history, yet there is no such

published information. This chapter reports apatite fission track and (U-Th)/He data from Kerala with the aims of:

1. Determining if the escarpment has evolved into a downwarped rift flank or an elevated rift flank.
2. Determining if the escarpment has developed in response to rifting between India and Madagascar or in response to rifting between India and The Seychelles.
3. Determining if this portion of the Western Indian margin is a volcanic rifted or a passive rifted margin (see section 1.2.1).

Nineteen samples were collected from a margin-normal transect east of Callicut and 30 samples were collected from a margin-normal transect east of Cochin (Figure 51 and Figure 52). Margin-normal transects were adopted for the sampling strategy because they include a wide range of elevations necessary to sample a range of palaeo-depths. Low temperature thermochronometric data from transects should display different trends between for the competing conceptual models of passive margin evolution (Gallagher, 1995). All samples are unweathered charnockites, gneisses or granites from either small quarries (on the coastal plain) or road-cutting and exposures (at the escarpment). AFTT data from 20 samples from the Cochin transect are reported in section 5.2, and (U-Th)/He data from 5 samples are reported in section 5.3, and the results of simultaneous inverse-modelling are reported in section 5.4. A summary and conclusions are provided in section 5.5. There are few published measurements on the present geothermal gradient of the Western Indian margin and even fewer estimates of the palaeogeothermal gradient and palaeosurface temperature (see section 4.1). Heat flow throughout the Southern Indian shield is highly variable (Agrawal and Pandey, 2004; Manglik, 2006; Roy and Rao, 2003) but similar to estimates from Goa and Karnataka. Consequently, a palaeogeothermal gradient of 20°C/km and a palaeosurface temperature of 20°C are used to convert the magnitude of cooling from low temperature thermochronometry into denudation.



Figure 51 Location of samples for Kerala

Samples are marked by red circles; the escarpment is marked by the ornated line.

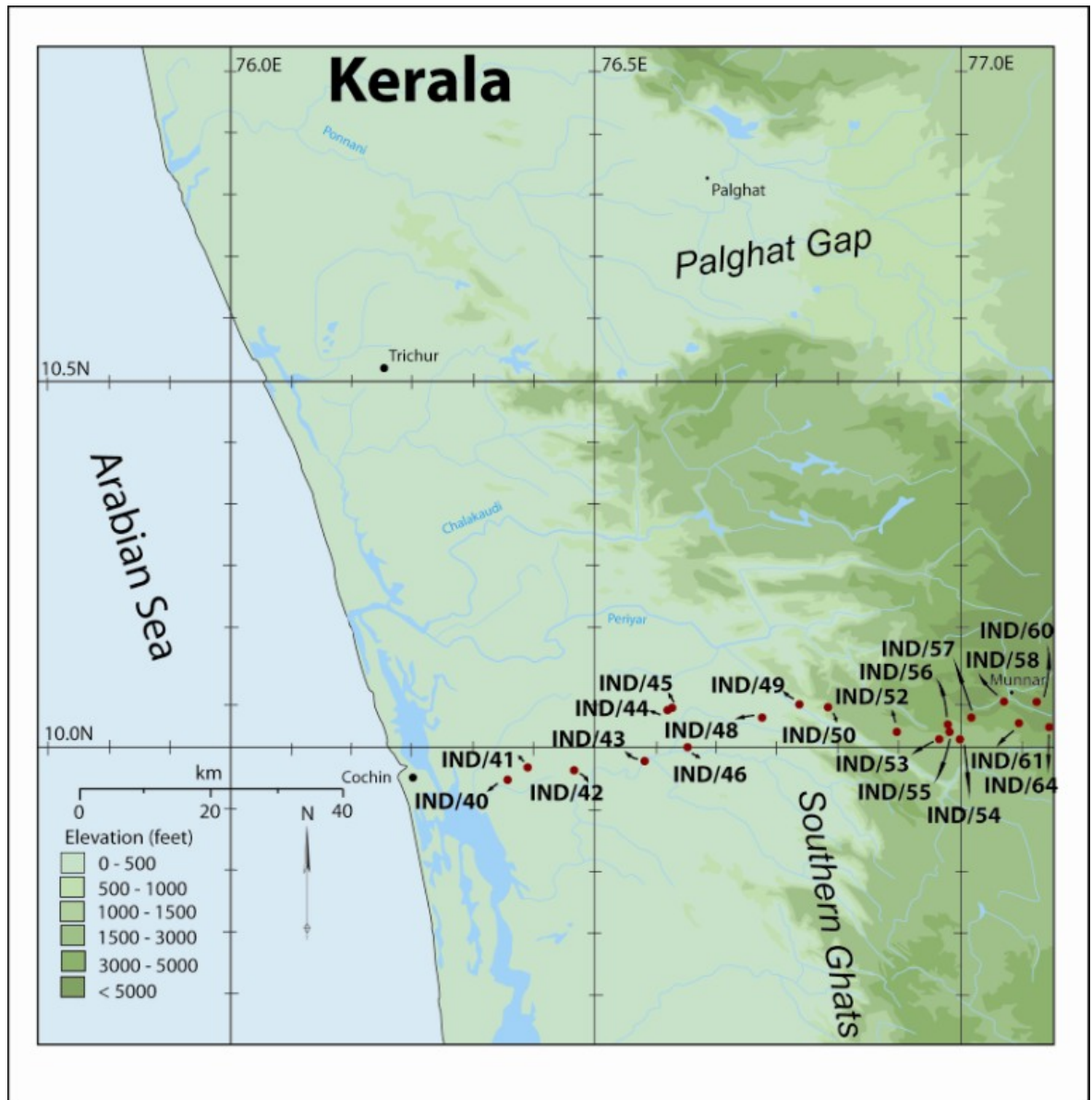


Figure 52 Location of analysed samples for Kerala

5.2 Apatite fission track data

Between 14 and 20 apatite crystals from each of the 20 samples from a transect between Cochin and Munnar were analysed using the external detector method (Gleadow and Duddy, 1981) and the zeta age calibration method (Hurford and Green, 1982, 1983) (Figure 52). Sample elevations range from sea level to over 1.5 km, covering the coastal plain, the escarpment face and the mountainous zone east of the escarpment around Munnar (Figure 52). Government restriction within Tamil Nadu prevented sampling of the elevated interior plateau further east. Figure 53, Table 9 & Table 10 report the location, elevation, fission track age, mean track length, 1σ uncertainties and average D_{par} values.

5.2.1 AFTT results

Apatite fission track (AFTT) ages range from 62 Ma to 314 Ma and mean track lengths range from 13.24 μm to 11.30 μm . The youngest AFTT age and longest mean TLD was obtained from the sample closest to the coast (IND/40/04). All other samples have AFTT ages older than 100 Ma and mean track lengths shorter than 13.09 μm . The general pattern is similar to AFTT results from Goa and Karnataka: samples closest to the coast are interpreted as having cooled rapidly from temperatures in excess of the PAZ at approximately the time of The Seychelles/India rift, and samples further inland have undergone smaller magnitudes of cooling and contain a proportion of fission tracks that have been partially annealed.

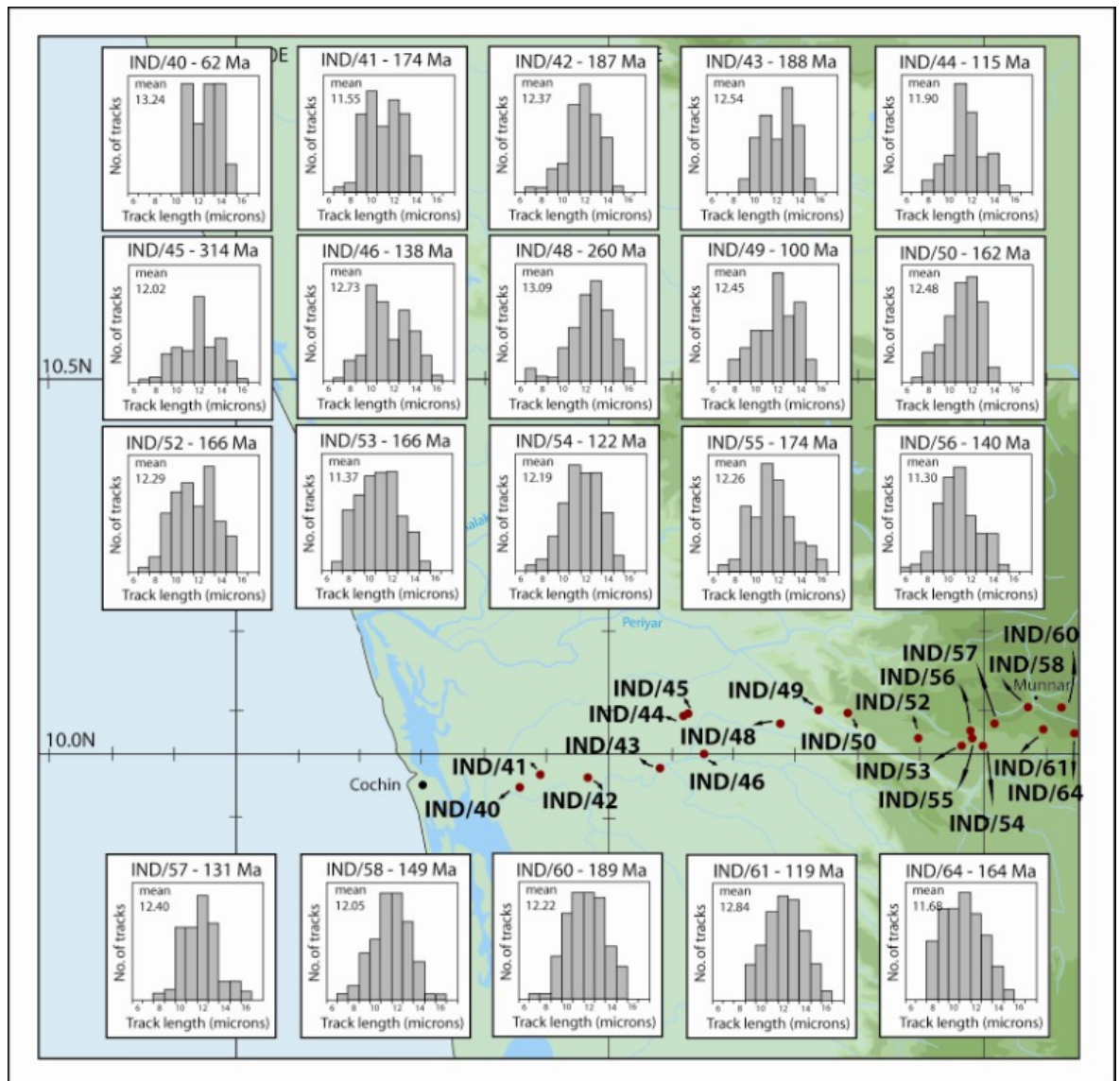


Figure 53 AFTT results for Kerala

Results of AFTT analysis (ages and corresponding TLD's) for selected samples in Kerala

Sample name	Degrees (N)	Degrees (E)	Dosimeter		No of grains	Spontaneous tracks		Induced tracks		Age dispersion		Central age (Ma)
			(ρ_d)	(N_d)		(ρ_s)	(N_s)	(ρ_i)	(N_i)	Chi-sq	P(%)	
IND40	9.9512	76.3871	12.77	7623	20	1.199	256	3.722	795	0.14	17.85	61.8
IND41	9.9715	76.4196	13.24	7482	20	5.086	1046	5.028	1034	0.15	7.99	173.6
IND42	9.9686	76.4750	13.35	7482	20	9.977	1911	9.591	1837	0.22	0.00	186.6
IND43	9.9881	76.5722	13.45	7482	20	0.661	58	0.627	55	0.01	90.68	187.9
IND44	10.0045	76.6353	13.55	7482	20	8.145	786	13.492	1302	0.31	0.00	114.8
IND45	10.0532	76.6004	13.22	7623	16	15.362	2656	8.497	1469	0.25	0.00	313.9
IND46	10.0534	76.6006	13.11	7623	20	7.184	1018	8.977	1272	0.17	0.84	138.1
IND48	10.0428	76.7374	13.67	7623	20	3.653	764	2.773	580	0.21	2.84	260.8
IND49	10.0584	76.7872	12.81	7238	20	5.793	1177	9.859	2003	0.07	15.52	100.3
IND50	10.0533	76.8243	12.80	7238	20	6.926	1228	7.31	1296	0.15	2.87	162.0
IND52	10.0187	76.9239	12.79	7238	20	23.312	3767	23.721	3833	0.13	0.01	165.7
IND53	10.0081	76.9723	12.78	7238	20	14.047	2508	14.193	2534	0.12	0.5	166.0
IND54	10.0099	77.0021	12.77	7238	20	11.543	2100	15.836	2881	0.15	0.04	122.1
IND55	10.0232	76.9873	12.76	7238	20	15.062	2502	14.659	2435	0.07	15.75	173.9
IND56	10.0348	76.9846	12.63	7482	14	14.097	2039	17.105	2474	0.19	0.00	139.8
IND57	10.0353	77.0177	12.75	7238	20	23.494	3077	30.015	3931	0.13	0.01	131.4
IND58	10.0575	77.0568	12.74	7238	20	17.768	2594	20.754	3030	0.18	0.00	148.7
IND60	10.0567	77.1021	12.94	7482	20	30.168	5393	27.136	4851	0.11	0.01	188.5
IND61	10.0350	77.0842	12.74	7238	13	29.272	2322	41.991	3331	0.15	0.00	119.0
IND64	10.0183	77.2075	9.32	5303	20	15.108	3329	11.514	2537	0.15	0.02	163.8

Table 9 AFTT age data for Kerala

Sample name	Degrees (N)	Degrees (E)	Number of tracks	Mean TLD		D _{par}	
				(μm)	($\pm 1\sigma$)	(μm)	($\pm 1\sigma$)
IND40	9.9512	76.3871	65	13.24	1.22	1.77	0.22
IND41	9.9715	76.4196	100	11.55	1.69	1.43	0.16
IND42	9.9686	76.4750	100	12.37	1.52	1.58	0.15
IND43	9.9881	76.5722	29	12.54	1.62	1.41	0.15
IND44	10.0045	76.6353	100	11.90	1.64	1.56	0.19
IND45	10.0532	76.6004	100	12.02	1.98	1.98	0.25
IND46	10.0534	76.6006	102	12.73	1.95	1.65	0.16
IND48	10.0428	76.7374	100	13.09	1.74	1.72	0.18
IND49	10.0584	76.7872	100	12.45	1.83	1.74	0.24
IND50	10.0533	76.8243	102	12.48	1.89	1.73	0.19
IND52	10.0187	76.9239	100	12.29	1.89	1.58	0.16
IND53	10.0081	76.9723	100	11.37	1.91	1.50	0.19
IND54	10.0099	77.0021	101	12.19	1.68	1.61	0.14
IND55	10.0232	76.9873	100	12.26	2.01	1.68	0.17
IND56	10.0348	76.9846	103	11.30	1.82	1.87	0.16
IND57	10.0353	77.0177	100	12.40	1.55	1.52	0.16
IND58	10.0575	77.0568	100	12.05	1.64	1.50	0.13
IND60	10.0567	77.1021	101	12.22	1.74	2.26	0.32
IND61	10.0350	77.0842	100	12.84	1.69	1.54	0.23
IND64	10.0183	77.2075	101	11.68	1.83	1.46	0.16

Table 10 Track length distribution and D_{par} data for Kerala

The “boomerang plot” in Figure 54a shows that there is not a strong relationship between AFTT age and TLD. However, the youngest sample with the longest mean TLD is contemporaneous with The Seychelles/India rift, and not the Madagascar/India rift (Figure 54a). Figure 54b indicates that there is no systematic geographic pattern within the AFTT age data (e.g., with distance from the coast), but the presence of the youngest sample at the coast makes it extremely difficult to envisage escarpment evolution into a downwarped rift margin where much older AFTT ages would be expected (Gallagher, 1995). In order to obtain constraints on the magnitude of cooling across the transect so as to be able to determine how the margin developed (downwarped rift flank versus elevated rift flank), as well as to ascertain the timing of the onset of this development, inverse-modelling is necessary. Inverse-modelling has only been undertaken on samples that pass the chi-squared test and have p-values greater than 0.05.

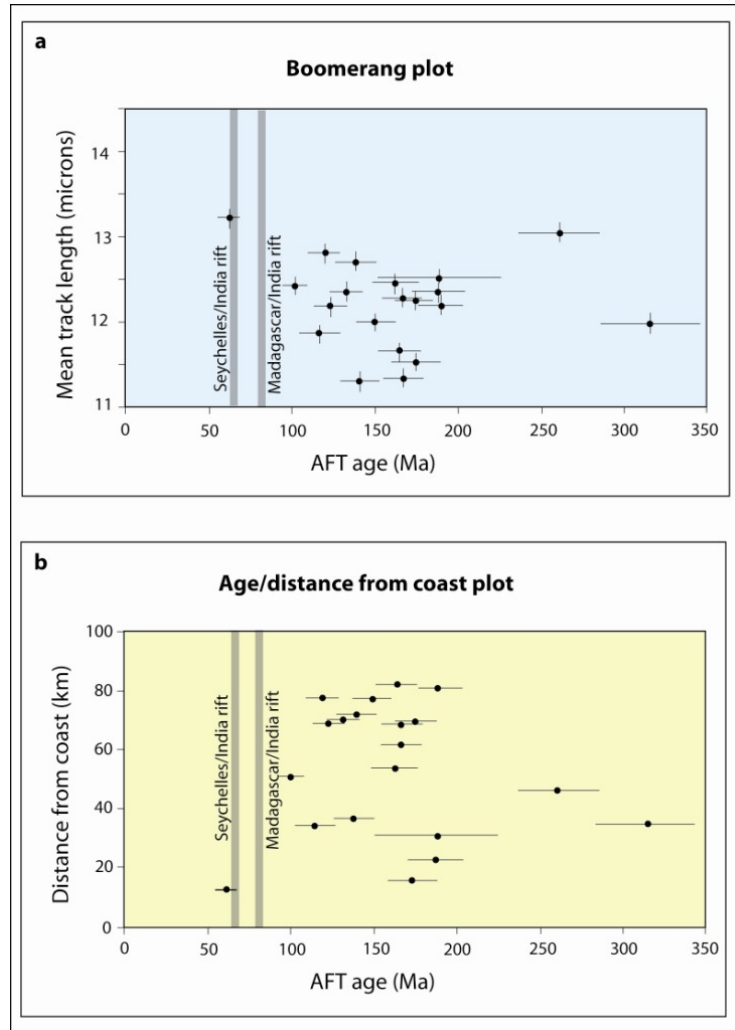


Figure 54 Boomerang plot and age vs distance from the coast for Kerala

a. Boomerang plot (AFTT age vs mean fission track length) for samples from Kerala.

b. AFTT age vs distance from the coast for samples from Kerala. The timing of The Seychelles/India rift and the Madagascar/India rift are marked by the solid bars.

Figure 13 displays the predicted AFTT results of all three conceptual models for constant escarpment formation initiated at 65 Ma (solid and dashed lines) and AFTT ages from the Cochin – Munnar traverse (see section 5.2) as solid circles. The trend and magnitude of the measured AFTT ages are reproduced adequately if the escarpment forms via the pinned divide model either with 4.5 km of rebound (more suitable fit to the data at the coast) or 3 km of rebound (more suitable fit to the data towards the escarpment).

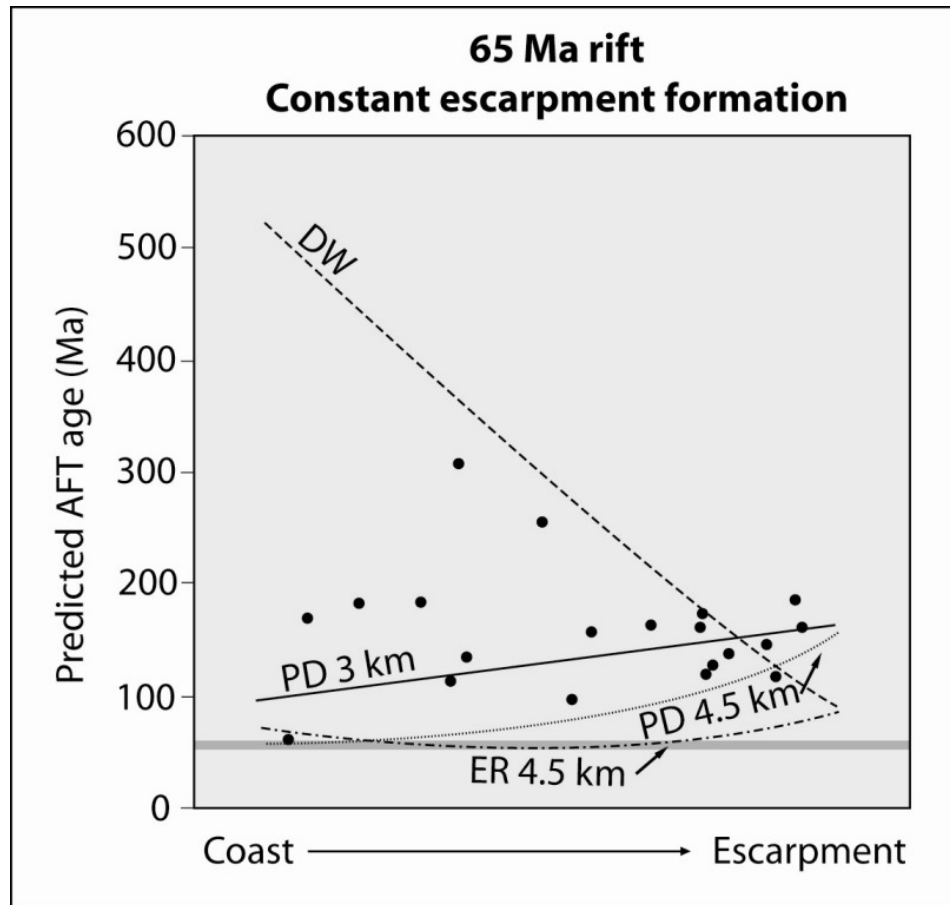


Figure 55 Predictive forward modelling results and measured data for Kerala

Predictive forward modelling results for all three conceptual models for constant escarpment retreat beginning at 65 Ma (solid and dashed lines) with measured data from the Cochin Munnar traverse (solid circles). The solid grey bar is the time of The Seychelles/India rifting event.

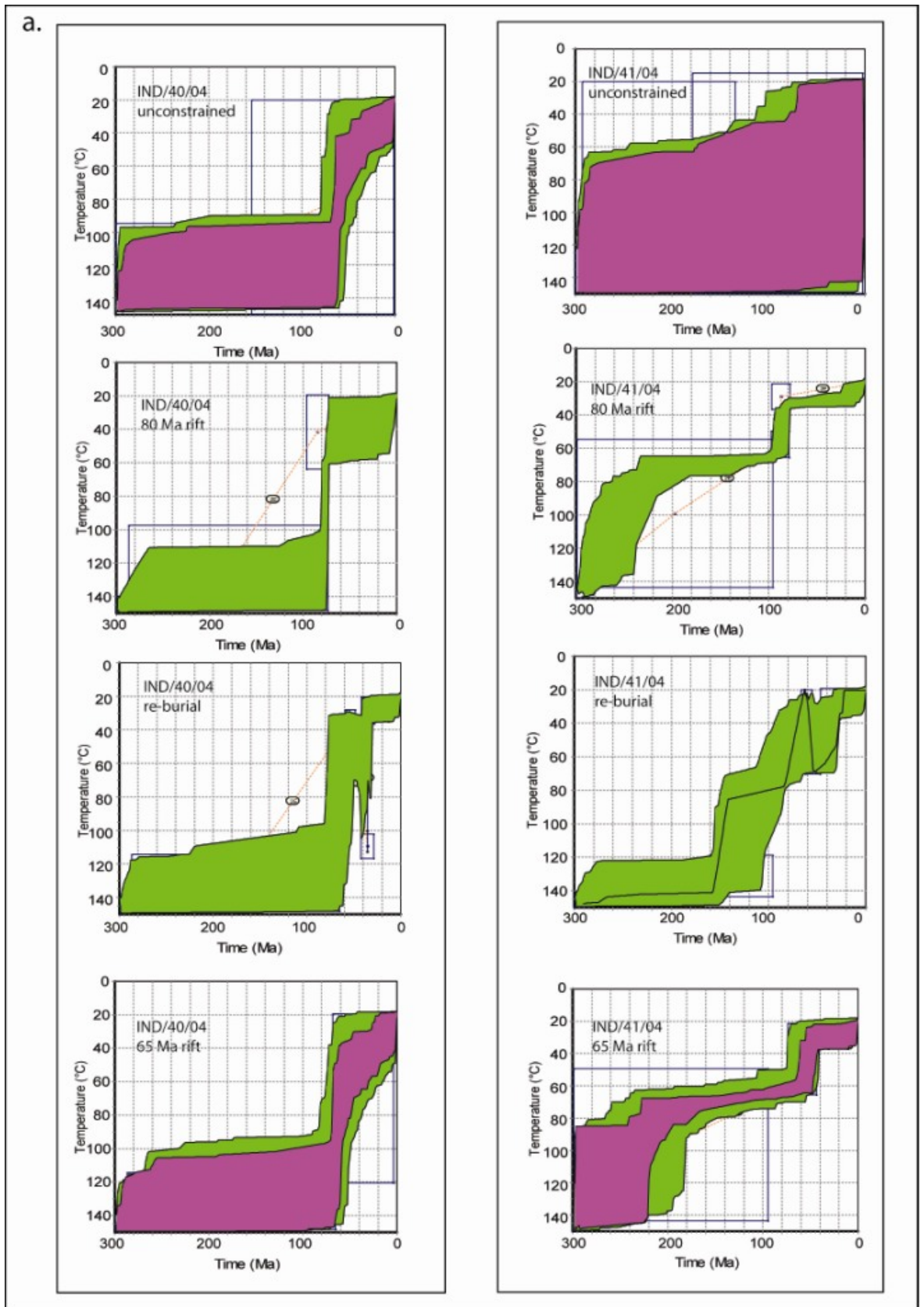
5.2.2 AFTT inverse-modelling

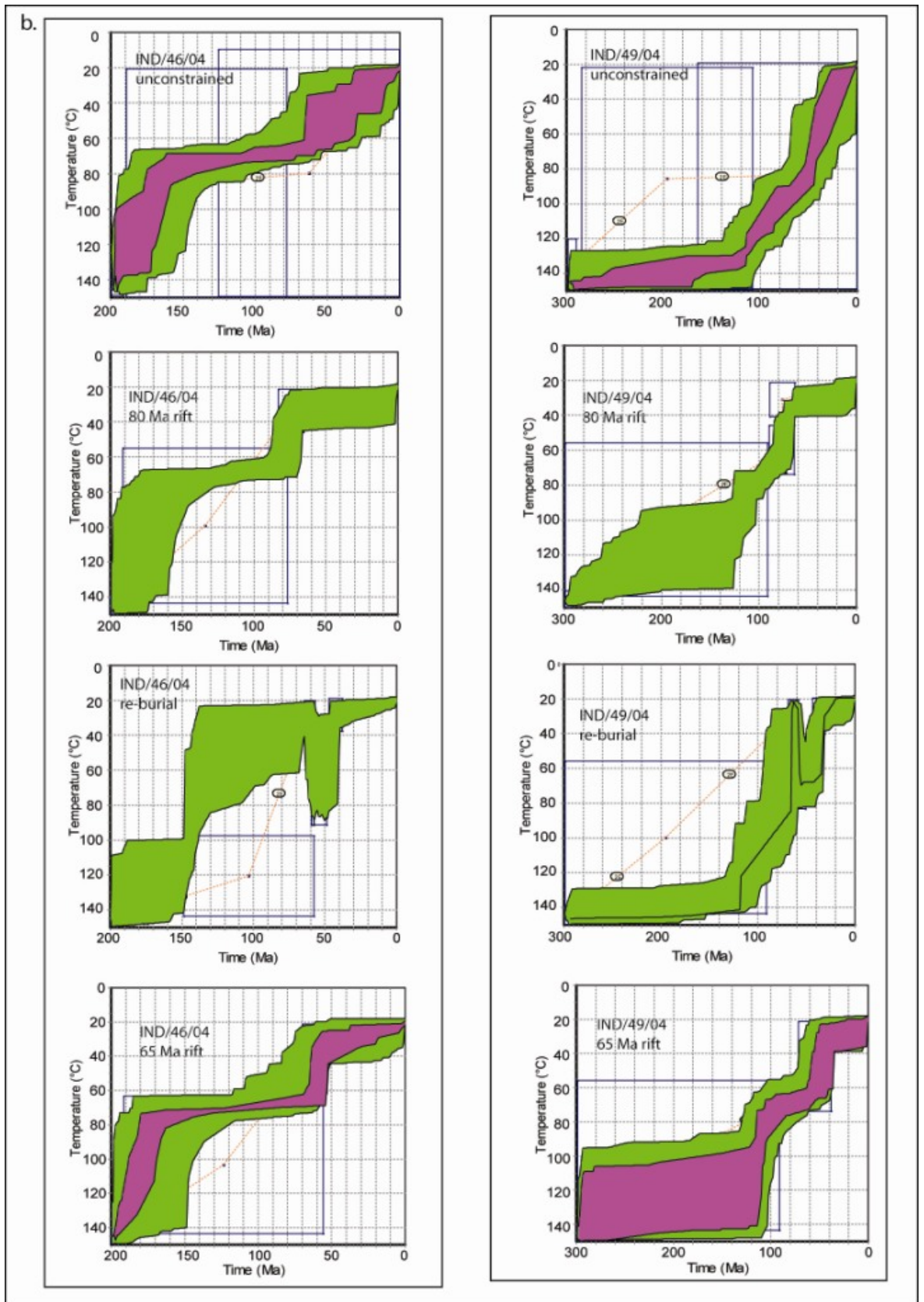
The Kerala AFTT data were inversely modelled using the same methods as applied to the Goa and Karnataka data (see section 4.2.2). The start conditions for all model inversions were such that the model run time exceeded the fission track age of the sample and the temperature of total annealing. The end conditions for each model run were 0 Ma and present day average surface temperature (20°C). Initial model runs were completely unconstrained. Subsequent model inversions were adapted to search for thermal histories that incorporate: re-burial accelerated cooling at 65 Ma and accelerated cooling at 80 Ma. Model inversions used the annealing algorithm of Ketcham et al. (1999), and they incorporated a c-axis projection correction for confined track lengths (Donelick et al., 1999) and the kinetic parameter D_{par} (see section 3.2.5.2). Each model run randomly searched for 10,000 thermal histories, and retained 'good' and 'acceptable' thermal histories at the end of each inversion.

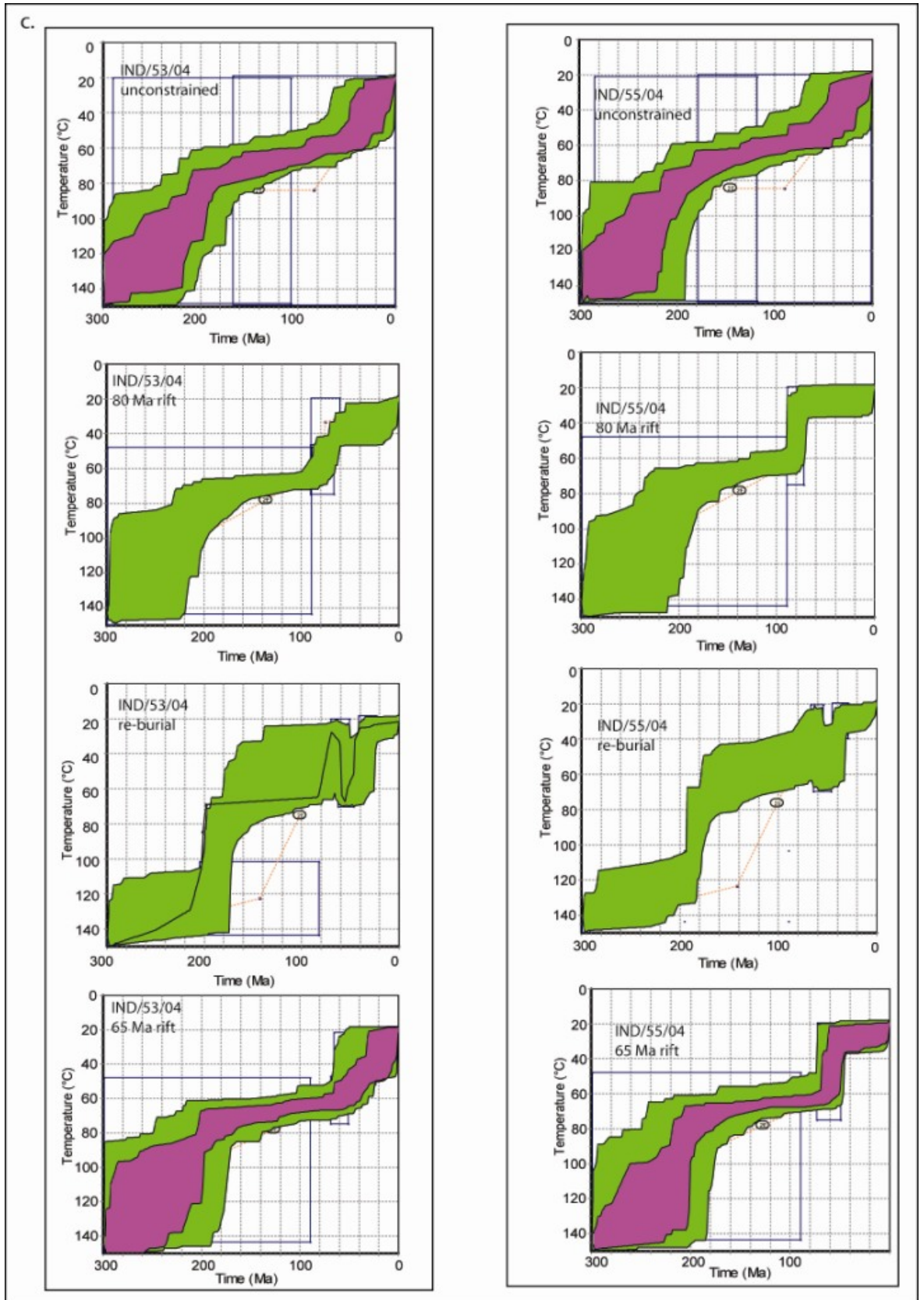
Inverse-modelling results are displayed in Figure 56a-d as time-temperature plots with the green envelopes encompassing acceptable thermal histories and the purple envelopes encompassing good thermal histories. IND/40/04 is the only sample that provides an age contemporaneous with The Seychelles/India rift. Inverse-modelling results from IND/40/04 indicate that the data are adequately reproduced if the sample cooled rapidly at 65 Ma. If the sample is allowed to rapidly cool earlier at 80 Ma or re-burial occurs, model inversions fail to locate any thermal histories that fit the data (Figure 56a). The coastal sample can be interpreted as having rapidly cooled from the base of the PAZ at the time of The Seychelles/India rift. IND/40/04 has apatite grains with an average D_{par} value of 1.77 μm , which will fully anneal at 111 °C. This cooling is equivalent to denudation in excess of 4.5 km for a palaeothermal gradient of 20°C/km and a palaeosurface temperature of 20°C.

Five further samples return inverse-modelling results that support accelerated cooling from within the PAZ at 65 Ma (Figure 56a-d and Figure 57). These samples are modelled as having a pre-rift history within the PAZ prior to accelerated cooling at 65 Ma from temperatures of between 70°C and 50°C. A pre-rift history within the PAZ is supported by the old AFTT ages and complex TLDs that indicate the fission tracks have been partially annealed. These data cannot adequately be reproduced if accelerated cooling occurs at 80 Ma or re-burial occurs (Figure 56a-c). Cooling from temperatures between 70°C and 50°C is equivalent to denudation of between 2.5 km and 1.5 km. These three samples and IND/40/04 support the hypothesis that The Seychelles/India rifting event triggered a denudational response and initiated the formation of the escarpment along the southern portion of the Western Indian margin.

Inverse-modelling of one samples (IND/50/04) provide ambiguous results that can be explained by accelerated cooling at either 65 Ma or 80 Ma (Figure 56d). There is no obvious explanation for IND/50/04 and the reason for successful inversion results for both simulated rifting events remains unclear. IND/50/04 could not be successfully inverse-modelled if re-burial occurs. This sample is bordered on either side by samples which rule out rapid cooling at 80 Ma. It is difficult to envisage some segments of the transect being affected by one rifting event and others by a different rifting event. Consequently, although this sample cannot provide robust constraints, they are not inconsistent with having also rapidly cooled at 65 Ma.







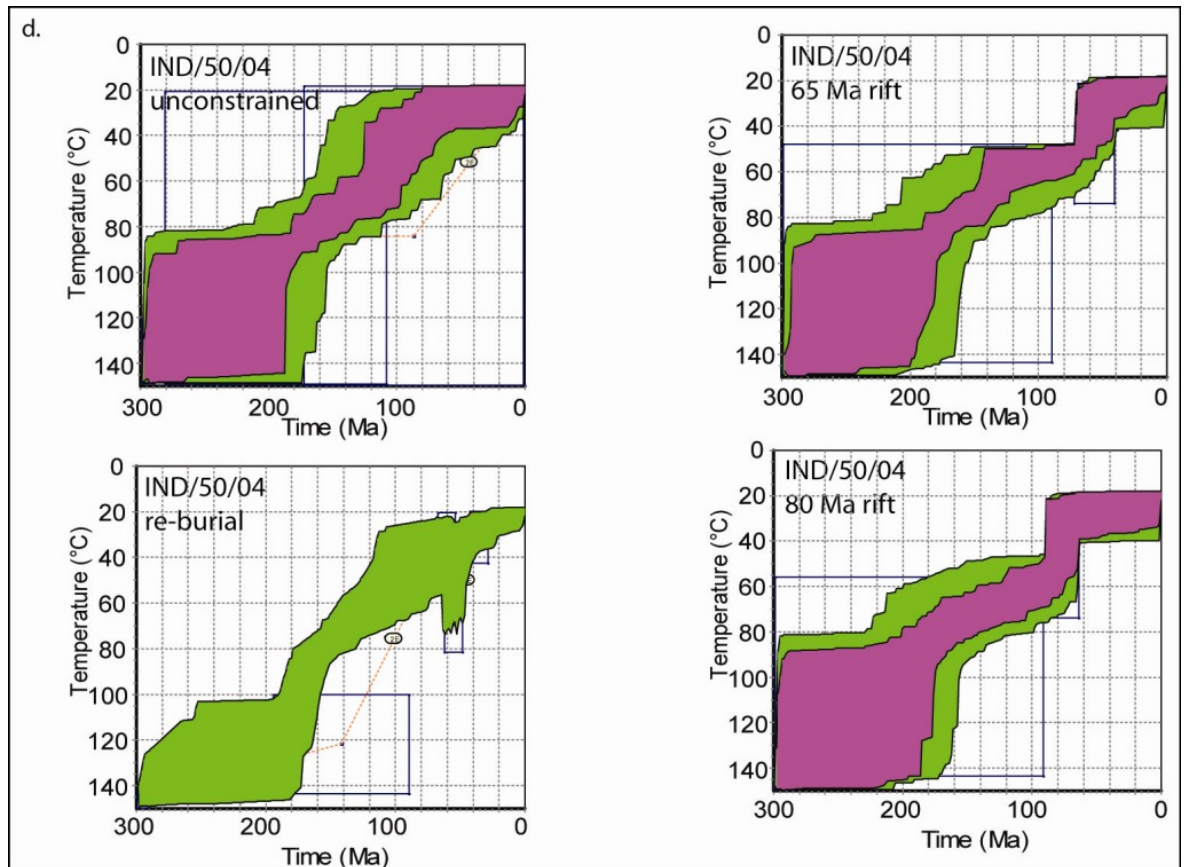


Figure 56 AFTT inverse-modelling results for Kerala

Green envelopes are ‘acceptable’ thermal histories, purple envelopes are ‘good’ thermal histories.

The amount of cooling inferred from the inverse-modelling is greatest close to the coast (from at least 111°C) and smaller further inland (from 70–50°C), a pattern of cooling that is compatible with escarpment formation into an elevated rift flank. It is difficult to envisage escarpment formation into a downwarped rift flank based on the results of inverse-modelling of AFTT data. Table 11 displays a summary of the magnitude of denudation for different palaeogeothermal gradients for samples from Kerala. As with the data from Goa and Karnataka, the magnitude of cooling further inland is small enough to test the sensitivity of the AFTT technique and constraining the post-rift cooling is challenging. Section 5.3 reports new (U-Th)/He data which are used to enhance constraints on post rift cooling.

Sample Name	Lat. (°N)	Long. (°E)	Post break-up cooling (°C) 65 Ma – 0 Ma	Magnitude of denudation (km) for variable palaeothermal gradients		
				20 °C/km	40 °C/km	60 °C/km
IND/40/04	9.9512	76.3871	90	4.50	2.25	1.50
IND/41/04	9.9715	76.4196	50	2.50	1.25	0.83
IND/42/04	9.9686	76.4750	30	1.50	0.75	0.33
IND/43/04	9.9881	76.5722	40	2.00	1.00	0.67
IND/45/04	10.0532	76.6004	50	2.50	1.25	0.83
IND/49/04	10.0584	76.7872	50	2.50	1.25	0.83
IND/52/04	10.0187	76.9239	50	2.50	1.25	0.83
IND/53/04	10.0081	76.9723	50	2.50	1.25	0.83
IND/54/04	10.0099	77.0021	50	2.50	1.25	0.83
IND/55/04	10.0232	76.9873	40	2.00	1.00	0.67
IND/56/04	10.0348	76.9846	30	1.50	0.75	0.33
IND/57/04	10.0353	77.0177	40	2.00	1.00	0.67
IND/58/04	10.0575	77.0568	40	2.00	1.00	0.67
IND/60/04	10.0567	77.1021	40	2.00	1.00	0.67
IND/61/04	10.0350	77.0842	50	2.50	1.25	0.83
IND/64/04	10.0183	77.2075	50	2.50	1.25	0.83

Table 11 Summary of magnitude of post break-up cooling for Kerala

Summary of magnitude of post break-up cooling from modelled AFTT data and magnitude of denudation based on variable palaeothermal gradients.

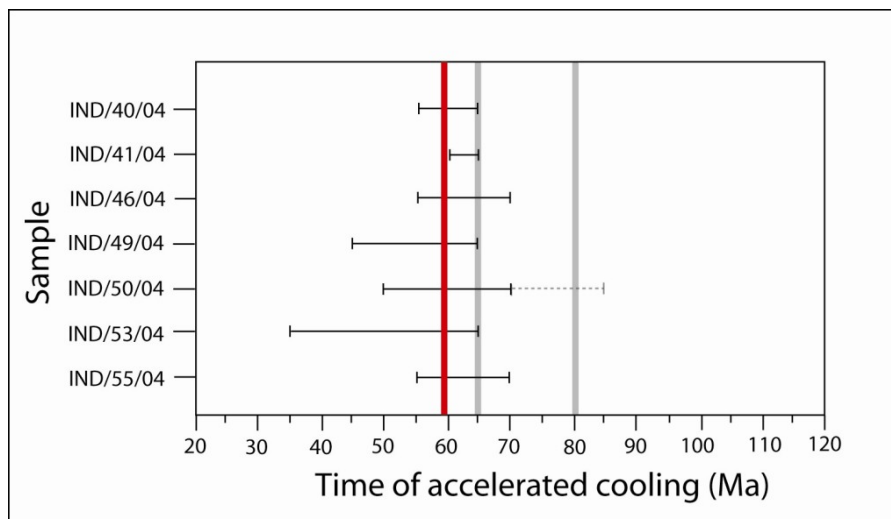


Figure 57 AFTT constraints on the time of accelerated cooling for Kerala

Apatite fission track constraints on the time of accelerated cooling (x-axis) for individual inverse-modelled samples (y-axis). The majority of samples can be successfully modelled with an accelerated cooling event at ~ 65 Ma (solid bars); however one sample (IND/50/04) can also be modelled successfully with accelerated cooling at ~ 80 Ma (dashed bars). The solid red line is the average time of cooling for the modelled samples (59Ma).

5.3 (U-Th)/He data

Compared to the samples from Goa and Karantaka, the apatites and zircons from Kerala were better quality (i.e. good apatite morphology and clean surfaces) and more abundant. Apatite (U-Th)/He (AHe) analyses were undertaken on IND/40/04, IND/42/04, IND/46/04, IND/52/04 and IND/64/04 (see Figure 52 and Table 12). IND/40/04 was also analysed for zircon (U-Th)/He (ZrHe) (see Table 13). Three to four inclusion free crystals were analysed per aliquot. Helium was extracted using a diode laser and analysis methods are reported in Appendix A. The samples were selected because they cover the major geomorphic features of the region – coastal plain, escarpment and elevated zone landward of the escarpment – and nearly the full range of elevations.

Table 12 displays the results for AHe and ZrHe analyses from Kerala. Alpha recoil-corrected AHe ages range from 36.8 Ma to 104.7 Ma and are all younger than AFTT ages from the same samples. Three samples on the coastal plain (IND/40/04, IND/42/04 and IND/46/04) all yielded AHe ages less than 65 Ma, whereas the remaining two samples located at the escarpment (IND/52/04) and in the elevated zone further east (IND/64/04) produce AHe ages greater than 65 Ma (Figure 58). This pattern in ages is very difficult to explain if the escarpment formed into a downwarped rift margin. The AHe ages at the coast are all younger than the time of The Seychelles/India rift suggesting that either these samples cooled rapidly after 65 Ma, or they cooled slowly through the PRZ starting at 65 Ma. In the next section the data are modelled in order to test if these ages could be produced from an increased cooling event in response to rifting between Madagascar and India.

Apatite (U-Th)/He

Sample name	Degrees (N)	Degrees (E)	Elevation (m)	Replicate	²³⁸ U (ng)	²³² Th (ng)	⁴ He (cc)	Uncorrected He age (Ma)	Corrected He age (Ma)	Mean age (Ma)	2σ	Analytical Error (Ma)	AFT age (Ma)
IND/40/04	9.9512	76.3871	0	I	0.0175	0.1189	1.588x10 ⁻¹⁰	28.7	36.8	48.0	26.5	0.9	61.8
IND/40/04				II	0.0656	0.0824	4.984x10 ⁻¹⁰	48.0	64.0				
IND/40/04				III	0.0352	0.3329	4.813x10 ⁻¹⁰	34.8	43.1				
IND/42/04	9.9686	76.4750	64	I	0.1137	0.3479	7.065x10 ⁻¹⁰	29.6	38.1	45.0	19.5	0.9	186.6
IND/42/04				II	0.0784	0.5932	1.100x10 ⁻⁰⁹	41.4	51.9				
IND/46/04	10.0534	76.6006	47	I	0.0922	0.1233	5.653x10 ⁻¹⁰	38.2	49.3	44.1	13.6	1.2	138.1
IND/46/04				II	0.0213	0.0647	1.127x10 ⁻¹⁰	25.3	36.4				
IND/46/04				III	0.0702	0.0965	4.007x10 ⁻¹⁰	35.4	46.6				
IND/52/04	10.0187	76.9239	548	I	0.4292	0.1307	3.535x10 ⁻⁰⁹	62.9	76.8	92.7	28.2	1.6	165.7
IND/52/04				II	0.0810	0.0538	8.968x10 ⁻¹⁰	78.2	103.6				
IND/52/04				III	0.0984	0.0480	1.005x10 ⁻⁰⁹	74.9	97.8				
IND/64/04	10.0183	77.2075	1303	I	0.3323	0.3718	4.407x10 ⁻⁰⁹	85.7	104.7	84.9	36.3	2.4	163.8
IND/64/04				II	0.0621	0.2263	7.427x10 ⁻¹⁰	52.8	69.0				
IND/64/04				III	0.1283	0.2590	1.423x10 ⁻⁰⁹	61.5	81.0				

Zircon (U-Th)/He

Sample name	Degrees (N)	Degrees (E)	Elevation (m)	Replicate	²³⁸ U (ng)	²³² Th (ng)	⁴ He (cc)	Uncorrected He age (Ma)	Corrected He age (Ma)	Mean age (Ma)	2σ	Analytical Error (Ma)	AFT age (Ma)
IND/40/04	9.9512	76.3871	0	I	1.2652	0.5148	4.768x10 ⁻⁰⁸	254.0	364.6	385.5	69.7	7.2	61.8
IND/40/04				II	1.1093	0.8068	5.977x10 ⁻⁰⁸	335.8	485.7				
IND/40/04				III	1.4716	0.4144	5.385x10 ⁻⁰⁸	255.7	367.1				
IND/40/04				IV	2.8599	0.5205	9.388x10 ⁻⁰⁸	243.1	324.2				

Table 12 and 13 (U-Th)/He data from Kerala

Errors are quoted to 2σ for multiple analyses. Single analyses are quoted to 6%, the same errors associated with analysis of Durnago apatite.

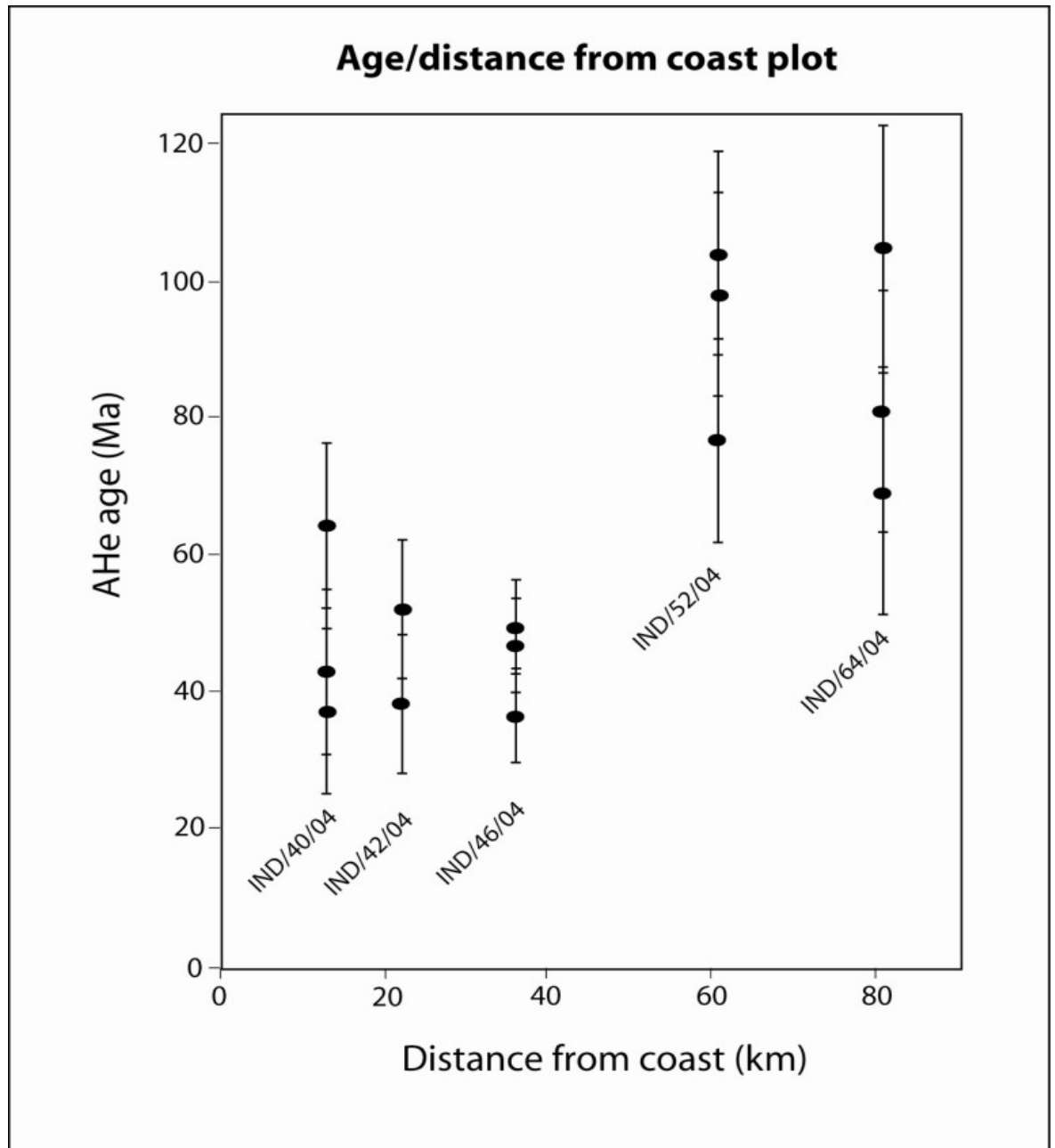


Figure 58 Apatite (U-Th)/He plot from Kerala

AHe age versus distance from the coast for samples analysed from Kerala. Error bars are 2 s.d. Younger ages are observed closest to the coast becoming older towards the escarpment, a pattern more consistent with denudation of an elevated rift flank.

The alpha recoil-corrected ZrHe ages for IND/40/04 are between 324.2 Ma and 485.7 Ma, much older than the AFTT age (62 Ma). These data indicate that although this sample has cooled from the base of the PAZ (as indicated by the AFTT data) it must have cooled from within the zircon PRZ prior to rifting to allow the accumulation and retention of He that would produce such an old ZrHe age. The temperature from which IND/40/04 has cooled from at 65 Ma is not immediately apparent from the data; however, inverse-modelling in the following section attempts to quantify this.

5.3.1 Inverse-modelling (U-Th)/He data

All five AHe samples and the single ZrHe sample were inversely modelled using the methods and model parameters outlined in section 4.2.2 except that a helium diffusion model (Farley, 2000; Reiners et al., 2004) was implemented instead of a fission track annealing model. Model runs were designed to simulate increased cooling at 80 Ma and 65 Ma. The average age and the average equivalent radius of each sample were used to carry out the model inversions.

AHe inverse-modelling results from IND/40/04 support the information provided by the AFTT data: the AHe data can be suitably reproduced if the sample is rapidly cooled from the base of the PRZ at 65 Ma. However, to reproduce the AHe age, the sample must remain within the PRZ during the post-rift period to allow a proportion of helium to diffuse out of the crystal and produce an AHe age less than 65 Ma. The inverse-modelling results demonstrate that the AHe data provide improved control on the post-rift segment of the thermal history of IND/40/04 (Figure 59a). The data from IND/40/04 cannot be adequately reproduced if the sample is modelled as having rapidly cooled from the base of the PRZ at 80 Ma unless the sample is held within the PRZ for the entire duration of the post-rift period and then cools rapidly (Figure 59a). A very late stage rapid cooling event is difficult to justify and there are no obvious mechanisms that could be responsible for such an event.

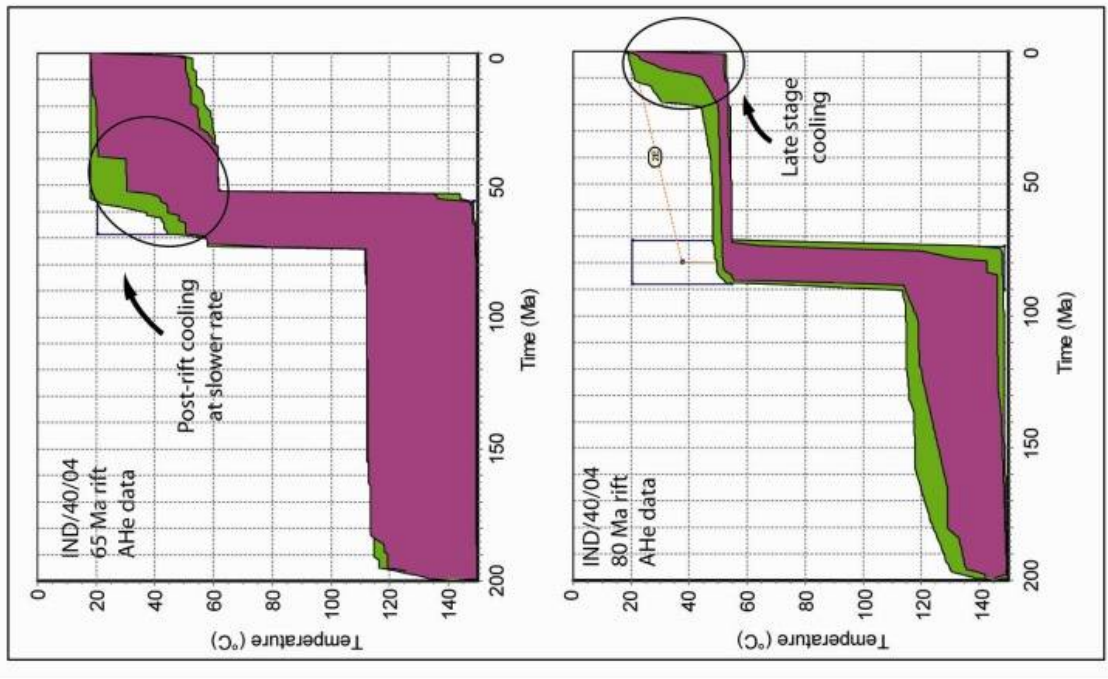
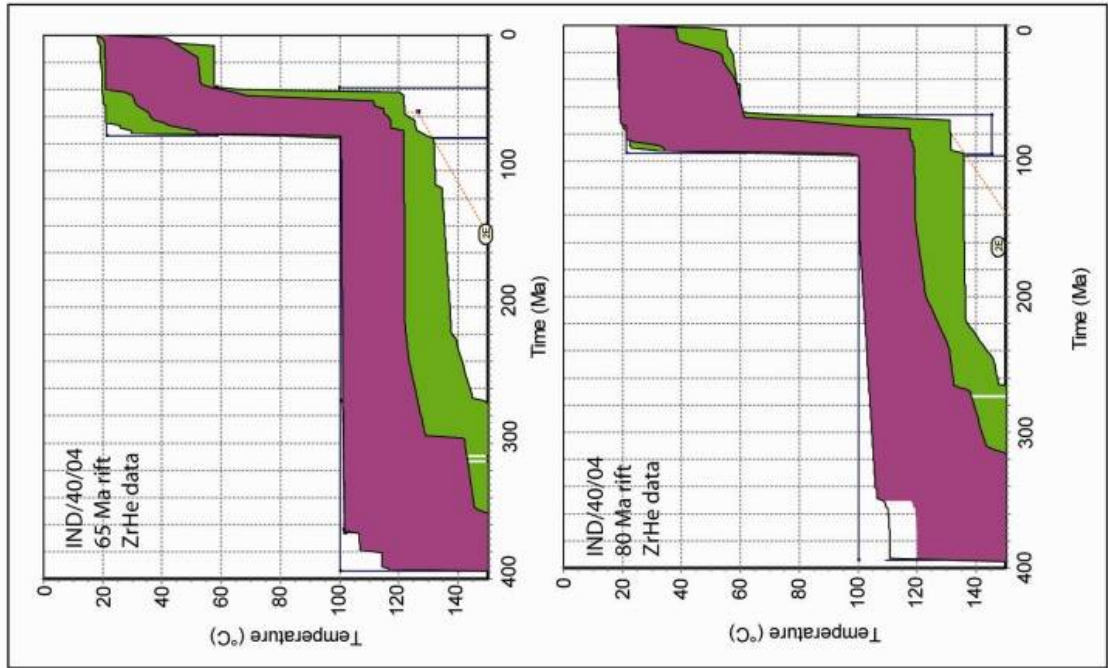
AFTT inverse-modelling results for IND/40/04 indicate that the data could be reproduced if the sample rapidly cooled from the base of the PAZ at 65 Ma. However, the AFTT data are unable to constrain how far below the PAZ the sample could have cooled from. ZrHe inverse-modelling results for IND/40/04 show that the data can be reproduced if the sample is allowed to cool from between 130°C and 110°C within the zircon PRZ (Figure 59a). If the sample cools from greater than 130°C the predicted ZrHe age is too young and if it cools from less than 110°C the predicted ZrHe age is too old. Inverse-modelling results also demonstrate that the ZrHe data are insensitive to the timing of the onset of rapid cooling and the data can be adequately reproduced for cooling at either 65 Ma or 80 Ma.

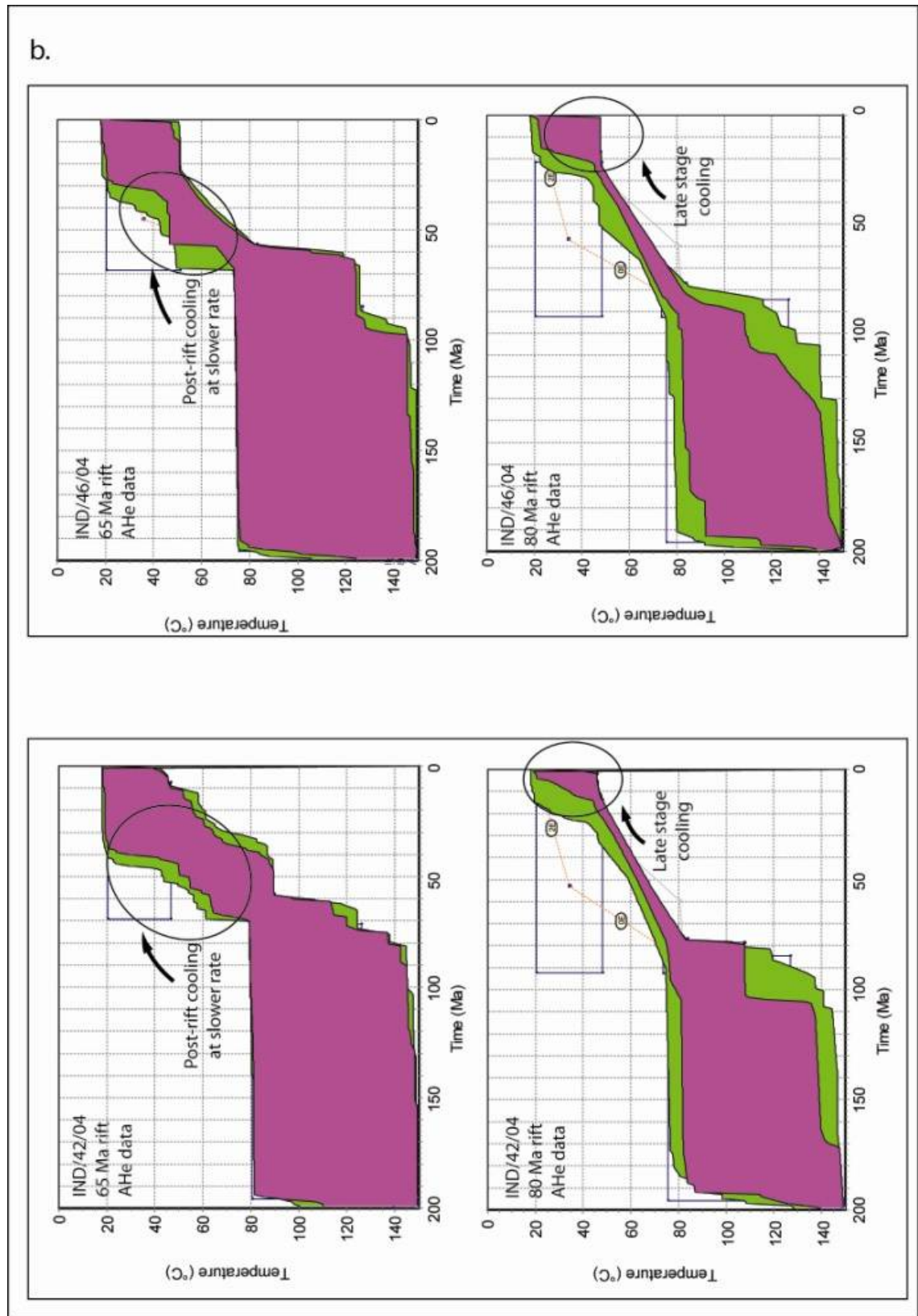
IND/42/04 and IND/46/04 produced similar AHe inverse-modelling results. If the samples are allowed to cool at 65 Ma the data can be reproduced successfully but only if the rate of cooling is between 1.7°C/Myr and 0.9°C/Myr (similar to the post-rift cooling rates predicted for IND/40/04) and only if they cool from greater than 80°C (Figure 59b). If these samples cool more rapidly at 65 Ma or cool from less than 80°C then the predicted AHe age is too old. When IND/42/04 and IND/46/04 are inversely modelled with cooling occurring at 80 Ma, then it is only possible to model the data successfully when the post-rift cooling rate is very slow and there is a late-stage rapid cooling event (Figure 59b).

AHe inverse-modelling results for IND/52/04 and IND/64/04 are less conclusive. Cooling at 65 Ma and cooling at 80 Ma both provide satisfactory modelled results that are consistent with the measured data. Samples must cool from between 60°C and 70°C, if cooling occurs at 65 Ma, or from greater than 80°C, if cooling occurs at 80 Ma (Figure 59c). It is difficult to envisage these samples to be recording a cooling signal from the Madagascar/India rifting event when samples further west on the coastal plain appear to be recording a cooling signal from The Seychelles/India rift.

The inverse-modelling of the apatite (U-Th)/He data provide support for the AFTT-derived conclusion that there was a strong denudational response to rifting between The Seychelles and India. Inverse-modelling also provides information on the magnitude of cooling across the region. For instance, IND/40/04 must have cooled from between 130°C and 110°C, which is equivalent to between 5.5 km and 4.5 km of denudation. The two samples on the coastal plain (IND/42/04 and IND/46/04) are modelled as having cooled from 80°C, corresponding to 3 km denudation. The two samples at the escarpment (IND/52/04 and IND/64/04) are modelled as having cooled from between 70°C and 60°C, equivalent to between 2.5 km and 2 km of denudation since 65 Ma. This pattern and magnitude of denudation is more consistent with escarpment formation into an elevated rift flank.

a.





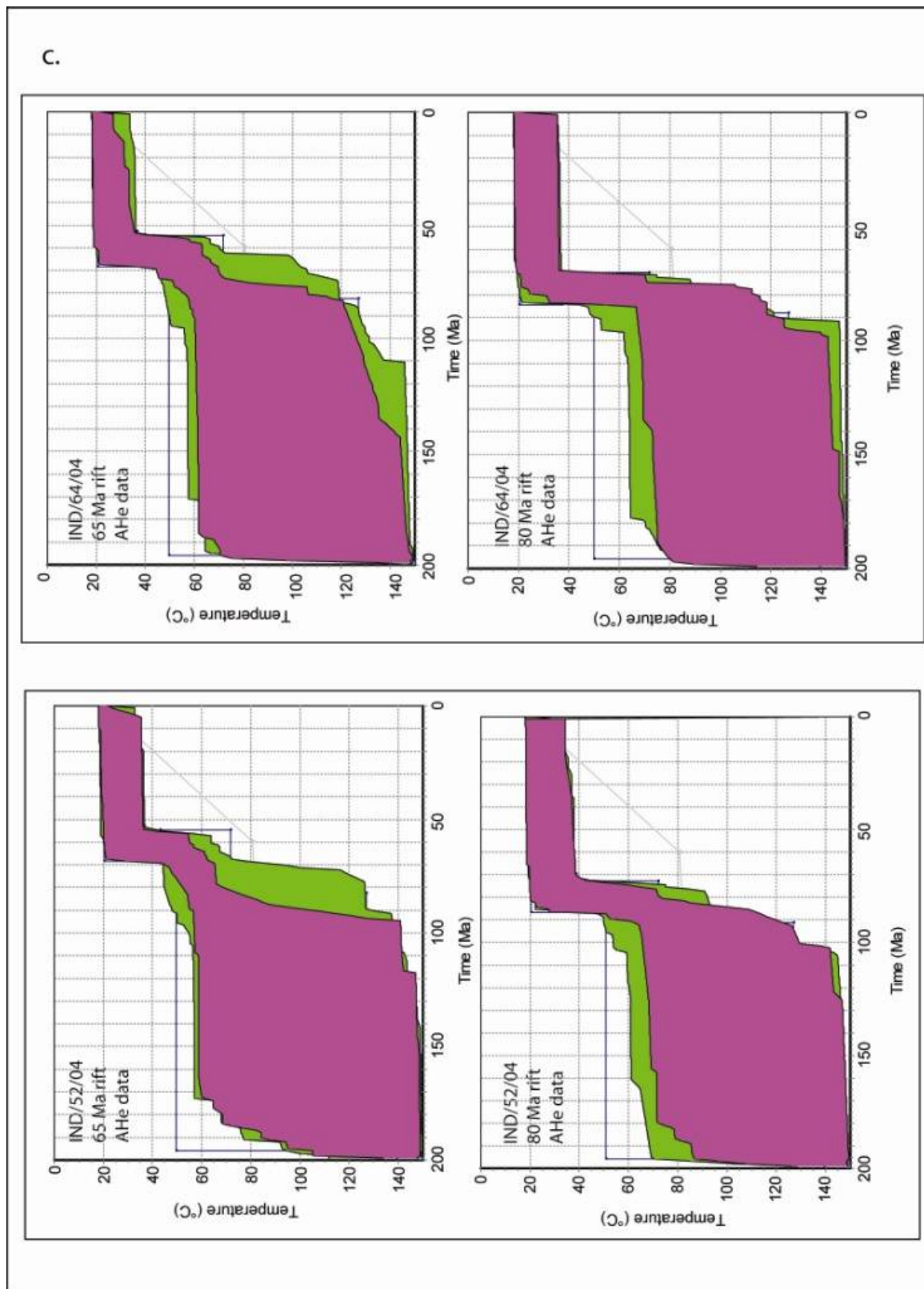


Figure 59 Results from apatite and zircon (U-Th)/He inverse-modelling of samples from Kerala

Green envelopes are 'acceptable' thermal histories, purple envelopes are 'good' thermal histories.

5.4 Simultaneous inverse-modelling

Simultaneous inverse-modelling was implemented for two samples, (IND/40/04 and IND/46/04). The parameters in each model run were the same as those used for the model inversion of each thermochronometer separately (section 0 and 5.3.1). The important difference from the modelling of the data from the individual thermochronometers is that with simultaneous inverse-modelling, successful inversion must satisfy both AFTT data and AHe data. Model runs were set up to test if a denudational response occurred in response to either rifting at 65 Ma or rifting at 80 Ma.

The results from IND/40/04 indicate that the data are best explained if the sample cooled rapidly from greater than 110°C to 60°C at 65 Ma followed by less rapid cooling (0.6°C/Ma) to present day temperatures. This supports the information provided from the inverse-modelling of each thermochronometer and confirms that there is no support for rapid cooling at 80 Ma (Figure 60). Cooling from greater than 110°C is equivalent to 4.5 km of denudation.

Modelling the combined thermochronometers from IND/46/04 is more challenging. Acceptable thermal histories that satisfy the AFTT and AHe data were located if the sample cools at a rate of 0.7°C/Myr – 0.6°C/Myr at 65 Ma from approximately 70°C, a similar rate to the post-rift cooling modelled for IND/40/04. No suitable thermal histories were recovered if the sample is allowed to cool at 80 Ma (Figure 60). Cooling from 70°C at 65 Ma corresponds to 2.5 km of denudation.

These results illustrate how simultaneous inverse-modelling can provide tighter constraints on the range of thermal histories for IND/40/04 and IND/46/04. The data that could be adequately modelled simultaneously provide support for rapid cooling at 65 Ma, consistent with a denudational response to rifting between The Seychelles and India. There is no evidence to support a denudational response to rifting between Madagascar and India. The pattern of denudation inferred from the simultaneous inverse-modelling results is 4.5 km closest to the coast (IND/40/04) decreasing to 2.5 km on the coastal plain. This pattern of denudation is consistent with escarpment evolution into an elevated rift flank, and is completely inconsistent with escarpment retreat into a downwarped rift flank.

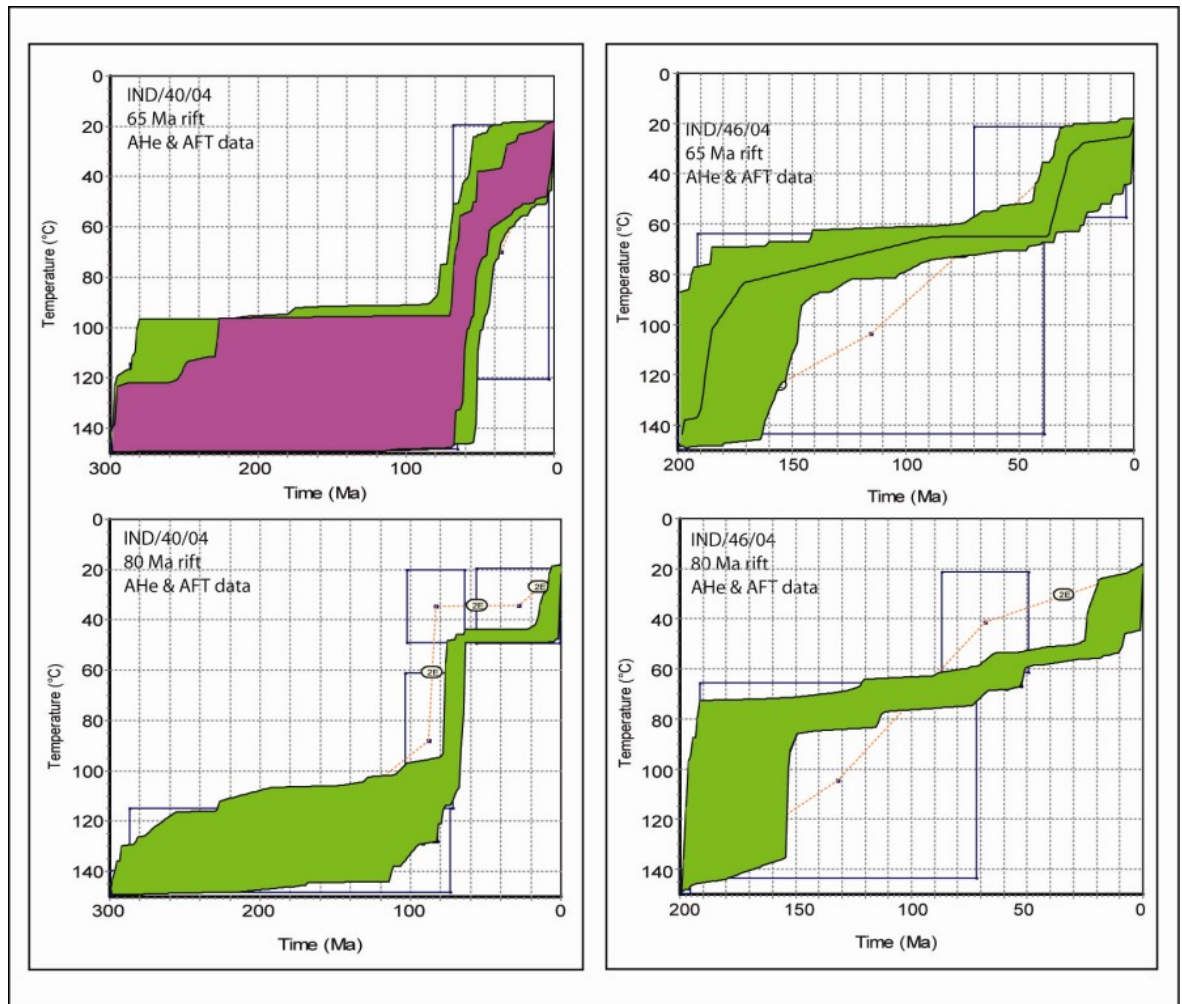


Figure 60 Simultaneous inverse-modelling results for Kerala

Simultaneous inverse-modelling results for IND/40/04 and IND/46/04

Green envelopes are 'acceptable' thermal histories, purple envelopes are 'good' thermal histories

5.5 Summary and conclusions

Low temperature thermochronometry of rocks from Kerala provides new information on the timing of the onset, and mode, of escarpment formation for this segment of the Western Indian margin. The sample closest to the coast (IND/40/04) has an AFTT age that is comparable to the age of the onset of rifting between The Seychelles and India. IND/40/04 also has a long, uni-modal TLD which can only be produced by rapid cooling from greater than 110°C. Inverse-modelling the IND/40/04 data supports the interpretation that this sample cooled rapidly from the base of the PAZ at the time of The Seychelles/India rift; there is no evidence to support a denudational response in Kerala to rifting between Madagascar and India.

Inverse-modelling of results from 15 samples from further inland indicate that data from the majority of these samples can be suitably reproduced if rapid cooling occurs from between 70 °C and 50 °C at approximately the time of The Seychelles/India rift. The data cannot be reproduced if rapid cooling occurs earlier, at the time of the Madagascar/India rift. Four

samples (Figure 56e) provide inverse-modelling results incorporating rapid cooling contemporaneous with either rifting event. However, these samples are tentatively interpreted as having rapidly cooled at the time of The Seychelles/India rift, consistent with the model inversions from surrounding samples. The pattern of cooling inferred from the AFTT data is inconsistent with escarpment retreat into a downwarped rift flank, and entirely consistent with escarpment evolution into an elevated rift flank (i.e. young rift ages at the coast, older ages inland). There is little evidence from any of the AFTT data to support active rifting incorporating pre-rift uplift with contemporaneous, denudationally-driven rapid cooling (see section 1.3).

It is difficult to provide constraints on the magnitude of cooling from AFTT data of IND/40/04 because it has cooled from at least the base of the AFTT PAZ. However, inverse-modelling results from ZrHe data can only be reproduced if IND/40/04 rapidly cools from between 130°C and 110°C. It is also challenging to provide accurate constraints on the magnitude of cooling for samples further inland because the data indicate that these samples have cooled from between 70°C – 50°C, temperatures which are at the limit of the sensitivity of the AFTT technique. Inverse-modelling of AHe data from five samples from the Cochin – Munnar transect provides results that adequately reproduce the measured data if rapid cooling occurs at 65 Ma (i.e. The Seychelles/India rift). However, the data can only be reproduced if the rate of post-rift cooling is between 1.7°C/Myr and 0.9°C/Myr. The pattern of cooling across the transect is consistent with escarpment evolution into an elevated rift flank.

Predictive forward modelling of AFTT data for a margin-normal transect provides different pattern of ages for the downwarp model and the elevated rift flank models. Forward-modelled AFTT ages for escarpment retreat into a downwarped rift flank are very old at the coast decreasing to ages that are much younger than the age of rifting (i.e., ~5 – 10 Ma) at the escarpment. Forward modelled AFTT ages for escarpment evolution into an elevated rift flank are indistinguishable from the age of rifting at the coast increasing towards the base of the escarpment. The measured AFTT data form a trend that is compatible with predictive forward modelled results for the pinned divide model with 4.5 km of rebound at the coast (decreasing to 2.5 km at the escarpment), initiated at the time of The Seychelles/India rift.

The results from simultaneous inverse-modelling of IND/42/04 and IND/64/04 highlight the potential challenges of this approach and model inversions for these samples were unsuccessful. However, simultaneous inverse-modelling of the remaining samples illustrates that this methodology is successful in providing tighter constraints on their thermal histories. Successful simultaneous model inversions are consistent with a denudational response to rifting between The Seychelles and India and escarpment evolution into an elevated rift flank.

Low temperature thermochronometry from both Goa and Karnataka, and Kerala demonstrate that the thermal histories for the Western Indian margin are best explained if an escarpment has developed into an elevated rift flank. The elevated rift flank models for passive margin evolution incorporate syn-rift lithospheric rift flank uplift (in direct response to rifting) and post-rift lithospheric flexure in response to denudational unloading onshore and sediment loading offshore (see section 1.2.2). Chapter 6 examines the lithospheric flexural response of the Western Indian margin using constraints from low temperature thermochronometry onshore (Chapter 4 & 5) and the sediment distribution offshore (Chapter 2).

6 Flexure of the lithosphere

6.1 Introduction

One of the key aims of this project is to test the competing groups of conceptual models for the evolution of the Western Indian high elevation passive margin. Apatite fission track and (U-Th)/He thermochronometry (chapters 4 and 5) indicate that the thermal history of the shallow lithosphere is best explained by a denudational response to escarpment development into an elevated rift flank. Similarly, the volume of clastic sediment deposited offshore of this segment of the Western Indian margin can only be accounted for by denudation of an elevated rift flank (chapter 2). The elevated rift flank models include ongoing flexural modification of the lithosphere as a result of denudational unloading onshore and sediment loading offshore. Lithospheric flexure is a potentially important mechanism influencing rock uplift, denudation and long-term landscape development (Gilchrist and Summerfield, 1990), yet it is poorly understood for the Western Indian margin.

This chapter examines the flexural isostatic response of the Western Indian margin to denudational unloading onshore (constrained from low temperature thermochronometry) and sediment loading offshore (constrained from basin geometry and sediment volume) to address the following questions:

1. Can rock uplift onshore and subsidence offshore be accounted for solely by flexural isostasy?
2. What are the flexural parameters necessary to generate rock uplift onshore and subsidence offshore, and are they compatible with natural conditions and with the characteristics of the Western Indian margin?
3. If flexural isostasy cannot explain the magnitude of rock uplift and subsidence, what additional mechanisms can be invoked?

Prior to discussing the theory of isostatic compensation (see section 6.2) it is necessary to examine the different types of vertical displacement acting on a passive margin (see Figure 14). England and Molnar (1990) defined the following relationship:

Surface uplift = Rock uplift – Denudation

Equation 7

Rock uplift occurs by tectonic uplift, thermal or dynamic mechanisms (e.g. plume/lithosphere interactions or mantle convection), isostatic adjustment to sub-lithospheric density variations (e.g. underplating or delamination) and isostatic adjustment to surface processes (see section 1.2.1). This chapter focuses on the isostatic adjustment to the surface processes of denudational unloading. If the isostatic response to denudational unloading is the only mechanisms generating rock uplift, and there has been no change in surface elevation, then it follows from Equation 7 that isostatic uplift (modelled in this chapter) should be equal to denudation (constrained from low temperature thermochronometry). If there is a mismatch between the isostatic response to denudational unloading and the magnitude of denudation then either the other mechanisms responsible for rock uplift need to be examined, or surface elevation has changed (Figure 61). Equation 7 can be modified for the depositional segment of the margin:

Change in basin elevation = Basin subsidence – (Sediment thickness + water)

Equation 8

Basin subsidence occurs either as tectonic subsidence, thermal subsidence or isostatic subsidence due to sediment and water loading (Allen and Allen, 2005). If it is assumed that the basin elevation has not changed and the only mechanism responsible for generating basin subsidence is isostatic adjustment to sediment loading, then the sediment thickness (constrained from offshore data, (chapter 2) should equal the modelled isostatic response to sediment loading. If there is a mismatch between the modelled isostatic response to sediment loading and the thickness of sediment present offshore, additional subsidence mechanisms must be considered or there has been a change in basin elevation (Figure 61).

Section 6.2 outlines the different forms of isostatic compensation, namely, local isostasy (Airy and Pratt models) and regional isostasy (flexural models). Section 6.3 examines isostasy in the context of the Western Indian margin and describes the methods used to model flexure of the Indian lithosphere. Section 6.4 reports the results and section 6.5 includes the discussion and conclusions.

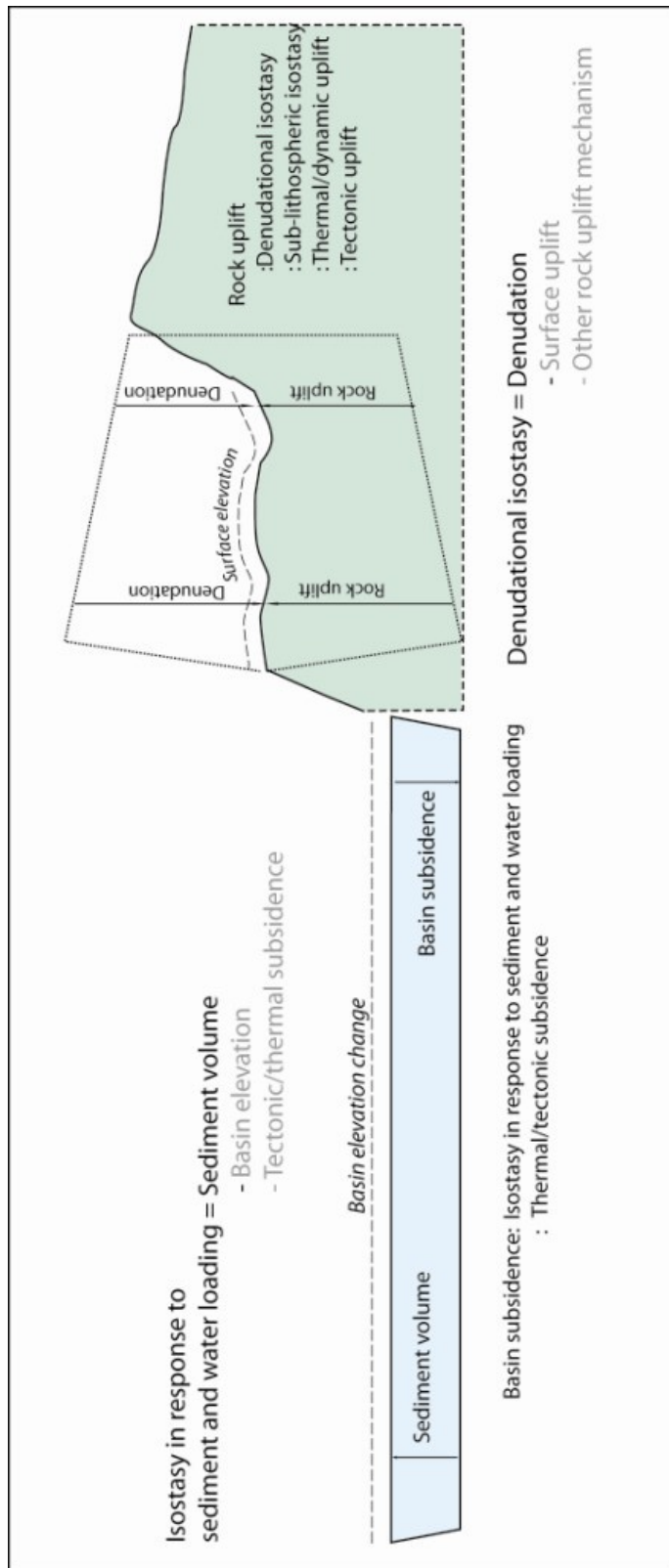


Figure 61 Uplift, subsidence and isostasy

Diagrammatic illustration of the relationship between denudationally driven isostasy, sediment load driven isostasy and additional uplift/subsidence mechanisms. Onshore denudationally driven isostasy is only the same as denudation if there is no tectonic uplift, no sub-lithospheric isostasy (e.g. magmatic underplating, lithospheric delamination), or no change in surface elevation. Similarly, offshore sediment load driven subsidence is only the same as sediment volume if there is no additional thermal/tectonic subsidence or no change in basin elevation.

6.2 Isostatic compensation mechanisms

Isostasy is the state of equilibrium between the lithosphere and asthenosphere whereby elevated and depressed areas of the Earth are compensated at depths. The compensation mechanism can be either local (see section 6.2.1) or regional (see section 6.2.2). Local isostasy treats the lithosphere as individual blocks responding to variations in density or thickness, and assumes that the lithosphere has no inherent strength. Local isostasy is an end-member condition where changes in the properties of the lithosphere will generate the greatest magnitude of rock uplift (or subsidence). Local isostasy has been included in the modelling procedure because it is an end-member condition (see section 6.4). Regional isostasy assumes that the lithosphere responds elastically over a much greater area and consequently generates smaller magnitudes of rock uplift depending on the strength of the lithosphere. For an elastically weak lithosphere, flexural isostasy approaches local isostasy and full compensation of loads of any size occurs. For an elastically strong lithosphere, flexural isostasy approaches completely uncompensated lithosphere capable of supporting large surface loads without any isostatic response.

6.2.1 Local isostasy

Local isostasy follows Archimedes Principle of hydrostatic equilibrium (first applied to isostasy by Fischer (1881)) where discrete, rigid lithospheric blocks move vertically and independently of each other while being supported on a fluid sub-stratum. There are two established models for local isostasy: the Airy hypothesis (Airy, 1855), subsequently developed by Heiskanen (1931), and the Pratt hypothesis (Pratt, 1859) later developed by Hayford (1909). The Airy-Heiskanen model assumes that the density of the lithosphere everywhere is equal such that areas of upstanding elevation are supported at their base by a ‘root’ of lithosphere which is less dense than the underlying asthenosphere. Depressed areas are supported at their base by an ‘anti-root’ composed of denser asthenosphere (Figure 62a). Airy isostatic equilibrium (i.e. the thickness of a root or anti-root) for an elevated lithospheric column is defined as:

$$r = \frac{h\rho_c}{(\rho_m - \rho_c)}$$

Equation 9

Where r is the thickness of the root, h is elevation of the lithospheric column, ρ_c is the average density of the lithosphere and ρ_m is the average density of the asthenosphere. The thickness of an anti-root for a depressed lithospheric column is defined as:

$$a = \frac{z(\rho_c - \rho_w)}{(\rho_m - \rho_c)}$$

Equation 10

Where z is the depth of water and ρ_w is the density of water.

The Pratt-Hayford model assumes that the thickness of the lithosphere everywhere is equal and isostatic equilibrium is achieved through variations in lithospheric density (Figure 62b). The density of an elevated area of the lithosphere is defined as:

$$\rho_e = \frac{T_c \rho_c}{(T_c + h)}$$

Equation 11

Where ρ_e is the density of the elevated lithospheric column and T_c is the normal thickness of lithosphere. The density of a depressed lithospheric column is defined as:

$$\rho_d = \frac{(T_c \rho_c - z \rho_w)}{(T_c - z)}$$

Equation 12

Local isostasy represents an end-member scenario capable of generating the maximum amount of rock uplift for a given amount of surface lowering. Using typical asthenosphere and lithosphere densities (3300 kg/m^3 and 2700 kg/m^3 respectively), surface lowering of 1 km will generate 4.5 km of rock uplift, and accordingly will require 5.5 km of denudation (Equation 9). Local isostasy assumes that the lithosphere has no rigidity and no matter how small the applied load, the lithosphere will reach isostatic equilibrium. Under certain conditions this assumption is valid where there are mechanisms (such as large scale faulting) to accommodate independent movement of discrete crustal blocks or the loads are significantly large. However, for many geological environments, the assumption that the lithosphere is weak is not appropriate (Banks et al., 1977). An alternative mechanism for achieving isostatic equilibrium is regional

compensation whereby the lithosphere is not treated as discrete blocks but responds via flexure over a broad area.

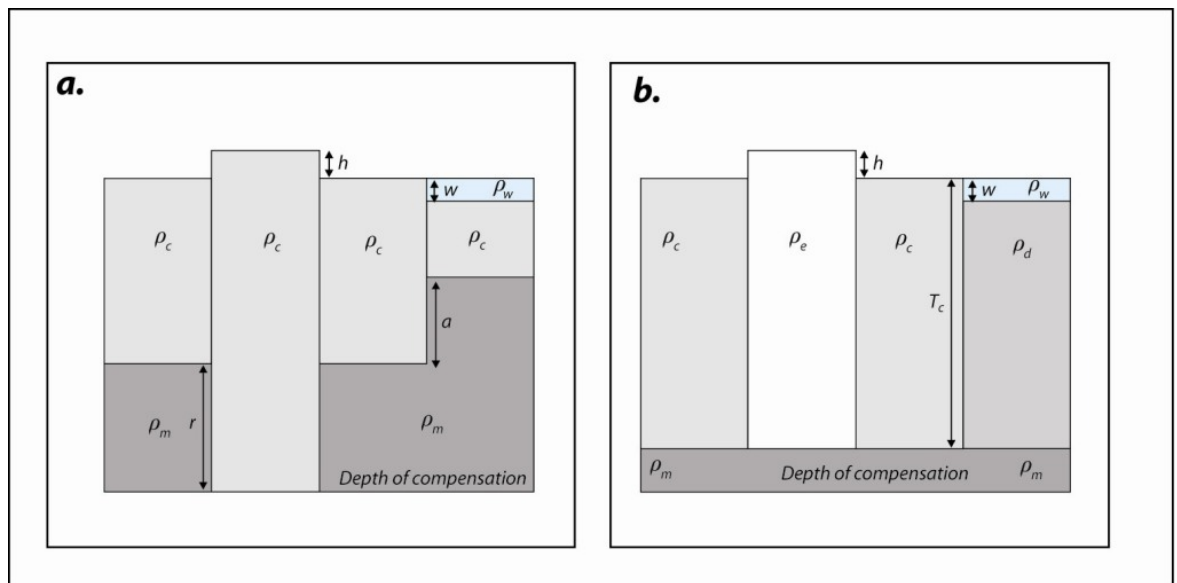


Figure 62 Models of local isostasy

- a. Airy compensation. Lithospheric blocks are all the same density but vary in thickness.
 b. Pratt compensation. Lithospheric blocks are all the same thickness but vary in density

6.2.2 Regional isostasy

Regional isostasy assumes that the lithosphere responds via flexural subsidence when loaded (e.g., by ice, sediments, lava emplacement) or via flexural uplift when unloaded (e.g., by deglaciation or denudational unloading) in the same manner as a thin, elastic plate overlying a fluid substratum (Gunn, 1943; Vening Meinesz, 1931; Walcott, 1970). A significant difference between local isostasy and regional isostasy is that deflection resulting from loading (or unloading) of the lithosphere is taken up laterally as well as vertically due to the intrinsic strength of the lithosphere. A fundamental consequence of lithospheric flexure is that the amount of deflection is reduced and spread over a wide area, the size of which is determined by the size of the load, its geometry and the mechanical properties of the lithosphere. A further effect of lithospheric flexure is the formation of ‘peripheral bulges’ adjacent to the region of deflection (Figure 63a and b).

Although the flexural response of the lithosphere can be model as a thin elastic plate, due to the large horizontal dimensions (relative to vertical thickness) it is also appropriate (and mathematically more simplistic) to model the flexural response of the lithosphere as a two dimensional elastic beam (Hetenyi, 1979; Timoshenko, 1958; Turcotte and Schubert, 2002;

Watts, 2001). The flexural response of the lithosphere modelled as an elastic beam takes the form of the fourth order differential equation (see Watts (2001) for derivation):

$$\frac{Dd^4W}{dx^4} + (\rho_m - \rho_{infill})gW = 0$$

Equation 13

Where D is the flexural rigidity (see below), W is the vertical stress, g is the acceleration due to gravity, ρ_m and ρ_{infill} are the mantle and infilling (or removed) material densities respectively. The flexural response of an elastic beam can be modelled as either continuous or semi-continuous (broken at one end). A continuous beam is analogous to an unfaulted section of lithosphere, a broken plate is analogous to a slab of lithosphere split by a major fault at one end. Equation 13 can be solved for a continuous beam (Equation 14) and a broken beam (Equation 15) (Pazzaglia and Gardner, 1994; Watts, 2001):

$$W_b(x) = W_0 e^{\frac{-x}{\alpha}} \left(\frac{\cos x}{\alpha} + \frac{\sin x}{\alpha} \right)$$

Equation 14

$$W_b(x) = W_0 e^{\frac{-x}{\alpha}} \frac{\cos x}{\alpha}$$

Equation 15

Where $W_b(x)$ is the deflection at distance x from W_0 the maximum deflection at the point of loading. W_0 is defined as (see Figure 63a):

$$W_0 = \frac{q\alpha^3}{8D}$$

Equation 16

Where D , the flexural rigidity, and α and q are flexural parameters defined by the following relationships (Pazzaglia and Gardner, 1994):

$$D = \frac{ET_e^3}{12(1-\nu^2)}$$

Equation 17

$$\alpha = \sqrt[4]{\frac{4D}{\rho_m g}}$$

Equation 18

$$q = \rho_{infill} g \Delta xy$$

Equation 19

Where E is the plate elasticity, ν is the Poisson's ratio and T_e is the effective elastic thickness, a parameter used to estimate the flexural rigidity of the lithosphere. For oceanic lithosphere the effective elastic thickness approximately corresponds to the depth of the 600°C isotherm (Watts, 2001). For continental lithosphere (which is structurally more complex), the effective elastic thickness does not correspond to a specific layer and is more challenging to estimate (Burov and Diament, 1996; Burov and Diament, 1995). Estimates of T_e for continental lithosphere range between 5km and 70km (Watts, 2001). The infilling material and mantle densities are ρ_{infill} and ρ_m respectively, Δxy is the cross-section that is loading (or unloading) the lithosphere at a particular point. Equations 14 and 15 must be solved for flexure deflection in response to both sediment loading (ρ_{infill} = sediment density and Δxy = the cross-section of sediment loading the lithosphere) and water loading (ρ_{infill} = water density and Δxy = the cross-section of water loading the lithosphere).

The geometry of the flexural response of the lithosphere can be calculated for the half width of the depression (X_0) analogous to the flexural wavelength (Equation 20), the distance from the point of maximum deflection to the peripheral bulge (X_{pb}) (Equation 21), and the magnitude of the peripheral bulge (W_{pb}) (Equation 22).

$$X_0 = \frac{3\pi\alpha}{4}$$

Equation 20

$$X_{pb} = \pi\alpha$$

Equation 21

$$W_{pb} = -W_0 e^{-\pi} = -0.0432W_0$$

Equation 22

Figure 63a illustrates the different parameters in Equation 13 - Equation 22 for modelling the lithosphere as a thin elastic beam.

Table 14 and Table 15 list the parameters necessary for modelling the isostatic flexural response of the lithosphere.

Constants		Variables	
ν	0.25	ρ_{infill} (offshore)	See section 6.3
E	70×10^9 Pa	ρ_{infill} (onshore)	for constraints for
g	9.8 ms ⁻²	Δxy	Western India
ρ_m	3300 kg/m ³	T_e	

Table 14 Constants for modelling lithospheric flexure

Table 15 Variables for modelling lithospheric flexure

The density of material deposited offshore (resulting in flexural subsidence from sediment loading) is constrained by the average density of the sediment in the Konkan-Kerala Basin (see chapter 2 and section 6.3). The density of the material that has been removed onshore (resulting in flexure uplift from denudational unloading) is constrained by the average density of crystalline rocks composing the Western Indian margin (section 6.3).

Distributed loads of various sizes result in contrasting flexural responses such that a narrow load flexes the lithosphere differently to a wide load. The geometry of the cross sectional area (Δxy) loading the lithosphere (offshore) and unloading the lithosphere (onshore) is constrained from the sediment distribution in the Konkan-Kerala Basin and low temperature thermochronometry of rocks onshore, respectively (section 6.3).

The effective elastic thickness (T_e) is a theoretical thickness that does not correspond to either a mechanical or thermal layer within the lithosphere (Stuwe, 2001). It is a useful variable, nonetheless, for altering the flexural properties of the lithosphere. Modifying T_e provides different magnitudes and geometries of deflection such that low T_e values generate large amounts of flexure over short distances (approaching local compensation) and large T_e values generate lower amounts of flexure but over greater distances (approaching no compensation and completely rigid lithosphere) (Figure 63b). Estimates for T_e are provided in section 6.3.

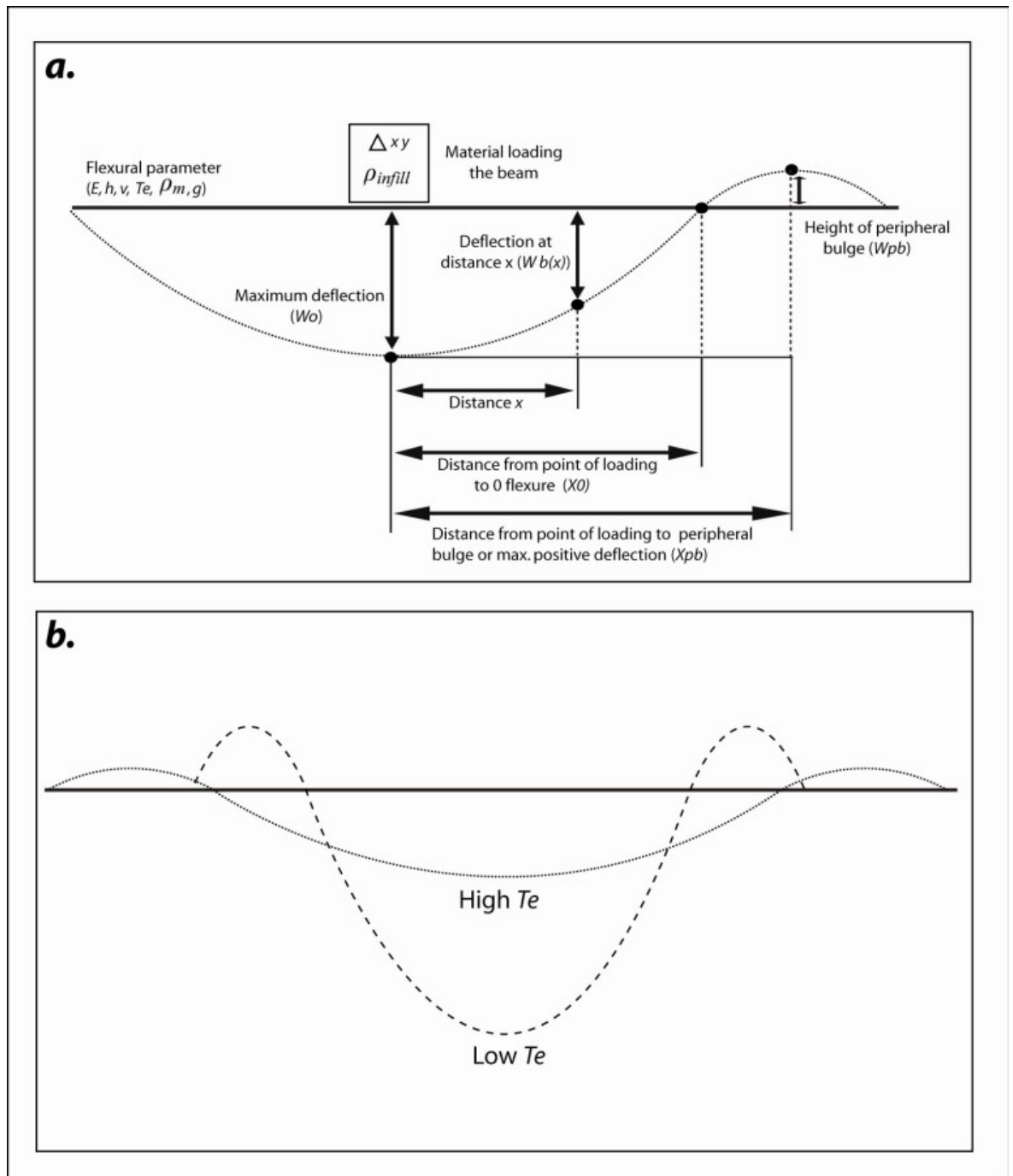


Figure 63 Regional isostasy

- a. Different parameters for modelling the flexural response of the lithosphere as a loaded beam (offshore). The same diagram reflected in the horizontal plain illustrates the different parameters for modelling the flexural response of the lithosphere as an unloaded beam (onshore).
- b. The geometry of flexure for different effective elastic thicknesses. High T_e represents flexurally stronger lithosphere with a small magnitude of deflection over a large horizontal distance. Peripheral bulges are also small and extend over large horizontal distances. Low T_e represents flexurally weak lithosphere with larger amounts of deflection over smaller horizontal distances and larger peripheral bulges.

6.3 Isostasy and the Western Indian margin

The flexural response of the Western Indian margin has previously been modelled as a continuous elastic beam, and a semi-continuous beam with one free end (Gunnell and Fleitout, 1998, 2000). The broken plate model simulates a break or fault that effectively de-couples the onshore and offshore portions of the margin. The much-debated, putative offshore West Coast Fault could represent such a de-coupling zone (Balakrishnan, 2001; Chandrasekharam, 1985). As a consequence of increased availability of borehole data offshore (Chapter 2) and the improved constraints from low temperature thermochronometry onshore (Chapters 4 and 5), flexure modelling in response to sediment loading and denudational unloading of the Western Indian lithosphere can now be refined. Section 6.3 (this section) outlines the parameters employed for flexural modelling (T_e , Δxy and ρ_{infill}) and the methods applied to simulate a continuous beam and a semi-continuous beam; section 6.4 presents the results.

Published constraints for the effective elastic thickness of the Indian sub-continent are rare and are summarised in Table 16.

Publication	T_e values	Method
Watts and Cox (1989)	100 km	Modelling Deccan lava emplacement
Gunnell and Fleitout (1998)and (2000)	35 km – 70 km	Finite difference numerical modelling
Stephen et al., (2004)	13 km	Gravity and topographic coherence function for the South Indian Shield
Rajesh and Mishra (2004)	12 km – 36 km	Multitaper spectral analysis
Chand and Subrahmanyam (2003)	10 km – 13 km	Gravity and bathymetry cross-spectral analysis
Tiwari et al.(2006)	10 km	Gravity and topography admittance for the Deccan Volcanic Province

Table 16 Published constraints for T_e of the Indian sub-continent.

In recognition of the large range of published T_e estimates for Western Indian, T_e values ranging from 10 km to 70 km have been modelled. The oceanic/continental crust transition is thought to occur west of the Chagos-Laccadive ridge (Kolla and Coumes, 1990) (Figure 5 and Figure 16), The lithosphere beneath the Konkan-Kerala basin therefore has similar rheological properties to the adjacent onshore lithosphere and the flexural properties (including T_e) should also be similar.

The modelled lithosphere was split into eight cells, five 100 km wide cells representing the lithosphere offshore and three for the lithosphere onshore (one 50 km wide cell seaward of the escarpment and two 100 km wide cells landward of the escarpment) (Figure 64a). The present day coast was taken as the boundary between the loaded offshore section of lithosphere and the

unloaded onshore section of the lithosphere. The position of the coastline is largely a function of Holocene eustatic sea level rise but it nonetheless marks a reasonable boundary between onshore erosion and offshore deposition. It is recognised that the position of the coast will have altered throughout the geological history of the Western Indian margin; however, there are no adequate constraints on coastal palaeoposition (see chapter 2) so the simplifying assumption is made that the coastline has, on average, effectively remained constant.

The flexural responses for each cell in the cross-section (including the flexural effects on neighbouring cells) were modelled for both a continuous beam (Equation 14) and a semi-continuous beam (Equation 15). The flexural effects of neighbouring cells were allowed to propagate throughout the modelled lithosphere for a continuous beam; however, for a semi-continuous beam, the flexural effects were not transmitted across the broken section of the beam (i.e., across the onshore/offshore boundary) (Figure 64b). The Δxy values for each of the five cells loading the lithosphere offshore were obtained by taking the average decompacted sediment thicknesses parallel to the margin from their position offshore using the sediment isopach maps of (Rao and Srivastava, 1984). The flexural effects of water loading each cell were also added using a density of 1000 kg/m^3 and Δxy values for the current average water depth (500m). Upper and lower limits for flexural deflection have also been calculated for water depths that are 200m higher than present day and 200m lower than present day (see Figure 18 and Table 17). The Δxy value for the cell seaward of the escarpment was obtained using constraints from low temperature thermochronometry, and the Δxy values for the two cells landward of the escarpment were obtained by assuming that 500 m of lithosphere has been denuded from the interior plateau since the onset of rifting. This is a reasonable value because there is evidence for the removal of ca. 500 m Deccan lavas inland of the escarpment north of the study area (Widdowson, 1997). The flexural effects from each loaded cell and neighbouring cells (including peripheral bulges) were then summed to provide the total deflection at a particular point along the modelled lithosphere (Figure 64a). A density of 1200 kg m^{-3} (average for shaley sandstone) was adopted for the offshore segment and a density of 2700 kg m^{-3} (average for crystalline rocks) for the onshore segment (Rust and Summerfield, 1990). Table 17 summarises the parameters for each of the eight cells used to model lithospheric flexure.

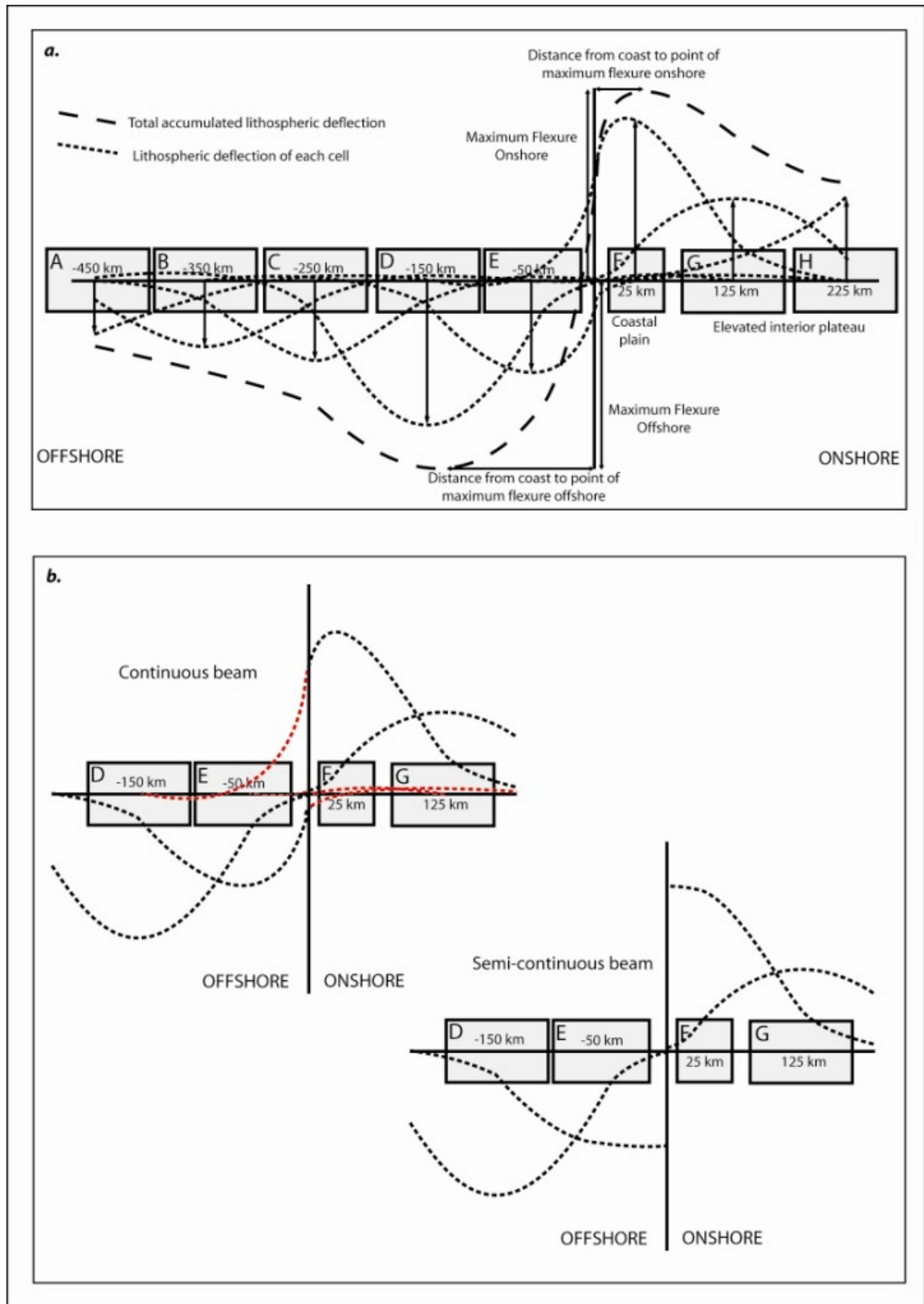


Figure 64 Flexural modelling set-up.

a. The lithosphere modelled as a thin elastic beam split into eight cells (A-H). Each cell exerts a flexural response on the elastic beam depending on if it is loaded or unloaded, what the density of the load is and what the cross sectional area of the load is (narrow dashed lines). The wide dashed lines indicate the total accumulated flexure for a particular point along the beam from the combined flexural effects of each cell.

b. Difference between the continuous beam and semi-continuous beam for cells adjacent to the onshore/offshore transition. Semi-continuous beam does not include the flexural effects propagating through the onshore/offshore transition (red dashed lines in the continuous beam model)

	Offshore					Onshore		
Cell	A	B	C	D	E	F	G	H
Dist. from coast (km)	-450	-350	-250	-150	-50	25	125	225
Δxy sediment (km ²)	74	90	109	195	125	100	50	50
ρ_{infill} sediment (kg/m ³)	1200	1200	1200	1200	1200	2700	2700	2700
Δxy water (km ²)	50 ±20	50 ±20	50 ±20	50 ±20	25 ±10	-	-	-
ρ_{infill} water (kg/m ³)	1000	1000	1000	1000	1000	-	-	-

Table 17 Summary of cell parameters

6.4 Results

Results of flexural isostatic modelling are summarised for a continuous beam in Table 18 and a semi-continuous beam in Table 19 for a range of effective elastic thicknesses. Results of modelling a beam with an effective elastic thickness of 2 km are included to model the end member situation for a loaded beam compensated locally (effectively Airy isostasy). Figure 65 and Figure 66 displays the results in diagrammatic form. The maximum offshore flexural subsidence is reported in columns 2 as negative values (\pm values are for water loading with sea level 200 m above and below present sea level). The maximum onshore flexural uplift is reported in column 4 as positive values. The maximum flexural deflection is important to determine if the amount of subsidence offshore and the magnitude of denudation onshore can be accounted for by flexural isostasy alone. Columns 3 and 5 report the distance from the point of zero flexure to the point of maximum flexure, analogous to the flexural wavelength; it should be noted that these values are for the individual cell, not the precise distance where maximum flexure occurs. The magnitude of the flexural wavelength is important to establish if the geometry of subsidence offshore and denudation onshore can be explained by flexural isostasy.

6.4.1 Continuous beam

The continuous beam model assumes that the offshore and onshore segments of the modelled lithosphere are completely connected such that the flexural effects propagate through adjacent segments influences total flexure of neighbouring segments. The maximum flexural subsidence offshore ranges from 1.4 km (for low T_e values) to 0.7 km (for high T_e values). Regardless of

the modelled effective elastic thickness, the flexural wavelength remains constant at 150 km for the offshore lithosphere. Onshore, the maximum flexural uplift ranges from 1.4 km (for low T_e values) to 0.5 km (for high T_e values). The flexural wavelength is 25 km for small T_e values (10 – 30 km) and 125 km for higher T_e values (50 – 70 km) (see Table 18 and Figure 65).

T_e (km)	Offshore		Onshore	
	W_0 , maximum deflection (km)	X_0 flexural wavelength (km)	W_0 , maximum deflection (km)	X_0 flexural wavelength (km)
2 (Airy)	-4.860 ± 0.34	-	4.620	-
10	-1.415 ± 0.12	150	1.350	25
30	-0.945 ± 0.10	150	0.699	25
50	-0.825 ± 0.09	150	0.536	125
70	-0.710 ± 0.08	150	0.532	125

Table 18 Results for a continuous beam

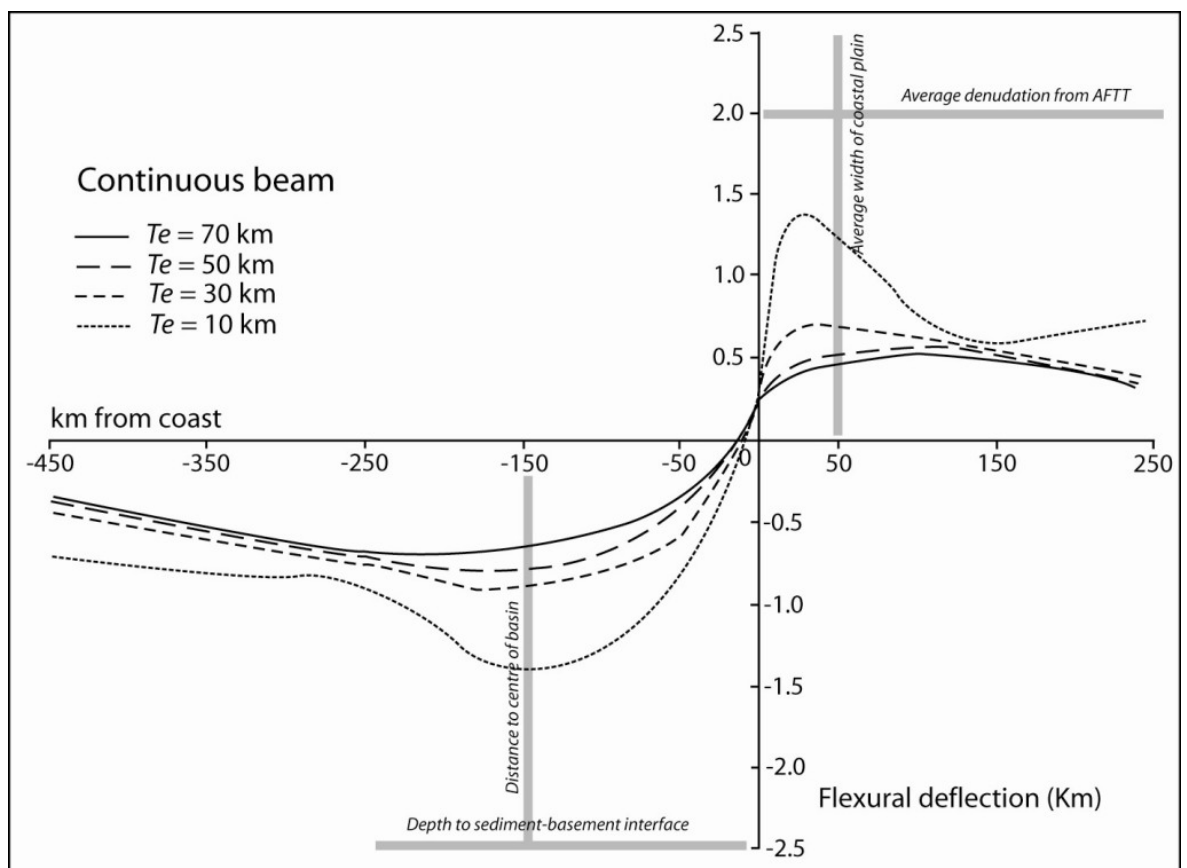


Figure 65 Model flexural isostatic response of a continuous beam for different effective elastic thicknesses.

6.4.2 Semi-continuous beam

The semi-continuous beam model assumes that there is no connection between the offshore and onshore segments of the modelled lithosphere and the flexural effects from one segment are not transmitted to the other segment. A semi-continuous beam is modelled by incorporating a weak zone (with very low T_e) across the transition between the offshore and onshore segments, effectively simulating the presence of a major fault. Results for maximum flexural subsidence offshore range from 1.4 km (low T_e values) to 0.5 km (high T_e values); flexural uplift onshore ranges from 1.5 km (low T_e values) to 0.4 km (high T_e values). The flexural wavelength is insensitive to the range of T_e values and remains constant at 150 km and 25 km for the offshore and onshore segments respectively (see Table 19 and Figure 66).

T_e (km)	Offshore		Onshore	
	W_o , maximum deflection (km)	X_o flexural wavelength (km)	W_o , maximum deflection (km)	X_o flexural wavelength (km)
2 (Airy)	-4.860 ±0.34	-	4.620	-
10	-1.417 ±0.06	150	1.510	25
30	-0.692 ±0.06	150	0.652	25
50	-0.578 ±0.06	150	0.478	25
70	-0.520 ±0.06	150	0.402	25

Table 19 Results for a semi-continuous beam

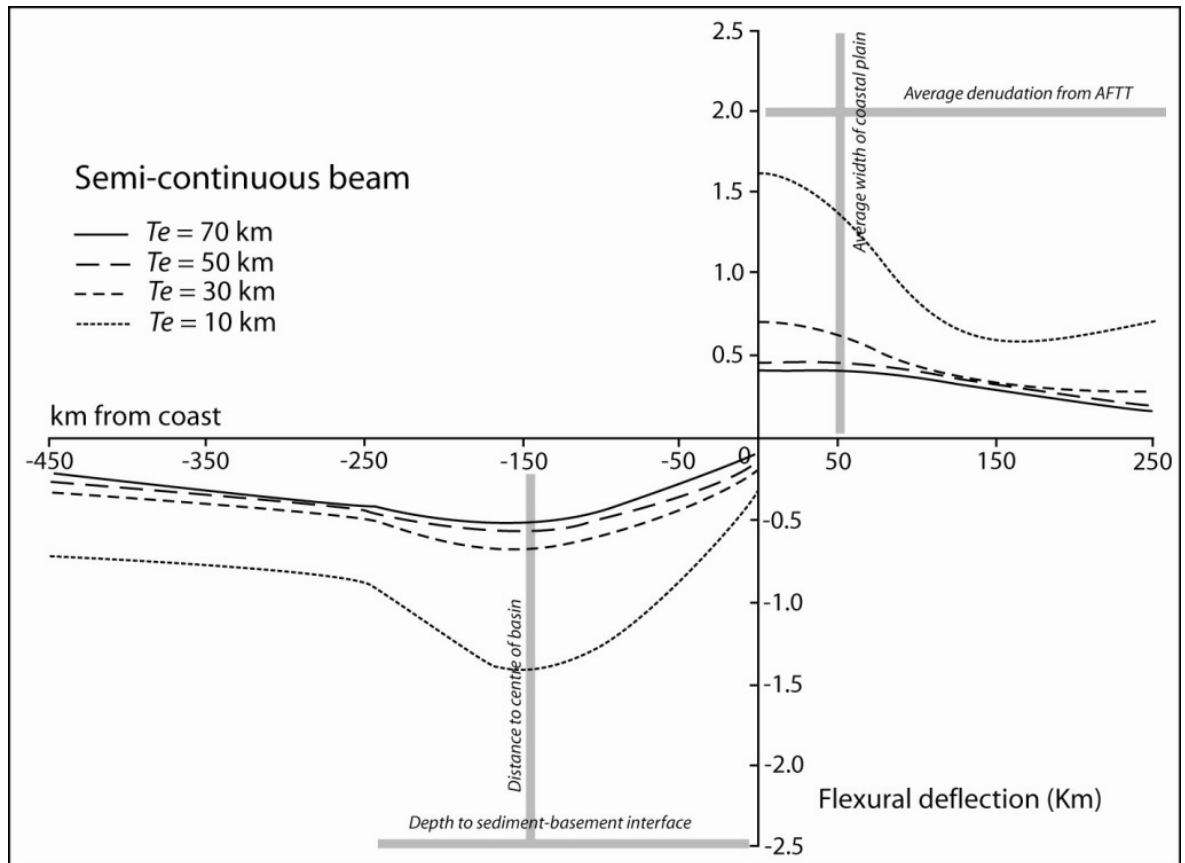


Figure 66 Model flexural isostatic response of a semi-continuous beam for different effective elastic thicknesses.

6.5 Conclusions

The maximum depth to the sediment-basement interface in the centre of the Konkan-Kerala basin, measured directly from seismic cross-sections (Figure 20) is 2.5 km. That average distance from coast to where the basin is at its deepest is 150km. If subsidence has occurred only in response to sediment loading, the depth to the sediment basement interface should be the same as the modelled isostatic response to sediment loading (Steckler and Watts, 1980). The greatest maximum flexural deflection offshore is generated if the modelled lithosphere has a low effective elastic thickness of 10 km. In order to produce the measured 2.5 km of subsidence from flexural isostasy alone the effective elastic thickness for the lithosphere would have to be less than 10 km. Despite the large range of published constraints for the effective elastic thickness of the Indian lithosphere, there is no evidence for low effective elastic thicknesses (i.e. less than 10 km). Flexural isostasy may be a contributing mechanism for subsidence; however, additional mechanisms must be invoked to account for the 2.5 km to the sediment-basement interface observed offshore. Post-rift thermal contraction accompanied by

sub-lithospheric thinning (Sleep, 1971; Sleep and Snell, 1976) or lithospheric stretching (Jarvis and McKenzie, 1980; McKenzie, 1978) are possible candidates for tectonic subsidence which could augment subsidence generated by sediment loading. The modelled flexural wavelength (for all T_e values) approximates the distance from the present coastline to the centre of the basin, implying that although flexural isostasy may not be the only mechanism contributing to the magnitude of subsidence, it may control the geometry of regional basin subsidence.

The low temperature thermochronometric data presented in Chapters 4 and 5 indicate that for a palaeogeothermal gradient of 20 °C/km the average magnitude of Cenozoic denudation across the coastal plain is 2-2.5 km. The maximum magnitude of flexural isostatic rock uplift that can be modelled is only ~1.5 km for a weak lithosphere with a low effective elastic thickness, falling short of the magnitude of denudation predicted from low temperature thermochronometry. Flexural isostasy alone does not adequately explain the magnitude of denudation, implicating additional rock uplift mechanisms. Tectonic rock uplift could be a possible cause but is often associated with crustal thickening in compressive tectonic settings and is difficult to justify in extensional tectonic settings. Alternative isostatic mechanisms such as magmatic underplating or lithospheric delamination could augment rock uplift already generated from denudational unloading. There is limited evidence for magmatic underplating beneath the Deccan volcanic province (Devey and Lightfoot, 1986); however, there is little justification for the thicknesses of underplating required to generate ca. 0.5 – 1 km of rock uplift needed to supplement the 1.5 km of rock uplift generated from flexural isostatic modelling (Gunnell and Fleitout, 1998). Similarly, there is little evidence that lithospheric delamination at passive margins can contribute significantly to rock uplift (Doin et al., 1996). An alternative explanation for the mismatch between the magnitude of denudation (constrained from LTT) and the modelled flexural deflection could be an elevated palaeosurface that has subsequently been eroded. Rock uplift (here modelled as flexural isostasy) is a combination of denudation and surface uplift (Equation 7 and Figure 61). If an elevated palaeosurface was present during the development of the margin, a lowering in this surface (i.e., a decrease in surface elevation) in combination with denudational flexural isostasy could account for the magnitude of denudation constrained from LTT.

The modelled flexural wavelength onshore is 25 km for all values of effective elastic thickness except for high T_e values of 50 – 70 km when the lithosphere is modelled as a continuous beam. A flexural wavelength of 25 km approximates the half-width of the coastal plain, suggesting that flexural isostasy operates at similar spatial scales to the large-scale geomorphic features of the Western Indian margin. However, samples located close to the present coastline yield low temperature thermochronometry data that are best explained if the magnitude of denudation (at the coast) is at least 4.5 km (for a palaeogeothermal gradient of 20 °C/km). Such extreme spatial variability in denudation (i.e., 4.5 km of denudation at the coast decreasing to 2km of denudation only 10–20 km further inland) is difficult to reconcile with a model of margin development incorporating lithospheric flexural isostasy only which predicts spatial variability in denudation over much longer wavelengths. One possible mechanism for generating such extreme spatial variability in denudation could be elevated rift flank uplift produced during the initial stages of continental rifting (Weissel and Karner, 1989). Brittle deformation of the lithosphere could be an alternative mechanism where the lithosphere deforms not only by flexural isostasy but also by vertical movement of major faults. The Western Indian margin contains several major shear-zones: Within the southern Granulite Terrane there is the Bavali shear-zone, Palghat-Cauvery shear-zone, Moyar shear-zone and Achankovil shear-zone (Radhakrishna et al., 2003). It has also been suggested that within the Deccan Volcanic province, the Panval Flexure may be a series of faults (Dessai and Bertrand, 1995; Sheth, 1998). These major structures could be possible candidates for accommodating brittle flexural deformation along the Western Indian margin.

The flexural isostatic modelling incorporates additional uplift from the formation of ‘peripheral bulges’ (see section 6.2.2). The effect of peripheral bulges was included in the total flexure modelled for each cell (see section 6.3 and Figure 64a). The peripheral bulges only exert an influence on adjacent cells with the continuous beam model because the flexural responses of individual cells are allowed to propagate across the onshore/offshore boundary (red dashed lines in Figure 64b). However, the effect of peripheral bulges is minimal, > 50 m for low T_e (10 km) and > 15 m for high T_e (70 km) and contributes very little to the total flexural isostatic response at any point along the beam. The limited influence of peripheral bulges has implications for the continuous and semi-continuous beam models, which provide very similar flexural modelling results. From a flexural modelling perspective, the properties of the lithosphere (and specifically whether it is broken by the West Coast Fault or not) appear to be largely irrelevant.

Both sediment mass balance results and low temperature thermochronometry support the hypothesis that the Western Indian margin has developed into an elevated rift flank. Flexural modelling also demonstrates that regional isostasy can explain a large amount of the observed subsidence offshore and denudation onshore using realistic parameters for the properties of the modelled lithosphere. However, flexural isostasy alone does not adequately account for the magnitude of subsidence or denudation unless low T_e values (which are difficult to justify for western India) are modelled. Additional mechanisms must be incorporated into models which endeavour to understand the evolution of the Western Indian margin. For the offshore segment of the margin, thermal subsidence could provide a complimentary mechanism for flexural isostasy. Additional mechanisms for generating uplift for the onshore segment of the margin are less clear; however, initial rift-flank uplift during the early stages of rifting, ongoing brittle deformation of the lithosphere or a (now denuded) elevated palaeosurface could be possible candidates.

7 Discussion and conclusions

7.1 Introduction

The tectonic history and subsequent landscape evolution of the Western Indian elevated passive margin is complex and challenging to understand. The timing of margin formation is enigmatic; was the Western Indian margin created in response to rifting between India and Madagascar, in response to rifting between India and The Seychelles, or a combination of both events? What mechanisms are involved in the rifting process and can these mechanisms be determined? Has the margin been actively rifted with associated hot spot interactions or passively rifted? What is the syn-rift and post-rift effect on long term landscape development and what mechanisms play a key role in the evolution of the Western Indian margin? These fundamental questions have been difficult to fully address with existing methodologies (Gunnell and Radhakrishna, 2001). Multiple applications of different methodologies used in this study utilising the offshore sedimentary record, onshore denudational record and the isostatic adjustment of the lithosphere has proved effective in resolving some of these long standing problems.

This chapter highlights the specific details drawn from the conclusions of this study and their implications for the aforementioned key questions. The connection between major tectonic events and the evolution of the Western Indian margin are then explored followed by a discussion of the mode of landscape evolution inferred from this study. Finally, methodological issues arising from dealing with offshore data, analysing low temperature thermochronometry data and numerical modelling are highlighted.

7.2 Plate tectonics and passive margin evolution

Passive margins are the end product of lithospheric extension, rupture and ocean basin formation which, within the framework of plate tectonics explains many of the large scale features of the Earth's surface such as the position of continents and oceans, and the formation of sedimentary basins (Beaumont et al., 2000; Kearey and Vine, 1996). Subsidence and the record provided by sedimentary deposits offshore has been

instrumental in our understanding of passive margin development within the context of plate tectonics (Allen and Allen, 2005; Gilchrist and Summerfield, 1994); however, the onshore elements of passive margins displaying persistent uplift have proved to be more challenging to incorporate into plate tectonic models (Beaumont et al., 2000; Gilchrist and Summerfield, 1994). Great escarpments at elevated passive margins provide a foundation for understanding the dynamics and timing of rifted margin development and provide the opportunity to examine the relationships between tectonic processes, surface processes and isostatic flexure (Braun et al., 2006; van der Beek, 1995). The principal questions needing addressed for the development of passive margins are: What is the timing of the onset of surface uplift (and denudation) and how is it related to the timing of rifting (i.e. active rifting or passive rifting)? What is the spatial distribution and magnitude of surface uplift and what implications are there for the existing conceptual models of passive margin development? These questions have been addressed for several passive margins including Southern Africa (Brown et al., 1990; Brown et al., 2002b; Gallagher and Brown, 1999; Gilchrist et al., 1994a; van der Beek et al., 2002), South Eastern Australia (Moore et al., 1986; Persano et al., 2002; Persano et al., 2005; van der Beek and Braun, 1998), South America (Gallagher et al., 1994), the Red Sea (Balestrieri et al., 2005; Omar and Steckler, 1995; Steckler et al., 1998) and Western India (Gunnell et al., 2003; Widdowson, 1997).

The tectonic evolution of the Western Indian margin is linked to both rifting between India and The Seychelles and rifting between India and Madagascar with no clear consensus on the spatial extent of either rift. Plate reconstructions place The Seychelles microcontinent adjacent to the northern third of the margin (Plummer and Belle, 1995; Reeves and de Wit, 2000) and the impingement of the Reunion plume with the subsequent emplacement of the Deccan lavas has been linked to separation of The Seychelles at ca. 65 Ma (Richards et al., 1989; Storey, 1995; White and McKenzie, 1995). However, the constraints on the timing of rifting for the southern segment of the margin are much poorer and intrusive igneous rocks have been linked to The Seychelles/India rift (Radhakrishna et al., 1994; Widdowson et al., 2000) but also the Madagascar/India rift (Pande et al., 2001).

Sediment mass balance analysis is one methodology which has been used to great effect to provide information on the evolution of the Southern African margin (Brown et al., 1990; Rust and Summerfield, 1990), the North Eastern Atlantic margin (Pazzaglia and Brandon, 1996; Pazzaglia and Gardner, 1994) and the Western Indian margin (Gunnell, 2001). The information provided from analysis of the sediments within the Konkan-Kerala basin (chapter 2) demonstrate that stretching of the lithosphere and basin initiation began during rifting between India and Madagascar creating small coast parallel grabens filled with Mesozoic sediments.

However, rifting between India and The Seychelles exerted a much greater influence over the development of the Konkan-Kerala basin, initiating major basin wide subsidence (Gombos et al., 1995) and increased the sediment flux from the onshore portion of the Western Indian margin (Chaubey et al., 2002; Rao and Srivastava, 1984; Singh and Lal, 1993).

The resolution of offshore data allow only spatially averaged information on sediment flux and corresponding onshore denudation rates; however, low temperature thermochronometry provides more powerful techniques for obtaining more rigorous constraints on the temporal and spatial extent of denudation. Low temperature thermochronometry has been used successfully to understand the development of passive margins (see reviews in Brown et al (1994), Gallagher (1995), Gallagher et al. (1998) and Kohn et al. (2005)). Low temperature thermochronometric data (chapters 4 and 5) for both Goa and Karnataka, and Kerala, modelling low temperature thermochronometry data show an increase in the magnitude and rate of cooling at 65 Ma with little evidence to support an increase in cooling at 80 Ma. The increase in cooling at 65 Ma can be linked to an increase in denudation in response to rifting between India and The Seychelles. Low temperature thermochronometry supports rifting in response to the breakup of India and The Seychelles for the entire length of the margin, not just the northern segments within the Deccan volcanic province. Although basin initiation offshore began at ca. 80 Ma, denudation of the onshore portion of the margin did not occur until 65 Ma. One possible explanation for rifting along the entire length of the margin during the Seychelles break-up event may be the re-activation of existing faults created during the Madagascar India rifting event (Chand and Subrahmanyam, 2003) or the exploitation of the pre-existing fabric within the Dharwar basement (Kolla and Coumes, 1990; Subrahmanyam et al., 1994; Subrahmanyam et al., 1995).

Passive margins represent the end stages of a sequence involving continental rifting, rupture and sea floor spreading. Two generalised models (each associated with different mechanisms and different sequences of events) describe how a continental rift evolves into a mature passive margin, active rifting and passive rifting. Active rifting involves plume-lithosphere interaction where uplift tends to precede rifting (White and McKenzie, 1989; White and McKenzie, 1995), with passive rifting, rifting tends to precede uplift (Braun and Beaumont, 1989; Steckler, 1985). The northern third of Western India has been cited as a volcanically (hence actively) rifted margin (Richards et al., 1989; Storey, 1995; White and McKenzie, 1995) and its development has been linked to the Reunion Plume (see chapter 1). However, the extent of plume impact and its influence on the development of the entire margin is less clear, and there is little evidence to support active rifting processes for the southern two thirds of the margin. Low temperature thermochronometry data from this study indicate that the timing of the onset of increased denudation is the same in Goa and Karnataka as it is further south in Kerala. If the

Reunion Plume is the primary cause of rifting, low temperature thermochronometry data should reveal younger accelerated denudation (in response to impingement of the plume) further south as India migrated north over the plume. Mechanisms associated with plume impacts are generally thermal and hence transient, yet increased denudation rates inferred from low temperature thermochronometry lasted throughout the Cenozoic. The Reunion Plume may have played a key role in the initiation of continental rapture, but it cannot be responsible for the generation and persistence of denudation across the whole margin throughout the Cenozoic.

The offshore mass balance data also highlighted a younger secondary pulse in sediment flux beginning in the late Miocene (see chapter 2). The timing of this younger pulse is challenging to explain with any rifting mechanism. Late Miocene increases in sediment flux have been observed throughout the Asian continent (Metivier et al., 1999; Molnar, 2004; Molnar and England, 1990) and is tempting to link the younger pulse within the Konkan-Kerala basin also to climate change (Prell and Kutzbach, 1992; Quade et al., 1989). However, with the limited information provided from the mass balance analysis the link between climate change and accelerated denudation remains tenuous and the hypothesis will need to be tested more fully with future work.

7.3 Long term landscape evolution of Western India

The classical conceptual models of elevated passive margin development are, escarpment retreat into a downwarped rift shoulder (King, 1967a; Ollier and Pain, 1997), and escarpment development into an elevated rift shoulder (Gilchrist and Summerfield, 1990, 1994; Gilchrist et al., 1994b; Kooi and Beaumont, 1994; Tucker and Slingerland, 1994). These two groups of competing conceptual models have been tested for the Southern African margin (van der Beek et al., 2002), the Red Sea (Balestrieri et al., 2005) and South Eastern Australia (Persano et al., 2002; Persano et al., 2005). The elevated rift flank models and the downwarp model have also been proposed for the post-rift evolution of Western India and both groups of models explain the topography of the margin adequately (Gunnell and Fleitout, 1998, 2000). Widdowson (1997) subsequently modified the downwarp model to incorporate post-rift isostatic flexure in response to sediment loading and denudational unloading to explain the morphology of the northern portion of the Western Indian margin (Widdowson, 1997; Widdowson and Cox, 1996; Widdowson and Mitchell, 1999). The methodologies utilised within this study target the fundamental differences between the conceptual models to determine the likely mode of escarpment development. The characteristics that separate the two groups of conceptual models and the methodologies employed to determine these characteristics are outlined in Table 20.

	Downwarped rift shoulder (Ollier)	Elevated rift shoulder	Methodology
Pattern of denudation across the coastal plain	Small closest to the coast (< few 100 m) increasing towards the base of the escarpment.	Greatest at the coast (several km) decreasing towards the base of the escarpment.	Low temperature thermochronometry (chapters 4 and 5)
Location and magnitude of maximum denudation	At the base of the escarpment, of the same order as the height of the escarpment (0.5 – 2.5 km)	At the coast, magnitude dependent on flexural strength of the lithosphere (1 – 5 km)	Low temperature thermochronometry (chapters 4 and 5)
Flexural response of the lithosphere	Lithosphere attains post-rift flexural rigidity with no flexural isostatic adjustments.	Lithosphere responds via flexural isostasy in response to sediment loading and denudational unloading	Flexural modelling of the lithosphere (chapter 6)
Presence of coastal facets	Yes	No	Geomorphological field evidence
Magnitude of sediment deposited offshore	Approximates the volume of a downwarped wedge of missing section removed from the coastal plain.	Approximates the volume of an inverted wedge of missing section removed from the coastal plain.	Mass balance analysis (chapter 2)

Table 20 Conceptual models and methodologies

Chapter 2 quantified the volume of sediment deposited in the Konkan-Kerala basin and compared it to the equivalent volume of missing sections onshore that would be predicted for a downwarped rift shoulder and an elevated rift shoulder. The assumptions were made that the Konkan-Kerala basin is a closed system, all the clastic sediment within the Konkan-Kerala basin is derived from the onshore segment used to calculate the missing section, and the onshore area has remained constant throughout the Cenozoic. These assumptions are justified in Chapter 2. The results indicate that the volume of clastic sediment deposited within the Konkan-Kerala basin is greater than the volume that would be expected from a denuded wedge predicted for a downwarped geometry. The volume of clastic sediment is more consistent with erosion of an inverted wedge predicted for an elevated rift shoulder. The downwarp model proposed by Widdowson (1997) differs from the downwarp model developed by Ollier and Pain (1997) by incorporating ongoing post-rift lithospheric flexure in response to denudational unloading. The Widdowson (1997) downwarp model can also account for the volume of sediments present offshore. Mass balance analysis can not differentiate between the elevated rift flank models and the Widdowson (1997) downwarp model because mass balance analysis provides constraints on the total volume of material denuded from the onshore portion of the margin, not the spatial pattern of denudation.

Surface uplift, rock uplift and denudation are all important processes for understanding models of long-term landscape development; however, quantifying denudation is the key to differentiating between the competing conceptual models. The spatial pattern and magnitude of denudation can be inferred from the cooling histories obtained from low temperature thermochronometry and marked differences in the age pattern across a margin normal transect are evident for each of the competing groups of conceptual models (Gallagher, 1995; Gallagher et al., 1998). Both Goa and Karnataka (chapters 4), and Kerala (chapter 5) display AFTT and AHe ages closest to the coast that, when modelled, are more consistent with rapid cooling from greater than ~ 110 °C. A reasonable assumption given the difficulty in extrapolating geothermal gradients over geological timescales where the lithologies are now largely absent is a palaeogeothermal gradient of 20 °C/km for the Western Indian margin (see chapters 4 and 5 for details). The corresponding depth of denudation is ~ 4.5 km at the coast, an amount that is inconsistent with more modest depth of denudation of only a few hundred meters expected for the downwarped rift shoulder model. LTT data across the coastal plains for both Goa and Karnataka, and Kerala are modelled as having more modest degrees of cooling from temperatures between 50 °C and 80 °C, equivalent to 1.5 – 3 km of denudation. This pattern of denudation with 4.5 km at the coast and 1.5 – 3 km further inland (with the smallest magnitude of denudation close to the escarpment) would be expected for a margin that has developed into an elevated rift shoulder with accompanying isostatic rebound.

Low temperature thermochronometry and in particular the use of AFTT and AHe simultaneously has been instrumental in highlighting more subtle differences in the style of cooling (and hence denudation) between the two field areas. Inverse-modelling of data from Goa and Karnataka are best explained by rocks that cool rapidly from either greater than 110 °C (at the coast) or within the PAZ and PRZ (further inland) to temperatures cooler than the top of the PRZ less than 10 Myrs after rifting at 65 Ma. Low temperature thermochronometry from Kerala can only be modelled if rocks are first rapidly cooled during rifting at 65 Ma but remain within the PRZ during the post-rift period cooling less rapidly. Although rifting between The Seychelles and India initiated an increase in denudation along the entire length of the margin, the regional effects for separate segments of the margin are different. It is unclear why there is a difference in the style of cooling between the two field areas but the LTT data indicate that the margin may be compartmentalised at a regional level or that the data are poor.

Flexural isostasy in response to sediment loading offshore and denudational unloading onshore has been cited as a possible mechanism accounting for persistence of rift flank uplift at passive margins (Gilchrist and Summerfield, 1990, 1994). Modelling the flexural response of the lithosphere to sediment loading and denudational unloading has been undertaken for the North Eastern Atlantic margin (Pazzaglia and Gardner, 1994), South Eastern Australian margin

(Bishop and Brown, 1992) and the Western Indian margin (Gunnell and Fleitout, 1998, 2000). The flexural properties of the lithosphere are a fundamental discriminator between the two groups of conceptual models, the downwarped rift shoulder model assumes that the lithosphere attains infinite strength, the elevated rift shoulder models assumes the lithosphere has finite strength. Chapter 6 examined the lithospheric flexural isostatic response of Western India to denudational unloading onshore and sediment loading offshore to determine the extent to which flexural isostasy may have influenced the development of the margin. Results from flexural isostatic modelling of the Western Indian lithosphere using a range of natural parameters for the flexural rigidity indicate that lithospheric flexure in response to denudational loading and sediment loading must be operating and the lithosphere cannot be infinitely strong. However, flexural isostasy cannot be the sole mechanism generating rock uplift and basin subsidence even if the modelled lithosphere is flexurally very weak (see chapter 6). Furthermore, the natural wavelengths over which the lithosphere responds flexurally are far too large to account for the inferred pattern of denudation (assuming denudation is equal to rock uplift) extracted from LTT data. The development of the Western Indian margin is clearly very complex and flexural isostasy is one of many mechanisms which need to be integrated into models of the Western Indian long-term landscape evolution.

7.4 Methodological issues and future work

The effectiveness of a mass balance analysis is dependant on the quality of offshore sedimentary data, knowledge of the dynamics of the offshore area (i.e. if there is sediment loss further offshore or sediment gain from adjacent offshore areas) and constraints on the spatial source area of the sediment (Allen and Allen, 2005; Hay et al., 1989; Summerfield, 1991b). Chapter 2 draws some important conclusions on the tectonic evolution and long-term landscape development of Western India, based on relatively sparse data which only provides partial constraints on the sedimentation history of the Konkan-Kerala basin (Chaubey et al., 2002; Rao and Srivastava, 1984; Rao and Rao, 1995; Singh and Lal, 1993). Offshore data for Western India is challenging to obtain, but despite the small quantity of data (relative to the area under study) used for the mass balance analysis, it was still possible to test different hypothesis regarding the mode of escarpment development (i.e. downwarped or elevated rift flank). The mass balance analysis concluded that the volume of sediment present offshore is inconsistent with Ollier and Pain's (1997) downwarp model, and as such the study is an advance on prior attempts at mass balance analysis for Western Indian (Gunnell, 2001). As more offshore data becomes available, future work will undoubtedly build a more detailed

picture of the sedimentary development of the Konkan-Kerala basin and a more robust understanding of the linkages between the onshore and offshore domains.

Apatite fission track and (U-Th)/He data for this study were inversely modelled to extract information on the cooling histories from different segments of the Western Indian margin. Successful model inversions depend on; the quality of data being modelled, the boundary conditions imposed on the modelling and the model input parameters (Donelick et al., 2005; Ketcham, 2005). For AFTT, data quality will be affected by; the number of grains used for AFTT age calculations, the number of tracks measured for TLD's, and uranium concentration. For (U-Th)/He, data quality will be affected by; helium, uranium and thorium concentrations, unquantified zonation of uranium and thorium, reproducibility and overall sample quality (identification of inclusions and/or cracks). Model boundary conditions include; the starting time and temperature, the finishing time and temperature, the number of model inversions, and the allowed complexity for each modelled thermal history. Model input parameters for AFTT comprise of; annealing algorithms, kinetic parameters (e.g. C_1 % or D_{par}), and c-axis projected lengths. Model parameters for (U-Th)/He are; diffusion calibrations, and modelled crystal geometry. All of these factors will influence the results obtained from inversely modelling LTT data which is why this study has chosen to use model results to test different hypotheses (i.e. accelerated cooling in response to different rifting events and re-burial in response to Deccan lava emplacement) as opposed to acquiring detailed quantitative information on the timing and magnitude of cooling for individual samples.

Inverse-modelling low temperature thermochronometric data results in multiple thermal histories and an inherent non-uniqueness making it problematic extracting absolute constraints on denudation. One possible solution is to simultaneously inverse-model different thermochronometers on the same sample (e.g. Persano et al. (2005)). Within this project simultaneous inverse-modelling proved effective for providing more robust constraints on modelled thermal histories (and hence denudation) for some samples (see sections 4.4 and 5.4). However other samples proved difficult or impossible to simultaneously inverse-model because the data being modelled were not good quality. Simultaneous inverse-modelling is a recent development and it is only within the last few years that user friendly software has become available and perhaps as a consequence it has not been used extensively throughout the thermochronometry community. If this methodology is to be utilised effectively, precise modelling strategies with careful sample selection and realistic model parameters will have to be employed.

Chapter 6 models flexural isostasy of the Western Indian lithosphere constrained from the volume of sediment offshore and the magnitude of denudation (from LTT) onshore. Modelling

was undertaken using theory developed for the flexure of beams from mechanical engineering (Hetenyi, 1979; Timoshenko, 1958), subsequently adapted to account for the properties of the lithosphere. Flexural isostatic studies have proved successful in explaining first order patterns of subsidence and uplift (Gunnell and Fleitout, 1998, 2000; Pazzaglia and Brandon, 1996; Pazzaglia and Gardner, 1994; Watts, 2001) and, for this study, successfully tested the different competing conceptual models of long-term landscape development. However, it still remains challenging extrapolating material properties of beams to less well constrained material properties of the lithosphere. Future work should attempt to quantify the flexural properties of the lithosphere more rigorously using region-specific methods that provide information on the composition, structure and isostatic condition of the lithosphere such as gravity, bathymetry, and seismic surveys (Chand et al., 2001; Chand and Subrahmanyam, 2003; Chandrasekharam, 1985; Rajesh and Mishra, 2004; Stephen et al., 2004; Tiwari and Mishra, 1999).

7.5 Conclusions and closing remarks

The following conclusions can be summarised from this study:

- The Western Indian margin began development in response to rifting between India and Madagascar, but the evolution of the margin (including the formation of the escarpment) was influenced primarily by rifting between India and The Seychelles.
- The India/Seychelles rifting event influenced the development of the entire length of the margin from the Deccan Volcanic Province to the Southern Granulite Terrane.
- The Reunion plume may have triggered rifting and sea-floor spreading during the development of the Western Indian margin, but did not play a significant role in triggering syn- and/or post-rift denudation. Passive rifting mechanisms are therefore more significant contributors to the development of the margin.
- The downwarp model of Ollier and Pain (1997) is not supported by the volume of sediment present within the Konkan-Kerala Basin or the pattern of denudation inferred from low temperature thermochronometry.
- Mass balance analysis cannot resolve the downwarp model of Widdowson (1997) from the elevated rift flank model; however, the pattern of denudation inferred

from apatite fission track and (U-Th)/He analysis can only be explained if the Western Indian margin formed into an elevated rift flank.

- The Western Indian margin appears to be compartmentalised with different styles of landscape development occurring on different segments of the margin. The Widdowson (1997) downwarp model provides a suitable explanation for the evolution of the escarpment within the Deccan Volcanic Province. Low temperature thermochronometry is more consistent with margin development into an elevated rift flank for the margin south of the Deccan.
- Modelling the flexural isostatic effects of sediment loading offshore and denudational unloading onshore indicate that flexural isostasy is a contributing mechanism but that other mechanisms must also be invoked to explain the subsidence and uplift patterns observed for Western India.

This study incorporates a variety of methodologies which individually are powerful techniques for addressing the questions regarding the tectonic evolution and long-term landscape evolution of the Western Indian elevated passive margin. However, mass balance analysis, new low temperature thermochronometry, and flexural modelling of the Western Indian margin each reveal issues which future work will need to address. The strength of this study comes from multiple applications of these different methodologies resulting in an improved understanding of the development of Western India.

Appendix A Analytical procedures for low temperature thermochronometry

A.1 Apatite and zircon mineral separation

Apatite and zircon are obtained by disaggregating 5 – 10 kg of the host rock using a jaw crusher and sieving to obtain a sand-sized fraction less than 300 μm . The fraction that is coarser than 300 μm is reprocessed in the jaw crusher until there is a sufficient volume of crushed rock. The material is then passed across a Wilfley table to wash the sample efficiently and provide a rough heavy mineral separate with grains between 300 μm and 65 μm in diameter. Once the sample has been dried at room temperature, magnetic minerals are removed using, first, a hand magnet and then a Frantz LB-1 magnetic separator. The non-magnetic fraction is then processed using standard heavy liquid separation. Firstly, Lithium Sodium Tungstate (2.8 g/cm^3) is used to remove minerals that are less dense than apatite (and zircon), in particular, quartz and feldspar. The dried heavy fraction is processed using Diiodomethane (density of 3.3 g/cm^3) to separate zircon (heavy fraction) from apatite (light fraction).

A.2 Apatite fission track analytical techniques

Apatite crystals from the separate are mounted in epoxy resin on a glass slide. The mount is ground and polished to reveal flat internal surfaces of the apatite crystals. The mounts are then etched in 5 % HNO_3 for 20 seconds at 20 °C followed by cleaning with water and alcohol to reveal spontaneous tracks. The method employed for this study is the external detector method requiring the attachment of a low uranium mica detector to the mount (Hurford and Green, 1982). To insure full contact of the mica and mount, the mica-mount pairs are secured by wrapping in heat-shrunk plastic film. Between 10 and 15 mounts with their detectors are stacked together with 2 - 3 mineral standards (e.g. Durango or FCT) interspersed throughout the stack and standard glasses (CN5 or European) at the top and base of the stack. The stack is then irradiated with neutrons at a well-thermalized reactor, for this study at the X-7 facility, Lucas Heights, Australia (Neutron fluence of $\sim 10^{16}$ thermal neutrons/ cm^2). After irradiation samples are separated and the mica sheets are etched in concentrated hydrofluoric acid for 40 minutes at 20 °C to reveal induced tracks. The mount and detector pairs are arranged together

on glass slides such that it is possible to match spontaneous track counts on individual grains to their corresponding induced track counts on prints on the mica detector (Figure 67). Induced tracks from the standard glasses at the top and base of the stack are also counted to correct for the fluence gradient across the stack created during each irradiation. Apatite fission track ages were obtained using the external detector method (Hurford and Green, 1982) and the zeta calibration method (Hurford and Green, 1983) (see Section B.2).

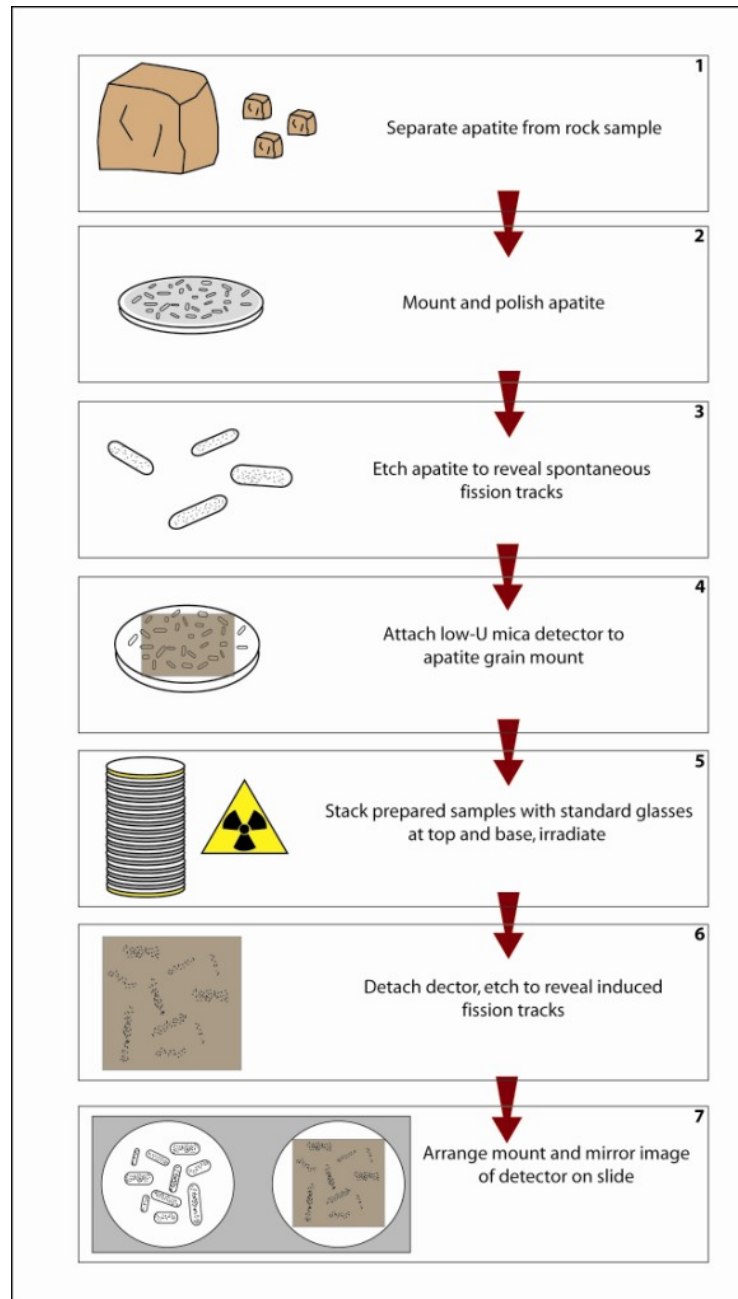


Figure 67 Apatite fission track sample preparation procedure

A.3 Apatite and zircon (U-Th)/He analytical techniques

A.3.1 Sample preparation

Apatite and zircon crystals were selected under a binocular polarising microscope at high magnification (x 500) to allow the identification of crystals with good morphology lacking any defects or inclusions. Defects or cracks can lead to rapid diffusion of helium out of the crystal lattice resulting in erroneously young ages. The presence of inclusions can result in erroneously old ages either by contributing parentless helium (e.g. in fluid inclusions) or He from a source where the parents cannot be measured (e.g. refractory mineral inclusions that do not dissolve during the conventional analytical protocol). A second experienced analyst checks suitable crystals. Acceptable crystals are then sketched and their dimensions measured using a 10 μm x 10 μm graticule. Only crystals with similar diameter in excess of 65 μm were used in each aliquot in this study to minimise the error associated with the alpha-recoil correction (Farley et al., 1996). The number of crystals per aliquot depends on the concentration of U and Th, and their age. For this study between two and five crystals were analysed in each aliquot.

Helium extraction was undertaken initially using an ultra-high vacuum doubled-walled resistance furnace following the procedure of (Persano et al., 2005) (apatite analyses only). Sample preparation requires that suitable crystals are loaded into individual re-usable stainless steel capsules approximately 2 mm in diameter which are then wrapped in degassed copper foil. The capsules are then placed into a Monax glass 'tree' which is mounted above the furnace. In later studies a diode laser was used to extract helium (apatite and zircon analyses). Crystals were loaded into 0.5 mm diameter Pt tubes which are crimped at both ends. The Pt packets are placed into 1.5 mm deep by 2 mm wide holes in a high purity copper laser pan following the procedure of (Foeken et al., 2006).

A.3.2 Helium analysis

Prior to He extraction, both the tree (for furnace extraction) and the laser pan (for laser extraction) are pumped to ultra-high vacuum using a turbo pump and a 301/second triode ion pump for approximately 2 hours. For the furnace method, prior to analyses, the furnace is isolated from the monax glass tree and degassed at 1200 °C for approximately 40 minutes. Single capsules are dropped sequentially from the tree into a de-gassed furnace and heated to 950 °C for 40 minutes. It has been demonstrated by (Persano et al., 2002) that this heating protocol results in complete degassing of apatite without volatilisation of U or Th. Following extraction, the gases are purified using hot and cold TiZr getters and liquid nitrogen-cooled charcoal prior to being measured using a Hidden HAL3F quadropole mass spectrometer.

During the extraction a ^3He spike is added prior to analysis (Persano et al., 2002). After each heating cycle, a re-heat cycle is undertaken in order to ensure complete sample de-gassing.

In later analyses the laser method was employed allowing more rapid sample throughput, smaller sample size and increased precision. For complete extraction of He from apatite, a 2 mm, 0.5 W beam is focused onto each sample separately in the laser pan. Helium extraction is achieved by heating the sample to 600 °C for 30 seconds (Foeken et al., 2006). For complete extraction of He from zircon, samples were heated to 1200 °C for 20 minutes using a 1.25 – 2.00 W de-focused beam (Foeken et al., 2006). Evolved gasses were purified and measured in an identical manner to the furnace method but without the necessity of a ^3He spike.

A.3.3 Uranium and thorium analysis

Following extraction of He, the samples are recovered for U and Th analysis using isotopic dilution. For apatite, each sample is dissolved using 2 ml of 5 % nitric acid, and spiked using 0.45 ng of ^{230}Th and 0.18 ng of ^{235}U . Spiked samples were left to equilibrate for 24 hours on a hotplate at 80 °C. For zircon, a new methodology was developed by Dobson (Dobson, 2006; Dobson et al., in press) involving acid digestion followed by simple cation exchange column chemistry for zircon dissolution and U-Th purification.

The U and Th are analysed using an Inductively Coupled Mass Plasma Spectrometer (ICPMS) following the procedure of (Balestrieri et al., 2005; Persano et al., 2002; Persano et al., 2005).

Appendix B Calculating AFTT ages

B.1 The AFTT age equation

Calculating the apatite fission track age follows the same general principles of other isotopic systems requiring knowledge of the concentration of the decaying parent element, the rate at which the parent element decays (decay constant) and the concentration of the daughter element. However, the basic age equation for a decaying radioisotope must be altered to account for two differences: 1) there is no daughter element and it is the accumulation of fission tracks that must be quantified; and 2) ^{238}U also decays via α -emission which must be corrected for. The fission track age is calculated using:

$$N_s = \frac{\lambda_f}{\lambda_\alpha} N_{^{238}\text{U}} (\exp^{\lambda_\alpha t} - 1)$$

Equation 23

Where N_s is the number of spontaneous fission tracks per unit volume, λ_f is the decay constant for spontaneous fission ($8.66 \times 10^{-17} \text{ y}^{-1}$ (Guedes et al., 2003)), λ_α is the decay constant for α -decay ($1.55125 \times 10^{-10} \text{ y}^{-1}$), $N_{^{238}\text{U}}$ is the number of spontaneous fission per unit volume, and t is the isotopic age (years).

Three additional alterations must be incorporated into the age equation to obtain a fission track age:

1. The concentration of ^{238}U cannot be measured directly and the standard procedure is to have samples irradiated to induce fission of ^{235}U . The external detector method records the fission of ^{235}U . The isotopic ratio of $^{235}\text{U}/^{238}\text{U}$ is 7.2527×10^{-3} (Hurford and Green, 1982) and, provided the cross section for induced nuclear fission of ^{235}U and the thermal neutron fluence are known, then the amount of ^{238}U can be determined. The concentration of ^{235}U can be determined from:

$$\rho_i = q^{235}\text{U}\phi\sigma$$

Equation 24

Where ρ_i is the induced track density from the fission of ^{235}U in the mica detector, q is the proportion of tracks intersecting a single plane, ^{235}U is the concentration of ^{235}U , ϕ is the thermal neutron flux per unit volume and σ is the cross section of ^{235}U for induced fission.

2. The decay constant for fission (λ_f) and the neutron fluence are difficult to measure; however, the zeta-calibration method (Hurford, 1990; Hurford and Green, 1982, 1983) circumnavigates this problem and also accounts for operator differences. The zeta-calibration method is now applied ubiquitously to fission track analysis (see Section B.2).
3. Both spontaneous and induced fission tracks are measured by counting the number of tracks that intersect the polished and etched surfaces of the sample and the detector respectively. The density of tracks and a geometry factor must be integrated into the age equation.

Taking into consideration the previous points, the standard age equation for calculating fission track ages is therefore:

$$t = \frac{1}{\lambda_\alpha} \ln \left\{ 1 + \lambda_\alpha \zeta \rho_D \left(\frac{\rho_s}{\rho_I} \right) G \right\}$$

Equation 25

Where ζ is the empirically obtained zeta-calibration and ρ_D is the induced fission track density of a U-doped standard glass irradiated with the sample. G is the geometry factor, ρ_s is the spontaneous track density and ρ_I is the induced track density.

B.2 The zeta calibration method

The empirically obtained zeta-calibration is defined in Equation 26, where induced fission of U-doped standard glasses are irradiated with known mineral standards and the track ratios are then compared (see Hurford and Green (1983) for details). Spontaneous fission tracks are sourced from both above (now polished away) and below the polished surface whereas induced tracks are only sourced from below the polished surface; therefore, a geometry factor of 0.5 is required (g). The spontaneous and induced track densities are ρ_s and ρ_I respectively. The zeta calibration is defined as:

$$\zeta = \frac{(e^{\lambda_{std}} - 1)}{\lambda(\rho_s / \rho_I)_{std} g}$$

Equation 26

Where B is an empirically-defined constant, I is the $^{235}\text{U}/^{238}\text{U}$ ratio, and σ_F is the cross section for induced nuclear fission of ^{235}U ($580.2 \times 10^{-24} \text{ cm}^2$) (see (Hurford and Green, 1983) for details).

Appendix C AFTT data

C.1 Western Indian AFTT ages

Trackkey plots for AFTT samples

p. 175- 186

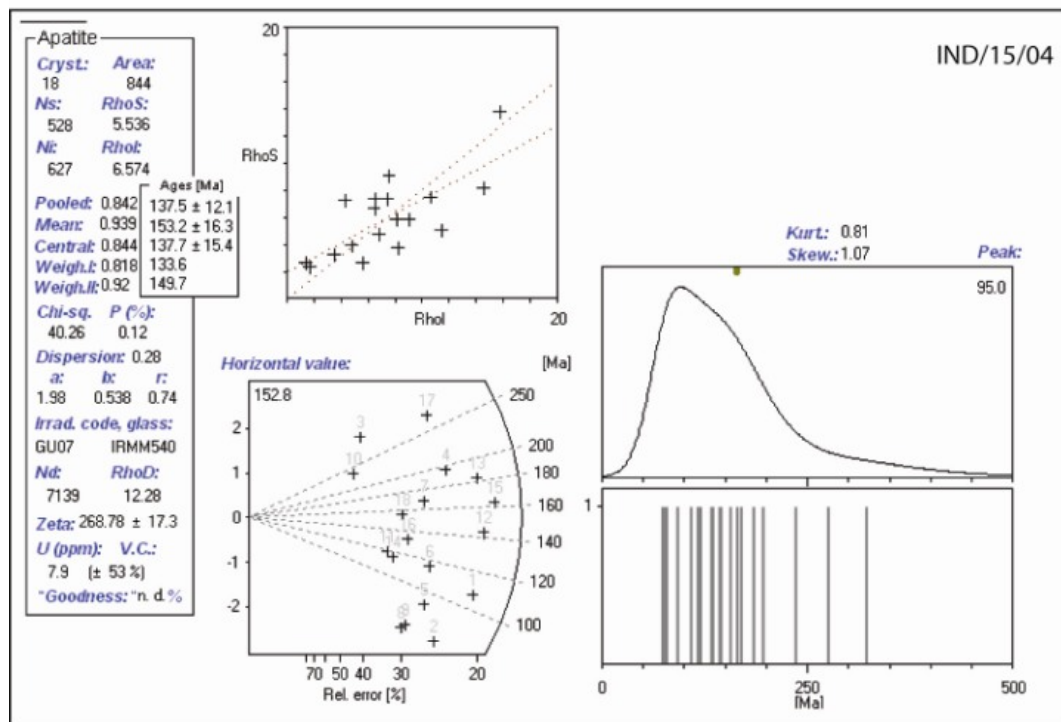
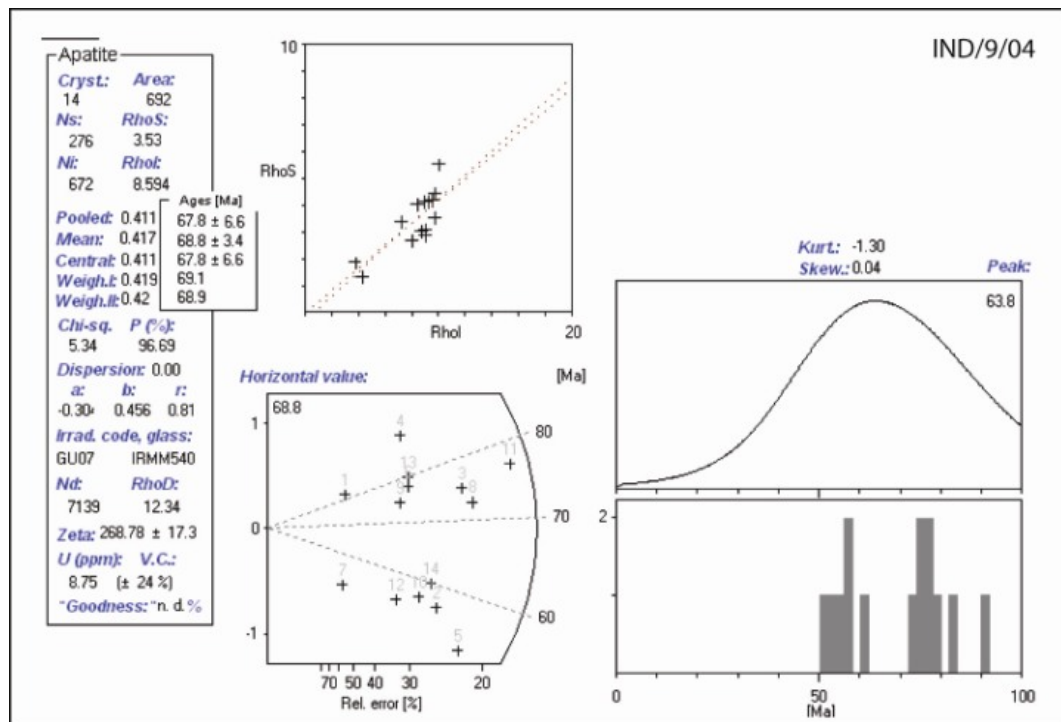
Table 21 AFTT TLD data for Goa and Karnataka

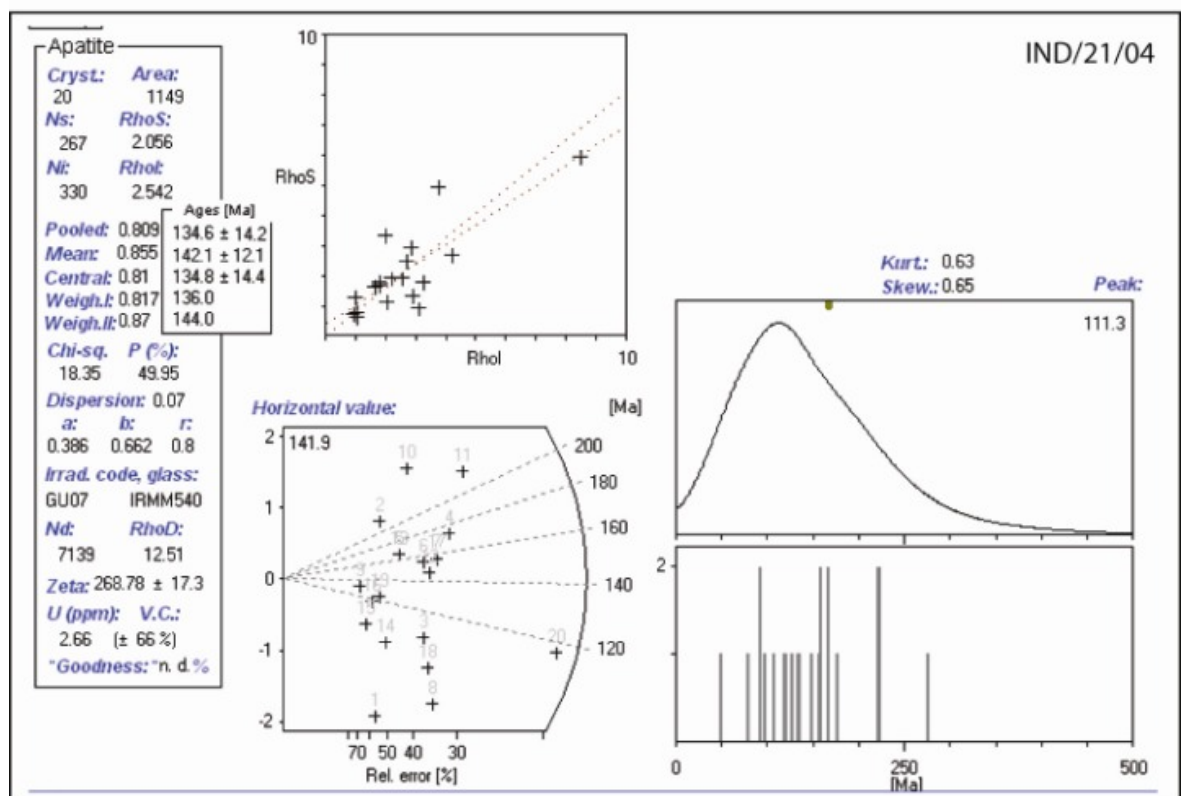
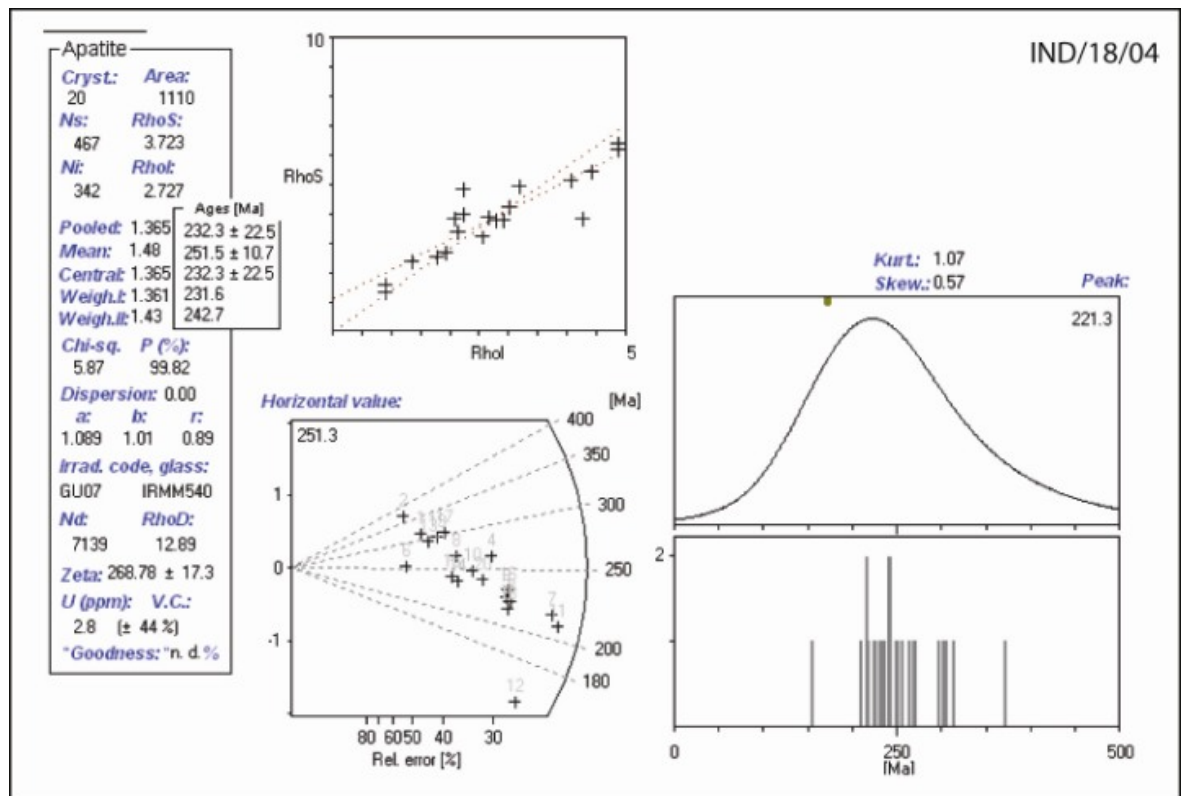
p. 187

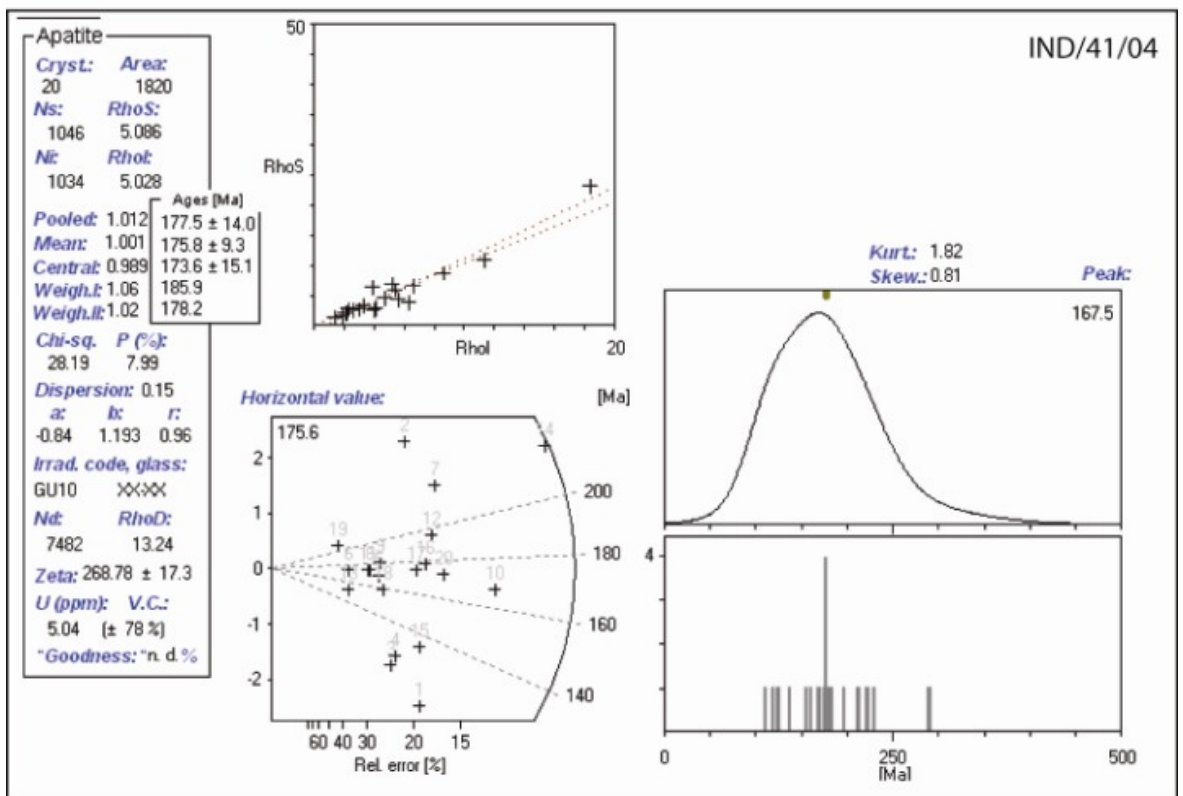
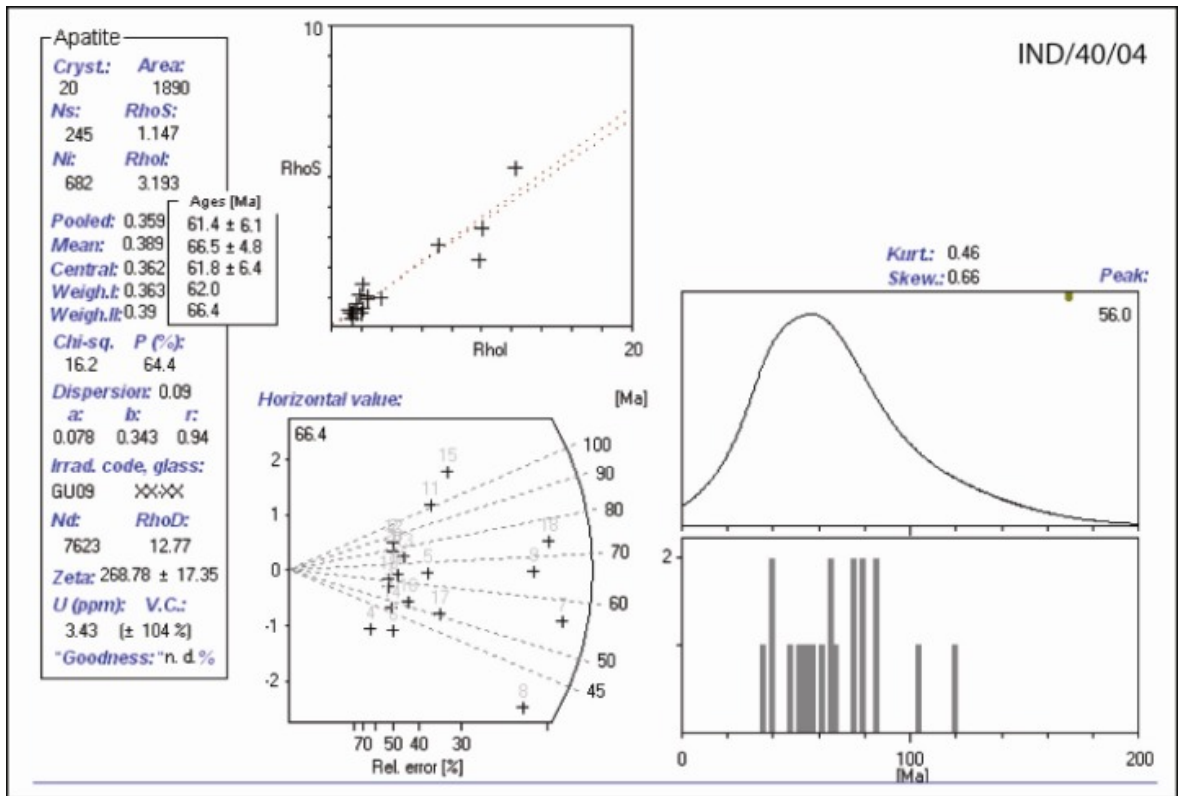
Table 22 AFTT TLD data for Kerala

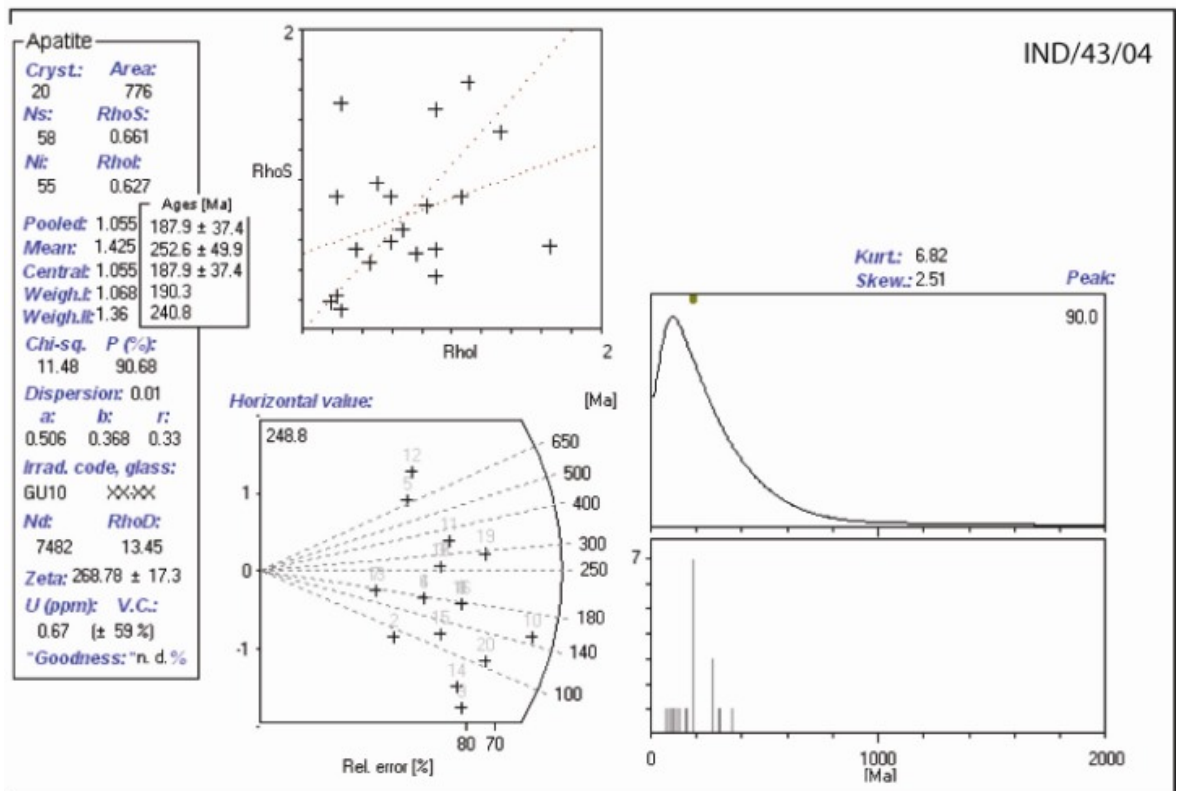
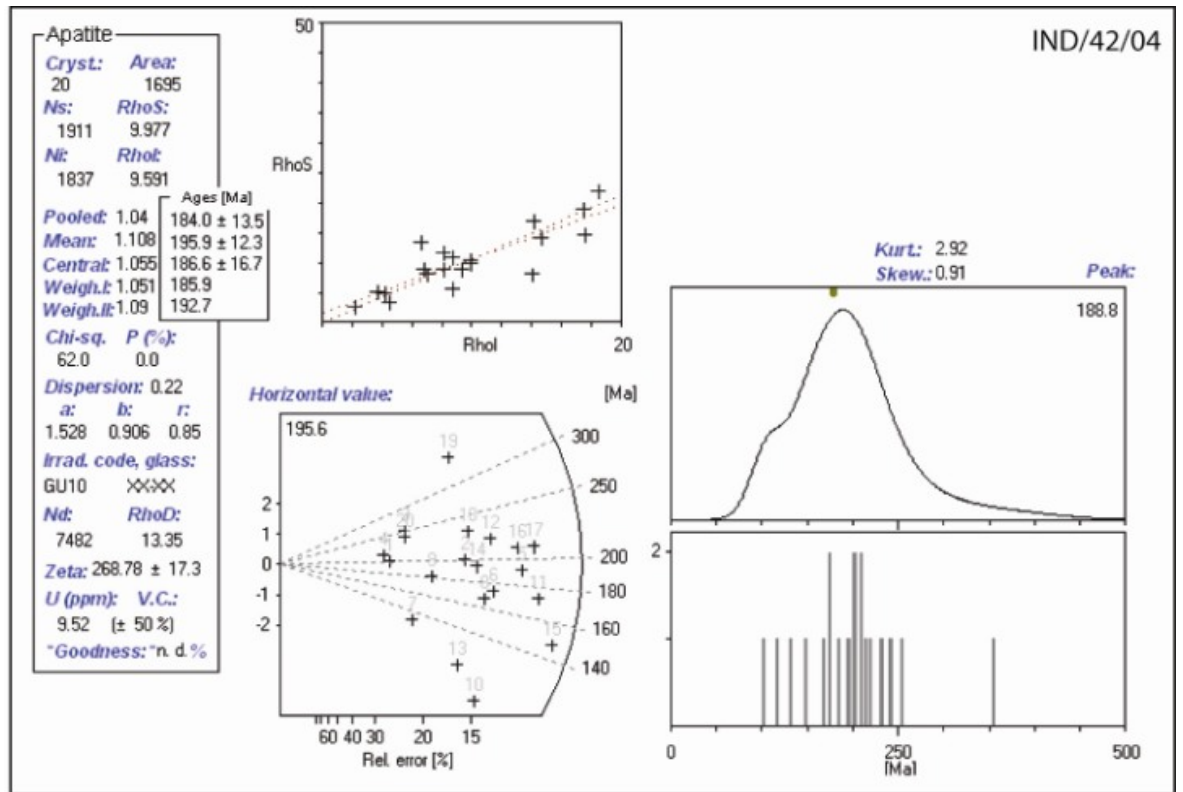
p. 188-189

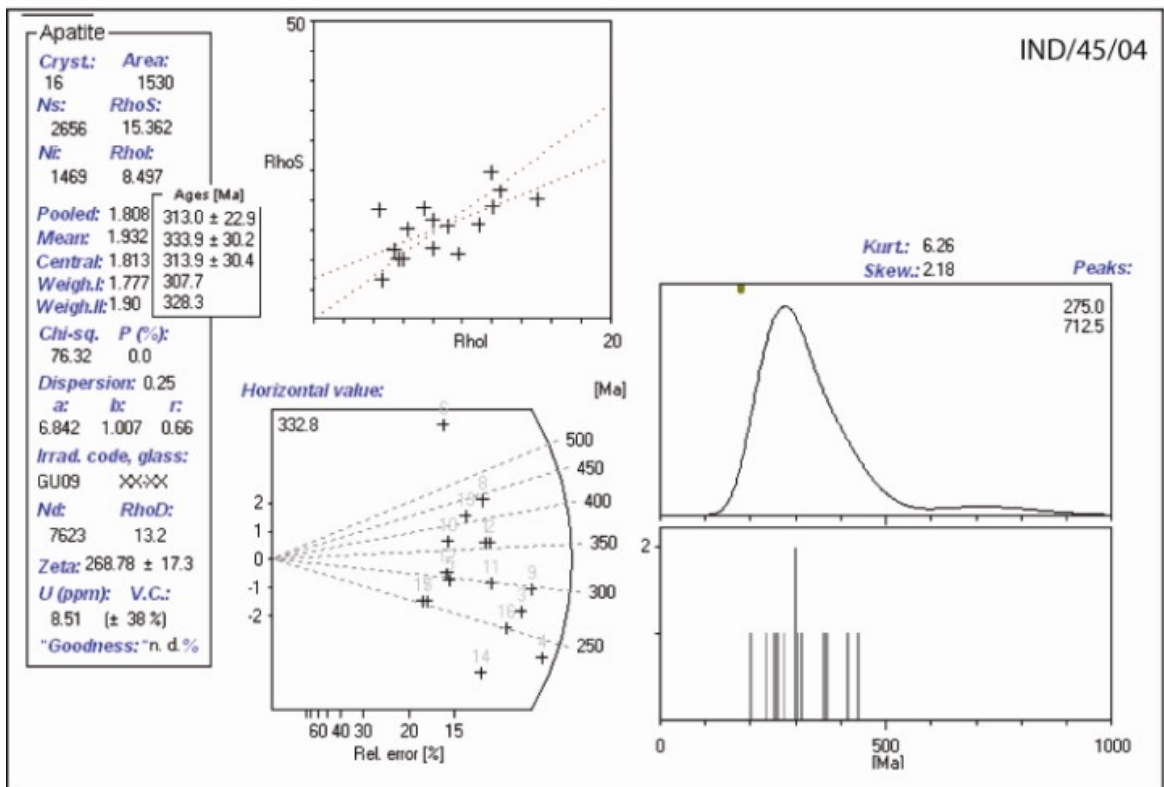
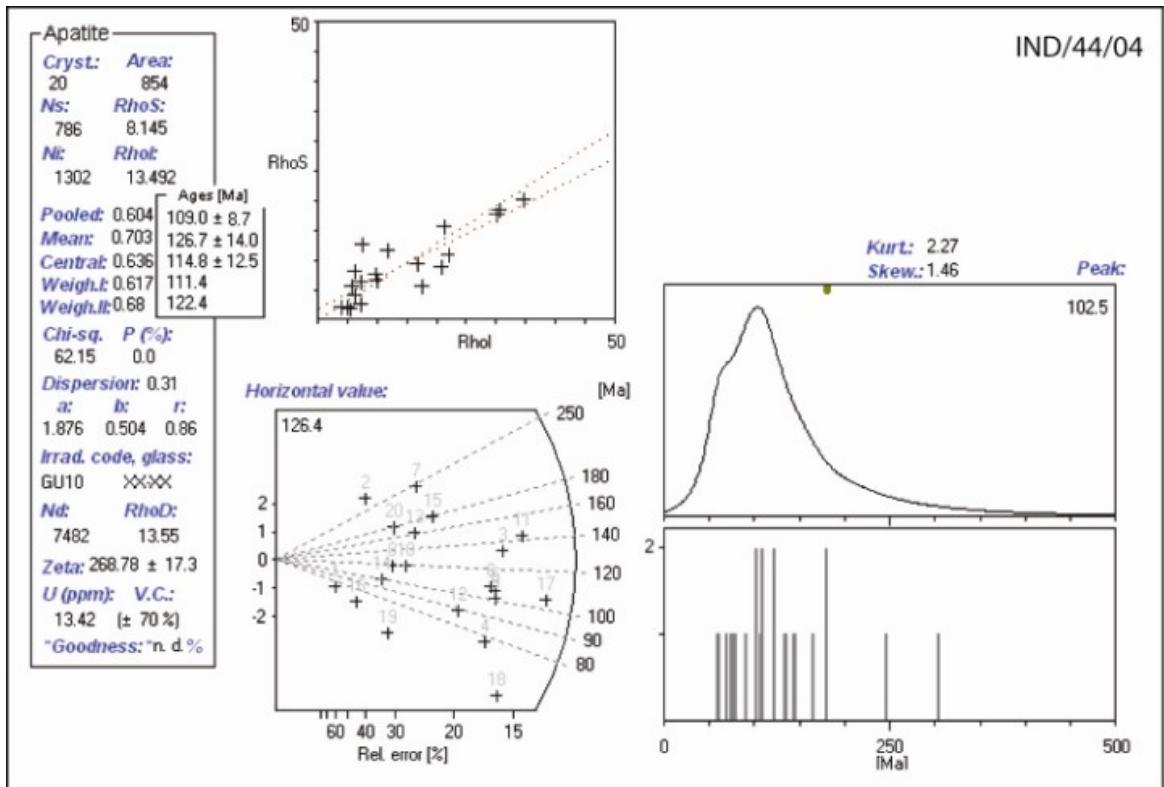
C.1.1 Trackkey plots

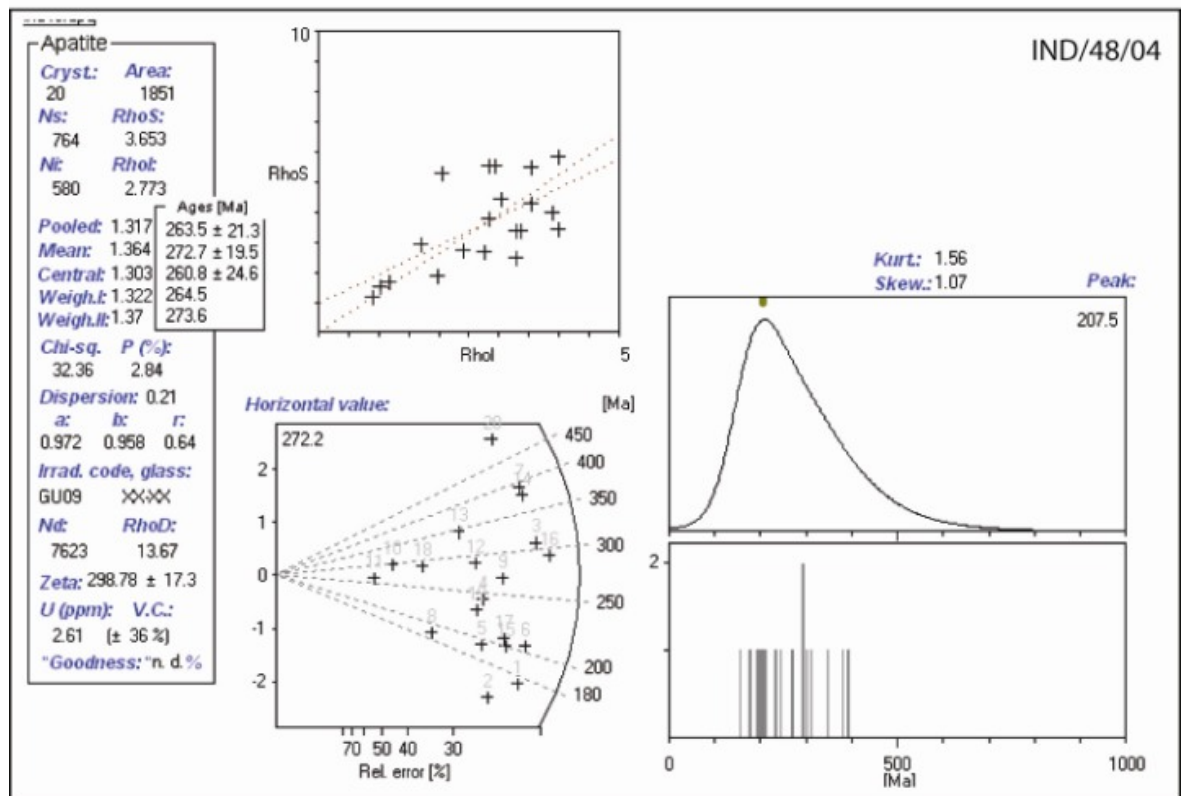
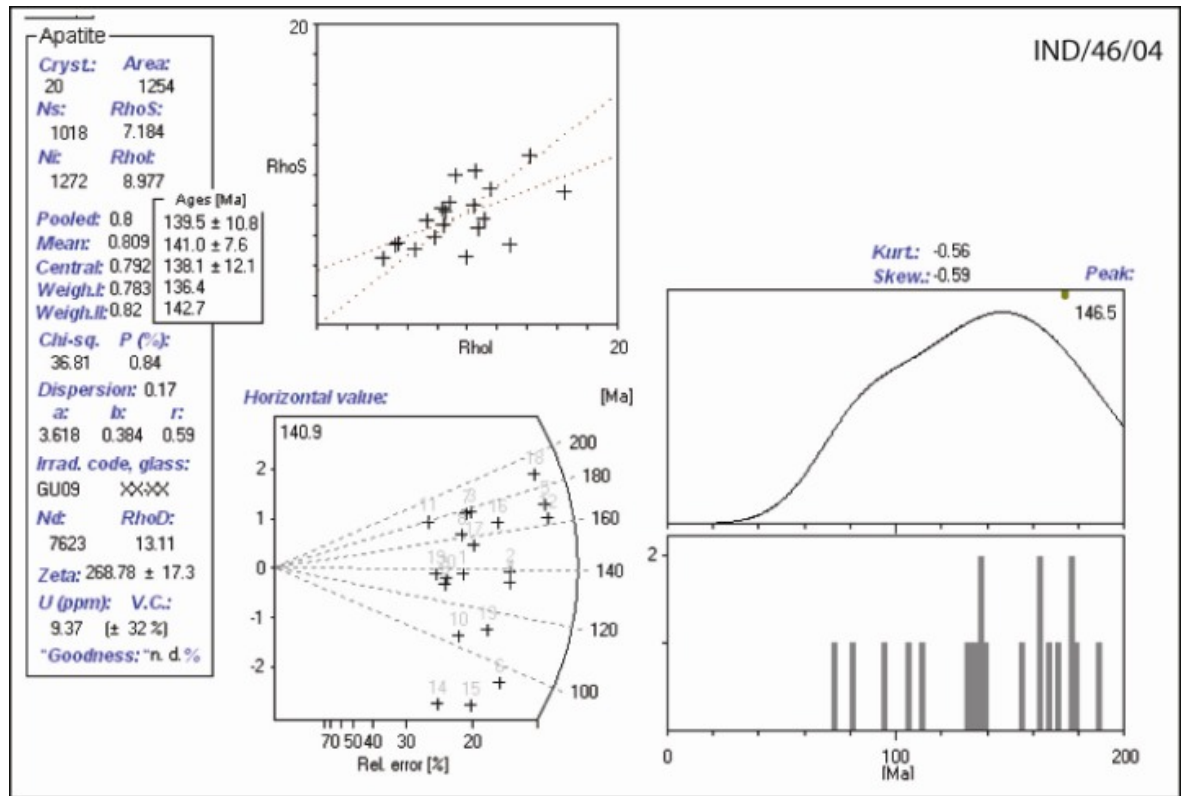


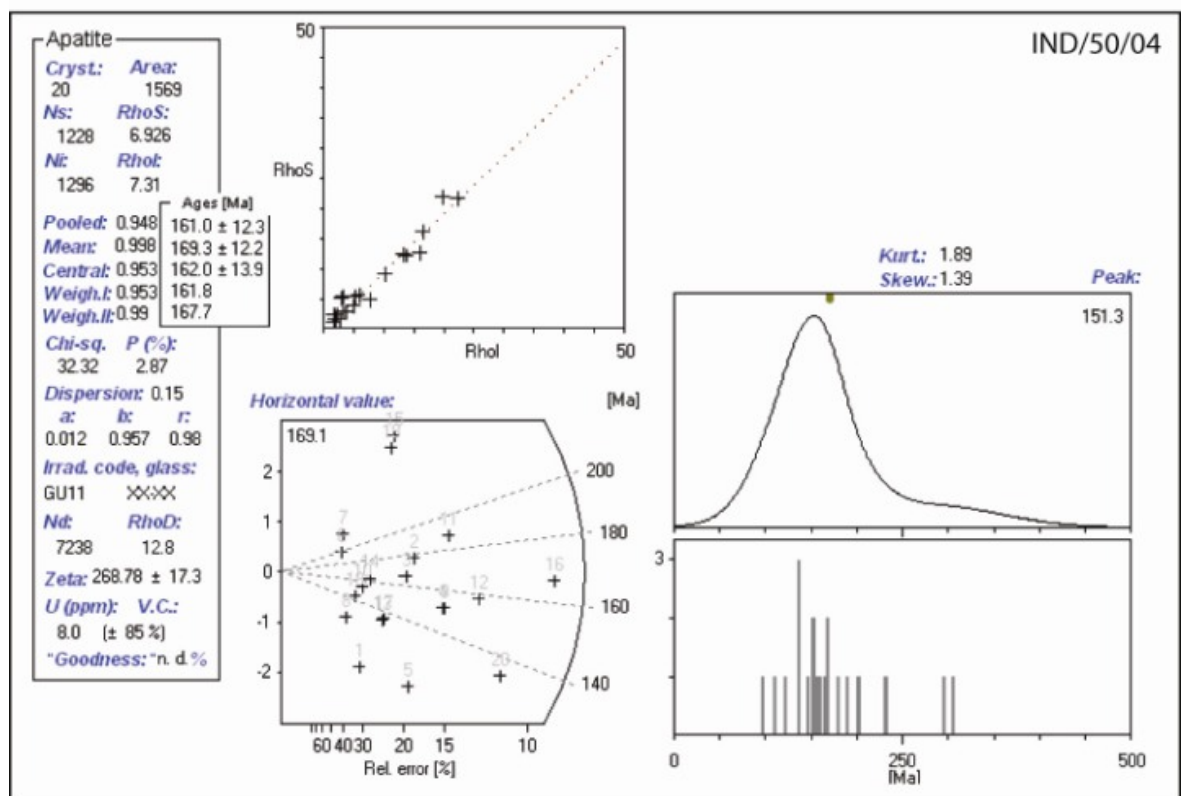
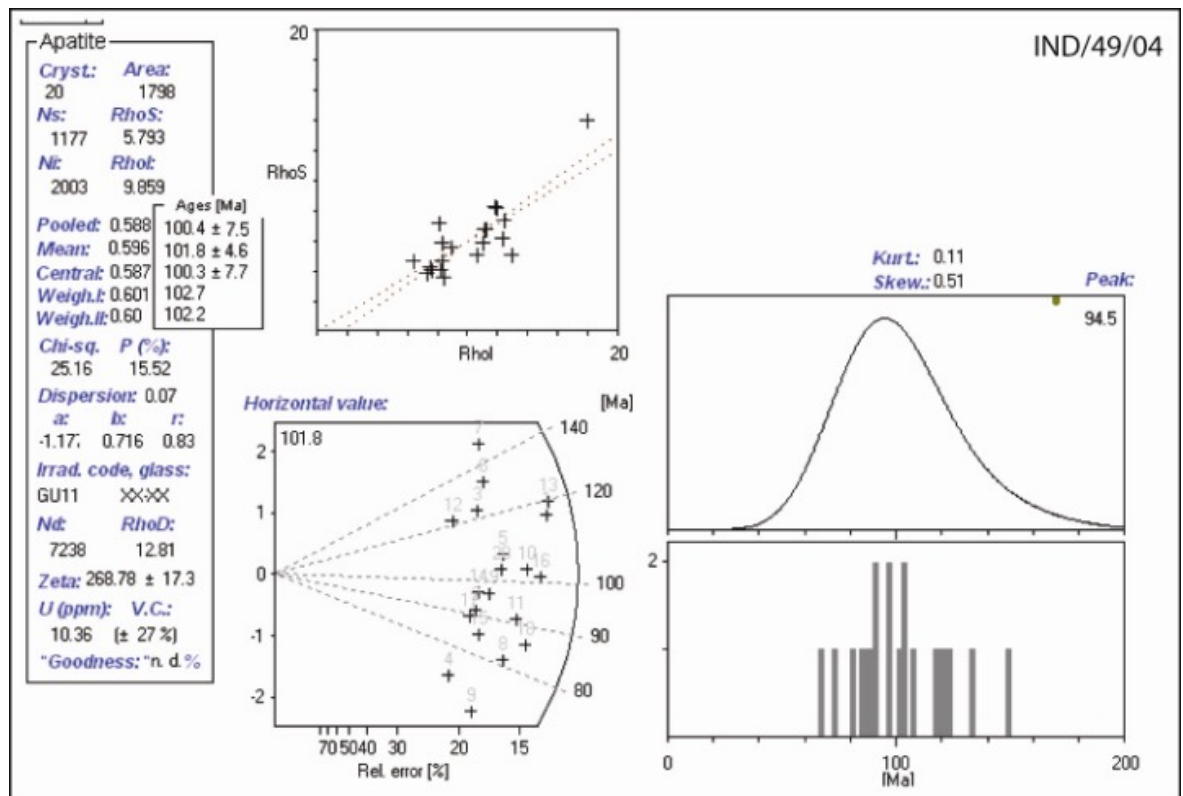


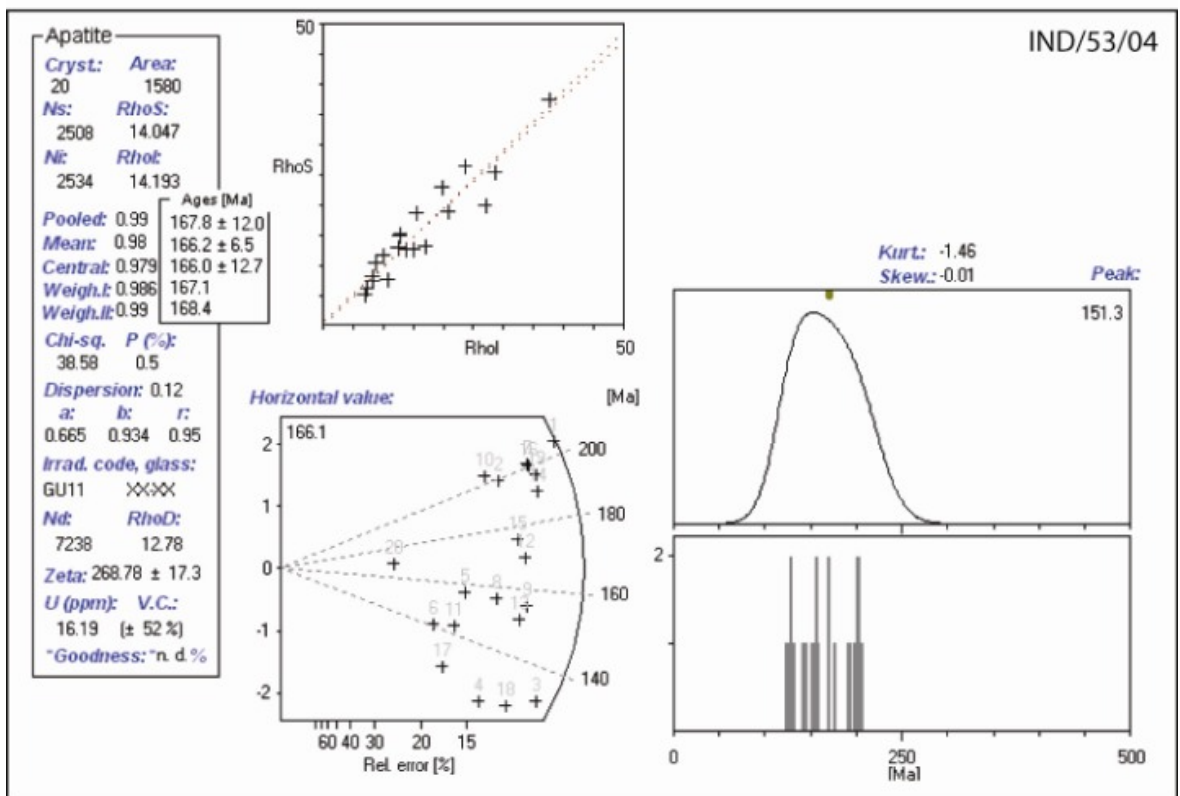
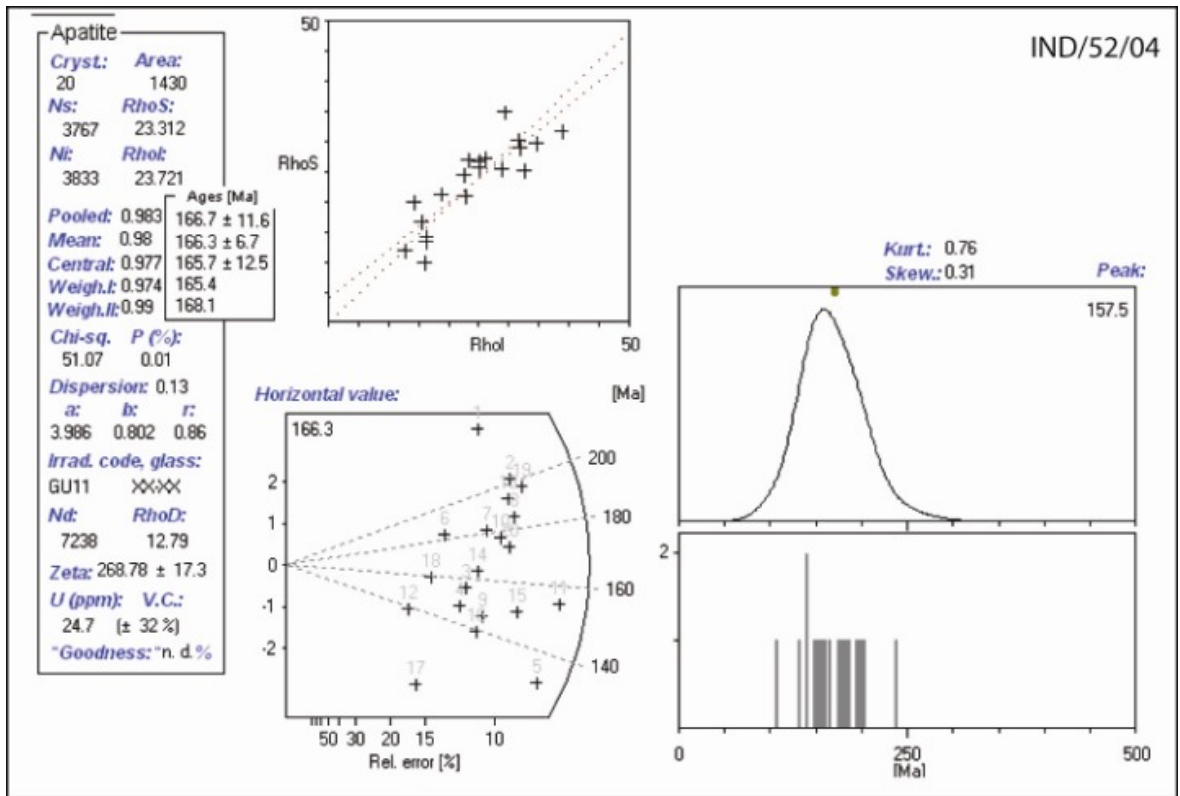


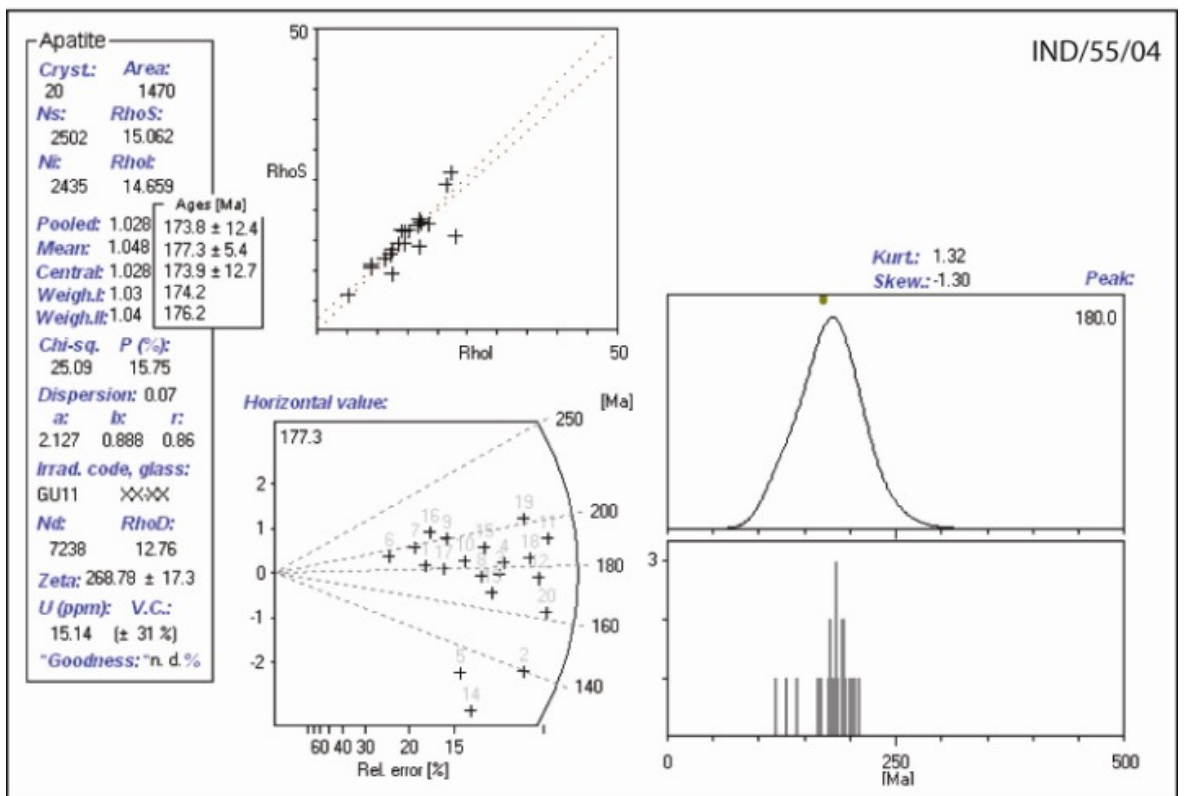
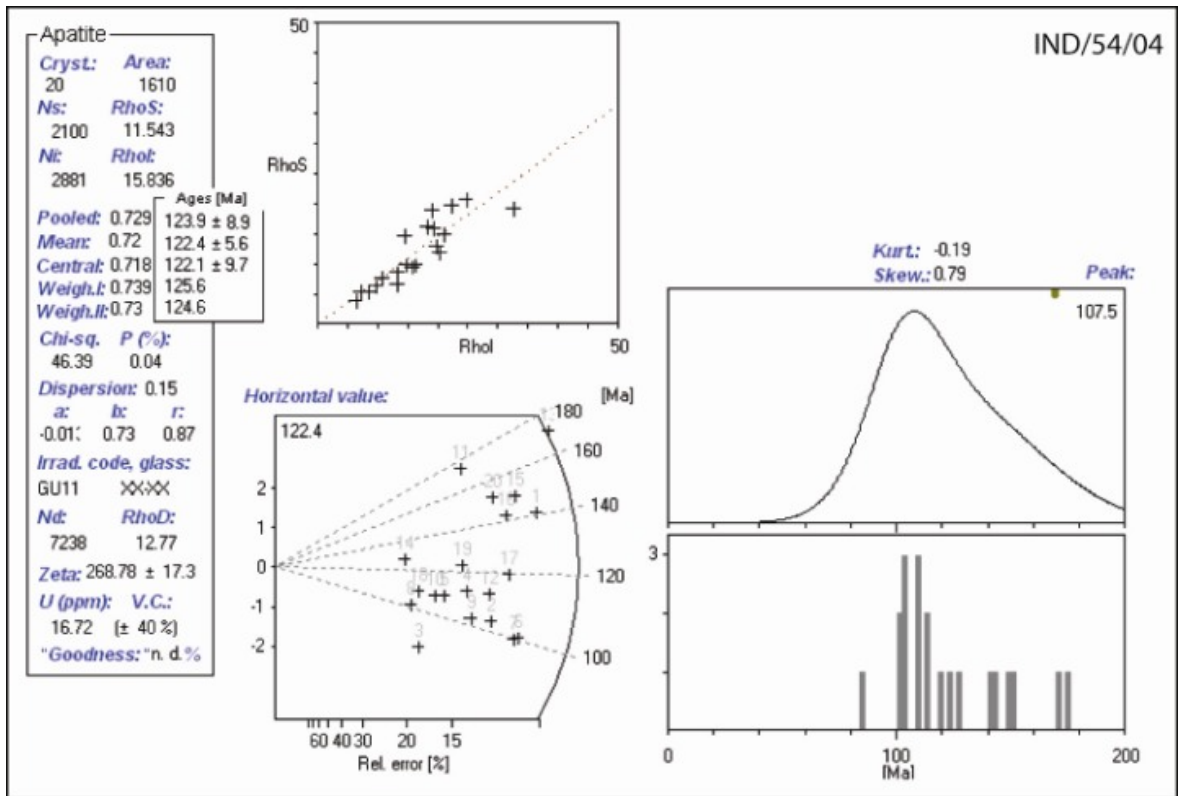


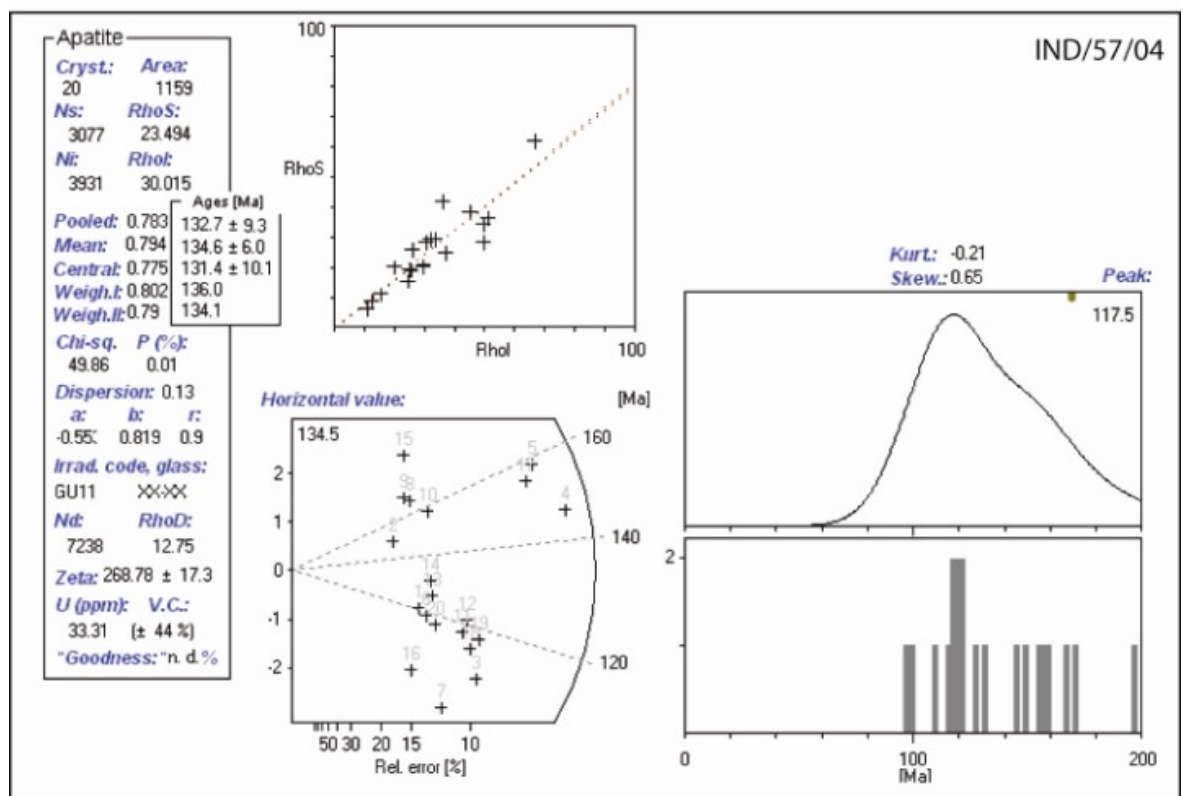
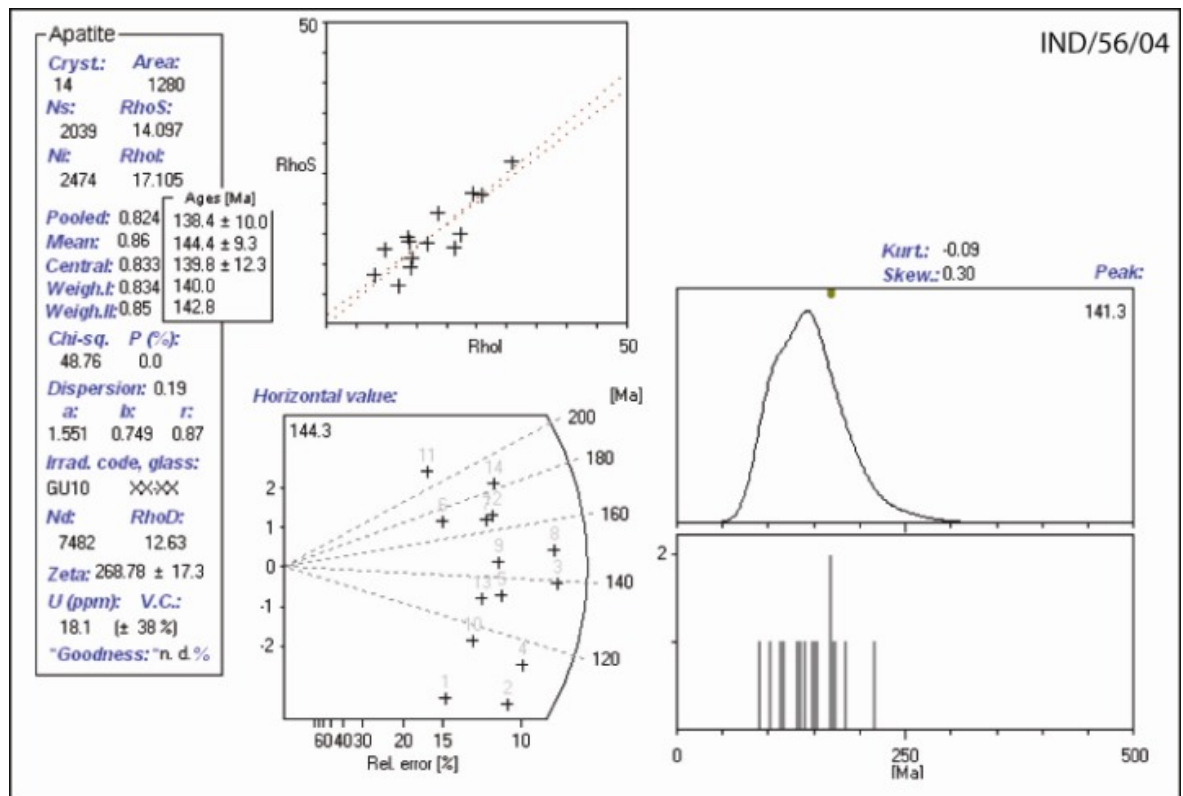


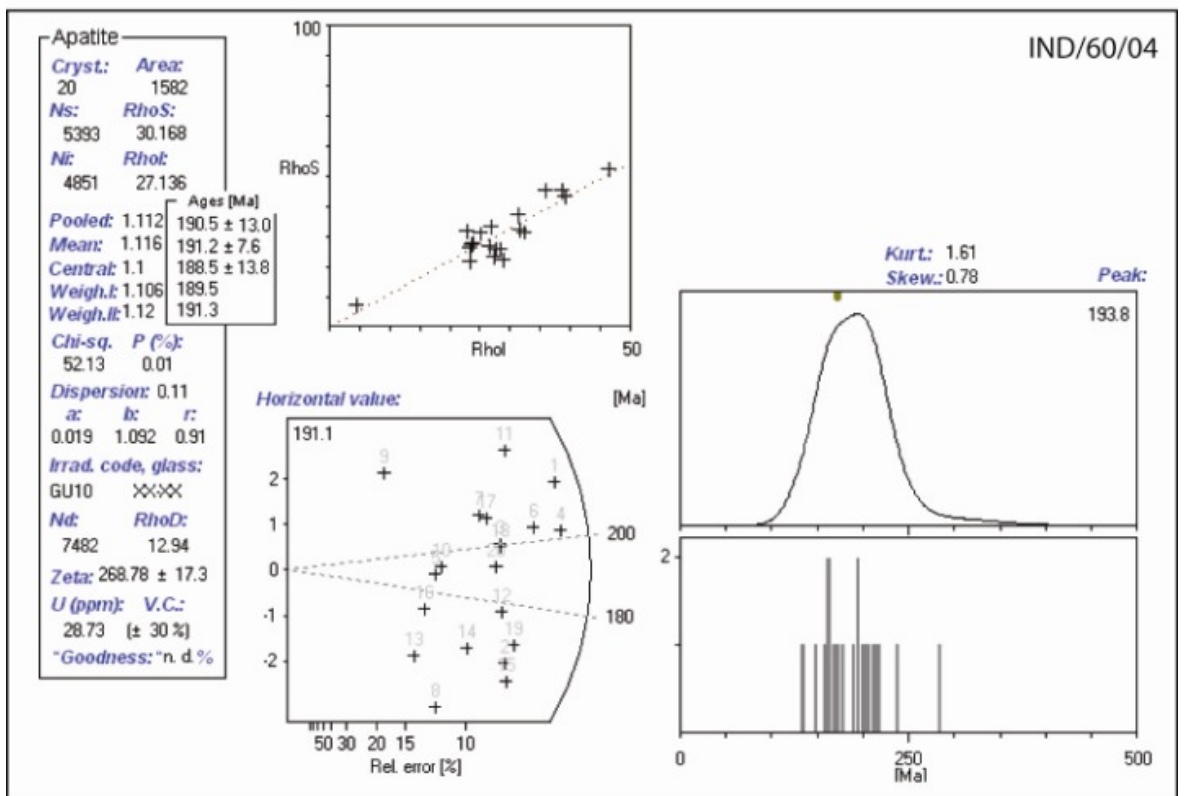
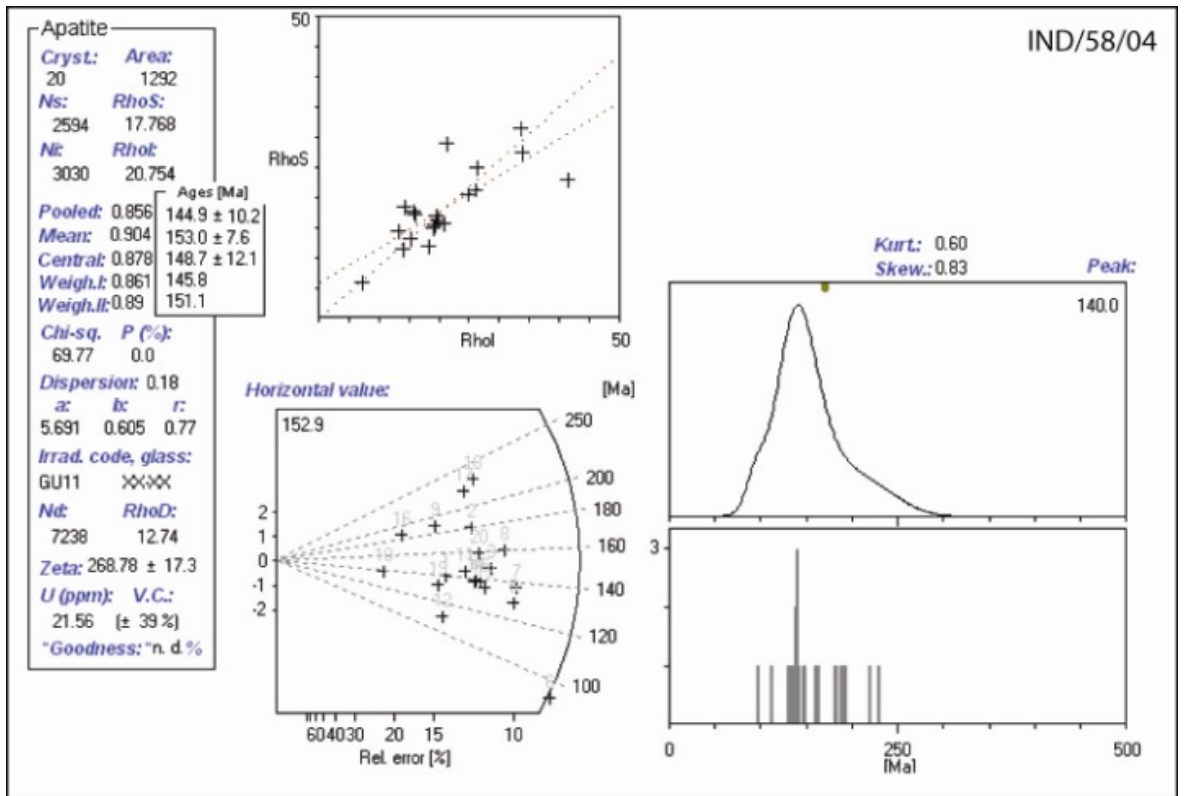


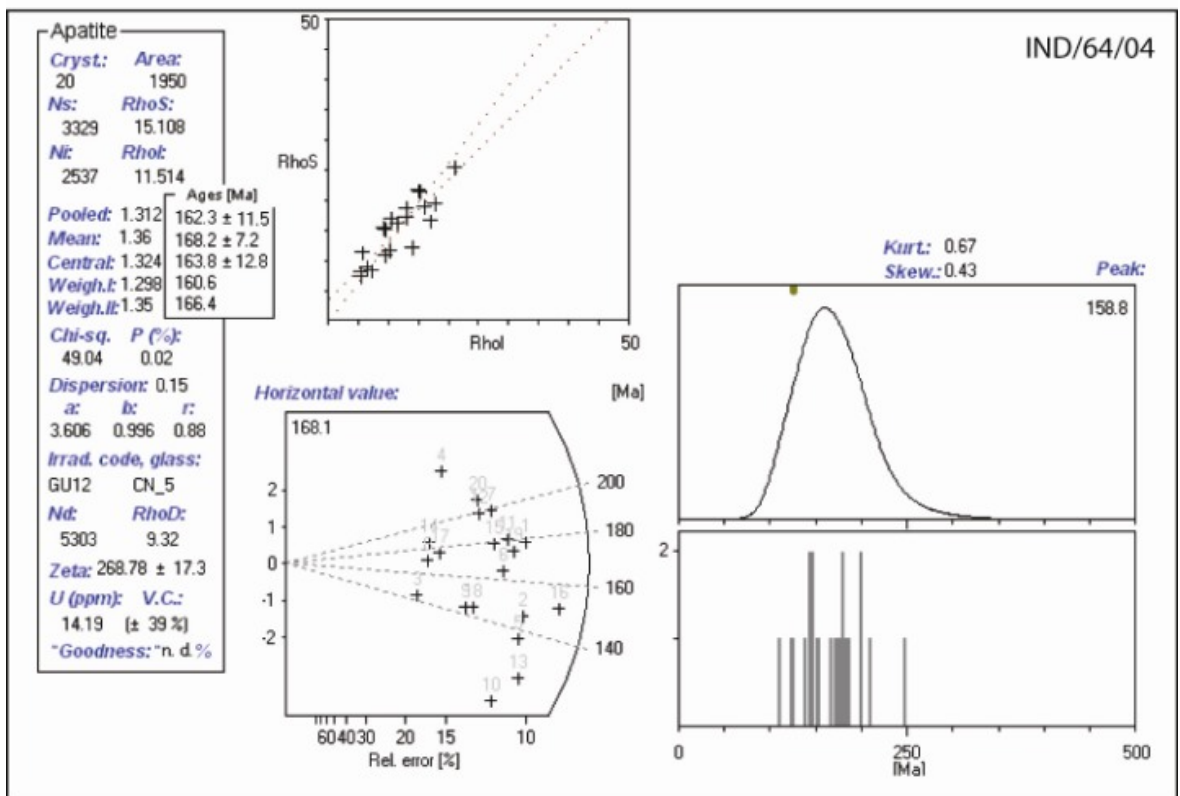
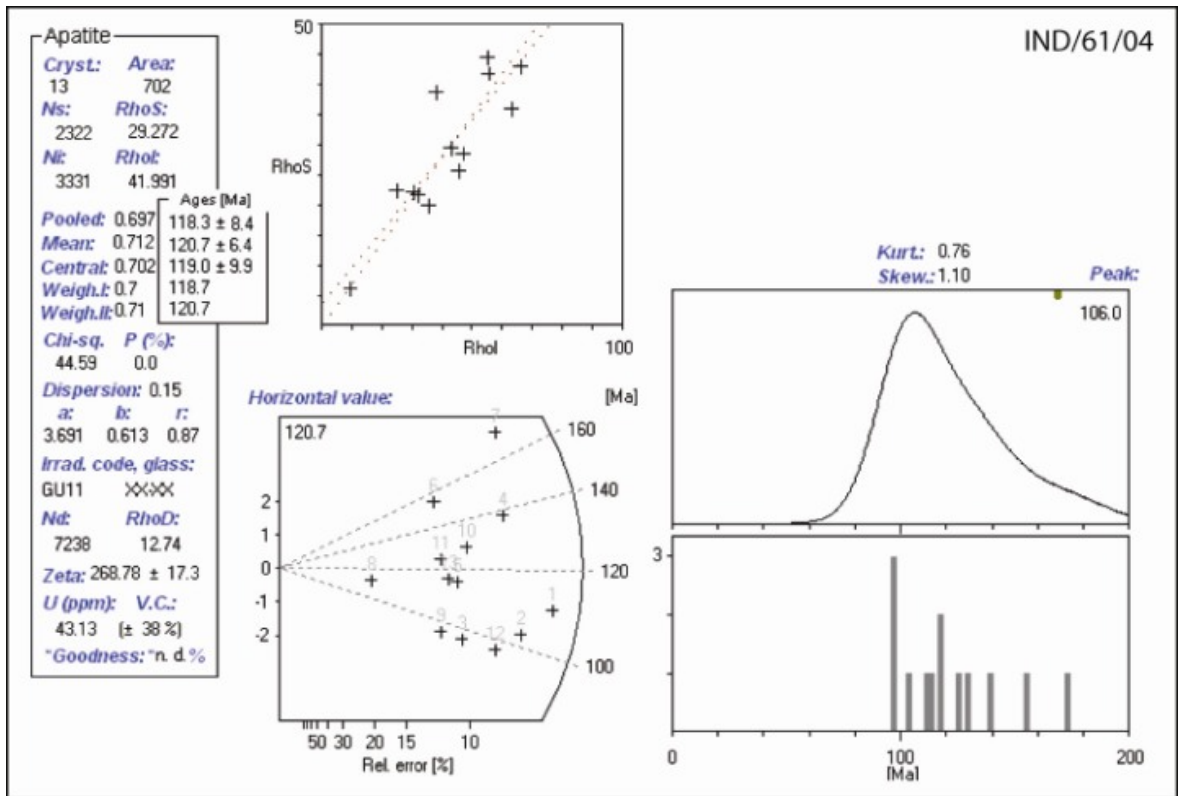






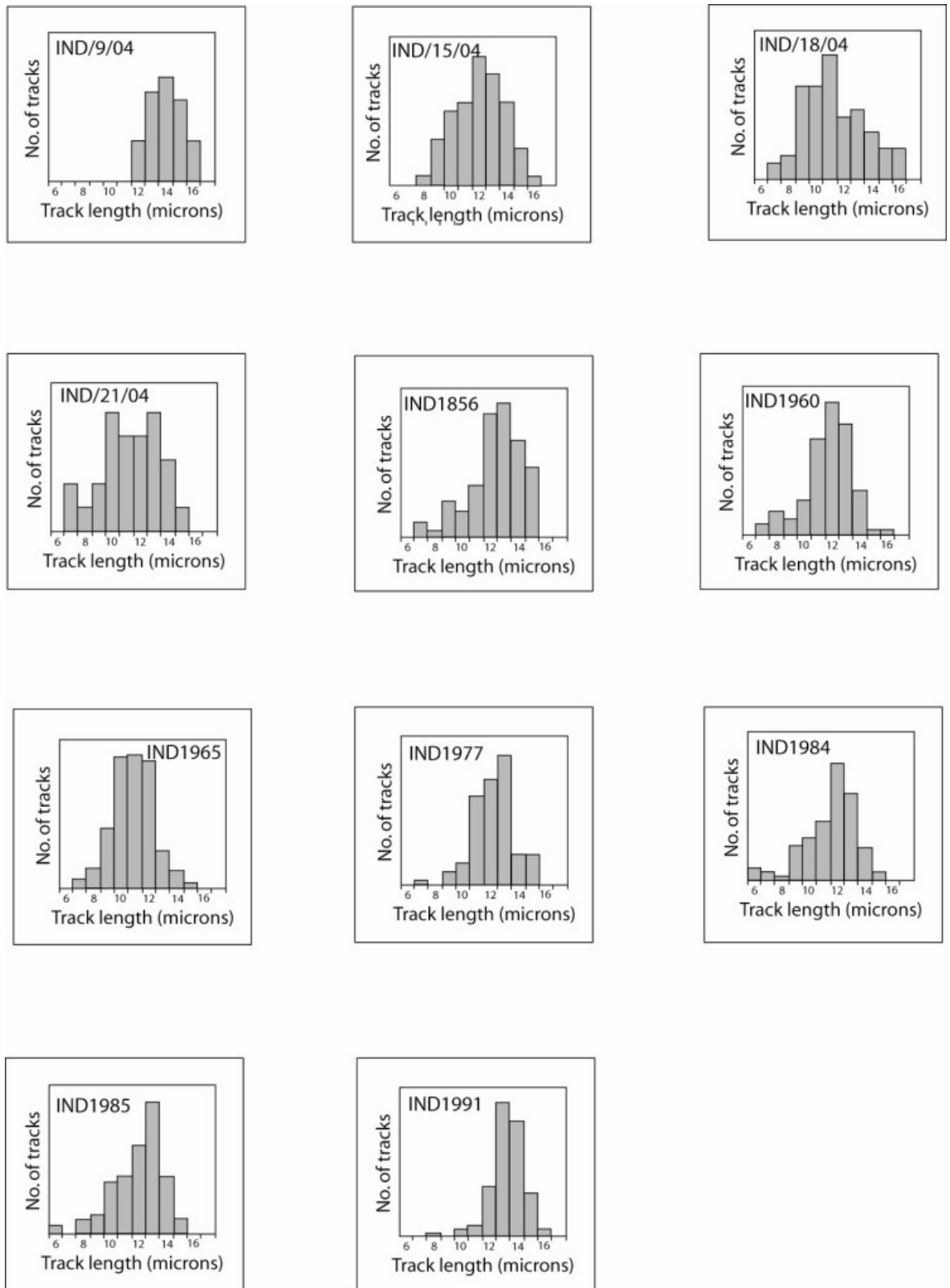




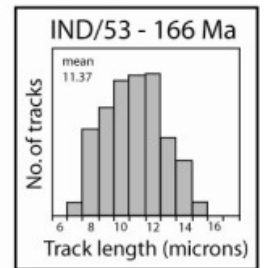
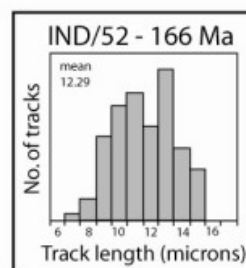
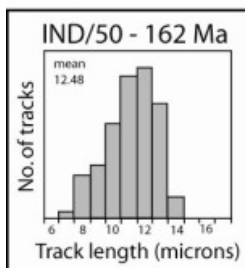
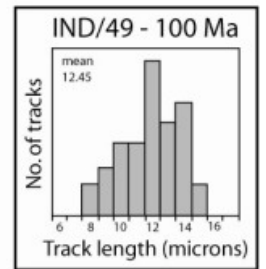
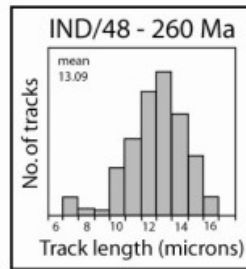
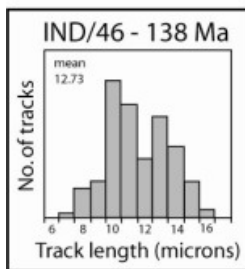
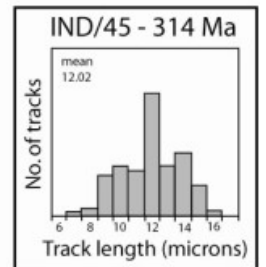
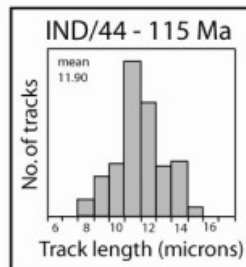
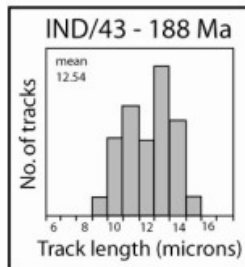
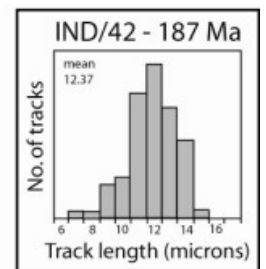
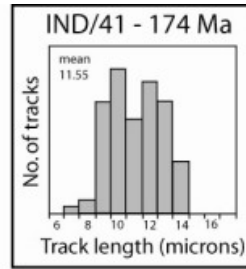
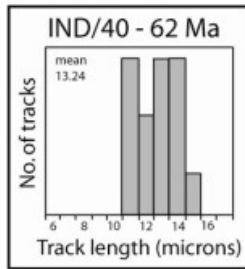


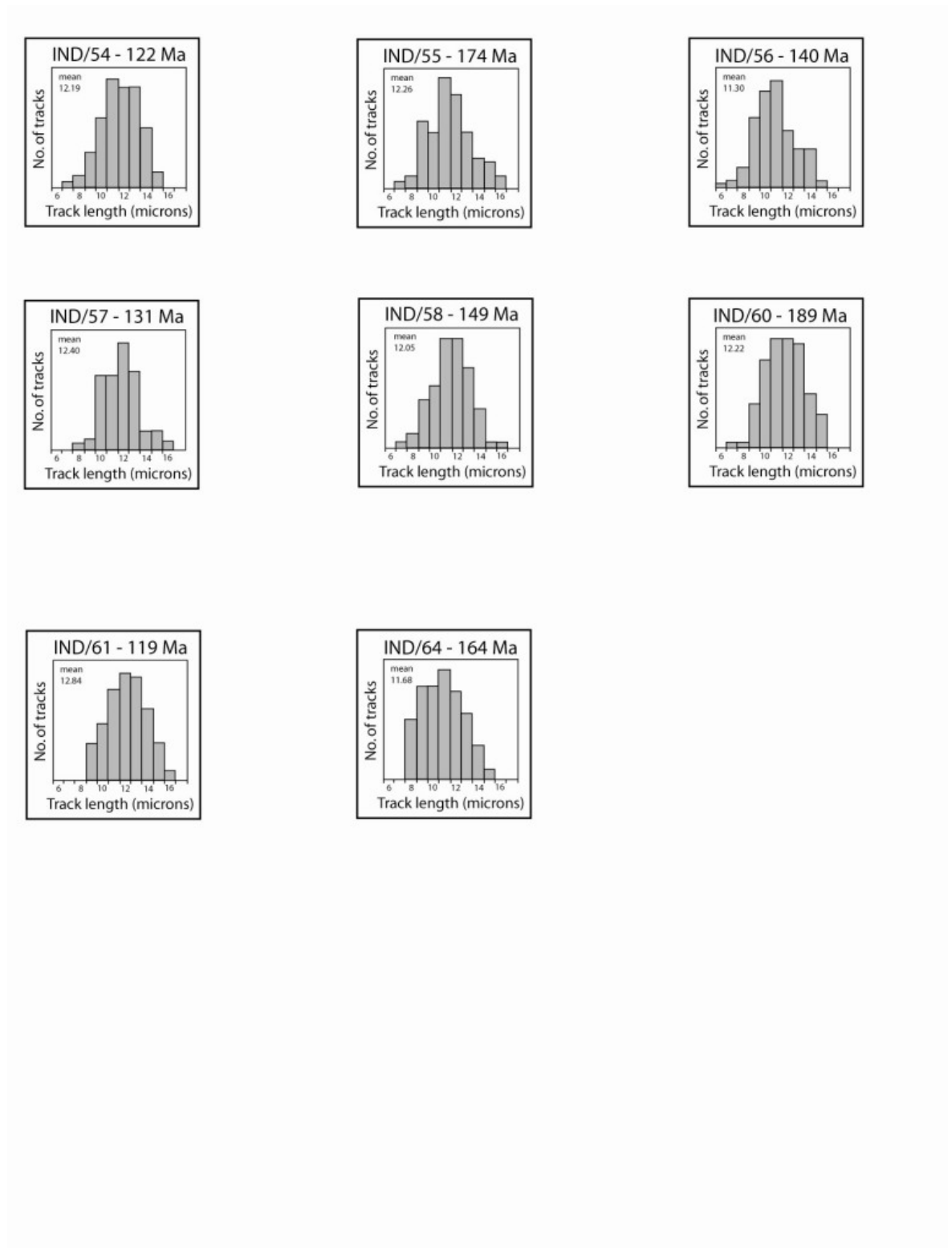
C.2 Western Indian TLD's

C.2.1 Goa and Karnataka



C.2.2 Kerala





References

Agrawal, P.K., and Pandey, O.P., 2004, Unusual lithospheric structure and evolutionary pattern of the cratonic segments of the South Indian shield: *Earth Planets And Space*, v. 56, p. 139-150.

Ahnert, F., 1970, Functional Relationships Between Denudation, Relief, And Uplift In Large Mid-Latitude Drainage Basins: *American Journal Of Science*, v. 268, p. 243-&.

Airy, G.B., 1855, On the computations of the effect of the attraction of mountain masses, as distributing the apparent astronomical latitudes of stations of geodetic surveys: *Philosophical Transactions of the Royal Society*, v. 145, p. 101-104.

Allegre, C.J., Birck, J.L., Capmas, F., and Courtillot, V., 1999, Age of the Deccan traps using Re-187-Os-187 systematics: *Earth And Planetary Science Letters*, v. 170, p. 197-204.

Allen, P.A., and Allen, J.R., 2005, *Basin Analysis*, Blackwell Science (UK), 445 p.

Anderson, D.L., 1994, The sublithospheric mantle as the source of continental flood basalts - The case against the continental lithosphere and plume head reservoirs: *Earth and Planetary Science Letters*, v. 123, p. 269-280.

Armstrong, P.A., 2005, Thermochronometers in sedimentary basins, *Low-Temperature Thermochronology: Techniques, Interpretations, And Applications, Volume 58: Reviews In Mineralogy & Geochemistry*, p. 499-525.

Arthur, T.J., MacGregor, D.S., and Cameron, N.R., 2003, *Petroleum geology of Africa - new themes and developing technologies: Geological Society Special Publication*, v. 207, p. 289.

Athy, L.F., 1930, Density, porosity and compaction of sedimentary rocks: *Bulletin American Association of Petroleum Geologists*, v. 14, p. 1-24.

Auden, J.B., 1949, Dykes in Western India - A discussion of their relationship with the Deccan Traps: *Transactions of the National Institute of Science, India*, v. 3, p. 123-159.

Audet, D.M., and McConnell, J.D.C., 1994, Establishing resolution limits for tectonic subsidence curves by forward basin modelling: *Marine and Petroleum Geology*, v. 11, p. 400-411.

Balakrishnan, T.S., 2001, Tectonics of Western India inferred from gravity patterns and geophysical exploration, *in* Gunnell, Y., and Radhakrishna, B.P., eds., *Sahyadri, the great escarpment of the Indian subcontinent. Patterns of landscape development in the Western Ghats*, Geological Society of India, Bangalore, p. 271-278.

Baldwin, B., and Butler, C.O., 1985, Compaction curves: *American Association of Petroleum Geologists Bulletin*, v. 69, p. 622-626.

- Balestrieri, M.L., Stuart, F.M., Persano, C., Abbate, E., and Bigazzi, G., 2005, Geomorphic development of the escarpment of the Eritrean margin, southern Red Sea from combined apatite fission-track and (U-Th)/He thermochronometry: *Earth And Planetary Science Letters*, v. 231, p. 97-110.
- Banks, R.J., Parker, R.L., and Huestis, S.P., 1977, Isostatic compensation on a continental scale - local versus regional mechanisms: *Geophysical Journal Of The Royal Astronomical Society*, v. 51, p. 431-452.
- Barbarand, J., Carter, A., Wood, I., and Hurford, T., 2003a, Compositional and structural control of fission-track annealing in apatite: *Chemical Geology*, v. 198, p. 107-137.
- Barbarand, J., Hurford, T., and Carter, A., 2003b, Variation in apatite fission-track length measurement: implications for thermal history modelling: *Chemical Geology*, v. 198, p. 77-106.
- Barbarand, J., and Pagel, M., 2001, Importance of the chemistry to characterise apatite fission-track annealing: *Comptes Rendus De L Academie Des Sciences Serie Ii Fascicule A-Sciences De La Terre Et Des Planetes*, v. 332, p. 259-265.
- Basu, D.N., Banerjee, A., and Tamhane, D.M., 1982, Facies distributions and petroleum geology of the Bombay offshore basin, India: *Indian Journal of Petroleum Geology*, v. 5, p. 51-75.
- Beane, J.E., Turner, C.A., Hooper, P.R., Subbarao, K.V., and Walsh, J.N., 1986, Stratigraphy, composition and form of the Deccan basalts, Western Ghats, India: *Bulletin of Volcanology*, v. 48, p. 61-83.
- Beaumont, C., Kooi, H., and Willet, S., 2000, Coupled tectonic-surface process models with applications to rifted continental margins and collisional orogens, *in* Summerfield, M.A., ed., *Geomorphology and Global Tectonics*, John Wiley & Son Ltd., Chichester, p. 28-55.
- Beckinsale, R.D., Drury, S.A., and Holt, R.W., 1980, 3,360-Myr old gneisses from the South Indian craton: *Nature*, v. 283, p. 469-470.
- Besse, J., and Courtillot, V., 1988, Paleogeographic maps of the continents bordering the Indian Ocean since the Early Jurassic: *Journal of Geophysical Research-Solid Earth and Planets*, v. 93, p. 11791-11808.
- Besse, J., and Courtillot, V., 1991, Revised and synthetic apparent polar wander paths of the African, Eurasian, North American and Indian plates, and true polar wander since 200 Ma: *Journal of Geophysical Research-Solid Earth and Planets*, v. 96, p. 4029-4050.
- Bikkar, A., Dunai, T.J., and Meesters, A.G.C.A., 2002, DECOMP. 1.1 FALW.
- Bishop, P., and Brown, R., 1992, Denudational Isostatic Rebound Of Intraplate Highlands - The Lachlan River Valley, Australia: *Earth Surface Processes And Landforms*, v. 17, p. 345-360.
- Braun, J., 2003, Pecube: a new finite-element code to solve the 3D heat transport equation including the effects of a time-varying, finite amplitude surface topography: *Computers & Geosciences*, v. 29, p. 787-794.
- Braun, J., 2005, Quantitative constraints on the rate of landform evolution derived from low-temperature thermochronology: *Reviews in Mineralogy and Geochemistry*, v. 351-374.

- Braun, J., and Beaumont, C., 1989, A Physical Explanation Of The Relation Between Flank Uplifts And The Breakup Unconformity At Rifted Continental Margins: *Geology*, v. 17, p. 760-764.
- Braun, J., and van der Beek, P., 2004, Evolution of passive margin escarpments: What can we learn from low-temperature thermochronology? *Journal Of Geophysical Research-Earth Surface*, v. 109.
- Braun, J., Van der Beek, P.A., and Batt, G., 2006, *Quantitative thermochronology*, Cambridge University Press, 258 p.
- Brown, R., Summerfield, M.A., and Gleadow, A.J.W., 1994, Apatite fission track analysis: its potential for the estimation of denudation rates and implications for models of long-term landscape evolution, *in* Kirkby, M.J., ed., *Process models and theoretical geomorphology*, John Wiley and Sons Ltd, p. 23-53.
- Brown, R.W., 1991, Backstacking apatite fission track "stratigraphy": A method for resolving the erosional and isostatic rebound components of tectonic uplift histories: *Geology*, v. 19, p. 74-77.
- Brown, R.W., Cockburn, H.A.P., Kohn, B.P., Belton, D., Fink, D., Gleadow, A.J.W., and Summerfield, M.A., 2002a, Combining low temperature apatite thermochronology and cosmogenic isotope analysis in quantitative landscape evolution studies: *Geochimica et Cosmochimica Acta*, v. 66, p. A106-A106.
- Brown, R.W., Rust, D.J., Summerfield, M.A., Gleadow, A.J.W., and de Wit, M.C.J., 1990, An early Cretaceous phase of accelerated erosion on the south-western margin of Africa: Evidence from apatite fission track analysis and the offshore sedimentary record: *Nuclear Tracks and Radiation Measurement*, v. 17, p. 339-350.
- Brown, R.W., Summerfield, M.A., and Gleadow, A.J.W., 2002b, Denudational history along a transect across the Drakensberg Escarpment of southern Africa derived from apatite fission track thermochronology: *Journal of Geophysical Research-Solid Earth*, v. 107.
- Burov, E., and Diament, M., 1996, Isostasy, equivalent elastic thickness, and inelastic rheology of continents and oceans: *Geology*, v. 24, p. 419-422.
- Burov, E.B., and Diament, M., 1995, The Effective Elastic Thickness (T-E) Of Continental Lithosphere - What Does It Really Mean: *Journal Of Geophysical Research-Solid Earth*, v. 100, p. 3905-3927.
- Cameron, N.R., Bate, R.H., and Clure, V.S., 1999, *The oil and gas habitats of the South Atlantic*: Special Publication Geological Society of London, v. 153.
- Campbell, I.H., and Griffiths, R.W., 1990, Implications of mantle plume structure for the evolution of flood basalts: *Earth And Planetary Science Letters*, v. 99, p. 79-93.
- Carlson, W.D., 1990, Mechanisms and kinetics of apatite fission-track annealing: *American Mineralogist*, v. 75, p. 1120-1139.
- Carlson, W.D., Donelick, R.A., and Ketcham, R.A., 1999, Variability of apatite fission-track annealing kinetics: I. Experimental results: *American Mineralogist*, v. 84, p. 1213-1223.
- Carter, T.J., Kohn, B.P., Foster, D.A., Gleadow, A.J.W., and Woodhead, J.D., 2006, Late-stage evolution of the Chemehuevi and Sacramento detachment faults from apatite (U-Th)/He

- thermochronometry - Evidence for mid-Miocene accelerated slip: Geological Society Of America Bulletin, v. 118, p. 689-709.
- Chadwick, B., Ramakrishnan, M., Vasudev, V.N., and Viswanatha, M.N., 1989, Facies distributions and structure of a Dharwar volcanosedimentary basin: evidence for Late Archean transpression in southern India? Journal of the Geological Society of London, v. 146, p. 825-834.
- Chadwick, B., Ramakrishnan, M., and Viswanatha, M.N., 1986, Stratigraphical and tectonic development of Late Archean, intracratonic volcanosedimentary basins (Dharwar Supergroup) in the Karnataka craton, Southern India: Journal of The Geological Society, v. 143, p. 967-968.
- Chand, S., Radhakrishna, M., and Subrahmanyam, C., 2001, India-East Antarctica conjugate margins: rift-shear tectonic setting inferred from gravity and bathymetry data: Earth and Planetary Science Letters, v. 185, p. 225.
- Chand, S., and Subrahmanyam, C., 2003, Rifting between India and Madagascar - mechanism and isostasy: Earth And Planetary Science Letters, v. 210, p. 317-332.
- Chandrasekharam, D., 1985, Structure and evolution of the western continental margin of India deduced from gravity, seismic, geomagnetic and geochronological studies: Physics of The Earth and Planetary Interiors, v. 41, p. 186-198.
- Chaubey, A.K., Bhattacharya, G.C., Murty, G.P.S., Srinivas, K., Ramprasad, T., and Rao, D.G., 1998, Early Tertiary seafloor spreading magnetic anomalies and paleo-propagators in the northern Arabian Sea: Earth and Planetary Science Letters, v. 154, p. 41-52.
- Chaubey, A.K., Rao, D.G., Srinivas, K., Ramprasad, T., Ramana, M.V., and Subrahmanyam, V., 2002, Analyses of multichannel seismic reflection, gravity and magnetic data along a regional profile across the central-western continental margin of India: Marine Geology, v. 182, p. 303-323.
- Clark, S.P., and Jäger, E., 1969, Denudation rate in Alps from geochronologic and heat flow data: American Journal of Science, v. 267, p. 1143-1160.
- Cockburn, H.A.P., Brown, R.W., Summerfield, M.A., and Seidl, M.A., 2000, Quantifying passive margin denudation and landscape development using a combined fission-track thermochronology and cosmogenic isotope analysis approach: Earth and Planetary Science Letters, v. 179, p. 429-435.
- Cooper, A.K., Davey, F.J., and Hinz, K., 1991, Crustal extension and origin of sedimentary basins beneath the Ross Sea and Ross Ice Shelf, Antarctica, *in* Thomson, M.R.A., Crame, J.A., and Thomson, J.W., eds., Geological evolution of Antarctica, Cambridge University Press, Cambridge, p. 285-291.
- Corrigan, J.D., 1993, Apatite fission-track analysis of oligocene strata in South Texas, Usa - testing annealing models: Chemical Geology, v. 104, p. 227-249.
- Courtillot, V., Besse, J., Vandamme, D., Montigny, R., Jaeger, J.J., and Cappetta, H., 1986, Deccan flood basalts at the Cretaceous Tertiary boundary: Earth and Planetary Science Letters, v. 80, p. 361-374.
- Courtillot, V., Jaupart, C., Manighetti, I., Tapponnier, P., and Besse, J., 1999, On causal links between flood basalts and continental breakup: Earth and Planetary Science Letters, v. 166, p. 177-195.

- Cox, K.G., 1980, A model for flood basalt vulcanism: *Journal of Petrology*, v. 21, p. 629-650.
- Cox, K.G., 1989, The role of mantle plumes in the development of continental drainage patterns: *Nature*, v. 342, p. 873-877.
- Cox, K.G., 1993, Continental magmatic underplating: *Philosophical Transactions of the Royal Society of London Series A - Mathematical Physical and Engineering Sciences*, v. 342, p. 155-166.
- Coyle, D.A., and Wagner, G.A., 1998, Positioning the titanite fission-track partial annealing zone: *Chemical Geology*, v. 149, p. 117-125.
- Crawford, A.R., 1969, Total rock Rb-Sr ages of over 3000-My in Southern India: *Transactions-American Geophysical Union*, v. 50, p. 331-&.
- Crowley, K.D., Cameron, M., and Schaefer, R.L., 1991, Experimental studies of annealing of etched fission tracks in fluorapatite: *Geochimica et Cosmochimica Acta*, v. 55, p. 1449-1465.
- Dahl, P.S., 1996, The effects of composition on retentivity of argon and oxygen in hornblende and related amphiboles: A field-tested empirical model: *Geochimica Et Cosmochimica Acta*, v. 60, p. 3687-3700.
- Damon, P.E., and Kulp, J.L., 1957, Determination of radiogenic helium in zircon by stable isotope dilution technique: *Transactions of the American Geophysical Union*, v. 38, p. 945-953.
- Das, A., Krishnaswami, S., Sarin, M.M., and Pande, K., 2005, Chemical weathering in the Krishna Basin and Western Ghats of the Deccan Traps, India: Rates of basalt weathering and their controls: *Geochimica et Cosmochimica Acta*, v. 69, p. 2067-2084.
- Davis, W.M., 1899, The geographical cycle: *Geographical Journal*, v. 14, p. 481-504.
- Dessai, A.G., and Bertrand, H., 1995, The Panvel-Flexure along the Western Indian continental margin - An extensional fault structure related to Deccan magmatism: *Tectonophysics*, v. 241, p. 165-178.
- Dessai, A.G., and Viegas, A.A.A.A., 1995, Multi generation mafic dyke swarms related to Deccan magmatism, south of Bombay: implications for the evolution of the Western Indian continental margin, *in* Devaraju, T.C., ed., *Dyke swarms of peninsular India*, Volume 33, *Memoirs of the Geological Society of India*, p. 435-451.
- Devey, C.W., and Lightfoot, P.C., 1986, Volcanological and tectonic control of stratigraphy and structure in the Western Deccan traps: *Bulletin of Volcanology*, v. 48, p. 195-207.
- Dobson, K.J., 2006, The zircon (U-Th)/He thermochronometry. Development and application of thermochronometers in igneous provinces: Glasgow, University of Glasgow.
- Dobson, K.J., Persano, C., and Stuart, F.M., in press, Quantitative constraints on mid- to shallow crustal processes using the zircon(U-Th)/He thermochronometer: *Journal of the Geological Society*, London. Special Publication.
- Dodson, M.H., 1973, Closure temperature in cooling geochronological and petrological systems: *Contributions to Mineralogy and Petrology*, v. 40, p. 259-274.

- Doin, M.P., Fleitout, L., and McKenzie, D., 1996, Geoid anomalies and the structure of continental and oceanic lithospheres: *Journal Of Geophysical Research-Solid Earth*, v. 101, p. 16119-16135.
- Donelick, R.A., 1991, Crystallographic orientation dependence of mean etchable fission-track length in apatite - an empirical-model and experimental-observations: *American Mineralogist*, v. 76, p. 83-91.
- Donelick, R.A., 1993, Apatite etching characteristics versus chemical composition: *Nuclear Tracks and Radiation Measurement*, v. 21, p. 604.
- Donelick, R.A., Farley, K., Asimow, P., and O'Sullivan, P., 2003, Pressure dependence of He diffusion and fission-track annealing kinetics in apatite? Experimental results: *Geochimica Et Cosmochimica Acta*, v. 67, p. A82-A82.
- Donelick, R.A., Ketcham, R.A., and Carlson, W.D., 1999, Variability of apatite fission-track annealing kinetics: II. Crystallographic orientation effects: *American Mineralogist*, v. 84, p. 1224-1234.
- Donelick, R.A., Ketcham, R.A., and Carlson, W.D., 2000, Variability of apatite fission-track annealing kinetics: II. Crystallographic orientation effects (vol 84, pg 1224, 1999): *American Mineralogist*, v. 85, p. 1565-1565.
- Donelick, R.A., O'Sullivan, P.B., and Ketcham, R.A., 2005, Apatite fission-track analysis, Low-Temperature Thermochronology: Techniques, Interpretations, And Applications, Volume 58: *Reviews In Mineralogy & Geochemistry*, p. 49-94.
- Donelick, R.A., Roden, M.K., Mooers, J.D., Carpenter, B.S., and Miller, D.S., 1990, Etchable length reduction of induced fission tracks in apatite at room-temperature (approximately 23-degrees-C) - crystallographic orientation effects and initial mean lengths: *Nuclear Tracks and Radiation Measurements*, v. 17, p. 261-265.
- Dunai, T.J., 2005, Forward modeling and interpretation of (U-Th)/He ages, Low-Temperature Thermochronology: Techniques, Interpretations, And Applications, Volume 58: *Reviews In Mineralogy & Geochemistry*, p. 259-274.
- Duncan, R.A., and Pyle, D.G., 1988, Rapid eruption of the Deccan flood basalts at the Cretaceous Tertiary boundary: *Nature*, v. 333, p. 841-843.
- Ehlers, T.A., 2005, Crustal thermal processes and the interpretation of thermochronometer data, Low-Temperature Thermochronology: Techniques, Interpretations, And Applications, Volume 58: *Reviews In Mineralogy & Geochemistry*, p. 315-350.
- Ehlers, T.A., and Farley, K.A., 2003, Apatite (U-Th)/He thermochronometry: methods and applications to problems in tectonic and surface processes: *Earth And Planetary Science Letters*, v. 206, p. 1-14.
- Einsele, G., and Hinderer, M., 1998, Quantifying denudation and sediment-accumulation systems (open and closed lakes): basic concepts and first results: *Palaeogeography Palaeoclimatology Palaeoecology*, v. 140, p. 7-21.
- Embleton, B.J.J., Veevers, J.J., Johnson, B.D., and Powell, C.M.A., 1980, Paleomagnetic comparison of a new fit of East and West Gondwanaland with the Smith and Hallam fit: *Tectonophysics*, v. 61, p. 381-390.

- England, P., and Molnar, P., 1990, Surface uplift, uplift of rocks, and exhumation of rocks: *Geology*, v. 18, p. 1173-1177.
- Falvey, D.A., and Deighton, I., 1982, Recent advances in burial and thermal geohistory analysis: *Journal of Australian Petroleum Exploration Association*, v. 22, p. 65-81.
- Farley, K.A., 2000, Helium diffusion from apatite: General behavior as illustrated by Durango fluorapatite: *Journal Of Geophysical Research-Solid Earth*, v. 105, p. 2903-2914.
- Farley, K.A., 2002, (U-Th)/He dating: Techniques, calibrations, and applications, *Noble Gases In Geochemistry And Cosmochemistry, Volume 47: Reviews In Mineralogy & Geochemistry*, p. 819-844.
- Farley, K.A., and Stockli, D.F., 2002, (U-Th)/He dating of phosphates: Apatite, monazite, and xenotime, *Phosphates: Geochemical, Geobiological, And Materials Importance, Volume 48: Reviews In Mineralogy & Geochemistry*, p. 559-577.
- Farley, K.A., Wolf, R.A., and Silver, L.T., 1996, The effects of long alpha-stopping distances on (U-Th)/He ages: *Geochimica Et Cosmochimica Acta*, v. 60, p. 4223-4229.
- Fischer, O., 1881, *Physics of the Earth's crust*, Macmillan and Co., London, 391 p.
- Fleischer, R.L., Price, P.B., and Walker, R.M., 1975, *Nuclear tracks in solids; Principles and applications*, University of California Press, Berkley, 627 p.
- Foeken, J.P.T., Stuart, F.M., Dobson, K.J., Persano, C., and Vilbert, D., 2006, A diode laser system for heating minerals for (U-Th)/He chronometry: *Geochemistry Geophysics Geosystems*, v. 7.
- Foote, R.B., 1876, *Geological features of the south Mahratta country and adjacent districts: Memoirs of the Geological Survey of India*, v. 12, p. 1-268.
- Gallagher, K., 1995, Evolving temperature histories from apatite fission-track data: *Earth and Planetary Science Letters*, v. 136, p. 421-435.
- Gallagher, K., and Brown, R., 1999, Denudation and uplift at passive margins: the record on the Atlantic Margin of southern Africa: *Philosophical Transactions Of The Royal Society Of London Series A-Mathematical Physical And Engineering Sciences*, v. 357, p. 835-857.
- Gallagher, K., Brown, R., and Johnson, C., 1998, Fission track analysis and its applications to geological problems: *Annual Review Of Earth And Planetary Sciences*, v. 26, p. 519-572.
- Gallagher, K., Hawkesworth, C.J., and Mantovani, M.S.M., 1994, The denudation history of the onshore continental margin of SE Brazil inferred from apatite fission track data: *Journal of Geophysical Research-Solid Earth*, v. 99, p. 18117-18145.
- Ghosh, B.N., and Zutshi, P.L., 1989, Indian west coast shelf break tectonic features: *Geological Survey of India Special Publication*, v. 24, p. 309-318.
- Gilchrist, A.R., Kooi, H., and Beaumont, C., 1994a, Post-Gondwana geomorphic evolution of Southwestern Africa - Implications for the controls on landscape development from observations and numerical experiments: *Journal of Geophysical Research-Solid Earth*, v. 99, p. 12211-12228.

- Gilchrist, A.R., and Summerfield, M.A., 1990, Differential denudation and flexural isostasy in formation of rifted margin upwarps: *Nature*, v. 346, p. 739-742.
- Gilchrist, A.R., and Summerfield, M.A., 1994, Tectonic models of passive margin evolution and their implications for theories of long-term landscape development, *in* Kirkby, M.J., ed., *Process Modles and Theoretical Geomorphology*, John Wiley & Son Ltd., Chichester, p. 55-84.
- Gilchrist, A.R., Summerfield, M.A., and Cockburn, H.A.P., 1994b, Landscape dissection, isostatic uplift, and the morphologic development of orogens: *Geology*, v. 22, p. 963-966.
- Gleadow, A.J.W., 1990, Fission track thermochronology - reconstructing the thermal and tectonic evolution of the crust: *Proceedings of the Pacific Rim '90 Congress*, p. 15-21.
- Gleadow, A.J.W., Belton, D.X., Kohn, B.P., and Brown, R.W., 2002, Fission track dating of phosphate minerals and the thermochronology of apatite, *Phosphates: Geochemical, Geobiological, And Materials Importance, Volume 48: Reviews In Mineralogy & Geochemistry*, p. 579-630.
- Gleadow, A.J.W., and Brown, R., 2000, Fission track thermochronology and teh long term dendautional response to tectonics, *in* Summerfield, M.A., ed., *Geomorphology and Global Tectonics*, John Wiley and Sons Ltd., p. 57-75.
- Gleadow, A.J.W., and Duddy, I.R., 1981, A Natural Long-Term Track Annealing Experiment For Apatite: *Nuclear Tracks And Radiation Measurements*, v. 5, p. 169-174.
- Gleadow, A.J.W., Duddy, I.R., Green, P.F., and Lovering, J.F., 1986, Confined fission-track lengths in apatite - a diagnostic-tool for thermal history analysis: *Contributions to Mineralogy and Petrology*, v. 94, p. 405-415.
- Gleadow, A.J.W., and Fitzgerald, P.G., 1987, Uplift history and structure of the Transantarctic Mountains - new evidence from fission-track dating of basement apatites in the dry valleys area, Southern Victoria Land: *Earth and Planetary Science Letters*, v. 82, p. 1-14.
- Gombos, A.M., Powell, W.G., and Norton, I.O., 1995, The tectonic evolution of Western India and its impact on hydrocarbon occurrences - An overview: *Sedimentary Geology*, v. 96, p. 119-129.
- Green, P.F., Crowhurst, P.V., Duddy, I.R., Japsen, T., and Holford, S.P., 2006, Conflicting (U-Th)/He and fission track ages in apatite: Enhanced He retention, not anomalous annealing behaviour: *Earth And Planetary Science Letters*, v. 250, p. 407-427.
- Green, P.F., and Duddy, I.R., 2006, Interpretation of apatite (U-Th)/He ages and fission track ages from cratons: *Earth And Planetary Science Letters*, v. 244, p. 541-547.
- Green, P.F., Duddy, I.R., Gleadow, A.J.W., Tingate, P.R., and Laslett, G.M., 1986, Thermal annealing of fission tracks in apatite. I. a qualitative description: *Chemical Geology*, v. 59, p. 237-253.
- Green, P.F., Duddy, I.R., and Hegarty, K.A., 2005, Comment on "Compositional and structural control of fission track annealing in apatite" by J. Barbarand, A. Carter, I. Wood and A.J. Hurford, *Chemical Geology*, 198 (2003) 107-137: *Chemical Geology*, v. 214, p. 351-358.
- Green, P.F., Duddy, I.R., Laslett, G.M., Hegarty, K.A., Gleadow, A.J.W., and Lovering, J.F., 1989, Thermal annealing of fission tracks in apatite.4. quantitative modeling techniques and extension to geological timescales: *Chemical Geology*, v. 79, p. 155-182.

- Grove, M., and Harrison, T.M., 1996, Ar-40(*) diffusion in Fe-rich biotite: *American Mineralogist*, v. 81, p. 940-951.
- Guedes, S., Hadler, N.J.C., Sarkis, J.E.S., Oliveira, K.M.G., Kakazu, M.H., Iunes, P.J., Saiki, M., Tello, S.C.A., and Paulo, S.R., 2003, Spontaneous-fission decay constant of ^{238}U measured by nuclear track techniques without neutron irradiation: *Journal of Radioanalytical and Nuclear Chemistry*, v. 258, p. 117-122.
- Gunn, R., 1943, A quantitative evaluation of the influence of the lithosphere on the anomalies of gravity: *J. Franklin Institute*, v. 236, p. 373-390.
- Gunnell, Y., 1998, The interaction between geological structure and global tectonics in multistoreyed landscape development: a denudation chronology of the South Indian shield: *Basin Research*, v. 10, p. 281-310.
- Gunnell, Y., 2001, Fluvial routing systems and the signatures of onshore denudation in the offshore sedimentary record of Western India: *Geological Society Of India*, v. 47, p. 279-293.
- Gunnell, Y., and Fleitout, L., 1998, Shoulder uplift of the Western Ghats passive margin, India: A denudational model: *Earth Surface Processes and Landforms*, v. 23, p. 391-404.
- Gunnell, Y., and Fleitout, L., 2000, Morphotectonic evolution of the Western Ghats, India, *in* Summerfield, M.A., ed., *Geomorphology and Global Tectonics*, John Wiley & Sons Ltd., Chichester, p. 321-338.
- Gunnell, Y., Gallagher, K., Carter, A., Widdowson, M., and Hurford, A.J., 2003, Denudation history of the continental margin of western peninsular India since the early Mesozoic - Reconciling apatite fission-track data with geomorphology: *Earth and Planetary Science Letters*, v. 215, p. 187-201.
- Gunnell, Y., and Radhakrishna, B.P., 2001, Sahyadri, the great escarpment of the Indian subcontinent. Patterns of landscape development in the Western Ghats, *Geological Society of India, Bangalore*, 717 p.
- Hames, W.E., and Bowring, S.A., 1994, An Empirical-Evaluation Of The Argon Diffusion Geometry In Muscovite: *Earth And Planetary Science Letters*, v. 124, p. 161-167.
- Hansen, E.C., Stern, R.J., Devaraju, T.C., Mahabaleswar, B., and Kenny, P.J., 1997, Rubidium-strontium whole-rock ages of banded and incipient charnockites from southern Karnataka: *Journal Of The Geological Society Of India*, v. 50, p. 267-275.
- Haq, B.U., Hardenbol, J., and Vail, P.R., 1987, Chronology Of Fluctuating Sea Levels Since The Triassic: *Science*, v. 235, p. 1156-1167.
- Harris, N., 1995, Significance of weathering Himalayan metasedimentary rocks and leukogranites for the Sr isotope evolution of seawater during the Early Miocene: *Geology*, v. 23, p. 795-798.
- Harrison, T.M., 1981, Diffusion Of Ar-40 In Hornblende: *Contributions To Mineralogy And Petrology*, v. 78, p. 324-331.
- Harrison, T.M., Duncan, I., and McDougall, I., 1985, Diffusion Of Ar-40 In Biotite - Temperature, Pressure And Compositional Effects: *Geochimica Et Cosmochimica Acta*, v. 49, p. 2461-2468.

- Harrison, T.M., and Zeitler, P.K., 2005, Fundamentals of noble gas thermochronometry, *Low-Temperature Thermochronology: Techniques, Interpretations, And Applications*, Volume 58: *Reviews In Mineralogy & Geochemistry*, p. 123-149.
- Hay, W.W., Shaw, C.A., and Wold, C.N., 1989, Mass-balanced paleogeographic reconstructions: *Geologische Rundschau*, v. 78/1, p. 207-242.
- Hayford, J.H., 1909, *The figure of the Earth and isostasy from measurements in the United States*: Washington D.C., Coast and Geodetic Service, Government Printing Office, v. 132.
- Hedberg, H.D., 1936, Gravitational compaction of clays and shales: *American Journal of Science*, v. 31, p. 241-287.
- Heiskanen, W.A., 1931, Isostatic tables for the reduction of gravimetric observations calculated on the basis of Airy's hypothesis: *Bullitin Géodéseque*, v. 30, p. 110-129.
- Hendriks, B.W.H., and Redfield, T.F., 2005, Apatite fission track and (U-Th)/He data from Fennoscandia: An example of underestimation of fission track annealing in apatite: *Earth And Planetary Science Letters*, v. 236, p. 443-458.
- Hetenyi, M., 1979, *Beams on elastic foundations*, The University of Michigan Press, 264 p.
- Hooper, P.R., 1990, The timing of crustal extension and the eruption of continental flood basalts: *Nature*, v. 345, p. 246-249.
- House, M.A., Wernicke, B.P., and Farley, K.A., 1998, Dating topography of the Sierra Nevada, California, using apatite (U-Th)/He ages: *Nature*, v. 396, p. 66-69.
- House, M.A., Wernicke, B.P., and Farley, K.A., 2001, Paleo-geomorphology of the Sierra Nevada, California, from (U-Th)/He ages in apatite: *American Journal Of Science*, v. 301, p. 77-102.
- Hubbard, R.J., 1988, Age and significance of sequence boundaries on Jurassic and Early Cretaceous rifted continental margins: *Aapg Bulletin-American Association of Petroleum Geologists*, v. 72, p. 49-72.
- Hurford, A.J., 1990, International-union-of-geological-sciences subcommission on geochronology recommendation for the standardization of fission-track dating calibration and data reporting: *Nuclear Tracks and Radiation Measurements*, v. 17, p. 233-236.
- Hurford, A.J., 1991, Uplift and cooling pathways derived from fission-track analysis and mica dating - a review: *Geologische Rundschau*, v. 80, p. 349-368.
- Hurford, A.J., and Green, P.F., 1982, A users guide to fission-track dating calibration: *Earth and Planetary Science Letters*, v. 59, p. 343-354.
- Hurford, A.J., and Green, P.F., 1983, The zeta-age calibration of fission-track dating: *Isotope Geoscience*, v. 1, p. 285-317.
- Hurley, P.M., 1954, The helium age method and the distribution and migration of helium in rocks, *in* Faul, H., ed., *Nuclear Geology*, Wiley and Sons, p. 301-329.
- Jarvis, G.T., and McKenzie, D.P., 1980, Sedimentary basin formation with finite extension rates: *Earth And Planetary Science Letters*, v. 48, p. 42-52.

- Joseph, S., and Nambiar, C.G., 1996, Alkaline nature and taphrogenetic affinity of felsic volcanic rocks of St Mary Islands, off Mangalore coast: *Current Science*, v. 70, p. 858-860.
- Kailasam, L.N., 1979, Plateau uplift in peninsular India: *Tectonophysics*, v. 61, p. 243-&.
- Kalaszad, S., Roden, M.K., Miller, D.S., and Morisawa, M., 1993, Evolution Of The Continental-Margin Of Western India - New Evidence From Apatite Fission-Track Dating: *Journal Of Geology*, v. 101, p. 667-673.
- Katz, M.B., and Premoli, C., 1979, India and Madagascar in Gondwanaland based on matching Precambrian lineaments: *Nature*, v. 279, p. 312-315.
- Kearey, P., and Vine, F.J., 1996, *Global tectonics*, Blackwell Science, Oxford, 333 p.
- Kent, R.W., Storey, M., and Saunders, A.D., 1992, Large igneous provinces - Sites of plume impact or plume incubation: *Geology*, v. 20, p. 891-894.
- Ketcham, R.A., 2005, Forward and inverse modeling of low-temperature thermochronometry data, *Low-Temperature Thermochronology: Techniques, Interpretations, And Applications, Volume 58: Reviews In Mineralogy & Geochemistry*, p. 275-314.
- Ketcham, R.A., Donelick, R.A., and Carlson, W.D., 1999, Variability of apatite fission-track annealing kinetics: III. Extrapolation to geological time scales: *American Mineralogist*, v. 84, p. 1235-1255.
- Ketcham, R.A., Donelick, R.A., and Donelick, M.B., 2003, AFTSolve: A program for multi-kinetic modeling of apatite fission-track data: *American Mineralogist*, v. 88, p. 929-929.
- King, L.C., 1950, The study of the World's plainlands: A new approach to geomorphology: *Quarterly Journal of the Royal Society of London*, v. 106, p. 101-127.
- King, L.C., 1955, Pediplanation and isostasy: an example from South Africa: *Quarterly Journal of the Geological Society of London*, v. 111, p. 353-359.
- King, L.C., 1967a, *The morphology of the Earth* (2nd edn.), Olliver & Boyd, Edinburgh, 699 p.
- King, L.C., 1967b, *The morphology of the Earth* (2nd edn.), Olliver & Boyd, Edinburgh.
- King, S.D., and Anderson, D.L., 1995, An alternative mechanism of flood basalt formation: *Earth and Planetary Science Letters*, v. 136, p. 269-279.
- Kohn, B.P., Belton, D.X., Brown, R.W., Gleadow, A.J.W., Green, P.F., and Lovering, J.F., 2003, Comment on: "Experimental evidence for the pressure dependence of fission track annealing in apatite" by A.S. Wendt et al. [*Earth Planet. Sci. Lett.* 201 (2002) 593-607]: *Earth And Planetary Science Letters*, v. 215, p. 299-306.
- Kohn, B.P., Gleadow, A.J.W., Brown, R.W., Gallagher, K., Lorencak, M., and Noble, W.P., 2005, Visualizing thermotectonic and denudation histories using apatite fission track thermochronology, *Low-Temperature Thermochronology: Techniques, Interpretations, And Applications, Volume 58: Reviews In Mineralogy & Geochemistry*, p. 527-565.

- Kohn, B.P., Gleadow, A.J.W., Raza, A., Kohlmann, F., and Brown, R.W., 2006, Re-evaluating low temperature apatite thermochronology in slowly cooled terranes: *Geochimica Et Cosmochimica Acta*, v. 70, p. A328-A328.
- Kolla, V., and Coumes, F., 1990, Extension of structural and tectonic trends from the Indian subcontinent into the Eastern Arabian Sea: *Marine and Petroleum Geology*, v. 7, p. 188-196.
- Kooi, H., and Beaumont, C., 1994, Escarpment evolution on high elevation rifted margins - Insights derived from a surface processes model that combines diffusion, advection, and reaction: *Journal of Geophysical Research-Solid Earth*, v. 99, p. 12191-12209.
- Laslett, G.M., Gleadow, A.J.W., and Duddy, I.R., 1984, The relationship between fission-track length and track density in apatite: *Nuclear Tracks And Radiation Measurements*, v. 9, p. 29-38.
- Laslett, G.M., Green, P.F., Duddy, I.R., and Gleadow, A.J.W., 1987, Thermal annealing of fission tracks in apatite.2. A quantitative-analysis: *Chemical Geology*, v. 65, p. 1-13.
- Lawrence, D.T., Doyle, M., and Aigner, T., 1990, Stratigraphic simulation of sedimentary basins - Concepts and calibration: *Aapg Bulletin-American Association of Petroleum Geologists*, v. 74, p. 273-295.
- Lorencak, M., 2003, Low temperature thermochronology of the Canadian and Fennoscandian Shields, University of Melbourne.
- Lovera, O.M., Grove, M., Harrison, T.M., and Mahon, K.I., 1997, Systematic analysis of K-feldspar Ar-40/Ar-39 step heating results.1. Significance of activation energy determinations: *Geochimica Et Cosmochimica Acta*, v. 61, p. 3171-3192.
- Manglik, A., 2006, Mantle heat flow and thermal structure of the northern block of Southern Granulite Terrain, India: *Journal Of Geodynamics*, v. 41, p. 510-519.
- Mathur, R.B., and Nair, K.R., 1993, Exploration of the Bombay offshore basin: Processes of the Second Seminar on Petroleum Basins of India. KDMIPE and ONGC, v. 2, p. 365-396.
- McKenzie, D., 1978, Some remarks on development of sedimentary basins: *Earth and Planetary Science Letters*, v. 40, p. 25-32.
- McKenzie, D., and Sclater, J.G., 1971, Evolution of Indian Ocean since Late Cretaceous: *Geophysical Journal of the Royal Astronomical Society*, v. 24, p. 437-&.
- Meesters, A., and Dunai, T.J., 2002a, Solving the production-diffusion equation for finite diffusion domains of various shapes - Part II. Application to cases with alpha-ejection and nonhomogeneous distribution of the source: *Chemical Geology*, v. 186, p. 57-73.
- Meesters, A., and Dunai, T.J., 2002b, Solving the production-diffusion equation for finite diffusion domains of various shapes Part 1. Implications for low-temperature (U-Th)/He thermochronology: *Chemical Geology*, v. 186, p. 333-344.
- Metivier, F., Gaudemer, Y., Tapponnier, P., and Klein, M., 1999, Mass accumulation rates in Asia during the Cenozoic: *Geophysical Journal International*, v. 137, p. 280-318.

- Miles, P.R., and Roest, W.R., 1993, Earliest sea floor spreading magnetic anomalies in the North Arabian Sea and the ocean-continent transition: *Geophysical Journal International*, v. 115, p. 1025-1031.
- Millot, R., Gaillardet, J., Dupre, B., and Allegre, C.J., 2002, The global control of silicate weathering rates and the coupling with physical erosion: new insights from rivers of the Canadian Shield: *Earth And Planetary Science Letters*, v. 196, p. 83-98.
- Mitchell, C., and Widdowson, M., 1991, A geological map of the southern Deccan Traps, India and its structural implications: *Journal of the Geological Society of London*, v. 148, p. 495-505.
- Mohriak, W.U., Karner, G.D., Dewey, J.F., and Maxwell, J.R., 1988, Structural and stratigraphic evolution of the Campos Basin, offshore Brazil, *in* Tankard, A.J., and Balkwill, H.R., eds., *Extensional tectonics and stratigraphy of the North Atlantic Margin*, Volume 46, American Association of Petroleum Geology Memoirs, p. 577-598.
- Molnar, P., 2004, Late Cenozoic increase in accumulation rates of terrestrial sediment: How might climate change have affected erosion rates? *Annual Review of Earth and Planetary Sciences.*, v. 32, p. 67-89.
- Molnar, P., and England, P., 1990, Late Cenozoic uplift of mountain-ranges and global climate change - Chicken or egg: *Nature*, v. 346, p. 29-34.
- Moore, M.E., Gleadow, A.J.W., and Lovering, J.F., 1986, Thermal evolution of rifted continental margins: new evidence from fission track dating of apatites from southeastern Australia: *Earth And Planetary Science Letters*, v. 78, p. 255-270.
- Morgan, W.J., 1981, Hot spot tracks and the opening of the Atlantic and Indian Ocean, *in* Emilani, C., ed., *The Sea*, John Wiley & Son Ltd., New York, p. 443-487.
- Muller, R.D., Royer, J.Y., and Lawver, L.A., 1993, Revised plate motions relative to the hotspots from combined Atlantic and Indian-Ocean hotspot tracks: *Geology*, v. 21, p. 275-278.
- Murrel, G.R., 2003, The long-term thermal evolution of central Fennoscandia, revealed by low temperature thermochronometry, Vrije Universiteit Amsterdam.
- Musset, A.E., 1960, Diffusion measurements and the potassium-argon method of dating: *Geophysical Journal of the Royal Astronomical Society*, v. 18, p. 253-303.
- Naeser, C.W., and Faul, H., 1967, Fission track annealing in apatite and sphene: *Journal of Geophysical Research*, v. 74, p. 705-710.
- Naeser, C.W., and Forbes, R.B., 1976, Variation Of Fission-Track Ages With Depth In 2 Deep Drill Holes: *Transactions-American Geophysical Union*, v. 57, p. 353-353.
- Naini, B.R., and Talwani, M., 1982, Structural framework and the evolutionary history of the continental margin of western India, *in* Watkins, J.S., and Drake, C.L., eds., *Studies in continental margin geology*, Volume 34, Am. Assoc. Pet. Geol. Mem., p. 167-191.
- Naqvi, S.M., and Rogers, J.J.W., 1987, Precambrian geology of India. *Oxford Monographs on Geology and Geophysics*, Oxford Monographs on Geology and Geophysics, Volume No. 6, Oxford University Press, Oxford.

- Norton, I.O., and Sclater, J.G., 1979, Model For The Evolution Of The Indian-Ocean And The Breakup Of Gondwanaland: *Journal Of Geophysical Research*, v. 84, p. 6803-6830.
- O'Sullivan, P.B., and Parrish, R.R., 1995, The importance of apatite composition and single-grain ages when interpreting fission-track data from plutonic rocks - a case-study from the Coast Ranges, British-Columbia: *Earth And Planetary Science Letters*, v. 132, p. 213-224.
- Ohmori, H., 1983, Erosion rates and their relationship to vegetation from the viewpoint of world-wide distribution: *Bulletin of the Department of Geography University of Tokyo*, v. 15, p. 77-91.
- Oldham, R.D., 1893, *A manual on the geology of India* (2nd edn.).
- Ollier, C.D., 1982, Geomorphology and tectonics of the Dorrigo Plateau, NSW: *Journal of the Geological Society of Australia*, v. 29, p. 431-435.
- Ollier, C.D., 1985, Morphotectonics of passive continental margins: introduction.: *Zeitschrift Fur Geomorphologie Supplement-band*, v. 54, p. 1-9.
- Ollier, C.D., and Pain, C.F., 1997, Equating the basal unconformity with the palaeoplain: A model for passive margins: *Geomorphology*, v. 19, p. 1-15.
- Ollier, C.D., and Power, K.B., 1985, The Western Ghats and morphotectonics of Peninsular India: *Zeitschrift Fur Geomorphologie Supplement-band*, v. 54, p. 37-56.
- Omar, G.I., and Steckler, M.S., 1995, Fission-Track Evidence On The Initial Rifting Of The Red-Sea - 2 Pulses, No Propagation: *Science*, v. 270, p. 1341-1344.
- Pande, K., 2002, Age and duration of the Deccan Traps, India: A review of radiometric and paleomagnetic constraints: *Proceedings Of The Indian Academy Of Sciences-Earth And Planetary Sciences*, v. 111, p. 115-123.
- Pande, K., Sheth, H.C., and Bhutani, R., 2001, Ar-40-Ar-39 age of the St. Mary's Islands volcanics, southern India: record of India-Madagascar break-up on the Indian subcontinent: *Earth and Planetary Science Letters*, v. 193, p. 39-46.
- Pandey, O.P., and Agrawal, P.K., 2000, Thermal regime, hydrocarbon maturation and geodynamic events along the western margin of India since late Cretaceous: *Journal Of Geodynamics*, v. 30, p. 439-459.
- Parida, G., and Mishra, Y.K., 1992, A late Palaeocene-Eocene fan-delta in Bombay offshore basin: *Bullitin ONGC*, v. 29, p. 105-120.
- Pascoe, E.H., 1964, *A manual of the geology of India and Burma*, Government of India Press, Calcutta.
- Pazzaglia, F.J., and Brandon, M.T., 1996, Macrogeomorphic evolution of the post-Triassic Appalachian mountains determined by deconvolution of the offshore basin sedimentary record: *Basin Research*, v. 8, p. 255-278.
- Pazzaglia, F.J., and Gardner, T.W., 1994, Late Cenozoic flexural deformation of the middle U.S. Atlantic passive margin: *Journal of Geophysical Research*, v. 99, p. 12143-12157.
- Penck, W., 1953, *Morphological analysis of landforms*, MacMillan, London, 429 p.

- Persano, C., Stuart, F.M., and Bishop, P., 2002, Low-T thermochronology constraints on the development of the Australian Great Escarpment: *Geochimica et Cosmochimica Acta*, v. 66, p. A593-A593.
- Persano, C., Stuart, F.M., Bishop, P., and Dempster, T.J., 2005, Deciphering continental breakup in eastern Australia using low-temperature thermochronometers: *Journal of Geophysical Research-Solid Earth*, v. 110.
- Plummer, P.S., and Belle, E.R., 1995, Mesozoic tectonostratigraphic evolution of The Seychelles microcontinent: *Sedimentary Geology*, v. 96, p. 73-91.
- Powell, C.M., Johnson, B.D., and Veevers, J.J., 1980, A revised fit of East and West Gondwanaland: *Tectonophysics*, v. 63, p. 13-29.
- Prasad, M.B.K., and Ramanatran, A.L., 2005, Solute sources and processes in the Achankovil River basin, Western Ghats, southern India: *Hydrological Sciences Journal-Journal Des Sciences Hydrologiques*, v. 50, p. 341-354.
- Pratt, J.H., 1859, On the deflection of the plumb-line in India, caused by the attraction of the Himalaya mountains and the elevated regions beyond; and its modification by the compensation effect of a deficiency of matter below the mountain mass: *Philosophical Transactions of the Royal Society*, v. 149, p. 745-796.
- Prell, W.L., and Kutzbach, J.E., 1992, Sensitivity of the Indian monsoon to forcing parameters and implications for its evolution: *Nature*, v. 360, p. 647-652.
- Price, P.B., and Walker, R.M., 1963, Fossil Tracks Of Charged Particles In Mica And Age Of Minerals: *Journal Of Geophysical Research*, v. 68, p. 4847-&.
- Purdy, J.W., and Jäger, E., 1976, K-Ar on rock-forming minerals from the Central Alps: *Memoirs of the Institute of Geology and Mineralogy University of Padova*, v. 30, p. 31.
- Quade, J., Cerling, T.E., and Bowman, J.R., 1989, Development of Asian monsoon revealed by marked ecological shift during the latest Miocene in Northern Pakistan: *Nature*, v. 342, p. 163-166.
- Radhakrishna, B.P., 1952, Mysore Plateau, its structural and physiographic evolution: *Bulletin of the Mysore Geological Association*, v. 3, p. 1-56.
- Radhakrishna, B.P., 1967, The Western Ghats of the Indian Peninsula: *Proc. seminars on geomorphological studies in India*, Nov, 1965, p. 5-13.
- Radhakrishna, B.P., 1993, Neogene uplift and geomorphic rejuvenation of the Indian peninsula: *Current Science*, v. 64, p. 787-792.
- Radhakrishna, M., Kurian, P.J., Nambiar, C.G., and Murty, B.V.S., 2003, Nature of the crust below the Southern Granulite Terrain (SGT) of Peninsular India across the Bavali shear zone based on analysis of gravity data: *Precambrian Research*, v. 124, p. 21-40.
- Radhakrishna, T., Dallmeyer, R.D., and Joseph, M., 1994, Paleomagnetism and Ar-36/Ar-40 vs Ar-39/Ar-40 isotope correlation ages of dyke swarms in central Kerala, India - tectonic implications: *Earth And Planetary Science Letters*, v. 121, p. 213-226.

- Rajesh, R.S., and Mishra, D.C., 2004, Lithospheric thickness and mechanical strength of the Indian shield: *Earth And Planetary Science Letters*, v. 225, p. 319-328.
- Raju, D.S.N., Bhandari, A., and Ramesh, P., 1999, Relative sea level fluctuations during Cretaceous and Cenozoic in India: *Bulletin ONGC*, v. 36, p. 185-202.
- Rao, P.R., and Srivastava, D.C., 1984, Regional seismic facies analysis of western offshore India.: *Bulletin of ONGC*, v. 21, p. 83-96.
- Rao, S.V., Dasgupta, D.K., Bhushan, K.S., Srinivas, M.S., and Ghosh, D.R., 2002, Sedimentary processes and structural framework of Konkan Basin – Western offshore, India: *Geological Survey of India Special Publication*, v. 76, p. 43-52.
- Rao, V.P., and Rao, B.R., 1995, Provenance and distribution of clay minerals in the sediments of the western continental shelf and slope of India: *Continental Shelf Research*, v. 15, p. 1757-1771.
- Rao, Y.H., Subrahmanyam, C., Sharma, S.R., Rastogi, A.A., and Deka, B., 2001, Estimates of geothermal gradients and heat flow from BSRs along the Western Continental Margin of india: *Geophysical Research Letters*, v. 28, p. 355-358.
- Ravenhurst, C.E., Roden-Tice, M.K., and Miller, D.S., 2003, Thermal annealing of fission tracks in fluorapatite, chlorapatite, manganoapatite, and Durango apatite: experimental results: *Canadian Journal Of Earth Sciences*, v. 40, p. 995-1007.
- Reeves, C., and de Wit, M., 2000, Making ends meet in Gondwana: retracing the transforms of the Indian Ocean and reconnecting continental shear zones: *Terra Nova*, v. 12, p. 272-280.
- Reiners, P.W., 2005, Zircon (U-Th)/He thermochronometry, *Low-Temperature Thermochronology: Techniques, Interpretations, And Applications, Volume 58: Reviews In Mineralogy & Geochemistry*, p. 151-179.
- Reiners, P.W., and Farley, K.A., 1999, Helium diffusion and (U-Th)/He thermochronometry of titanite: *Geochimica Et Cosmochimica Acta*, v. 63, p. 3845-3859.
- Reiners, P.W., and Farley, K.A., 2001, Influence of crystal size on apatite (U-Th)/He thermochronology: an example from the Bighorn Mountains, Wyoming: *Earth and Planetary Science Letters*, v. 188, p. 413-420.
- Reiners, P.W., Farley, K.A., and Hickes, H.J., 2002, He diffusion and (U-Th)/He thermochronometry of zircon: initial results from Fish Canyon Tuff and Gold Butte: *Tectonophysics*, v. 349, p. 297-308.
- Reiners, P.W., Spell, T.L., Nicolescu, S., and Zanetti, K.A., 2004, Zircon (U-Th)/He thermochronometry: He diffusion and comparisons with Ar-40/Ar-39 dating: *Geochimica Et Cosmochimica Acta*, v. 68, p. 1857-1887.
- Richards, M.A., Duncan, A.R., and Courtillot, V.E., 1989, Flood basalts and hot-spot tracks: plume heads and tails: *Science*, v. 246, p. 103-107.
- Rowley, D.B., and Sahagain, D., 1988, Depth-dependant stretching: a different approach: *Geology*, v. 14, p. 32-35.

Roy, S., and Rao, R.U.M., 2000, Heat flow in the Indian shield: *Journal Of Geophysical Research-Solid Earth*, v. 105, p. 25587-25604.

Roy, S., and Rao, R.U.M., 2003, Towards a crustal thermal model for the Archaean Dharwar craton, southern India: *Physics And Chemistry Of The Earth*, v. 28, p. 361-373.

Rust, D.J., and Summerfield, M.A., 1990, Isopach and borehole data as indicators of rifted margin evolution in southwestern Africa: *Marine and Petroleum Geology*, v. 7, p. 277-287.

Rutherford, E., 1904, *Radioactivity*, Cambridge University Press, 287 p.

Rutherford, E., 1906, *Radioactive transformations*, Charles Scribner's Sons, New York, 287 p.

Santosh, M., Collins, A.S., Tamashiro, I., Koshimoto, S., Tsutsumi, Y., and Yokoyama, K., 2006, The timing of ultrahigh-temperature metamorphism in Southern India: U-Th-Pb electron microprobe ages from zircon and monazite in sapphirine-bearing granulites: *Gondwana Research*, v. 10, p. 128-155.

Schlich, R., 1982, The Indian-Ocean - Aseismic ridges, spreading centers, and oceanic basins: *Ocean Basins and Margins*, v. 6, p. 51-147.

Scotese, C.R., Gahagan, L.M., and Larson, R.L., 1988, Plate tectonic reconstructions of the Cretaceous and Cenozoic ocean basins: *Tectonophysics*, v. 155, p. 27-48.

Seranne, M., and Anka, Z., 2005, South Atlantic continental margins of Africa: A comparison of the tectonic vs climate interplay on the evolution of equatorial west Africa and SW Africa margins: *Journal of African Earth Sciences*, v. 43, p. 283-300.

Shankar, U., Thakur, N.K., and Reddi, S.I., 2004, Estimation of geothermal gradients and heat flow from bottom simulating reflector along the Kerala-Konkan basin of western continental margin of India: *Current Science*, v. 87, p. 250-253.

Sheth, H.C., 1998, A reappraisal of the coastal Panvel flexure, Deccan Traps, as a listric-fault-controlled reverse drag structure: *Tectonophysics*, v. 294, p. 143-149.

Sheth, H.C., 2005, From Deccan to Reunion: no trace of a mantle plume, *in* Foulger, G.R., ed., *Plates, plumes and paradigms*, Volume 388, *Geol. Soc. Am. Spec. Pap.*, p. 477-501.

Shuster, D.L., Flowers, R.M., and Farley, K.A., 2006, The influence of natural radiation damage on helium diffusion kinetics in apatite: *Earth And Planetary Science Letters*, v. 249, p. 148-161.

Singh, N.K., and Lal, N.K., 1993, Geology and petroleum prospects of Konkan-Kerala basin, *in* Biswas, S.K., ed., *Proc. Second Seminar on petroliferous basins of India*, Volume 2, Indian petroleum Publishers, Dehra Dun, India, p. 461-469.

Singh, R.P., Rawat, S., and Chandra, K., 1999, Hydrocarbon potential in Indian deep waters: *Exploration Geophysics*, v. 30, p. 83-95.

Sleep, N.H., 1971, Thermal effects of formation of Atlantic continental margins by continental break up: *Geophysical Journal Of The Royal Astronomical Society*, v. 24, p. 325-&.

Sleep, N.H., and Snell, N.S., 1976, Thermal contraction and flexure of mid-continent and Atlantic marginal basins: *Geophysical Journal Of The Royal Astronomical Society*, v. 45, p. 125-154.

- Soman, K., 1997, *Geology of Kerala*, Geological Society of India, Bangalore, 335 p.
- Spotila, J.A., 2005, Applications of low-temperature thermochronometry to quantification of recent exhumation in mountain belts, *Low-Temperature Thermochronology: Techniques, Interpretations, And Applications*, Volume 58: Reviews In Mineralogy & Geochemistry, p. 449-466.
- Steckler, M.S., 1985, Uplift and extension at the Gulf of Suez indications of induced mantle convection: *Nature*, v. 309, p. 536-538.
- Steckler, M.S., Feinstein, S., Kohn, B.P., Lavier, L.L., and Eyal, M., 1998, Pattern of mantle thinning from subsidence and heat flow measurements in the Gulf of Suez: Evidence for the rotation of Sinai and along-strike flow from the Red Sea: *Tectonics*, v. 17, p. 903-920.
- Steckler, M.S., Omar, G.I., Karner, G.D., and Kohn, B.P., 1993, Pattern of hydrothermal circulation within the Newark Basin from fission-track analysis: *Geology*, v. 21, p. 735-738.
- Steckler, M.S., and Watts, A.B., 1980, The Gulf Of Lion - Subsidence Of A Young Continental-Margin: *Nature*, v. 287, p. 425-429.
- Stephen, J., Singh, S.B., and Yedekar, D.B., 2004, Evidence of low lithospheric strength for the South Indian Shield: Deep continental studies in India, v. 14, p. 22-24.
- Stockli, D.F., Dumitru, T.A., McWilliams, M.O., and Farley, K.A., 2003, Cenozoic tectonic evolution of the White Mountains, California and Nevada: *Geological Society Of America Bulletin*, v. 115, p. 788-816.
- Storey, B.C., 1995, The role of mantle plumes in continental breakup: case histories from Gondwanaland: *Nature*, v. 377, p. 301.
- Strutt, R.J., 1908, On the accumulation of helium in geological time: *Proceedings Of The Royal Society Of London Series A-Containing Papers Of A Mathematical And Physical Character*, v. 81, p. 272-277.
- Stuwe, K., 2001, *Geodynamics of the lithosphere*, Springer, 449 p.
- Subbarao, K.V., Chandrasekharam, D., Navaneethakrishnan, P., and Hooper, P.R., 1994, Stratigraphy and structure of parts of the central Deccan Province; eruptive models, *in* Subbarao, K.V., ed., *Volcanism (Radhakrishna volume)*, Wiley Eastern Ltd, New Delhi, p. 321-332.
- Subrahmanya, K.R., 1987, Evolution of the Western Ghats, India - a simple model: *Journal of the Geological Society of India*, v. 29, p. 446-449.
- Subrahmanyam, C., and Chand, S., 2006, Evolution of the passive continental margins of India - a geophysical appraisal: *Gondwana Research*, v. 10, p. 167-178.
- Subrahmanyam, V., Krishna, K.S., Murthy, G.P.S., Rao, D.G., Ramana, M.V., and Rao, M.G., 1994, Structural interpretation of the Konkan basin, southwestern continental margin of India, based on magnetic and bathymetric data.: *Geo-Marine Letters*, v. 14, p. 1432-1457.
- Subrahmanyam, V., Rao, D.G., Ramana, M.V., Krishna, K.S., and Rao, M.G., 1995, Structure and tectonics of the southwestern continental margin of India.: *Tectonophysics*, v. 249, p. 267-282.

- Summerfield, M.A., 1985, Plate tectonics and landscape development on the African continent, *in* Morisawa, M., and Hack, J.T., eds., *Tectonic Geomorphology*, Allen & Unwin, Boston, p. 27-51.
- Summerfield, M.A., 1991a, *Global Geomorphology*, John Wiley & Sons, New York, 537 p.
- Summerfield, M.A., 1991b, *Tectonic Geomorphology: Progress in Physical Geography*, v. 15, p. 193-205.
- Summerfield, M.A., and Hulton, N.J., 1994, Natural controls on fluvial denudation rates in major world drainage basins: *Journal of Geophysical Research*, v. 99, p. 13871-13883.
- Tagami, T., 2005, Zircon fission-track thermochronology and applications to fault studies, *Low-Temperature Thermochronology: Techniques, Interpretations, And Applications, Volume 58: Reviews In Mineralogy & Geochemistry*, p. 95-122.
- Tagami, T., and O'Sullivan, P.B., 2005, *Fundamentals of fission track thermochronology: Reviews in Mineralogy and Geochemistry*, v. 58, p. 19-47.
- Tagami, T., and Shimada, C., 1996, Natural long-term annealing of the zircon fission track system around a granitic pluton: *Journal Of Geophysical Research-Solid Earth*, v. 101, p. 8245-8255.
- Taylor, P.N., Chadwick, B., Moorbath, S., Ramakrishnan, M., and Viswanatha, M.N., 1984, Petrography, chemistry and isotopic ages of peninsular gneiss, Dharwar acid volcanic-rocks and the Chitradurga granite with special reference to the late archean evolution of the Karnataka Craton, Southern India: *Precambrian Research*, v. 23, p. 349-375.
- Thakur, N.K., and Nagarajan, N., 1992, Geotectonic remobilization of the lower crustal segment of southern peninsular India: *Physics of the Earth and Planetary Interiors*, v. 73, p. 153-162.
- Timoshenko, S., 1958, *Strength and materials. Part II. Advanced theory and problems*, New York, D. Van Nostrand Co.
- Tiwari, P.K., Surve, G., and Mohan, G., 2006, Crustal constraints on the uplift mechanism of the Western Ghats of India: *Geophysical Journal International*, v. 167, p. 1309-1316.
- Tiwari, V.M., and Mishra, D.C., 1999, Estimation of effective elastic thickness from gravity and topography data under the Deccan Volcanic Province, India: *Earth And Planetary Science Letters*, v. 171, p. 289-299.
- Todal, A., and Edholm, O., 1998, Continental margin off Western India and Deccan Large Igneous Province: *Marine Geophysical Researches*, v. 20, p. 273-291.
- Torsvik, T.H., Tucker, R.D., Ashwal, L.D., Carter, L.M., Jamtveit, B., Vidyadharan, K.T., and Venkataramana, P., 2000, Late Cretaceous India-Madagascar fit and timing of break-up related magmatism: *Terra Nova*, v. 12, p. 220-224.
- Tucker, G.E., and Slingerland, R.L., 1994, Erosional dynamics, flexural isostasy, and long-lived escarpments - A numerical modeling study: *Journal of Geophysical Research-Solid Earth*, v. 99, p. 12229-12243.
- Turcotte, D.L., and Schubert, G., 2002, *Geodynamics (2nd edn)*, Cambridge University Press, 456 p.

- Vaidyanadhan, R., 1977, Recent advances in geomorphic studies of Peninsular India: a review: *Indian Journal of Earth Science*, v. S. Ray vol., p. 13-35.
- van Balen, R.T., van der Beek, P.A., and Cloetingh, S.A.P.L., 1995, The effect of rift shoulder erosion on stratal patterns at passive margins: Implications for sequence stratigraphy: *Earth and Planetary Science Letters*, v. 134, p. 527-544.
- van der Beek, P., 1995, Morphotectonic evolution of rifted continental margins: inferences from coupled tectonic-surface process models and fission track thermochronology: *Tectonics*, v. 14, p. 406-421.
- van der Beek, P., and Braun, J., 1998, Numerical modelling of landscape evolution on geological time-scales: A parameter analysis and comparison with the south-eastern highlands of Australia: *Basin Research*, v. 10, p. 49-68.
- van der Beek, P., Summerfield, M.A., Braun, J., Brown, R.W., and Fleming, A., 2002, Modeling postbreakup landscape development and denudational history across the southeast African (Drakensberg Escarpment) margin: *Journal of Geophysical Research-Solid Earth*, v. 107.
- Vening Meinesz, F.A., 1931, Une nouvelle methode pour la réduction isostatique régionale de l'intensité de la pesanteur: *Bulltin Géodésique*, v. 29, p. 33-51.
- Verma, R.K., 1991, *Geodynamics of the Indian peninsula and the Indian plate margin*, Oxford and IBH publishing company, New Delhi, 357 p.
- Wadia, D.M., 1989, *Geology of India*, Tata McGraw-Hill, New Delhi, 460 p.
- Wagner, G.A., Reimer, G.M., and Jäger, E., 1977, Cooling ages derived from apatite fission track, mica Rb-Sr, and K-Ar dating: The uplift and cooling history: *Memoirs of the Institute of Geology and Mineralogy University of Padova*, v. 30, p. 1-27.
- Wagner, G.A., and Van den Haute, 1992, *Fission track dating*, Elsevier, Amsterdam.
- Walcott, R.I., 1970, Flexural rigidity, thickness, and viscosity of the lithosphere: *Journal of Geophysical Research*, v. 75, p. 3941-3953.
- Walker, P.M.B., 2002, *Dictionary of Science and Technology*, Chambers, 1152 p.
- Watt, S., and Durrani, S.A., 1985, Thermal-stability of fission tracks in apatite and sphene - using confined-track-length measurements: *Nuclear Tracks And Radiation Measurements*, v. 10, p. 349-357.
- Watts, A.B., 2001, *Isostasy and flexure of the lithosphere*, Cambridge University Press, 458 p.
- Watts, A.B., and Cox, K.G., 1989, The Deccan Traps: an interpretation in terms of progressive lithospheric flexure in response to a migrating load: *Earth And Planetary Science Letters*, v. 93, p. 85-97.
- Weissel, J.K., and Karner, G.D., 1989, Flexural uplift of rift flanks due to mechanical unloading of the lithosphere during extension: *Journal of Geophysical Research-Solid Earth and Planets*, v. 94, p. 13919-13950.

- Wendt, A.S., Vidal, O., and Chadderton, L.T., 2002, Experimental evidence for the pressure dependence of fission track annealing in apatite: *Earth And Planetary Science Letters*, v. 201, p. 593-607.
- Wendt, A.S., Vidal, O., and Chadderton, L.T., 2003, The effect of simultaneous temperature, pressure and stress on the experimental annealing of spontaneous fission tracks in apatite: a brief overview: *Radiation Measurements*, v. 36, p. 339-342.
- White, R., and McKenzie, D., 1989, Magmatism at rift zones - The generation of volcanic continental margins and flood basalts: *Journal of Geophysical Research-Solid Earth and Planets*, v. 94, p. 7685-7729.
- White, R.S., and McKenzie, D., 1995, Mantle plumes and flood basalts: *Journal of Geophysical Research-Solid Earth*, v. 100, p. 17543-17585.
- Widdowson, M., 1997, Tertiary palaeosurfaces of the SW Deccan, Western India: implications for passive margin uplift, *in* Widdowson, M., ed., *Palaeosurfaces: recognition, reconstruction and paleoenvironmental interpretation*, Volume 120, Geological Society of London Special Publication, p. 221-248.
- Widdowson, M., and Cox, K.G., 1996, Uplift and erosional history of the Deccan Traps, India: Evidence from laterites and drainage patterns of the Western Ghats and Konkan Coast: *Earth and Planetary Science Letters*, v. 137, p. 57-69.
- Widdowson, M., and Gunnell, Y., 1999, Lateritization, geomorphology and geodynamics of a passive continental margin: The Konkan and Kanara coastal lowlands of western peninsular India: *Special Publication of the International Association of Sedimentologists*, v. 27, p. 245-274.
- Widdowson, M., and Mitchell, C., 1999, Large-scale stratigraphy, structural and geomorphological constraints for earthquakes in the Southern Deccan Traps, India: The case for denudationally-driven seismicity: *Memoirs of the Geological Society of India*, v. 43, p. 425-452.
- Widdowson, M., Pringle, M.S., and Fernandez, O.A., 2000, A post K-T boundary (Early Palaeocene) age for Deccan-type feeder dykes, Goa, India: *Journal Of Petrology*, v. 41, p. 1177-1194.
- Wolf, R.A., Farley, K.A., and Kass, D.M., 1998, Modeling of the temperature sensitivity of the apatite (U-Th)/He thermochronometer: *Chemical Geology*, v. 148, p. 105-114.
- Wolf, R.A., Farley, K.A., and Silver, L.T., 1996, Helium diffusion and low-temperature thermochronometry of apatite: *Geochimica Et Cosmochimica Acta*, v. 60, p. 4231-4240.
- Zeitler, P.K., Herczeg, A.L., McDougall, I., and Honda, M., 1987, U-Th-He Dating Of Apatite - A Potential Thermochronometer: *Geochimica Et Cosmochimica Acta*, v. 51, p. 2865-2868.